University of Nottingham

UK | CHINA | MALAYSIA

3D Printing of a Medical Device Designed for Sustained Drug Delivery to the Ear

Waleed Yousof A. Rizg,

Pharm.D, MSc Pharmaceutical Sciences

Thesis submitted to the University of Nottingham

for the degree of Doctor of Philosophy

Division of Molecular Therapeutics and Formulation

School of Pharmacy

July 2020

Declaration

I would like to declare that the work conducted in this thesis titled “3D Printing of a Medical Device Designed for Sustained Drug Delivery to the Ear” is my own work and performed at the University of Nottingham between April 2017- Feb 2021 under the supervisions of Dr Jonathan Burley, Professor Clive Roberts, and Professor Ricky Wildman.

Waleed Yousof Rizg

Abstract

Ear infections are a common ear problem that can affect the human ear at all ages. Otitis externa (OE) is an external inflammatory ear condition of the outer auditory canal with or without an ear infection. Such ear inflammation might be located within the auditory canal with or without the involvement of the ear pinna or tragus. Most acute otitis externa (AOE) can be treated with over-the-counter ear drops, and in severe cases, patients may need to take oral or intravenous antibiotics. Topical ear drops are preferred for many reasons, including the ability to directly deliver them to the site of action with a higher local drug concentration, reduced ototoxicity, the ability to bypass the blood labyrinth barrier (BLB), less possibility of bacterial antibiotic resistance, and reduced systemic side effects. However, otic drops have limitations, including the frequency of daily dosing, whereby the patient has to lie down, and a reduction in the ease of self-administration. Ototopical treatments with a gelling system via the external ear canal can provide advantages over-ear drops, including improved patient compliance by reducing the frequency of daily dosing, increased contact time of the administered drug at the site of action, prolonged release of the drug at the desired site of action, and no need for the patient to lie down to prevent the drug escaping from the outer ear. We propose to develop an in-ear prototype device using 3D printing to deliver dexamethasone (DXM) as an anti-inflammatory medication through a hydroxypropyl methylcellulose (HPMC) gelling system to the external ear canal. DXM would be able to show a sustained release after being inserted into a patient's external canal for the treatment of AOE.

In chapter three, various ear prototype devices with a range of basic and realistic geometries were successfully printed using two kinds of 3D printing technologies, including fused deposition modelling (FDM) and stereolithography (SLA). FDM was successfully utilised with a PLA thread to develop an in-ear prototype device with pores to facilitate drug release. Electron microscopy confirmed that the FDM-printed PLA

devices have uniformly distributed layers without cracking or unwanted pores between the deposited layers. Also, there were no overlaps between the printed layers.

After the proper design was reached, various concentrations of HPMC hydrogels were successfully prepared. The rheological data show that the concentrations of the prepared HPMC samples (1-6% HPMC w/w) have liquid-like behaviours. In comparison, the 7% HPMC w/w sample showed an elastic-like behaviour after 15 Hz frequency. Furthermore, the flow curve data showed that the HPMC samples exhibited non-Newtonian shear-thinning behaviours. The releases of the HPMC hydrogel samples (1-7% HPMC w/w) through various FDM PLA printed ear prototype devices with simple geometries containing various pore numbers and locations were affected by different factors, including increasing the pore numbers, decreasing the concentrations of the HPMC polymer, raising the temperature from room temperature to body temperature, and changing the pore locations of the prototype devices. The 7% HPMC was selected to be utilised with the developed ear prototype device as a vehicle for the extended drug release of DXM.

In the final experimental chapter, two tablets, including DXM/methyl-β-cyclodextrin and DXM-lactose, were successfully formulated. The manufactured tablets have the same dose of DXM used in the treatment regimen of OE patients (≈ 2 mg of DXM). The DXM successfully diffused through the selected 7% HPMC hydrogel according to the Raman data. The Raman results confirmed that the intensity and area under the curve (AUC) of the characterised molecular peak of the C=O group, located at 1660 cm^{-1}, decreased from day 1 to day 7. Finally, the *in vitro* release experiment showed that the DXM had a sustained release for the typical period of the treatment regimen for AOE, i.e. 7 days.

Acknowledgements

In the name of Allah, the Most Gracious and the Most Merciful. I would like to thank Allah for enriching me with integrity, courage, compassion, endurance and patience in addition to facilitating my pursuit of completing this work.

I would also like to give specific thanks to my main supervisor, Dr Jonathan Burley, for accepting me in his lab. Furthermore, I would also like to thank him for providing motivation, patience, guidance, revising my writing, continuously supporting me in my PhD study and research. His continuous guidance profoundly helped me while designing this thesis and conducting the research project. I learned a lot from him.

I would also like to give specific thanks to my co-supervisors, Professor Clive Roberts and Professor Ricky Wildman, for their motivation, guidance, encouragement, and assistance during designing this project. I would also like to thank Professor Clive Roberts for his constant support and assisting me through the difficulties faced in the lab. Also, I would like to thank Professor Ricky Wildman for facilitating my access to the engineering labs to use the lab's facilities.

I would also like to thank Professor David Baguley and Dr Anand Kasbekar, for their guidance during the research, answering our questions, supports, and provide us with the facility in the hearing research centre.

I would also like to thank the team and staff in the engineering labs for answering our questions and guiding me in the lab. I would also like to especially thank Dr Ehab Saleh for his guidance, support, motivation, encouragement, helping me to improve the design of the printed devices and answering my questions. In addition, I would also like to thank Dr Hagit Gilon for assisting me in the lab with the FDM 3D printer. Moreover, I would like to thank Dr Vincenzo Taresco for his advice, helping me in the lab, and answering my questions.

I would also like to thank my colleagues and friends in D19 and D20 offices, Awaji Safhi, Dr Wathiq AL-Hachami, Mohammed Alissa, Dr Mohammed Al-Natour, Rayan Mushtaq, Dr Amjad Abouselo, Thatayaone Monkgogi, George Bebawy, and for their helping, motivating and supporting me during my work.

I would also like to extend specific thanks to my mother, Dr Shadia Matbouli, her supporting, motivation, prayers, and encouragement throughout my life. I would also like to thank my family, Nouf Hanbazaza, Malak Rizg, and Mohammed Rizg, Moayad Rizg, for their constant patience, support, motivation, and encouragement.

I would also like to thank King Abdul-Aziz University and the pharmaceutics department of the Faculty of Pharmacy for giving me this great opportunity to receive my higher education in the United Kingdom, and for their support during my studies. Last but not least, I would also like to thank the Saudi Arabian Cultural Bureau in London for their financial support.

Table of Contents

Table of Contents

List of Figures

List of Tables

List of Abbreviations

%	**Percentage**
3D	**Three-Dimensional**
A	**Area**
ABS	**Acrylonitrile Butadiene Styrene**
AOE	**Acute Otitis Externa**
AOM	**Acute Otitis Media**
API	**Active Pharmaceutical Ingredient**
BLB	**Blood Labyrinth Barrier**
CAD	**Computer Aided Designe**
CCD	**Charge Coupled Device**
CD	**Cyclodextrin**
CR	**Controlled Release**
CJ	**Continous Jet**
COE	**Chronic Otitis Externa**
D	**Displacement**
DDS	**Drug Delivery System**
DOD	**Drop on Demand**
DES	**Drug Eluting Stents**
DF	**Dossage Form**
DRI	**Drug Releasing Implant**
DSC	**Differential Scanning Calorimetry**
DXM	**Dexamethasone**
ER	**Extended Rlease**
F	**Force**
FDA	**Food and Drug Administration**
FDM	**Fused Deposition Modeling**
GIT	**Gastrointestinal Tract**
H	**Hight**
HCL	**Hydrochloric Acid**
HPLC	**High-Performance Liquid Chromatography**
HPMC	**Hydroxypropyl Methylcellulose**
HSM	**Hot Stage Microscopy**
IDDS	**Implantable Drug Delivery Systems**
IJ	**Ink Jet**
IPS	**Implantable Pump System**
IR	**Immediate Release**
IV	**Intravenous**
KCL	**Potassium Chloride**
KH_2PO_4	**Potassium Dihydrogen Phosphate**
LDD	**Local Drug Delivery**
ME	**Middle Ear**
MD	**Meniere's Disease**
Na_2HPO_4	**Disodium Hydrogen Phosphate**
NaCL	**Sodium Chloride**
NIR	**Near Infrared**
ODD	**Otic Drug Delivery**
OE	**Otitis Externa**
OM	**Otitis Media**

OWM	**Oval Window Membrane**
Pa	**Pascal**
PBS	**Phosphate Buffered Saline**
PCL	**Polycaprolactone**
PE	**Polyethylene**
PEG	**Polyethylene Glycol**
PET	**Poly(ethylene terephthalate)**
PLA	**Poly(lactic acid)**
PLGA	**Poly(Lactic-Co-Glycolic Acid)**
PMMA	**Poly(methyl methacrylate)**
PU	**Polyurethanes**
PVA	**Polyvinyl Alcohol**
PEVA	**Poly Ethylene Vinylacetate**
RS	**Raman Spectroscopy**
RM	**Raman Mapping**
RWM	**Round Window Membrane**
SDD	**Systemic Drug Delivery**
SE	**Side Effect**
SEM	**Scanning Electrone Microscopy**
SLA	**Stereolithography**
SLS	**Selective Laser Sentring**
TC	**Tympanic Cavity**
Tg	**Glass Transition**
MP	**Melting Point**
TM	**Tympanic Membrane**
TPU	**Thermoplastic Polyurethane**
USP	**United States Pharmacopea**
V	**Velocity**
γ	**Shear Strain**
γ.	**Shear Rate**
η	**Viscosity**
τ	**Shear Stress**
LVER	**Linear Viscoelastic Region**
AS	**Amplitude Sweep**
FS	**Frequency Sweep**
G’	**Storage Modulus**
G’’	**Loss Modulus**

Chapter 1: Introduction

The human ear is mainly responsible for receiving surrounding sounds and a sense of balance. The ability to hear is critical to our ability to interact with others and understand the surrounding world. Hearing dysfunction is the most common sensory disability in people and affects new-borns, children, adults and elderly people [1]. Many people worldwide suffer from different ear diseases and associated conditions, including otitis media (OM), otitis externa (OE), Meniere's disease (MD) and hearing loss. Chronic OE or OM affects about 3-5% of the U.S population, with a yearly cost of more than $2.98 billion [2]–[4]. If ear diseases are not treated properly, infections can spread to the surrounding tissues and become life-threatening, especially for immunocompromised patients. Ear diseases, such as MD, clearly decrease an individual's quality of life [5]–[7].

Due to the prevalence of ear diseases, there are many efforts to develop new therapeutic agents, with some attempts directed toward the progress of drug delivery systems (DDS) to improve the efficacy of treatments. The demand for ear medications is significant, with a global market of around $10 billion in the USA [8]. Fortunately, many ear diseases can be treated in the early stages if they are properly diagnosed [9], [10].

The human ear is a complicated organ, and it is an anatomically protected organ. Thus, there are many challenges for otic drug delivery (ODD). For external ear diseases, such as OE, current treatments focus on local treatment with ear drop medications, such as a topical analgesic, acetic acid solution, antibiotic alone or with steroids. In some cases, patients take systemic antibiotics. Topical DDS may have numerous benefits over systemic DDS, including maximising drug concentrations at the site of action and decreasing the systemic side effects [1].

The next part of this thesis reviews the essential parts of the human ear and the main barriers affecting drug delivery.

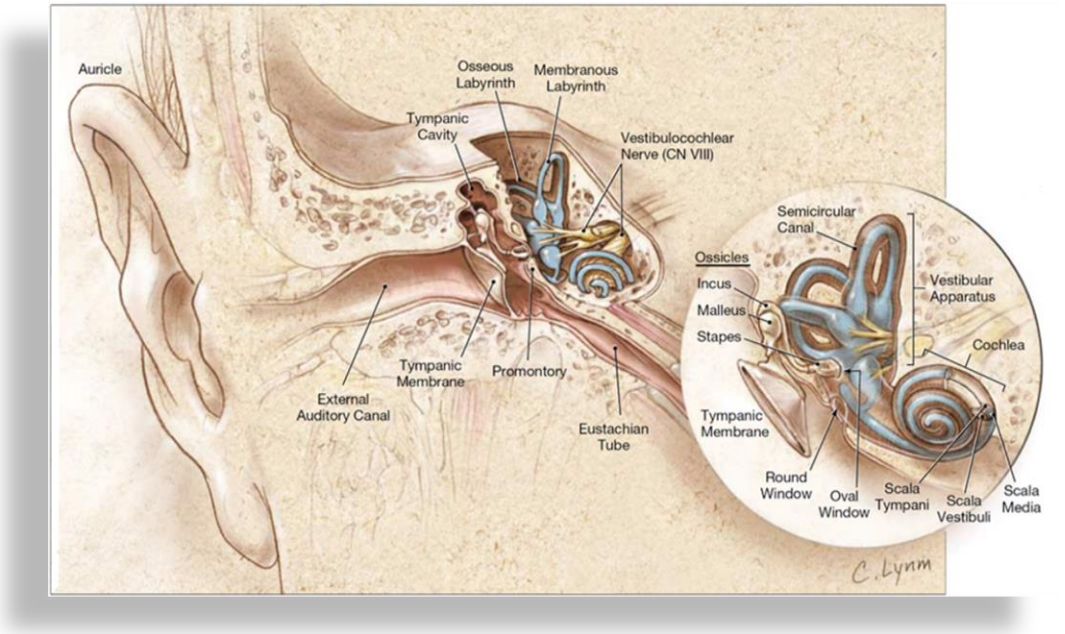

Figure 1.1 Schematic illustration of different human ear compartments and their compositions [11].

1.1 Human Ear Anatomy and Physiology

The human ear is mainly divided into three primary parts, the external, middle and inner ear **(Figure 1.1)**. The outer ear is composed of several components, including the ear pinna (auricle), which is the visible concave cartilaginous structure of the ear. The ear canal connects the ear auricle to the tympanic membrane (TM), which is also called the eardrum. It serves the function of collecting and magnifying sound waves. Moreover, it protects the elasticity of the TM by maintaining the proper humidity and temperature in the ear canal part [12].

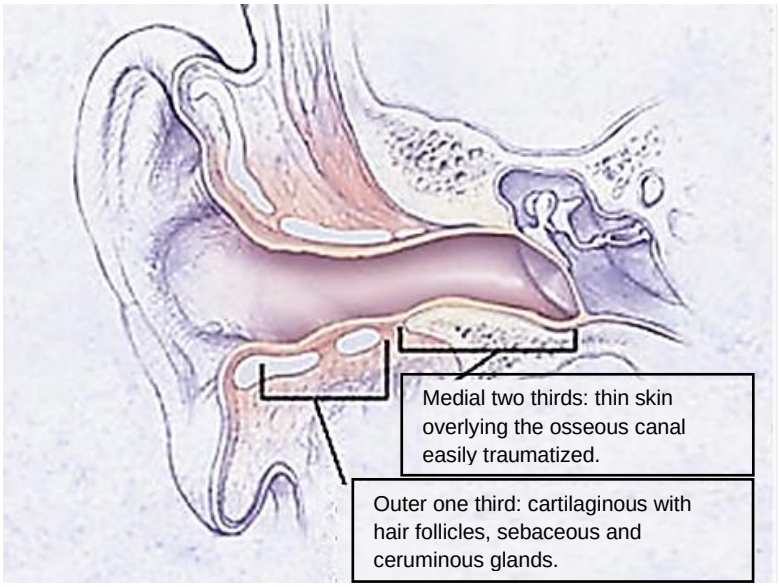

Figure 1.2 Anatomy of the external auditory part with the cartilaginous and bony part covered with skin [13].

The external auditory canal can be divided into different parts, namely a lateral outer one third and inner two thirds **(Figure 1.2)**. The outer third part is cartilaginous and covered by 1 mm thick skin. However, the inner part is bony and covered by thinner 0.2 mm skin [14]. The outer part enters the temporal bone [15]; the sebaceous glands, hair follicles and modified apocrine sweat glands are localised in this part. The cerumen, which is also called ear wax, is a mixture of secretion glands (sebaceous and modified apocrine sweat glands) [14], [16]. A healthy human auditory canal is slightly acidic, and its pH value lies between 5.0 and 5.7. This acidic range can inhibit bacterial growth [17], [18]. The ear cerumen acts together with the available hairs to limit dust and small objects entering the canal [15]. The bony part of the auditory canal does not have any hairs or secretion producing glands [19].

The TM is located at the end of the external auditory canal, and it separates the external ear from the middle ear. The TM vibrates to transmit the received sound signals from the outer ear to the internal ear [20]. The auditory canal length varies among adults and young individuals. Douglass et al.'s study showed different measurements of the ear canal lengths and diameters of people of different ages. The ear

canal lengths in the mentioned study ranged from 14 to 23 mm [21]. The average length of the auditory canal in an adult is about 25 mm and is about 5% longer in men than in women. The ear canal has an oval shape with an average diameter of 7-8 mm [15].

The next part of the human ear is the middle ear (ME), which comprises different smaller parts. It is composed of the tympanic cavity (TC), which contains the ossicular chain, which itself contains the three smallest bones in the human body, including the incus, malleus and stapes. Furthermore, it is composed of a mucosal lining that keeps the internal environment of the ME moist [22], and it contains the Eustachian tube, which allows the airing of the TC through the nasopharynx to facilitate the equalisation of the ME pressure [12]. The ossicular chain serves the function of transferring received sound signals from the ME to the internal ear [20].

The final part of the human ear is the inner ear. It is embedded deep in the petrous bone, which is one of the most hardened bones of the human body. It is composed of different components, including a) the cochlea, b) vestibuli and c) semi-circular canals [12]. The cochlea is a bony coiled tube that resembles a snail's shell [23]. This organ is divided into different fluid-filled compartments, including a) the scala tympani, b) scala media, and c) scala vestibuli [24].

Generally, during the auditory process, all sound waves are collected by the ear pinna and directed into the ear canal to produce TM vibration. The generated vibrations affect the three ossicular chains and cause their movement. After that, the stapes transfers the received pressure wave to the internal ear fluids via the oval window using a piston-like motion. Then, the internal ear hair cells vibrate and convert the received acoustic information into a bioelectric signal. After that, the converted signal is transmitted by the cochlear nerve to the brainstem. Finally, it is transmitted to the cerebral cortex, where the information is interpreted into hearing sensations [22].

Various barriers separate the cochlea from the ME and the circulatory system, including the round window membrane (RWM), the blood labyrinth barrier (BLB), and the oval window membrane (OWM). However, the central obstacle that isolates the external ear from the middle ear is called the TM [12].

The TM is elliptical and slightly conical in shape. This membrane is approximately 0.1 mm in thickness, and it is mainly comprised of different layers, including a) an outer epidermal layer, b) a middle fibrous layer with collagen that gives the TM its physical integrity, and c) an inner mucosal layer. The epidermal layer acts as a drug delivery barrier due to the presence of the stratum corneum layer [25]. Drug delivery to the ME through the transtympanic route must pass all three layers of the TM unless it is physically ruptured prior to that [26].

The RWM and OWM are the second main drug delivery barriers to the inner ear after the TM. These membranes are semipermeable and are located at the base of the cochlea. They separate the cochlea from the ME, and they are considered inner ear barriers. Moreover, they are regarded as pathways for drug delivery to the ear cochlea [22], [27].

The third major barrier is the BLB. This barrier is a physical and biochemical barrier between both the cochlea and systemic circulation. This barrier is distinguished by a continuous capillary endothelium, which links the blood vessels in the inner cochlea. These cells are attached by tight junctions [28]. This barrier protects the human ear, such as from potential toxins in systemic circulation that could damage the ear [29].

1.2 Major Ear Disease

Several diseases can affect human ear components. **Table 1.1** shows the major ear diseases affecting the three different parts of the human ear.

Table 1.1 The major ear disorders associated with the different parts of the human ear [22].

	Outer ear part	Middle ear part	Inner ear part
Ear Diseases	OE	OM	Hearing loss, MD and autoimmune inner ear disease, tinnitus

In this thesis, we focus on one of the major diseases affecting the outer ear part, which is acute OE. However, many other disorders can affect the outer ear, including malignant external otitis, cholesteatoma, obstructions of the ear canal (wax, foreign bodies) and tumours of the auricles and the outer ear canal [30].

1.2.1 External Ear Disease (Otitis externa)

OE is one of the most common problems affecting the outer ear **(Figure 1.3)**. It is defined as an inflammation of the lining of the external auditory canal, and it may also occur in the ear tragus or pinna. OE can be subdivided into two types, including a) acute otitis externa (AOE) or b) chronic otitis externa (COE). AOE may take less than six weeks to overcome, and most cases of this type are infectious. However, COE may take more than three months to treat fully, and the common reasons for this are allergies or a dermatological condition [31].

1.2.1.1 Acute Otitis Externa (AOE)

The majority (>95%) of OE cases are acute, occurring in children aged 18 years or younger [32]. AOE happens due to a bacterial infection, which causes 90% of AOE cases or fungal infection, which causes 10% of AOE cases [22].

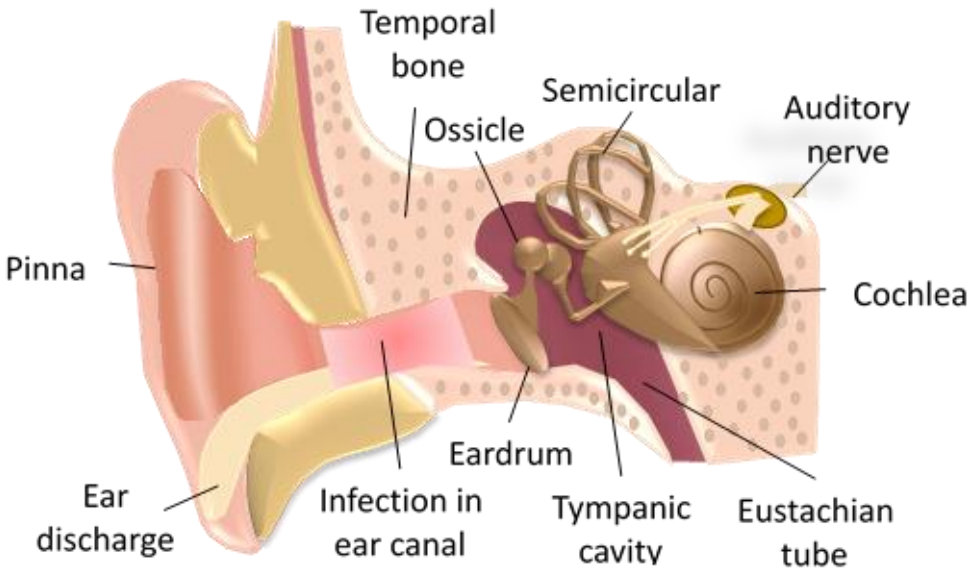

Figure 1.3 Schematic diagram of human ear anatomy with AOE.

Table 1.2 Risk factors of OE [32], [33].

Canal obstruction	▪ Ear wax obstruction ▪ Foreign body ▪ Sebaceous cyst
Earwax/epithelial cells integrity	▪ Using hearing aid devices ▪ Using of earplugs ▪ Earwax removal ▪ Instrumentation/itching
Water in the external ear canal	▪ Humidity ▪ Sweating ▪ Swimming or prolonged water exposure
Dermatologic conditions	▪ Psoriasis ▪ Eczema
Anatomic abnormalities	▪ Stenosis of the ear canal ▪ Exostoses ▪ Hairy ear canals
Miscellaneous	▪ stress ▪ using of soap ▪ purulent otorrhea from OM

1.2.1.1.1 Risk Factors

Many risk factors can influence the progress of this kind of disease in patients. **Table 1.2** shows the different risk factors that may impact OE. These risk factors affect the protective earwax barrier as well as disrupt the epithelial layer of the external ear canal and increase the pH of the external auditory ear canal [17], [33], [34].

1.2.1.1.2 Pathophysiology

The most frequently detected pathogens in AOE are *Staphylococcus spp* and *Pseudomonas aeruginosa*. AOE can also be caused due to fungal infections (otomycosis), such as *Candida or Aspergillus* infections. Though fungal infections are uncommon, they may be seen in some AOE patients after they have been treated with topical antibiotics [31], [35].

Ear wax protects the ear canal in various ways. Firstly, it protects the epithelium layer of the skin from breakdown by providing a waxy barrier. Also, it inhibits bacterial or fungal growth due to its acidity [36]. Even a little small amount of ear wax can protect the auditory canal from infection. However, ear wax that accumulates excessively in the canal can cause canal obstruction, infection and retention of debris and water [3]. Self-cleaning of the canal by any materials, such as cotton swabs, can damage the lining of the external canal. Moreover, excessive exposure to water may cause canal maceration and epithelial lining breakdown [31].

1.2.1.1.3 Diagnosis

There are several symptoms of AOE, including itching, otalgia, pain on chewing and in some cases, hearing loss. The most common hallmarks of AOE are tenderness of the pinna or tragus [37]. During a physical examination with an otoscope, the auditory ear canal may appear erythematous and slightly oedematous with otorrhea. The infection in the external ear of an AOE patient may spread to the surrounding structures of the canal and lead to many diseases, such as facial or auricular cellulitis, or chondritis [31]. Moreover, a continuing chronic infection may

develop into canal stenosis and conductive hearing loss [38]. In untreated cases, the infection can spread to the surrounding bone (temporal bone), causing osteomyelitis and systemic toxicity [31].

1.2.1.1.4 Treatment of AOE

Successful treatments of AOE, include a) aural toilet, b) treatment of infection, c) pain control, and d) avoiding any promoting factors. Removing any impacted cerumen and debris facilitates drug penetration to the desired site [31]. Topical administration of antimicrobial medication with or without corticosteroid drugs is used for the treatment of uncomplicated AOE patients. The most commonly used antimicrobial agents include quinolones, aminoglycosides, acetic acid and polymyxin B [39]. The administration of topical corticosteroid medication provides a rapid improvement in symptoms, such as erythema, external canal oedema, and ear pain [32], [40]. Steroid drugs are available with several antibiotic preparations, and affected patients need to be treated for 7-10 days [32]. **Table 1.3** presents the most common otic medications used for the treatment of AOE.

Table 1.3 The most common topical formulations for AOE [1], [31].

Component	Brand	Dosage	Comments
Acetic Acid 2% solution	VoSol	3-5 drops every 4-6 hours	Avoid if TM ruptured, because it may cause irritation
Acetic Acid 2%/hydrocortisone 1% solution	VoSol HC	3-5 drops every 4-6 hours	Avoid if TM ruptured, because it may cause irritation
Neomycin/polymyxin B/Hydrocortisone solution	Cortisporin	3-4 drops every 6-8 hours	Avoid if TM ruptured
Ciprofloxacin 0.2% solution	Cetraxal otic	3-4 drops every 12 hours	Single-use container
Ciprofloxacin 0.2%/ Hydrocortisone 1% suspension	Cipro HC	3-4 drops every 12 hours	7 days course
Ciprofloxacin 0.3%/ DXM 0.1% suspension	Ciprodex	3-4 drops every 12 hours	7 days course
Ofloxacin 0.3% solution	Floxin Otic	10 drops once daily	7 days course
DXM 0.1 % suspension	Maxidex	-	-

While the topical administration of antibiotics is beneficial for AOE patients, oral antibiotics have limited utility [41]. Around 20-40% of AOE patients take systemic antibiotic delivery via the oral route with or without topical drug delivery [42]–[44]. Topical antibiotics, such as aminoglycosides and fluoroquinolone, are beneficial for most AOE cases, and they cover both *Pseudomonas aeruginosa* and *Staphylococcus spp* pathogens. The selection of topical antibiotics should be based on different factors, including cost, availability, contact sensitivity, ototoxicity, dosing schedules, and patient compliance [1]. In AOE patients with canal debris or otorrhea, the ear canals can be cleaned using irrigation, gentle suction, and then gently drying the area with cotton. The affected patients need to take the ear drops for one week. If they still have symptoms, they need to continue for up to more one week. If the symptoms are still present on day 14, the treatment should be considered a failure [1]. The patients need to take the ear drops appropriately, and they often need to have someone else to conduct the procedure for it to be more effective. The patients need to lie on their side with the affected ear on top, and the ear preparations are placed to run along the bottom of the ear canal until the canal is filled. Then, the pinna is gently moved to remove trapped air and to confirm that the canal filled with drugs. Finally, the patient should stay in the same position for 3-5 minutes [1].

Topical acetic acid preparations can be used because they have anti-infective activity and drying action. However, the efficacy of this kind of preparation diminishes if it is used for more than one week [45]. The topical administration of pain control medications can be used for AOE patients, including over-the-counter medications, such as ibuprofen or acetaminophen. AOE patients should be aware of and avoid precipitating factors, such as swimming or using hearing aids or earplugs until the symptoms have resolved as well as minimise moisture exposure and any source of ear trauma [1].

In this thesis, DXM was selected as a model of an anti-inflammatory drug to quickly relieve the inflammation, itching, and squamation that occurs in the auditory canal in people suffering from AOE [46]. Moreover, DXM has been approved by the U.S. FDA to be used topically with the antibiotic ciprofloxacin, which is available commercially as Ciprodex®, in the ME to treat acute otitis media (AOM) in paediatric cases with a tympanostomy tube and external ear to treat AOE [47], [48].

1.2.2 Administration Routes for Otic Drug Delivery (ODD)

Numerous routes have been used for ODD. The choice of the appropriate route of administration depends on the otic disease that needs to be treated and the physicochemical properties of the active pharmaceutical ingredients (API). The ODD route of administration can be classified into systemic and local drug delivery routes of administration [22].

1.2.2.1 Systemic Drug Delivery (SDD)

SDD to a human ear can be classified into oral and IV drug deliveries. The oral route of administration is commonly used to treat people who suffer from the inner ear and ME disorders because this route of administration is convenient and preferred by patients [40], [49]. The IV route of administration is used to treat severe ME disorders, such as acute mastoiditis [22].

1.2.2.2 Local Drug Delivery (LDD)

LDD has several advantages over SDD, including the ability to bypass the BLB, minimise the systemic side effects and increase the API concentration at the site of action. LDD can be classified into topical, transtympanic, intratympanic, and cochlear drug delivery [22].

1.2.2.2.1 Topical Drug Delivery

In this type of drug delivery, the API is directly applied to the external ear canal of the human ear. The most commonly used medications include antifungal and antibiotic ear drops [50] and gels [25].

1.2.2.2.2 Transtympanic Drug Administration

The first barrier to drug delivery from the external ear to the ME and inner ear is the TM. Successful transtympanic drug delivery depends on API diffusion through the undamaged TM from the outer auditory canal to the middle and inner auditory parts. Transtympanic drug delivery can be enhanced by using chemical permeation enhancers. A research study, utilised localized and sustained antibiotic (ciprofloxacin) delivery through the transtympanic administration to the ME by using different chemical penetration enhancers (bupivacaine, limonene, sodium dodecyl sulfate), in a gelling system (poloxamer 40) [25].

1.2.2.2.3 Intratympanic Drug Administration

This route of administration comprises injecting the API into the ME cavity. After that, the injected drug diffuses into the cochlea via the RWM along the concentration gradient. Also, small pharmaceutical devices, such as microWicks (1 mm in diameter, and 9 mm in length), osmotic pumps, and microcatheters (1.5, 2.0 or 2.5 mm in diameter) have been used for Intratympanic ODD [51]. Some clinical studies used steroids through intratympanic injection to treat a variety of diseases, such as hearing loss and MD [52]–[55].

1.2.2.2.4 Intracochlear Drug Administration

In this route of administration, the drug is administered directly on the cochlea [56]. Different intracochlear methods have been used, such as cochlear implants and osmotic mini-pumps [57]. Cochlear osmotic pumps and implants offer the preferred methods for the controlled, automatic and complex dosing of different compounds into the inner ear cochlea. These two routes of administrations are invasive [58].

The next sections are brief backgrounds about the IDDS, including their classifications, applications, and some implant systems available on the pharmaceutical market.

1.3 Implantable Drug Delivery Systems (IDDS)

Current treatments of AOE are mainly focused on the local treatment of ear canal infections with ear drops medication, including analgesics, acetic acid solutions, and antibiotics alone or with steroid drops. In some cases, the patients take systemic antibiotics when the infection has spread outside the ear canal. The oral administration has some limitations, such as drug stability, bioavailability, bacterial resistance, toxicity, and duration of release [1].

Although the local treatment of AOE with ear drops is preferable to the oral administration, it has various drawbacks, including patient compliance, which may be affected by the frequency of daily dosing, the need for someone else to apply the medications to gain full efficacy, and the use of hearing aids, as patients may stop using these devices until the disease has been treated. In some cases, the patients may move to a more invasive surgery situation. A controlled drug delivery system is required to resolve these issues [59]. Drug-releasing implants (DRI) have clearly emerged as a possible alternative to the topical administration of clinical treatments based on ear drops. DRIs have a variety of benefits and drawbacks; these are described in **Table 1.4.** Implants can be defined as a dosage form that can be placed directly inside the body subcutaneously or inserted into an internal body cavity. This kind of dosage form is designed to release the API over a prolonged period [60]. It is used as a delivery system for delivering drugs locally or systemically to produce therapeutic effects [61].

Table 1.4 Advantages and disadvantages associated with IDDS [62]–[64].

Advantages	Disadvantages
▪ Targeted DD can be achieved.	▪ Implantation is often associated with minor or major surgery.
▪ Can deliver the API that cannot be provided by oral and IV.	▪ The implantation procedure needs expert physicians and personnel.
▪ Drug release commonly follows zero-order kinetics.	▪ The surgery might be traumatic and may produce some complications for the patient, such as scars.
▪ It offers sustained drug release for extended periods.	▪ The by-products from the biodegradable implantable systems can be harmful to the body.
▪ It has a wide range of flexibility in the choice of materials, supplies, manufacturing methods, formulating, and modulation of drug release.	▪ Reducing the size of the implant may limit the drug loading capacity.
▪ Macromolecules that have a shorter in vivo half-life, poor permeability characteristics, or are subject to enzymatic degradation can be delivered successfully by IDDS, e.g., peptides and proteins.	▪ It is required to be correctly placed at the targeted site to avoid any adverse reaction that may occur due to this dosage form.
▪ Immediate removal is possible in case of adverse reaction experience or allergic reaction after implantation.	▪ The design is time-consuming and more expensive compared to other oral dosage forms.
▪ It facilitates a higher therapeutic efficacy compared to traditional routes of administration.	▪ Insertion of this dosage form inside the body for more extended periods may lead to the formation of fibrous capsules that may affect drug release.

Generally, IDDS can be classified into different categories, including passive and active implants. Passive implants can be subcategorized into biodegradable and non-biodegradable polymeric implants [59], [62]. In this thesis, we focus on the first category, which is passive implants.

1.3.1 Passive Polymeric Implantable Systems

These kinds of implantable systems have no moving parts. Moreover, they depend on a passive diffusion mediated phenomenon to control APIs release [65]. Passive polymeric implants can be categorised into two categories: 1) Non-biodegradable and 2) biodegradable implantable polymeric systems [59], [62]. These two types utilise the application of polymer and polymeric membranes to achieve controlled drug molecule release within biological systems [59].

1.3.1.1 Non-biodegradable Polymeric Implantable Systems

Various types of non-biodegradable IDDS have been approved and are available on the pharmaceutical market. However, the most common forms of this type of polymeric system include 1) reservoir implant systems and 2) matrix implant systems (**Figure 1.4**). Non-biodegradable implantable polymeric systems are primarily composed of a variety of polymers, including silicones, ethylene vinyl acetate, urethanes, acrylates and their copolymers, vinylidene fluoride copolymers, poly(ethylene vinyl acetate) (PEVA), and polysulfone polymers [62], [63].

The reservoir system comprises a central compact drug core, which is surrounded by a permeable polymeric non-biodegradable membrane (**Figure 1.4A**). The permeable membrane controls the release rate of the drug [63]. There are certain drawbacks to this kind of system, including a) high manufacturing cost, b) the challenge of designing with macromolecules due to their poor diffusion through the permeable membrane, and c) the potential for “drug dumping” due to the rupture of the polymeric membrane during therapy. The possibility of a membrane break renders the reservoir system a less popular method of drug delivery compared to the matrix system. If the membrane breaks, the concentration of the administered drug will increase instantly within the body. Consequently, this will produce dose-related toxicity. For example, transdermal reservoir patches can provide dose dumping when the rate-controlling membrane is destroyed [59], [63], [66].

Matrix systems consist of a uniform dispersion of drug molecules within the non-biodegradable polymer system (**Figure 1.4B**) [63]. This kind of system depends on the diffusion of drug molecules through the non-biodegradable polymer matrix network to achieve a sustained-release of the drug [59], [63].

Matrix systems offer multiple advantages, including 1) low manufacturing cost, 2) safety in terms of drug leakage, and 3) the formulation of macromolecules, such as enzymes, antibodies, and insulin [59], [66].

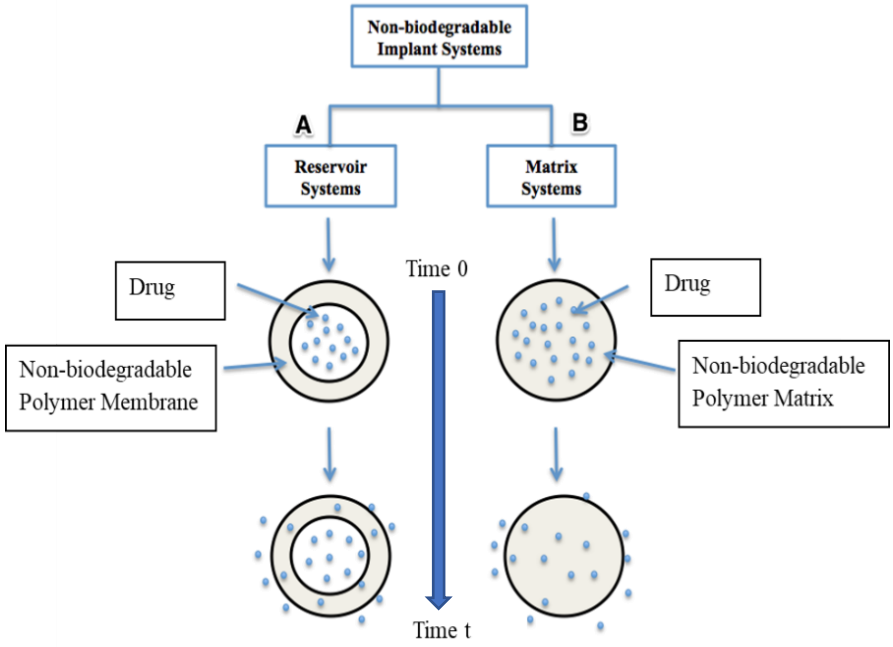

Figure 1.4 Schematic diagram of non-biodegradable A) reservoir and B) matrix implant systems.

1.3.1.2 Biodegradable Implantable Systems

This type was developed to overcome the limitations of non-biodegradable implantable systems. Biodegradable implantable systems are prepared using polymer or block copolymer that can be cracked into small parts. These fragments are excreted or absorbed by the human body [67], [68]. In biodegradable implantable systems, there is no requirement to remove the implants after implantation, as they degrade inside biological systems into non-toxic metabolites are excreted by the body [69]. Biodegradable polymeric systems follow the same classification as for non-biodegradable implants, namely the reservoir and matrix systems [63]. **Figure 1.5** shows a schematic diagram of a biodegradable matrix system.

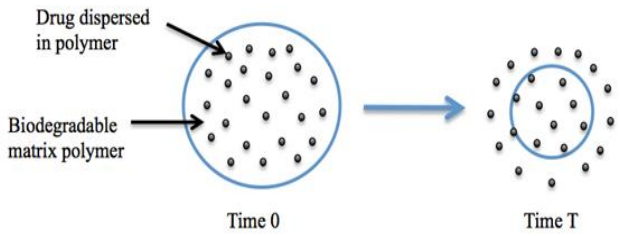

Figure 1.5 Schematic diagram of a biodegradable matrix system. The drug molecules are released by an erosion mechanism. The black dots represent the drug molecules.

Various polymers are utilised to fabricate a biodegradable system, including polylactic acid (PLA), poly anhydride, polyglycolic acid, hydroxypropyl methylcellulose (HPMC), poly(lactic-co-glycolic acid) (PLGA), polyvinylpyrrolidone, polycaprolactone (PCL), polyhydroxy butyrate, and polyethylene glycol (PEG) [59], [63]. The polymers utilised in biodegradable implants can be further characterised as either natural and synthetic polymers [69]. This type is more complicated to manufacture than non-degradable implantable systems [65].

1.3.2 Applications of Polymeric Implantable Systems

The major clinical applications of both non-biodegradable and biodegradable polymeric implantable systems include the delivery of a variety of therapeutic agents, such as anticancer agents, contraceptive steroids, ocular therapeutics, and cardiovascular treatments [62]. Polymeric IDDS can be applied as a hormonal contraceptive. The most commonly used reservoir system for birth control is the levonorgestrel sustained release implant system known as Norplant®. The Food and Drug Administration (FDA) in the USA approved the use of Norplant® in 1990 **(Figure 1.6A)** [59], [62], [69]. Norplant® is composed of 6 thin, flexible silicone capsules. Each one is loaded with levonorgestrel hormone (36 mg), and the contraceptive can be inserted subcutaneously into the upper arm of female consumers [70]. Furthermore, IDDS can be used for ocular drug delivery to treat a variety of ocular diseases, such as cytomegalovirus retinitis, diabetic retinopathy, and glaucoma [71]. There are multiple ophthalmic IDDS available on the pharmaceutical market, such as Vitrasert®, Retisert®, Surodex®, and Ozurdex® **(Figure**

1.6B) [72], [73]. Additionally, they represent an appropriate approach for minimally invasive and localised cancer treatment. They can be utilised to treat cancer patients, and they can be placed on different sites within the body. For instance, they can be placed directly on a tumour (intratumoral site), subcutaneously or on intramuscular sites [63]. There are many anti-cancer drug-eluting implants currently available on the market, such as Gliadel® **(Figure 1.6C)**, OncoGel®, Lupron Depot®, and Zoladex® [74]. Finally, they can be utilised in the treatment of cardiovascular diseases. Drug-eluting stents (DES) form an important example of a non-biodegradable as well as biodegradable IDDS application. There are two versions of biodegradable DES, including a biodegradable coating on a permanent stent and a fully biodegradable system [62]. There are different types of DES available commercially, including the sirolimus-eluting Cypher™ stent **(Figure 1.6D)** and the Taxus™ stent [75]. **Table 1.5** shows different examples of IDDS that are used for ocular disease, anticancer treatment, in women's health (contraceptive), and in central nervous systems disorders and infectious diseases.

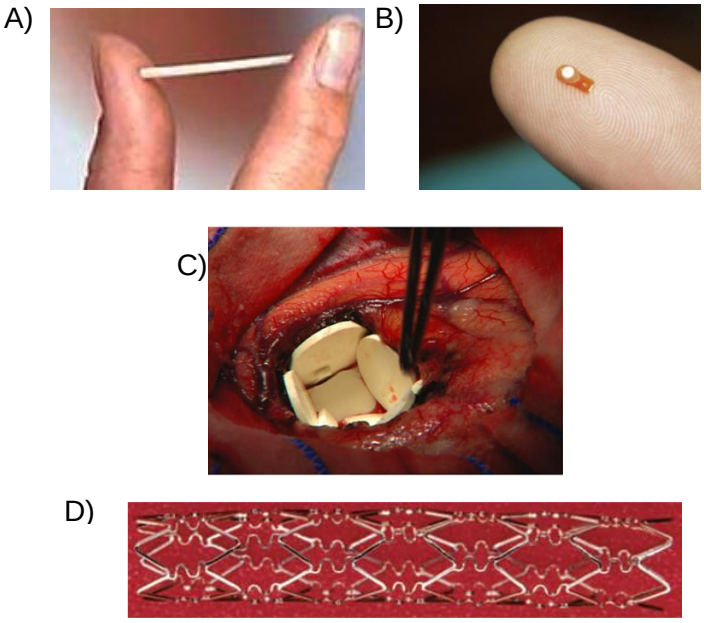

Figure 1.6 Various examples of IDDS and their applications, including A) contraceptive implants (Implanon®) [76], B) ocular drug delivery (Retisert®) [72], C) cancer drug delivery (Gliadel®) [77], and D) cardiovascular disease treatment (Cyper®) stent [78].

Table 1.5 Examples of IDDS, including cancer therapy, contraceptives, ocular therapies, pain management, and central nervous systems.

Product names	Implant type	Material used	Drug used	Indication	References
Norplant®	Sub-cutaneous	silicone	Levonorgestrel	Contraception	[79]
Implanon®	Sub-cutaneous	PEVA	Etonogestrel	Contraception	[80]
Nuvaring®	Intra-vaginal	PEVA	Etonogestrel, Ethinyl estradiol	Contraception	[81], [82]
Estring®	Intra-vaginal	silicone	Estradiol	Menopausal symptoms	[83]
Zoladex®	Sub-cutaneous	PLGA	Goserelin	Prostate cancer	[84]
Gliadel Wafers®	Inta-tumoral	Silicone	Carmustine (BVNU)	Primary malignant glioma	[85]
Oncogel®	Inta-tumoral	PLGA-PEG-PLGA	Paclitaxel	Oesophageal cancer	[86]
Vantas® Sub	Sub-cutaneous	Methacrylate based hydrogel	Histrelin	Prostate cancer	[87]
Ocusert®	Intra-ocular	PEVA	Pilocarpine, Alginic acid	Open-angle glaucoma	[88]
Retisert®	Intra-ocular	Microcrystalline cellulose, PVA, Magnesium stearate	Fluocinolone	Non-infectious uveitis	[89]
Vitrasert®	Intra-ocular	PVA, PEVA	Ganciclovir	CMV retinitis in AIDS patients	[90]
Probuphine®	Sub-cutaneous	PEVA	Buprenorphine	Opioid abuse	[91]
LiRIS®	Intra-vesical	Silicone	Lidocaine	Interstitial cystitis/bladder pain syndrome	[92]
Med-Launch	Sub-cutaneous	PLGA	Risperidone	Schizophrenia	[93]
Risperdal consta®	Intra-muscular	PLGA	Risperidone	Schizophrenia	[94]

Other types of implants are dynamic and electromechanical implants. The dynamic implant system utilises a positive driving force to deliver and control API release. Most of these are electronic devices made from metallic items, although some polymeric implants are used, such as osmotic pumps. Dynamic IDDSs are mostly pump-type implants [65].

1.3.3 Drug Release Mechanism from Polymeric IDDS

IDDS API release mechanisms are divided into several categories, including controlled swelling, matrix degradation, passive diffusion and osmotic pumping [95].

In controlled swelling systems, the rate of release is controlled by the solvent penetration into the utilised matrix of an implanted device [96]. Alternatively, passive diffusions and osmotic pumps mechanisms drug delivery are promising systems for linear drug delivery. On the other hand, osmosis is a concept defined as the overall movement of water from a site of a dilute solution to a site of a more concentrated solution via a permeable membrane. Thereby, it produces a hydrostatic pressure difference between both sites [97]. Osmotic pumping is a phenomenon that uses the osmosis concept to control the API drug rate. Consequently, IDDS devices based on osmotic pumping display a constant drug release rate produced by solvent absorption driving the transport of a drug [98]. Diffusion is another drug release mechanism, defined as a process by which API molecules move spontaneously from one place to another to equilibrate thermodynamic activity or chemical potential. In this mechanism, the driving force is the concentration gradient [95]. The drug release mechanisms can be divided into two categories, including drug release mechanisms from a) biodegradable and b) non-biodegradable implants.

1.3.3.1 Drug Release Mechanisms from Biodegradable Implants

IDDS devices are commonly involved in a drug-polymer mixture or a drug reservoir surrounded by a polymer [99]. After the IDDS is inserted into the desired area, the utilised drug is released at a controlled rate as the used polymer degrades. The API release from an IDDS contains a reservoir system that is mainly controlled by different factors, including the polymer degradation rate or API dissolution into the polymer wall and then diffusion through the polymer wall, or a combination of both.

In contrast, there are different API release mechanisms from a drug-polymer mixture, such as swelling, erosion, or diffusion. The API release from these systems mainly depends on drug solubility, drug load, drug permeability in the used polymer, and the degradation rate of the polymer inside the human body [99]. The degradation of the polymer and subsequently the drug release can occur due through hydrolysis, enzyme

degradation, oxidation, physical degradation or a combination thereof [100], [101].

1.3.3.2 Drug Release Mechanism from Non-Biodegradable Implants

The primary release mechanism in this kind of implant is passive diffusion. The reservoir system maintains a constant release rate that is not affected by a concentration gradient; however, it is related to the permeability or thickness of the rate-controlling membrane (zero-order release) [102]. On the other hand, the release mechanism in the matrix system is mediated by Fickian diffusion, which is affected by the concentration gradient [103], [104]. Moreover, these systems provide sustained drug release. However, the release kinetics are reliant on the volume fraction of the API in the matrix, indicating that the drugs released from these systems are directly proportional to the API contained within the matrix [96].

1.3.4 Methods of Polymeric Implantable Manufacture

Various methods are used to manufacture the implants, including A) compression, B) hot-melt extrusion, C) solvent casting, D) injection moulding and E) 3D printing technologies [65]. A thermoplastic polymer such as PLA can be manufactured as an IDDS using several fabricating techniques, including compression, injection moulding, moulding or extrusion [105].

1.3.4.1 Compression technique

This technique has been used for the fabrication of implantable DDS containing heat- or solvent- sensitive compounds, includes peptides and proteins [106]. However, the implants manufactured using this technique showed a faster release profile than other manufacturing techniques. Also, to prolong the drug release, an additional method may be required, such as coating the implant. Fialho et al. utilised the compression and hot moulding methods to compare the influence of the used methods on the degradation of polymeric matrices and the release of the drug (DXM acetate) [105].

1.3.4.2 Solvent casting

In this method, the used polymer is dissolved into an appropriate solvent. Subsequently, the produced solution is cast into a mould. Then, the used solvent is removed by evaporation [107]. The fabricated implants result in films or laminar implants [108]–[110]. Prata Al et al. utilised this method to produce a polymeric-based biodegradable ophthalmic implant to deliver DXM to treat diseases affecting the posterior segments of the eye [111].

1.3.4.3 Hot-melt extrusion

This method has several steps, including mixing, melting, and forcing a polymer through a small hole named a die [107]. The polymer used in this method needs to be thermoplastic, such as PLGA and PLA [112]. Follonier et al. utilised this method to manufacture sustained drug release pellets. They used the drug diltiazem HCl. After they made the pellets, they filled them into hard gelatine capsules and studied the drug release *in vitro* [113].

1.3.4.4 Injection moulding

Thermoplastic polymers such as PLA or PLGA can be used with this method. In the beginning, the used polymer is heated. Then, it is injected into a specific mould. Finally, the used polymer is allowed to solidify [65].

1.3.4.5 3D Printing

This technology is currently utilised to create different kinds of implantable systems, including dental implants, prostheses and orthopaedic implants [114]. Three-dimensional (3D) printing technologies are promising in the fabrication of IDDS. 3D printing technology is a cost-effective, reproducible, highly adaptable method, and it could be a promising technology in the fabrication of implantable drug delivery devices [114].

The next section affords a brief overview of 3D printing technologies, the current methods utilised for drug delivery, their principles, and their various applications.

1.4 3D Printing of IDDS

3D printing technology is a fabricating method in which items are manufactured through the process of fusing or depositing materials, such as ceramics, powders, plastic, liquids, living cells, and metal, in layers to form 3D objects [115]–[118]. 3D printing is also referred to as rapid prototyping, additive manufacturing or solid free-form technology [119].

3D printing technology relies on computer-aided design (CAD) (**Figure 1.7**) to attain flexibility, time-efficiency, and exceptional fabricating capabilities for pharmaceutical products [120]. This technology has gained increasing attention in pharmaceutical formulation development due to its efficacy in overcoming the challenges associated with conventional pharmaceutical unit operations, such as mixing, granulation, and compression. Traditional manufacturing can lead to the creation of variable qualities of final products in terms of drug loading, drug stability, drug release, and the stability of the pharmaceutical dosage form [121]. The attempts to develop 3D printing technology for pharmaceutical product development led to the first FDA approval for 3D printed tablets for Levetiracetam (Spritam®) [122].

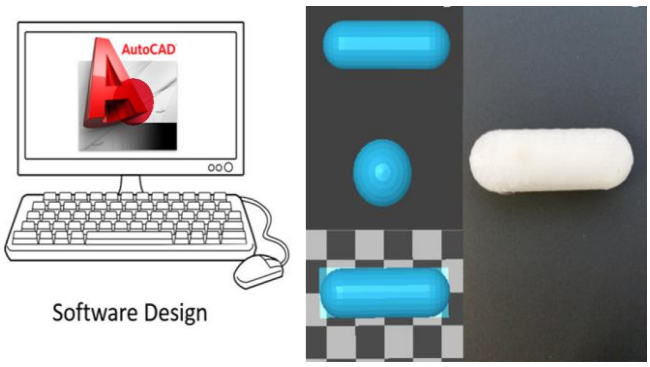

Figure 1.7 Schematic diagram of CAD design (left); a capsule designed in CAD (middle); a capsule printed with a 3D printer (right) [123].

1.4.1 Current 3D and AM Printing Techniques Applied in Drug Delivery Systems

There are different categories of 3D printing techniques that are utilised in the manufacture of the solid-free form of drugs. Some of these include stereolithography (SLA), inkjet (IJ) printing, selective laser sintering (SLS), fused deposition modelling (FDM), and semisolid printing (**Figure 1.8**) [123]–[125]. Multiple DDS have been developed through 3D printing techniques, including oral controlled-release (CR) systems, drug delivery microchip, rapidly dissolving DDS, CR pills, and multiple phase DDS [126]–[131]. Also, 3D printing has been applied for the preparation of a variety of sophisticated IDDS with complex design features due to their ability in terms of the particular spatial deposition of multiple materials or drugs and control over local composition and microstructure [132]. 3D printing techniques that are applied in DDS currently exist only in research labs.

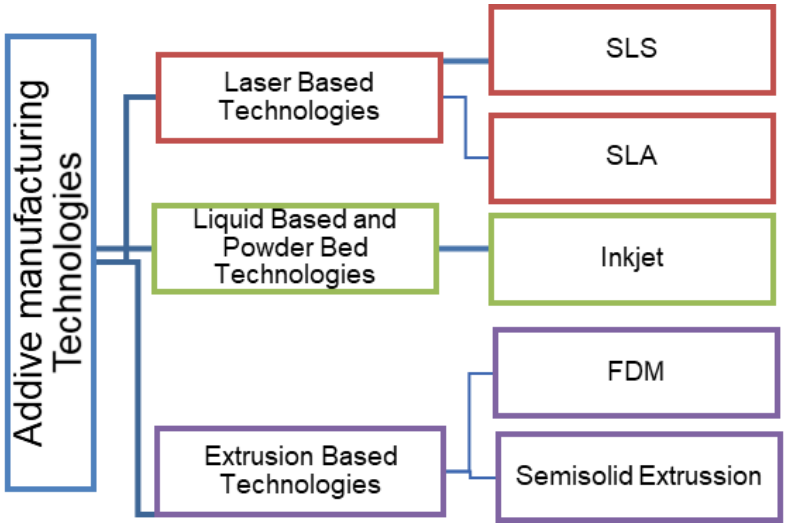

Figure 1.8 Schematic diagram for the classification of printing technologies applied in DDS.

1.4.1.1 Stereolithography (SLA)

Charles Hull developed the first SLA printer in the 1980s [133]. In this kind of 3D printer, a photopolymerisable resin is exposed to high-energy light, such as UV light, to polymerise and solidify of the loaded resin. After the resin is solidified to a specific depth, the building plate is lowered vertically along the z-axis. Then, the hardened layer is submerged in resin, and the procedure is repeated until the 3D object is finished layer by layer [134] **(Figure 1.9 A)**. SLA technology has been applied in different fields, including pharmaceutical applications [135] and tissue engineering [136]. For instance, Wang et al. utilised an SLA 3D printer to manufacture modified-release tablets containing paracetamol and 4-aminosalicylic acid [135]. The SLA printer technique and materials that have been used in this thesis are described in detail in **chapter 2, sections 2.1 and 2.4.2.**

1.4.1.2 Selective Laser Sintering (SLS)

SLS printing is a powder-based 3D model manufacturing method. This kind of printer utilises a high-power laser to sinter polymer powders to produce a 3D object [137]. At the beginning of the procedure, a layer of polymer powder is spread uniformly onto a platform by a roller. Subsequently, the powder is heated to a temperature just below the powder's melting point. Afterwards, a laser beam is selectively scanned over the polymer powder, increasing the local temperature to equal the powder's melting point to fuse the powder particles. After the completion of this process, another layer of powder is supplied, levelled, and sintered in the desired area. Thereafter, the above-mentioned steps are repeated until the 3D model is attained. The remaining powdered materials can be recycled **(Figure 1.9B)** [124]. Several materials can be employed by an SLS 3D printer, such as polyvinylchloride, polycarbonate, acrylonitrile butadiene styrene (ABS), nylon, metal, polyester and ceramic powder [124], [138], [139]. This kind of 3D printer has been used in tissue engineering [140] and drug delivery devices [141].

1.4.1.3 Powder Bed Inkjet (IJ) and Inkjet 3D Printing

Traditional desktop printers apply two concepts: drop-on-demand (DOD) and continuous jet (CJ) printing. In both printing types, the liquid passes through a nozzle or orifice [124]. In CJ printing, the fluid is pushed through the nozzle continuously. Subsequently, the jet breaks into a stream of droplets. In DOD 3D printing, microdroplets are dispensed at the desired sites layer by layer to create the 3D object [123]. Further, an additional class of IJ printer utilises a powder bed. In this printer, layers of solid particles are bonded together by a printed liquid material for the production of a 3D object. Specifically, a layer of powder is spread with the help of a roller uniformly on the top of a supported stage. Subsequently, droplets of liquid binding materials are printed from the head of an IJ printer onto the distributed powder at the required area of solidification. After that, the printing stage lowers, and another layer is first spread evenly and then selectively combined with the printing binding material. The previous steps are repeated until a 3D model is produced **(Figure 1.9 C)** [124]. A 3D powder-based bed IJ printed model is usually heat-treated to increase the binding of the particles in the required regions. Unbound powder serves as a supporting material during the printing process and is removed after its completion. Various types of powders can be utilised, such as a polymer, glass, or ceramic [124], [142]. This kind of 3D printer has been used in research labs to manufacture oral dosage forms (tablets) [143].

1.4.1.4 Fused Deposition Modelling (FDM)

At present, the FDM printer is one of the most commonly used manufacturing technologies for rapid prototyping. FDM printers manufacture a 3D object by extruding thermoplastic materials and depositing the semi-molten materials onto a stage layer by layer [119] **(Figure 1.9 D)**. This kind of 3D printer has been used in medicine; for example, surgeons print 3D anatomical guidance and organs to deal with the challenges experienced during the operation [144]. Also, this method has been used in dentistry [145], the creation of customised prosthetic

limbs, the automotive industry, and drug delivery [146]. FDM technique and materials are described briefly in more detail in **chapter 2, sections 2.1 and 2.4.1.**

1.4.1.5 Semisolid extrusion

This kind of 3D printer is a syringe-like system, and it extrudes gels or pastes above the building plate a layer by layer **(Figure 1.9 E)**. The extruded materials solidify after extrusion by either cooling or evaporation of the solvent. This technology has been used to formulate oral dosage forms [147].

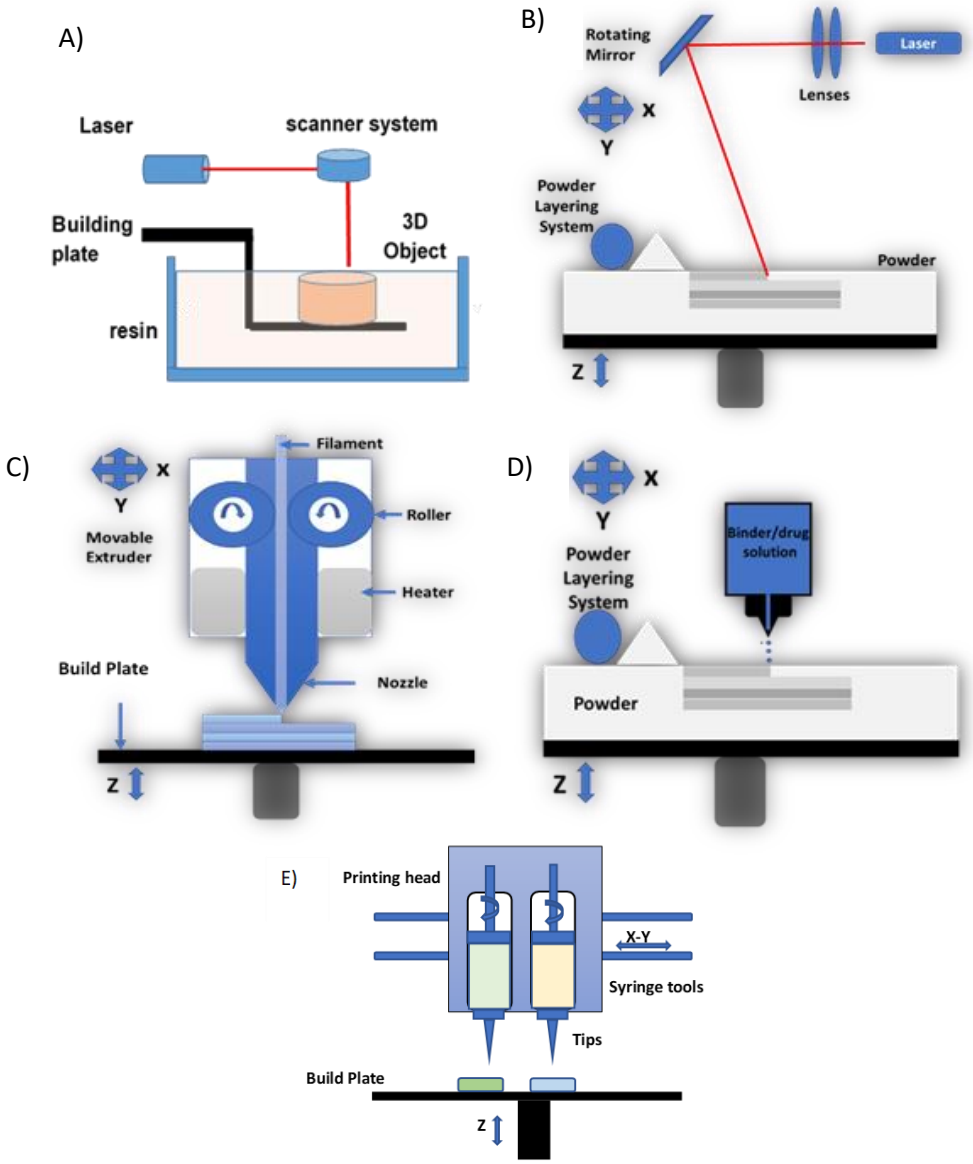

Figure 1.9 Schematic diagram of different kinds of 3D printers, including A) SLA, B) SLS, C) FDM, D) inkjet, and E) semisolid extrusion printer. These schematic diagrams are adapted from [134], [147], [148].

Table 1.6 Summary of 3D and AM printing techniques [134], [149]–[173].

Technique	Working Principle	Substrate	Advantages	Limitations
SLA	Laser scanning and UV induced curing	Liquid (photopolymer)	• High printing resolution • Suitable for thermolabile APIs	• Material limitation, • Cytotoxicity • High cost
SLS	Laser scanning and heat-induced sintering	Solid particles (metal, polymer or plastic)	• Good strength • Easy removal of support powder • Extensive selection of starting materials • Increased porosity with matrix	• High cost • Powdery surface • Wastage of powder • Limited speed for laser sintering • High energy may degrade starting materials
FDM	Extrusion and deposition	Thread (thermoplastic, e.g. PLA, PVA, PCL, ABS)	• Low-cost printing and wide availability • Multi-material capability • Good strength • High drug uniformity • No post-printing process is required	• High temperature may degrade the API and excipients • Nozzle Clogging • Requires preparing filament before printing • Limited to thermoplastic polymers
IJ Powder-Based	DOD binder Printing	Solid particles (sand, polymer, plaster)	• Low cost • Multi-material capability • Easy removal of support powder • A more porous matrix system as compared to conventional tabletting. • Selection of materials	• Clogging of binder jet • Binder contamination • Requires post-printing drying • Requires unique powder facility
Semisolid Extrusion	Pressurized syringe extrusion, and heat or UV-assisted curing	Semisolid, softened (gel or paste)	• High printing resolution • Soft materials capability	• Low mechanical strength • Slow

1.4.2 Advantages and Limitations of 3D Printing Technologies

3D printing technologies offer a variety of benefits compared to other manufacturing techniques prevalent in the medical field. 3D printing is essential to the development of personalised devices and equipment. For instance, it can be utilised to manufacture customised medicines, prosthetics and hearing aids [117], [171]. Furthermore, using 3D printing technologies could revolutionise the way of making oral tablet dosage form, moving away from a ‘one-size-fits-all’ approach to permit the

personalization of medicines. Oral tablets can be fabricated in different strengths to ensure a safe and therapeutic effect for the majority of the population [174] as one dose might not fit all, due to patients' disease states, genetic profile, and other factors, including age [175], weight [176], and gender [177].

Personalized medicine commonly refers to those treatments given to a patient based on their characteristics, requirements, and preferences during the treatment process. 3D printing technology can formulate a tablet dosage form in small batches directly at the point of care. The tablet can be designed to comprise API combinations, with an appropriate dose for each API, formulation type and/ or any addition to suit the patient [178]. For instance, dosing requirements for paediatric cases or adults are different due to the differences in their physical characteristics, such as age and body weight, and pharmacokinetic factors, such as organ function and metabolic capacity, and drug clearance [179], [180]. Also, some drugs with a narrow therapeutic index [174], need exact dosing to maintain treatment efficacy and patient safety. This can be problematic for tablets with a single strength or formulation type. For example, the patient or caregiver can split the tablets or physicians can prepare formulations by crushing licensed tablets or by opening capsules and using their contents to achieve the required dose. However, this may lead to inaccurate dosing as well as dose variations from time to time [181], [182] and may produce dose dumping for enteric-coated tablets, which could have severe therapeutic consequences [183], [184].

3D printing technology can be utilised to manufacture a tablet containing an exact amount of APIs. This could simplify drug administration and decrease the risk of dose variation and medication errors. Furthermore, 3D printing technology can also be used to simplify medication administration, especially for drugs that have rapid dose changes on initiation or for reducing regimens. For instance, 3D printing has been used to dispense exact doses of prednisolone [185]. Moreover, 3D

printing can allow multiple APIs to be combined within a single tablet to produce personalize ‘polypills’, which can improve medication adherence and decrease administration errors. Several studies have used 3D printing technology to fabricate polypills [186], [187].

3D printing technology enables drug products to be adapted for on-demand and prescription-specific production. The ability of this technology to provide on-the-spot medication manufacture will have major effects in emergency drugs and for APIs that have a short half-life. Additionally, this technology can be utilised for patients on an individualised basis. The modification of drug dosing and combinations for each patient can be performed using 3D printing technology. The conventional APIs fabricating process cannot meet these requirements as they focus on large-scale production batches [188]. The conventional methods have a little flexibility in the fabrication process and need many steps, making it difficult to adapt to small batches. On the other hand, 3D printing technology has been used to fabricate drug products and allows these to be changed between prescriptions [124]. 3D printing also offers the flexibility to design and manufacture 3D objects with complex geometries and architecture using a variety of materials. For example, it can be utilised for the fabrication of irregular complex shapes, such as titanium orthopaedic and dental implants [124].

Although 3D printing technology provides a variety of advantages, it also entails certain disadvantages.

The main constraints of this technology are the manufacturing cost involved in fabricating large quantities of dosage forms in comparison to traditional methods. However, the 3D printing technique is an economical option for small-scale production [118]. An additional limitation of this technology comprises the regulatory concerns this process entails. These concerns may delay the widespread medical application of 3D printing for large-scale production [190]. The issues of safety and security are other limitations of this technology as it could be utilised to counterfeit low standard medications or medical devices [116]. Furthermore, 3D

printing also raises patent and copyright concerns. Finally, another limitation lies in the fact that there is no single universal 3D printer that can accommodate all materials and applications [191].

1.4.3 Applications of 3D Printing Techniques

3D printing techniques offer a broad range of applications. These techniques have been utilised across various fields, including the aerospace, automotive, jewellery, art, fashion, architecture, food, and medical **(Figure 1.10)** [192].

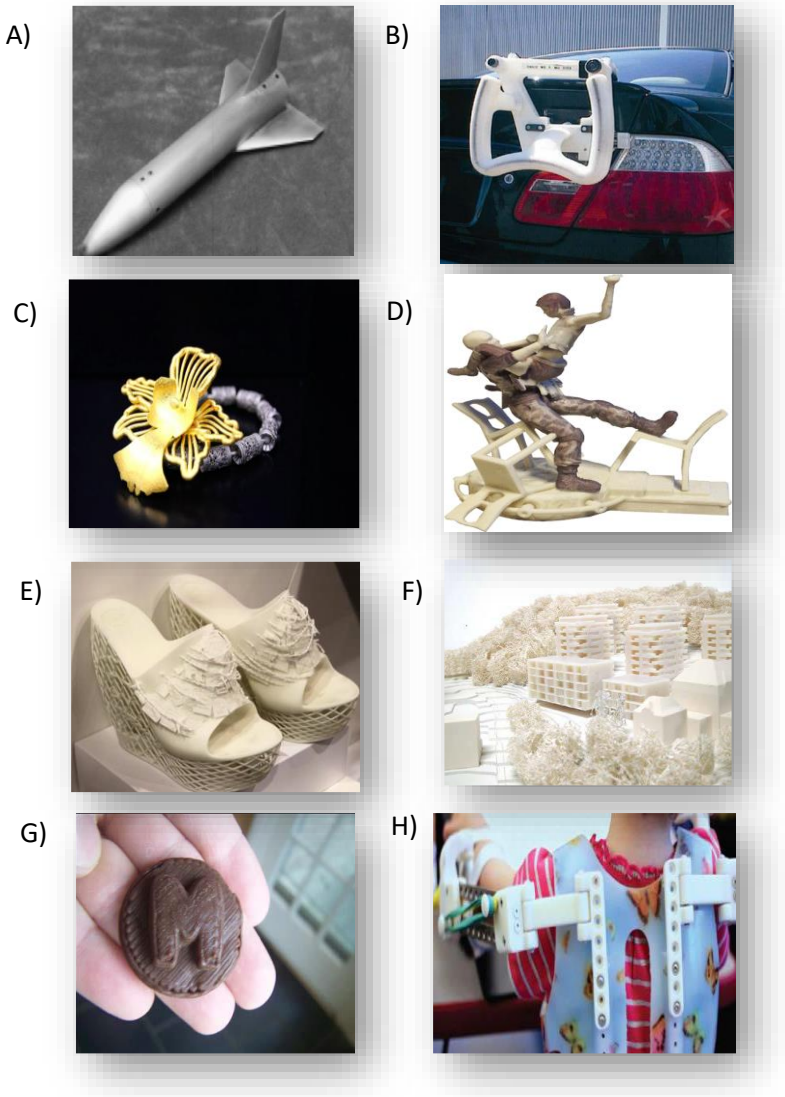

Figure 1.10 Different fields that utilise 3D printing technology: A) aerospace [193], B) automotive [194], C) jewellery [195], D) art [115], E) fashion [196], F) architecture [194], G) food (chocolate bar) [197], and H) medical [194].

1.4.3.1 Medical Applications of 3D Printing Technologies

3D printing has been applied in the field of medicine since the early 2000s when it was first employed to produce custom prosthetics and dental implants [119], [198]. Medical applications of 3D printing are growing rapidly. Recently, 3D printing has been utilised across a variety of applications, including bones, cell cultures, stem cells, ears, exoskeletons, vascular networks, blood vessel, tissue, organs, and windpipes, as well as novel dosage forms and drug delivery devices [115], [117], [191]. The current medical use of this technology is categorised into tissue and organ fabrication; pharmaceutical research concerning drug delivery, discovery and dosage forms; and the creation of custom-built prosthetics, implants, and anatomical models. Further, 3D printing has been used to fabricate a variety of IDDS, including cardiovascular stents, orthopaedic, dental, ocular and transdermal implants **(Figure 1.11)** [199].

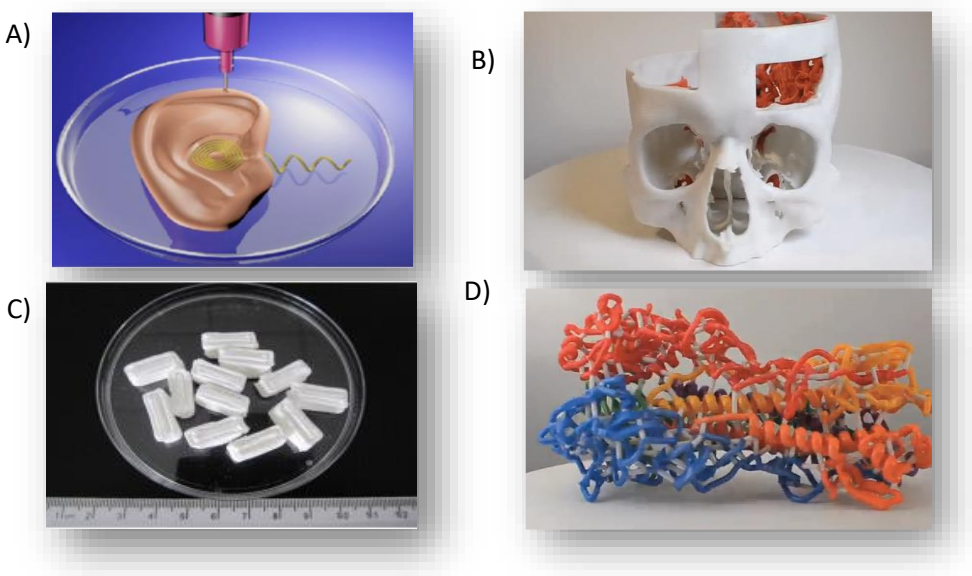

Figure 1.11 Various applications of 3D printing in medicine. 3D printing of A) an organ (bionic ear) [149], B) anatomical model for surgical preparation [200], C) pharmaceutical dosage forms (bilayer tablet) [147], and D) disease modelling (biological and biochemical structure of an influenza hemagglutinin primer) [200].

1.5 3D Printing Hearing Aids

3D printing technology has had a big influence on the manufacture of hearing aid devices. Nowadays, around 99% of hearing aids that fit in the human ear are custom-made using 3D printing techniques [117]. A hearing aid is defined as a small electronic device that can be worn in or behind the human ear. This electronic device makes some sounds louder so that a person who suffers from hearing loss can listen, communicate, and participate more fully in daily activities. The major components of a hearing aid device include an electronic signal processor, a microphone, a battery and a loudspeaker. These components are placed inside the hearing aid shell [201]. Digital hearing aids can be custom-made according to the individual's hearing needs. Moreover, they provide frequency-specific amplification at levels that enable improved speech recognition whilst amplifying background noise to a lesser extent [201]. The use of 3D printing technology can produce custom-shaped devices cost-effectively and efficiently. Many companies are using 3D printing to produce customizable hearing aids, such as CAMISHA, which makes the world's smallest hearing aids, a Danish company, and Widex [117].

Although hearing aid devices are beneficial for hearing impaired patients, they can cause OE disease due to the following reasons. They may produce irritations within the auditory canal because of allergic contact dermatitis from ear mould materials [202], [203]. Moreover, bacterial or fungal infection can produce OE due to accumulations of these microorganisms on hearing aid shells [204], [205]. Some studies have reported an accumulation of a wide range of fungi and bacterial contamination on the hearing aid devices of patients [204]–[207]. Furthermore, the insertion of hearing aid devices into the ear canal can produce wax impaction and occlusion of the ear canal, increasing the tendency for moisture accumulation and thus putting the hearing aid device utiliser at a considerable risk of OE [208]. It has been reported in the literature that when hearing aid devices obstruct the ear canal, the ear canal becomes darker, warmer and more moist than normal, which

affects the canal pH and the area becomes conducive for microbial proliferation [204], [206], [209], [210].

Some hearing aid users suffering from OE become dissatisfied with using their devices, while others stop using the hearing devices due to the problems they experience, such as irritation, otorrhea and itching [208]. Consequently, some ear specialists prefer fitting the hearing aid devices via alternatives routes that are more invasive, such as ME implants [211]–[213].

OE disease needs to be treated early to avoid any complications that may affect the patient's life. This disease affects the outer ear part, and it has a high incidence rate in children and adults [1]. The effective management of OE disease is usually managed using locally acidifying solutions, local analgesics and/or antibiotic ear drops alone or in combination with steroid drugs [214]. Topical ear drops are preferred for many reasons, including the fact that they can be delivered directly to the site of action with a higher local drug concentration, the ability to bypass the BLB barrier, and reduced systemic side effects. However, OE patients need to take ear drops 3-5 times daily for seven days [1], and the patients need to lie on their sides with the affected ear up for their treatment to be administered. Also, they need someone else to provide the medication while they are lying down. Studies have shown that around 40% of OE patients who self-medicate take their otic drops medications appropriately, but the effectiveness of the treatment increases when another person applies the drops for them [215], [216].

In this situation, there is a need for a one-time application of a constant drug release system, which would decrease the requirement for multiple daily drug dosing and improve patient compliance by maintaining their hearing during the treatment regimen. The current technologies do not provide this kind of drug-releasing systems. Therefore, we are looking to overcome the previous challenges by developing a drug-release system that can deliver otic medication locally without affecting the patent’s

hearing ability during the medication regimen. This might improve patient compliance and treatment outcomes.

1.6 Aims and Objectives

The general aim of this thesis is to develop a personalised in-ear prototype device. This device can be incorporated with a gelling system and an anti-inflammatory drug for sustained release after insertion into an AOE patient's external canal. The compressed tablet acts as a reservoir, and the gelling system acts to deliver the drug to the outside of the printed device at a rate determined by the diffusivity of the drug in the gelling system and the solubility of the drug in the hydrogel. In the longer term, it may be possible to couple the ear prototype device with hearing aid components to obtain personalised drug-eluting hearing aids.

In this dissertation, the following objectives will be clarified.

- Firstly, to fabricate 3D printed in-ear prototype devices with different geometries (realistic and simple geometries) using different 3D printing technologies. Moreover, to utilise various materials with solid and rubbery characteristics to print the designed devices. Furthermore, to characterise the manufactured ear prototype devices using SEM. In addition, to determine the dimensions of the printed ear prototype models using a digital calliper. Also, to develop a realistic ear prototype device that can incorporate a gelling system and a drug tablet and contains pores to facilitate drug release into the canal area.
- Secondly, to formulate various concentrations of a thermogelling system (HPMC hydrogel) and investigate the rheological behaviours to determine the concentration that provides elastic-like behaviour. Moreover, to investigate the flows of the prepared concentrations through one of the 3D printed ear prototype devices containing different pore numbers and locations to select one of the concentrations that can be incorporated within the developed prototype ear device.

- Thirdly, to fabricate two different tablets that contain DXM using a single hydraulic compression press machine. Moreover, to investigate the diffusion of DXM through one of the selected hydrogelic systems using Raman spectroscopic instrument. Furthermore, to study the *in vitro* release of DXM through the developed ear prototype device using one of the United States pharmacopoeia USA apparatuses (basket). This can be attained by incorporating the developed ear prototype device with the selected hydrogel system and the fabricated tablets. Also, to investigate the DXM release with or without covering the device with a synthetic Strat-m membrane.

Figure 1.12 showed a schematic illustration of A) a model of the designed ear prototype device that can be loaded with a drug tablet and a gelling system and B) the model system after insertion into an external auditory canal area.

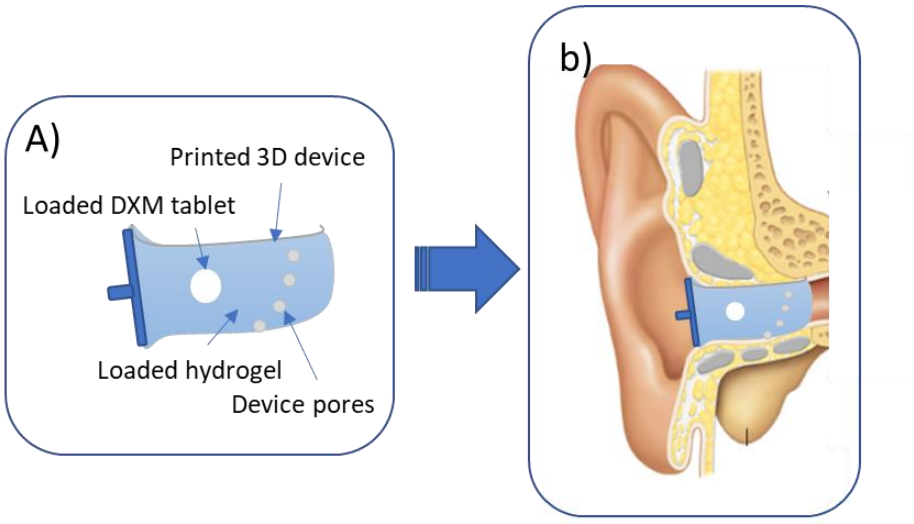

Figure 1.12 Schematic illustration of A) a designed ear prototype device with a realistic geometry that contains a gelling system and a drug tablet, and B) the designed drug delivery system after insertion in an external auditory canal area.

The detailed aims of each experimental chapter are specified at the start of each chapter. Moreover, the experimental results, limitations and future work are debated throughout this thesis.

Chapter 2: Materials and Experimental Techniques

This chapter aims to describe all the materials and experimental techniques used in this research study to achieve its goals. Moreover, the reasons for selecting the research elements and methods are briefly described in this chapter. The full details of each experiment are discussed in the experimental sections of **chapters 3, 4, and 5.**

2.1 Materials

2.1.1 Materials Utilised for 3D Printing

Poly(lactic acid) (PLA) (Black (UM 9014A), silver metallic (00216075), blue and red colours, melting point (MP) 145-160℃, and 2.85 mm diameter), polyvinyl alcohol (PVA) (Natural colour, 9732, MP 163℃, and 2.85 mm diameter) and thermoplastic polyurethane (TPU) commercial (Silver colour, MP 220℃, and 2.85 mm in diameter) filaments were purchased from Ultimaker, Lancashire, UK. Flexible resin (a mixture of methacrylic acid esters, proprietary pigment, additive package, and photoinitiators) and tough resin (a mixture of methacrylic and acrylic acid esters, and photoinitiators) were obtained from Formlabs Inc., USA.

2.1.2 Materials Utilised for Hydrogel Preparation and Tablet Fabrication

Hydroxypropyl Methylcellulose (HPMC) ($C_{56}H_{108}O_{30}$) (9040ST01, 90SH-4000SR, Meltolose®) was attained from Shin-Etsu Chemical Co, Tokyo, Japan. DXM/cyclodextrin complex (SLBW5982) and methyl-β-cyclodextrin ($C_{54}H_{94}O_{35}$) (A0403692) were purchased by Sigma Aldrich (Gillingham, UK). Alpha-D-lactose ($C_{12}H_{22}O_{11}$) and DXM drug (10210224) were obtained from Fisher Scientific Co., New Jersey, USA.

2.1.3 Materials Utilised for Buffer Preparation and Release Study Testing

Phosphate buffered saline (PBS) (RNBH4650), disodium hydrogen phosphate (Na_2HPO_4) (BCBM0149V), sodium chloride (NaCl) (1557310), Strat-M™ membrane (47 mm Disks, SKB04760) were

provided by Sigma Aldrich, Gillingham, UK. Potassium chloride (KCl) (CAS No. 7447-40-7) was attained from Riedel-de Haen, Seelze, Germany. Hydrochloric acid (HCl) (1540376) was supplied from Fisher Scientific, Loughborough, UK. Potassium dihydrogen phosphate (KH_2PO_4) (A0354394) was bought from Acros Organics, Geel, Belgium.

2.2 Drug Used in This Research Project:

2.2.1 Dexamethasone (DXM)

DXM is a synthetic derivative of the glucocorticoid hydrocortisone anti-inflammatory drug. It has a long history of treatment for humans, and it is commonly used to minimise inflammation in the central nervous system [217] [218]. This drug has an empirical formula of $C_{22}H_{29}FO_5$, and it has a molecular weight of 392.461 g/mol. It is identified chemically as 9-fluoro-11(beta), 17, 21-trihydroxy-16(alpha)-methylpregna-1, 4-diene-3, 20 dione. Furthermore, DXM has an MP range of 262-264^{o}C [219]. The chemical structure of DXM is presented in **Figure 2.1** [220]. DXM is available as an odourless, white, crystalline powder. This drug powder is stable in air, and it is practically insoluble in water. Moreover, it is slightly soluble in methyl chloride, and sparingly soluble in ethanol [220], [221].

DXM was approved by the U.S. FDA to usage topically with the antibiotic ciprofloxacin, which is available commercially as Ciprodex®, in the ME to treat acute otitis media (AOM) in paediatric cases with tympanostomy tube and external ear to treat AOE [47], [48]. Furthermore, DXM is commonly used in the treatment of different ophthalmic conditions via topical preparations [222]. DXM supports the decrease in itching, inflammation, and squamation [46]. In this project, this drug was selected as a model of an anti-inflammatory drug to relieve fast the inflammation that occurs in the auditory canal in people suffering from AOE.

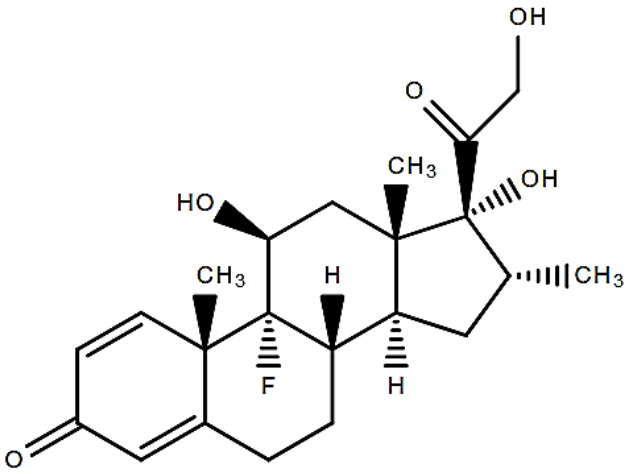

Figure 2.1 Chemical structure of DXM.

2.3 Polymers Used in This Research Project

2.3.1 Poly(lactic acid) PLA

PLA is a biodegradable, biocompatible, high-strength, thermoplastic, and biosafe polymer. This polymer belongs to the family of aliphatic polyesters, and it is derived from renewable resources, such as corn, chips or starch [223], making it inexpensive and obtainable for biomedical applications [224], [225]. The PLA was approved by the FDA for use in direct contact with biological fluids because it is safe. This polymer can be processed by using different techniques due to its thermal processability, including film casting, extrusion, blow moulding or fibre spinning methods [224].

The PLA is available as a white powder [226]. The melting temperature of PLA polymer ranges from 150 to 160℃, which makes energy saving during the manufacturing process [164], [227]. PLA has a low glass transition temperature (T_g) of 60-65℃ [228]. PLA has two stereoisomers, including D and L of lactic acid [226]. PLA can be made using both types of monomers D and L. The PLA prepared from the D monomer is crystalline, while the PLA from the L monomer is semi-crystalline [226]. Furthermore, PLA made of either can be used to obtain an amorphous

polymer. PLA is soluble in different organic solvents, such as chloroform, acetonitrile, dioxane, benzene and tetrahydrofuran. This polymer is insoluble in ethanol, methanol, and aliphatic hydrocarbons [226]. PLA has been used in the medical field, such as for implant devices and tissue scaffolding [207], [229], [230]. Therefore, this thermoplastic polymer was selected for this thesis.

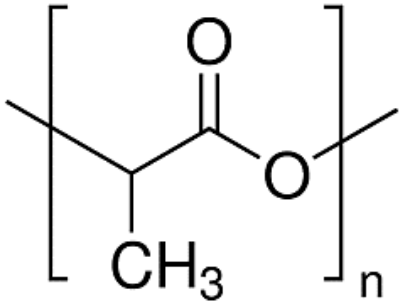

Figure 2.2 Chemical structure of PLA [231].

2.3.2 Cyclodextrins (CDs)

CDs are cyclic oligosaccharides, which are composed of D glucopyranoside units (glucose). These are unit-linked by α-1.4 glycosidic bonds. CDs are obtained from biotechnological processes involving the enzymatic degradation of natural corn starch. CD molecules have a truncated cone shape with a central lipophilic cavity due to the chair conformation of the glucopyranose units **(Figure 2.3).** The outer surface of a CD molecule is hydrophilic due to the presence of hydroxyl groups [232]. The lipophilic character of the central cavity of CD molecules is due to the presence of the skeletal carbon and ethereal oxygens of the glucose residues. CDs molecules structure gives them the ability to form water-soluble inclusion complexes with the hydrophobic molecules of APIs that have a suitable size.

The most common natural CDs, α-CD, β-CD, and γ-CD, have six, seven and eight glucopyranose units, respectively [233]. **Figure 2.2** illustrates the structure of the β-CD molecule, which is the most frequent type of natural CDs used in the pharmaceutical field [234]. The β-CD molecule

cavity size is suitable for forming inclusion complexes with various lipophilic API molecules [235]. The formed complexes produce changes in the physicochemical properties of the API drug molecule, including increased drug solubility, better stability, and an enhanced dissolution rate [236]. Several chemically modified derivatives of β-CDs are available commercially. They are obtained by replacing some of the hydroxyl groups of the β-CDs that are available on the outer surface with other functional groups, including methyl, hydroxypropyl, and sulfobutyl ether. Thus, the results of these modifications improve the aqueous solubility [237]. Methyl-β-CD is used with DXM to enhance solubility, stability, and facilitate the compression in forming a tablet. This tablet is added to one of the formulated HPMC hydrogel concentrations to investigate the diffusion and the releases of DXM **(see chapter 5)**.

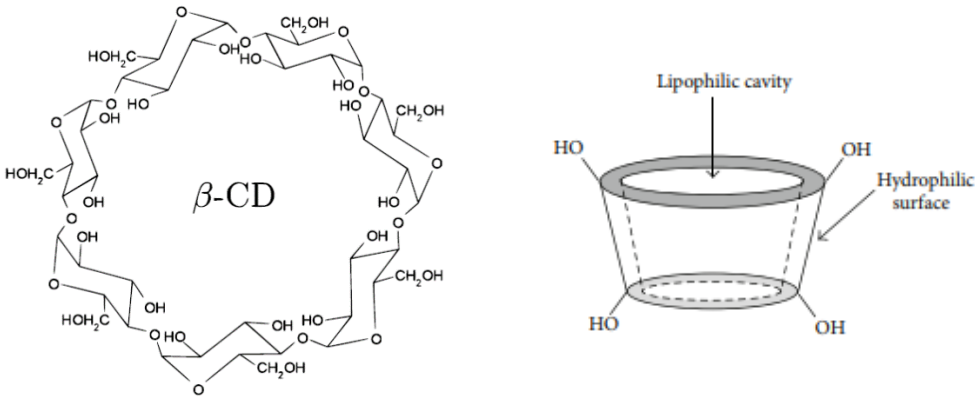

Figure 2.3 Left: Chemical structure of β-cyclodextrin [238]; right: its toroidal structure [232].

2.3.3 Hydroxypropyl Methylcellulose (HPMC)

HPMC, also called Hypromellose, is widely in used cellulose ether in the development of hydrophilic matrices. This polymer facilitates API release in a controlled way. It effectively raises the API release duration of action in order to prolong its therapeutic effect. HPMC is a water-soluble (hydrophilic), biocompatible, biodegradable polymer. Moreover, it is available as white to slightly off white, odourless, and tasteless powder. HPMC polymer swells and forms a gel when it hydrates. The formed hydrogel system is stable over the pH range of 3-11 [239]–[242]. In

addition, the gelation temperature for this polymer is 75-90℃. The HPMC chains are hydrated at lower temperatures; however, they start dehydrating as the temperature rises [243]. HPMC is widely utilised in the food industry as an emulsifier, stabiliser, thickener, surfactant, binder, film former, and suspension agent. Furthermore, it also used as a tablet binder and tablet matrix for extended drug release [244]. The USP differentiates four types of HPMC according to their percentage (%) methoxyl and % hydroxypropyl substitution, namely HPMC 1828, 2208, 2906 and 2910. The HPMC utilised in this thesis is HPMC 2208 (90SH4000SR) manufactured by the Shin-Etsu company under the name Metlose®. This polymer was selected to form the hydrogel system. We aim to incorporate one of the prepared HPMC hydrogel concentrations within the manufactured FDM device that contains pores. The selected hydrogel needs to stay for an extended period (7 days) in order to deliver an anti-inflammatory drug (DXM) locally at the ear canal wall to treat patients suffering from AOE.

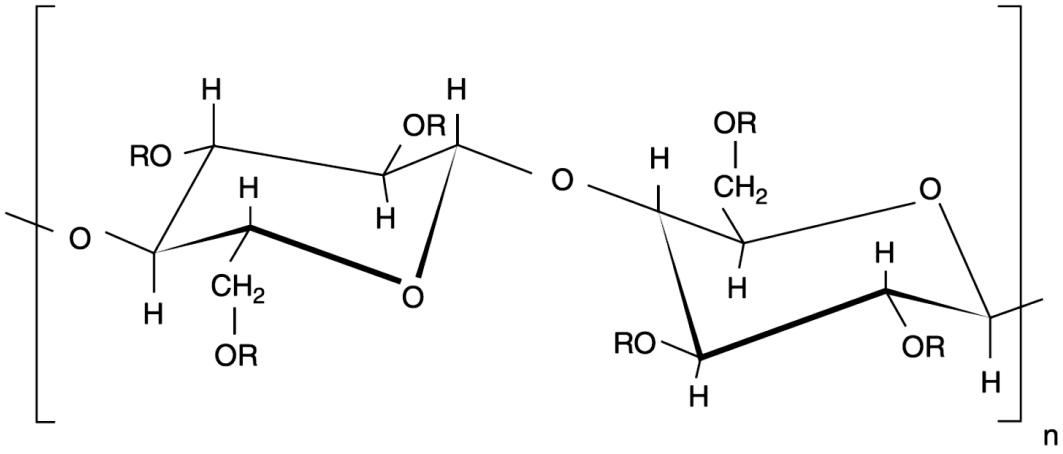

Figure 2.4 The chemical structure of HPMC. The substituent R represents either a CH_3, or a $CH_2CH(CH_3)OH$ group, or a hydrogen atom [245].

2.4 Instrumentations:

Equipment	Manufacturers	Specifications
Differential Scanning Calorimeter	Perkin Elmer, USA	DSC 8000
Optical Microscope	Lecia, Germany Prior, UK	MZ16 PX023POL
Anton Paar Rheometer	Anton Paar, Germany	MCR 302
SEM	Hitachi, Japan	Hitachi TM3030
Vacuum Sputter Coater Chamber	Leica	EM SCD005
FDM 3D Printer	Ultimaker BN, Geldermalsen, Netherlands	Ultimaker^{2+}
SLA 3D Printer	Formlabs Inc., Somerville, USA	Formlabs 2
Ultramicrotome	RMC Inc., Tucson, AZ, USA	PowerTome PC
Manual Hydraulic Single Press	Specac, Orpington, UK	Atlas™
Uv-Visible Spectrophotometer	Varian Australia Pty Ltd., Mulgrave, Australia	Cary, 50 Bio
Electronic Calliper	Hardened model, UK	Stainless®
Incubator Oven	Thermo Scientific, USA	Heratherm
Dissolution Apparatus	Copley Scientific Limited, UK	Dis8000
Raman Instrument	Horiba-Jobin-Yvon Ltd., Middlesex, UK	Confocal Horiba

2.5 Software

Equipment	Softwares
Differential Scanning Calorimeter	Trios v4.4.0
Optical Microscope	Linksys 32 v2.4.3
Anton Paar Rheometer	Rheoplus
FDM 3D Printer	Cura 3.6
SLA 3D Printer	PreForm 2.19.2
Raman Confocal Instrument	LabSpec 6

2.6 Methods

2.6.1 Designing of the 3D Object

In this thesis, online software (Tinkercad) was utilised to design and modify different prototype ear devices **(Figure 2.5)**. Various other software are available for creating 3D objects, including materialise magic, SketchUp, selfCAD, and free CAD. The CAD software enables the creation, optimisation, modification and analysis of designs (3D and 2D) in the form of an electronic file, which is in the .stl format. This file format is suitable for the 3D printing process [123].

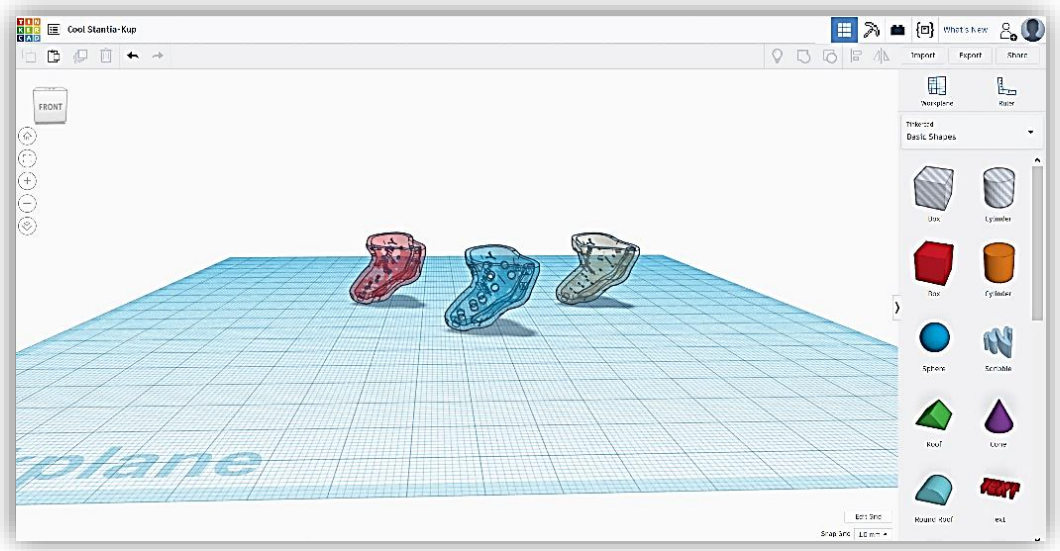

Figure 2.5 View of the interface of the Tinkercad online CAD software.

2.6.2 3D Printing Technique Used in This Thesis

2.6.2.1 Fused Deposition Modelling (FDM)

The FDM printer technology is a nozzle-based deposition system. This system allows the direct printing of a 3D object designed in CAD software to create a 3D shape layer by layer. FDM is widely utilised in drug delivery research, and it has several advantages, including the possibility to fabricate patient-tailored tablets [246], [247] or drug capsules with high accuracy and the production of many geometric devices with controlled and immediate drug release properties [248].

FDM printers manufacture a 3D object by extruding thermoplastic materials and depositing semi-molten materials onto a build stage layer by layer [119]. The loaded filament is heated at the nozzle head in order to reach the filament semi-molten state. After that, the thread is extruded onto the build plate or on the top of previously printed layers **(Figure 2.6)**. The feature (thermoplasticity) of the utilised polymers is an essential property for this method as it allows the threads to fuse during the printing process. After that, it enables the fused layers to solidify at room temperature after printing process [249]. Various thermoplastic polymers are utilised in the FDM printing process, such as PVA [246], PLA [227], polycaprolactone (PCL) [250] and acrylonitrile butadiene styrene (ABS) [251].

The Ultimaker^{2+} printer is a commercial FDM 3D printer that can manufacture 3D substances. It is used in this thesis **(Figure 2.7)** to fabricate different prototype ear medical devices. This printer is mainly composed of a movable printing head, printing nozzle, loading tube, two rotator rollers, building plate, push/rotate button, feeder, USB socket, SD card slot, printing head cable, display screen, and filament holder.

Different printing parameters need to be adjusted to obtain a printed object with good morphological resolution, including infill%, printing speed, layer height, wall thickness, top/bottom thickness, printing temperature, build plate adhesion, generate support layers, and build plate temperature. Different nozzle sizes come with the Ultimaker^{2+} FDM 3D printer, including those 0.8, 0.6, 0.4, and 0.25 mm in diameter.

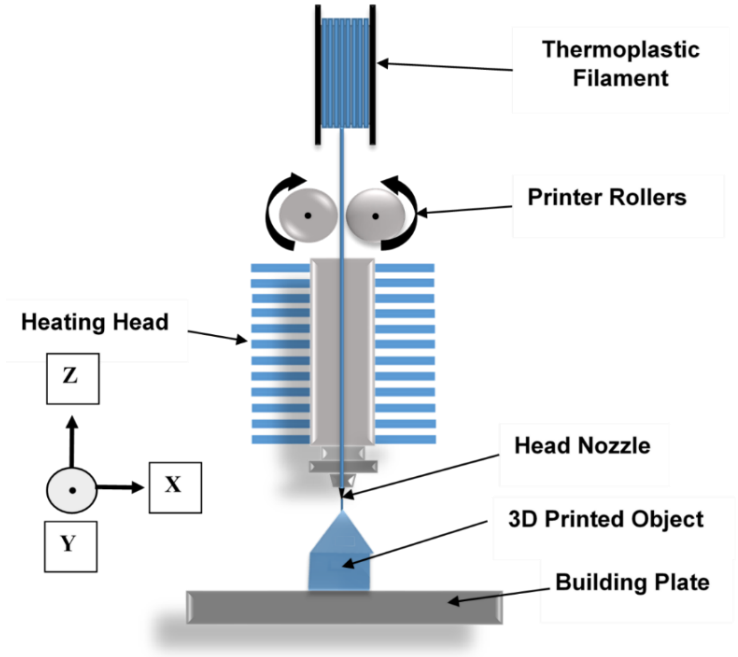

Figure 2.6 Schematic illustration of the FDM loading filament and the fabrication process of a 3D object.

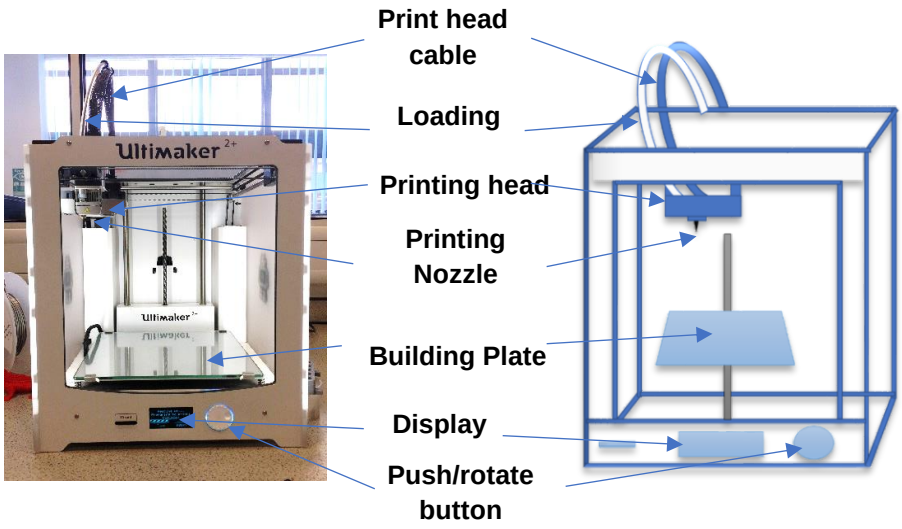

Figure 2.7 Photograph (left) and schematic diagram (right) of the Ultimaker^{2+} 3D FDM printer. The Ultimaker^{2+} has the dimensions 357 x 342 x 388 mm.

2.6.2.2 Stereolithography (SLA)

SLA is an AM technique that is widely used commercially. This type of printer was developed in 1986 [252]. It uses either a UV light source or an electron beam to produce a chain reaction on the loaded resin layers or monomer solution. The method uses different monomers, such as acrylic, which can be activated by a UV source and converted to polymer chains. After the polymerisation process, a resin layer is solidified to hold an additional layer, and the unreacted resin is removed after the printing finish. There is a post-treatment process, including heating or photo-curing, that can be used for some 3D printed parts to achieve the desired mechanical performance [249].

Formlabs 2 (Formlabs Inc., Somerville, USA) produced the commercial SLA 3D printers utilised in this research to manufacture 3D objects, here specifically the fabrication of different prototype ear objects **(Figure 2.8)**. This printer consists of a movable build plate, resin tank, resin cartilage, resin wiper, control button, curing UV laser, and display screen. Different printing parameters need to be adjusted in order to obtain a printed object with good morphological resolution, including layer thickness.

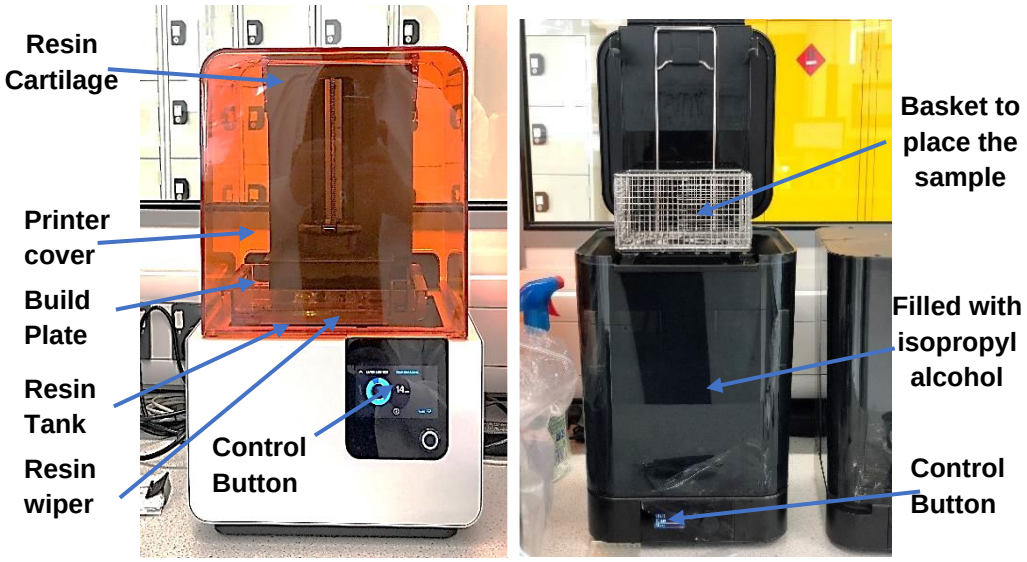

Figure 2.8 Schematic illustration of an SLA Formlabs^{2+} Printer (left) and form wash (right). The Formlabs 2 SLA 3D printer has the dimensions 350 x 330 x 520 mm, and the form wash has the dimensions 262 x 293 x 340 mm.

2.6.3 Characterisation of the Printed Prototype Devices and Filaments

2.6.3.1 Differential Scanning Calorimetry (DSC)

DSC is a thermal analytical technique that was developed in the early 1960s [253]. It measures the temperatures and heat flows related to transitions, examining samples as a function of temperature and time in a controlled temperature environment [254]. DSC is a useful technique because it gives detailed information on a substance in terms of its energetic and physical properties. It provides quantitative information about endothermic (acquired energy), exothermic (released energy), and heat capacity changes as a function of temperature and time (for example purity, melting, and glass transition temperature) [255].

This technique mainly uses a two-pan configuration (reference and sample pan). The sample pan generally comprises a known mass of material that needs to be examined, and the reference includes an empty pan. The difference in the heat flow rate between both pans is measured as they are heated or cooled in a controlled DSC temperature environment. The difference in temperature between both pans changes each time, and the sample goes through different transitions, including exothermic or endothermic transition [254].

DSC is commonly used in the pharmaceutical industry to characterise the thermal behaviours of a component, such as the melting temperature (T_m), glass transition temperature (T_g), crystallisation, dehydration, and sublimation [255]. In this thesis, a differential scanning calorimeter (Perkin Elmer DSC 8000, Waltham, MA, USA) is used to conduct the thermal analysis for the 3D printing FDM filaments (PLA) to determine the T_m and T_g temperatures of the used thread **(Figure 2.9)**.

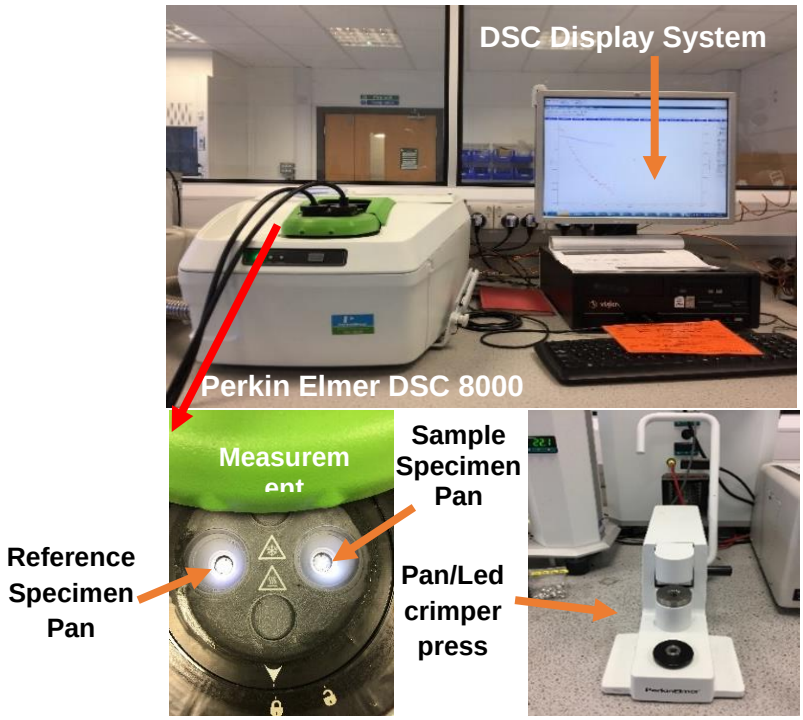

Figure 2.9 Photographs of a Perkin Elmer DSC 8000 and Perkin Elmer crimper press.

2.6.3.2 Scanning Electron Microscope (SEM)

An SEM is a type of electron microscope. It scans the surface of a prepared sample with a focused beam of electrons to form an image based on the interaction between the electron beam and the specimen. The detector measures the intensities of several areas of interactions. The most commonly used detectors are the secondary and backscattered electron detectors [256]. **Figure 2.11** shows a schematic diagram of the major components of an SEM, which are the electron source, anode, magnetic lens, scanning coil, secondary scatter electron detector, backscatter electron detector, TV scanner, and specimen stage.

An SEM gives point-by-point information about the tested specimen surface with an electron beam. This beam is generated by an electron gun, and it goes down the SEM column and onto a series of electromagnetic lenses, which focus the beam onto the specimen

surface. The SEM operator can control the beam magnifications and determine the area to be scanned. Specimens need some preparation before scanning, and they are subsequently placed in a vacuum chamber. After the focused electrons contact the set sample, energetic electrons are released from the sample surface. Different detectors attract various types of scattered electrons, such as secondary electrons, backscattered electrons and x-rays. The SEM provides 3D images in black and white [256]. In this thesis, an SEM (TM3030, Hitachi, Tokyo, Japan) was utilised to characterise the structure of some 3D printed objects **(Figure 2.10 bottom)**. All objects were coated with gold using a vacuum sputter coater chamber, namely a Leica EM SCD005 sputter coater (Leica Microsystems GmbH, Wetzlar, Germany) **(Figure 2.10 top)**. All images were attained by using Hitachi TM3030 software.

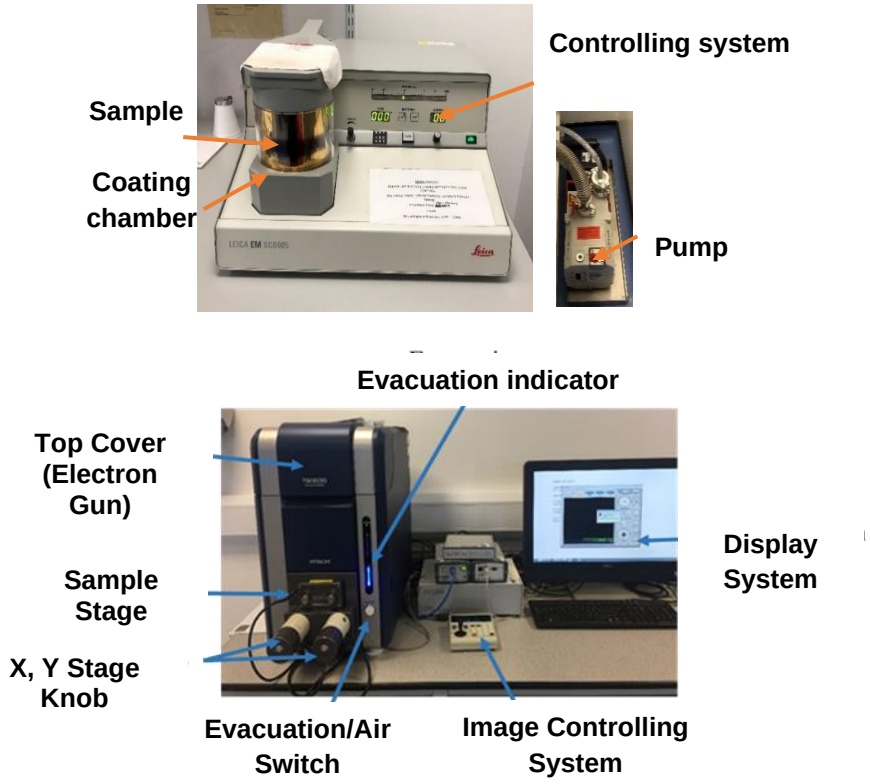

Figure 2.10 Photographs of a vacuum sputter coater (top) and an SEM tabletop TM3030 (bottom).

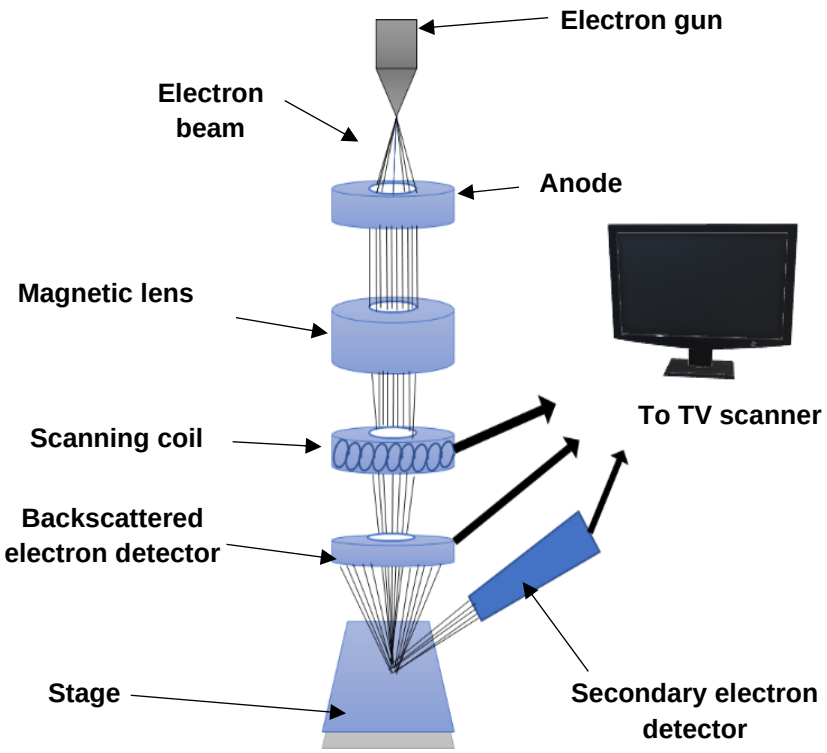

Figure 2.11 Schematic diagram of SEM. This diagram is inspired from this chapter. This diagram was adapted from [257].

2.6.3.3 Optical Microscope (OM) and Hot-Stage Microscope (HSM)

HSM, also called thermomicroscopy, is a combination of optical microscopy with thermal analysis components. This technique is primarily utilised to allow the study and physical characterisation of ingredients as a function of time and temperature. It is used to characterise the solid-state properties of materials, and it enables the observation of the physical appearance as well as the characterisation of the tested samples to rapidly find valuable data about its solid-state properties [258].

An HSM consist of a heating stage, digital programmable temperature controller, polariser, optical stereo microscope, digital camera and computer, and the software for the capture and analysis of micrographs **(Figure 2.12)**. The specimen is heated by transferring heat from a metal

block available on the hot stage plate, which is heated thermoelectrically. The tested sample can be cooled slowly to the required temperature at the desired rate. Some HSM instruments use liquid nitrogen to quench cool the sample, while some others have vacuum pumps, high-pressure pumps or purge gas that are connect to the hot stage plate [258]. HSM can be combined with different instruments, including DSC, Fourier transform infrared spectroscopy, Raman and confocal microscopy, SEM, and atomic force microscopy.

HSM can be used to study various materials in their solid states, such as APIs, excipients, polymers and lipids. Also, several observations can be made with thermal microscopy, such as solid-liquid transformations, compound morphology (solid, semi-solid, liquid, amorphous, crystalline, or crystal habit), solid-solid transformations, crystal growth and rate, and interactions between different compounds [258].

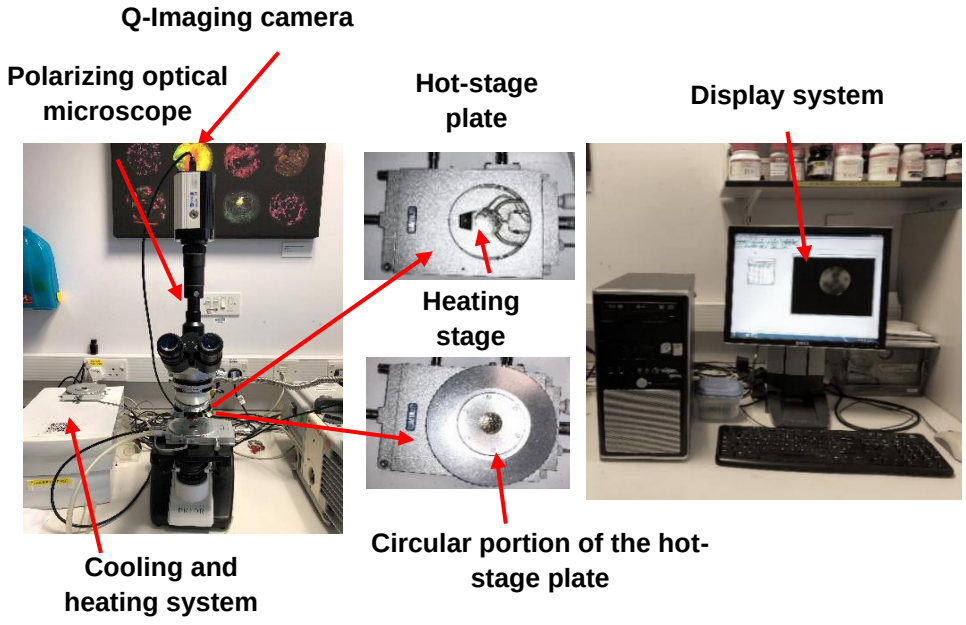

Figure 2.12 Photograph of an optical microscope with a hot stage control plate.

In this thesis, an optical microscope (Prior, PX023POL, Cambridge, UK) was used to observe the MP of the utilised 3D printing threads and conduct a comparison with results obtained from the DSC experiment. This microscope was equipped with a controlling temperature plate (Linkam, model T95-PE, Tadworth, UK), and it was fitted with a Q-IMAGING camera (QICAM, FAST1394, Surry, Canada) **(Figure 2.12)**. Furthermore, it was equipped with a 12V, 30W halogen lamp and moveable brightness control. This microscope was also equipped with various magnifications, including 4x, 10x, 20x, and 40x. All images were obtained using Linksys32 software.

Another OM was used to investigate the 3D printed prototype ear devices with different pore sizes, namely a Leica optical microscope (Lecia, MZ16, Germany). This microscope was fitted with various magnifications, including 0.71x, 1.0x, 1.25x, 1.6x, 2.0x, 2.5x, 3.2x, 4.0x, 5.0x, 6.3x, 8.0x, 10x, 11.5x. In addition, it was equipped with a digital camera (Leica EC3) and two light source boxes (Lecia, KL 1500 LCD and Lecia CLS 100x). Different images were captured under the calibrated magnification.

2.6.4 Formulations

2.6.4.1 Preparation of Hydroxypropyl Methylcellulose Hydrogel

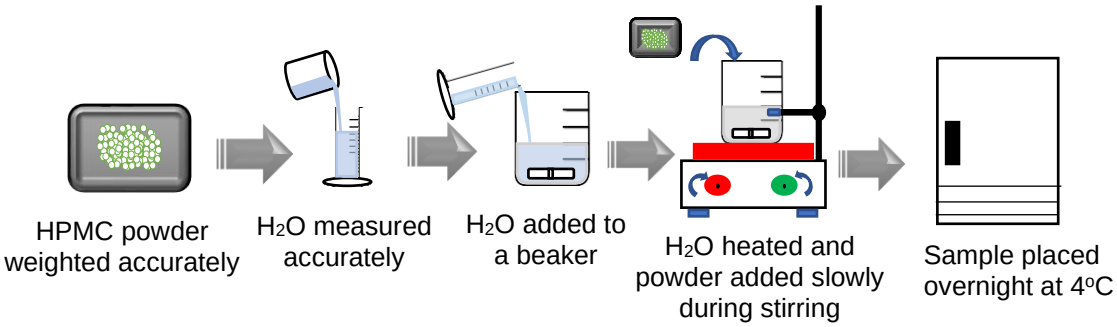

Figure 2.13 Schematic illustration of the preparation of HPMC hydrogel.

In this part, HPMC hydrogels were prepared with different polymer concentrations, including 1-7%, 9%, 10%, 15% and 20% of HPMC (w/w). Briefly, the amounts of HPMC powder were weighed accurately using an electronic balance (Make-Mettler Toledo, Model-AL-204, Switzerland). Then, an amount of distilled water (H_2O) was accurately measured using a gradual measuring cylinder and placed within a 50 mL glass beaker. Next, a magnetic stirrer bar was placed within the beaker, and they were both positioned above a magnetic stirrer apparatus (Asynt, ADS_HP_NT). The temperature of the magnetic stirrer plate was set on 90℃. After the heat reached a specific level, the stirrer was turned on, and the weighed amount of polymer was slowly added to the water within the beaker (around 1-2 minutes). After that, the formulations were kept above the magnetic stirrer for 24 hours at room temperature. Finally, they were placed within a refrigerator at 4℃ overnight **(Figure 2.14)**.

The main idea was to obtain a gelling system that could be incorporated within the 3D printed prototype ear devices to provide sustained drug release (DXM) via the printed pores.

2.6.4.1.1 Rheometer

Rheology is the science of the deformation and flow of the tested materials. Rheometry is a measuring technology, which is used to determine the rheological data. Specifically, it measures the viscosity (η) of a fluid. Moreover, it measures the effectiveness of shear strain and stress on the substances being tested [259]. The rheological measurement is made on a specimen that is placed between two components, including one stationary and one moving (rotating) component. Various kinds of measurement geometries are available; however, in this research work, the parallel plate geometry was utilised **(Figure 2.14)** [259].

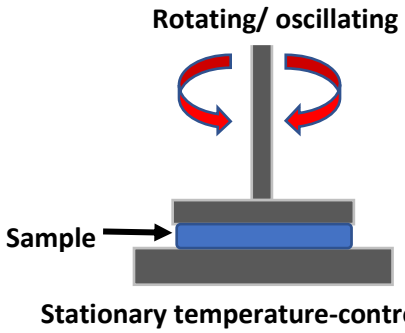

Figure 2.14 Schematic diagram illustrating the Anton Paar Rheometer parallel plate (PP 25 mm) geometry used for the rheological determinations of HPMC hydrogel samples.

2.6.4.1.2 Flow measurements:

The two parallel plate model was used to measure the rheological properties, as presented in **(Figure 2.15)**. In this model, the fluid can be imagined as a mini-scale amount of layers set on top of one another, similar a stacked deck of cards. The last layer at the bottom is a stationary layer, and the top layer is moved at a constant velocity. The layers under the top layer move with a velocity (V) directly proportional to the layer distance from the fixed bottom layer. In the rheometer instrument, a rotational force is applied. The rotationally applied force also shears the fluid in a laminar way. The measurement of sample viscosity is dependent upon the shear stress (τ) and shear rate (γ). **Table 2.1** shows these terms, their definitions, equations, and units.

Table 2.1 Flow measurements' definitions, equations, and units [259].

Measurement	Definition	Equation	Unit
Shear stress (τ)	The force (F) acting on an applied surface of a sample divided by the area of that surface.	$(\boldsymbol{\tau}) = \frac{\boldsymbol{F}}{\boldsymbol{A}}$	Pascal (Pa)
The shear strain (γ)	The displacement (D) divided by the height (H) of the applied sample	$(\gamma) = \frac{D}{H}$	
Shear rate (γ.)	The velocity of rotation divided by the gap size of the applied sample	$(\gamma.) = \frac{V}{H}$	reciprocal seconds (s^{-1})
Viscosity $(\boldsymbol{\eta})$	The ratio between the shear stress and shear rate.	$(\eta) = \frac{\tau}{\gamma.}$	pascal-seconds (Pa.s)

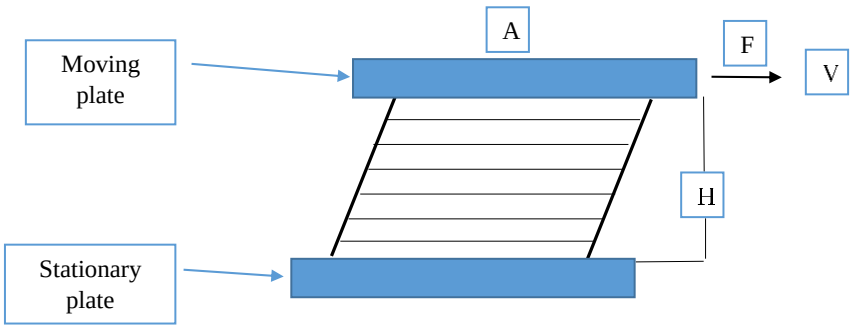

Figure 2.15 Illustration of the parallel plate model for shear tests to show the velocity distribution of the liquid flow in the shear gap.

The viscosity of the fluid can be described as its resistance to movement or flow. Liquids can be classified into two different categories, namely Newtonian or Non-Newtonian. For instance, a simple fluid, such as water, that has a constant viscosity not related to its shear rate is called a Newtonian fluid **(Figure 2.16)** [259].

In Newtonian liquids, the relationship between the shear rate (γ.) and the shear stress ($\boldsymbol{\tau}$) is a straight line. Furthermore, as the shear rate is varied, the viscosity of the liquid remains constant. On the other hand, the relationship between the shear rate and shear stress for a non-Newtonian fluid is not constant. Non-Newtonian liquids can be clarified as fluids containing a mixture of molecules that have different sizes and shapes [260]. Non-Newtonian fluids can be categorized into different types, including pseudoplastic flow, plastic flow, and dilatant flow [259]. Pseudo-plasticity, which also called shear-thinning, is time-independent and is characterised by an apparent viscosity that decreases with an increasing shear rate. Examples include paints and emulsions [261]. The second type is dilatant fluids. With these, the apparent viscosity increases with increasing shear rate. Moreover, there are also time-independent fluids called shear-thickening fluids [261]. Several examples of this type are available, including concentrated suspensions, such as sand/water mixtures, and compounds of candy [261], [262]. The last type of non-Newtonian fluid is called plastic fluid. This type is time-independent, and it behaves as a solid under static conditions. There is a specific amount of stress that needs to be applied to the contained fluid before any flow is made, known as the yield stress (f). On the other hand, if the applied stress is smaller than the yield stress, the tested material will deform elastically [263], [264].

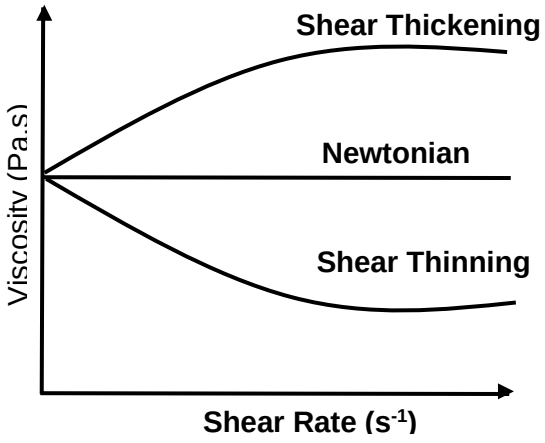

Figure 2.16 Representing the effects of the shear rate on the Newtonian and non-Newtonian behaviour of liquids samples regarding shear rate and viscosity.

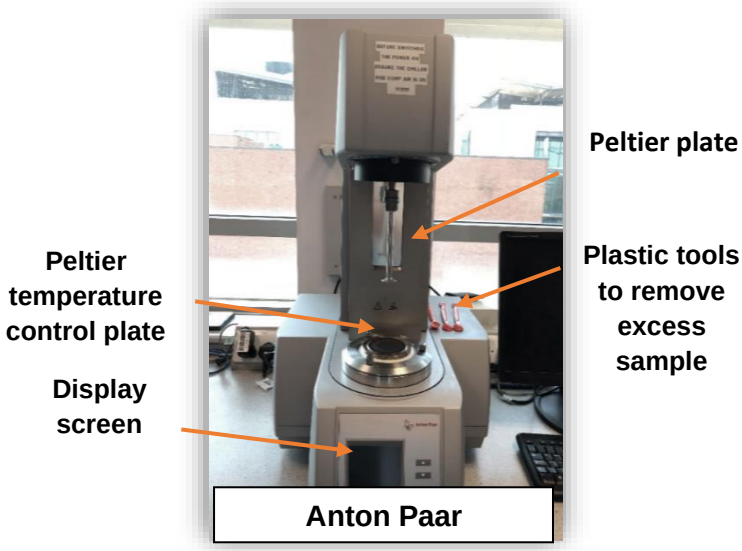

Figure 2.17 Photograph of an Anton Paar Rheometer (MCR 302).

In this work, an Anton Paar (MCR 302, Anton Paar, Germany) Rheometer **(Figure 2.17)** was used to investigate the rheological behaviours of the prepared HPMC hydrogels, including 2-7% HPMC hydrogels (w/w). Various tests were done, including the amplitude sweep test, frequency sweep test and viscosity test measurement.

2.6.4.2 Tablet Manufacturing

This kind of dosage form can be prepared by powder compression. The compression is provided by the action of the upper and lower punches of a die, through which the compressed force is applied. There are different stages in the processing of tabletting. First, the die is filled with a prepared powder, which normally flows by gravitational flow through a hopper via a die table. The lower punch is closed with the die at its bottom. Second, after the powder enters the die, the upper punch moves down and enters the die to compress the powder into a tablet. The lower punch can be either stationary or move up within the die hole during the compression phase. Then, the upper punch leaves its position when it reaches the maximum force needed. Finally, the last step is the tablet ejection. In this part, the lower punch rises until its upper level reach the

upper part of the die, and a pushing device removes the prepared tablet from the top of the die [265].

Different types of processes are used for tablet production, including A) single punch press, B) rotary press, and C) computerised hydraulic press. The single punch press is mainly composed of a set of punches (upper and lower punch) and one die **(Figure 2.18).** This type can manufacture small batches of a tablet either during formulation development and or the manufacture for clinical trials. For instance, automated versions can produce 200 tablets per minute. The other type of tablet compression machine is a rotary press **(Figure 2.19)**. This kind of machine was established to raise the output of tablet production. It can produce 10,000 tablets per minute, and it utilises several punches (upper and lower punches) and dies. The last one is the hydraulic press. This one is commonly utilised in the research field, and in development work, for instance, it is used for the initial evaluation of the tabletting properties of powders. Moreover, it used for the prediction of the effect of scale-up on the properties of the formed tablet [265].

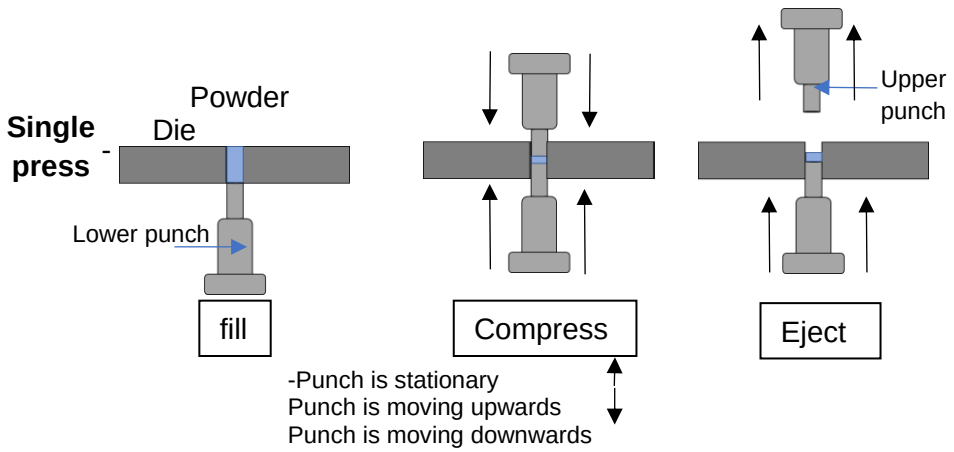

Figure 2.18 Schematic illustration of the sequence used in the fabrication of tablets with a single punch press tabletting instrument.

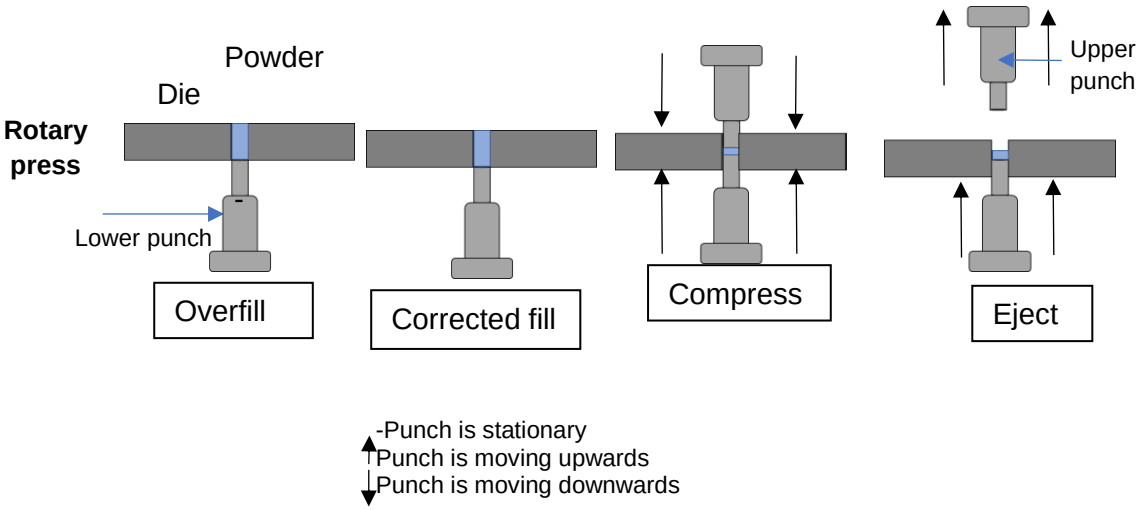

Figure 2.19 Schematic illustration of the rotary press tabletting process.

In this thesis, a manual hydraulic press 15 Ton (Atlas™, Specac, Orpington, UK) was used to compress several DXM/methyl-β-CD inclusion complexes and DXM/lactose drug tablets. The hydraulic press instrument is mainly composed of different parts, including a pump handle, leadscrew handle, bottom piston, top bolster pressing face, pressure/load gauge, and pressure release handle (**Figure 2.20**). Also, it comes with different evacuable pellet dies, punches and two stainless steel pellets, which are 5, 13, 20, 32, and 42 mm in diameter. This instrument is designed to compress the powder into small tablets one at a time. Furthermore, the compression pressure of this hydraulic press machine can be observed and monitored in tonnes. In this thesis, the sets of punches and dies 6 mm in diameter were used to compress different tablets.

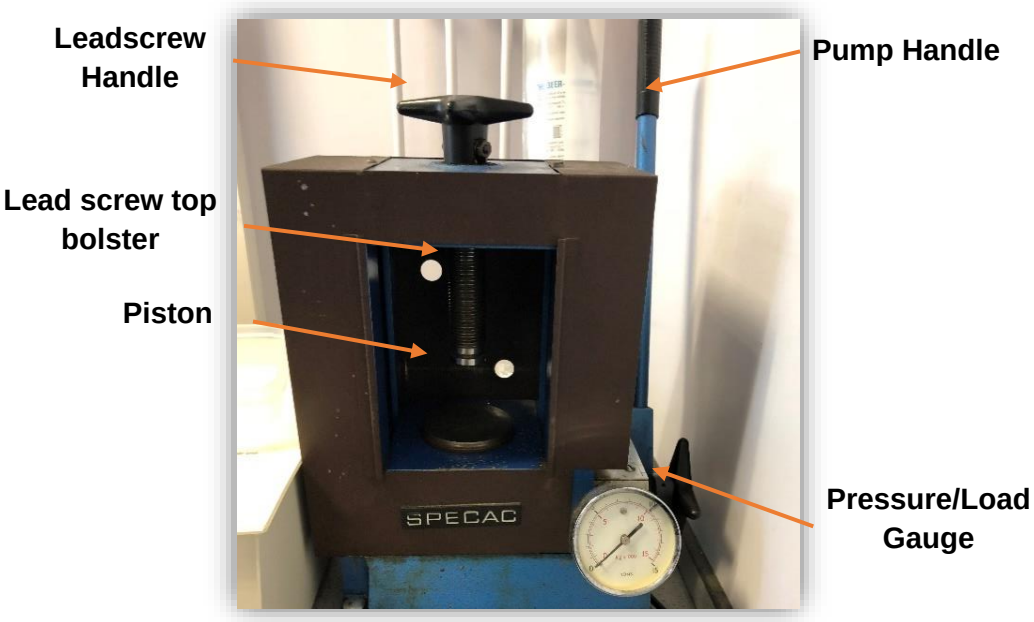

Figure 2.20 Photograph of an Atlas™ Manual 15 Ton (15 T) Hydraulic Press.

2.6.5 Study Drug Diffusion

2.6.5.1 Raman Spectroscopy (RS)

2.6.5.1.1 Principles of Raman Spectroscopy

RS is based on Raman scattering, which is a phenomenon discovered by Sir C. V. Raman [266]. The principles of Raman spectroscopy are related to the ability of this instrument to measure Raman scattering. The scattering happens when a tested sample is subjected to a specific light source (monochromatic light). The light interacts with the sample molecules, creating a short-lived excited state, named the virtual state. Different scattering events which arise, including elastic and inelastic scattering. The first event is called Rayleigh scattering. In this event, the incident and scattered photons have a similar energy. Secondly, a small portion of photons is scattered at shifted wavelengths in different directions, which is called Raman scattering. This type of scattering is directly associated with the frequency of molecular vibrations. Raman scattering can be categorised into two scattering categories, namely Stokes or anti-Stokes scattering [267].

In Stokes scattering, after exposure to an exciting source, the tested molecule moves from a vibrational state to a virtual state by absorbing an arriving photon. After that, the excited molecule moves back from the virtual state to a high-energy vibrational state. Then, a photon is released with less energy and longer wavelength. The difference in the wavelength of the incoming photon and the new photon is named a Raman shift. In anti-Stokes scattering, the molecule travels from the vibrational state (high energy) to the ground state after interacting with the photon. Then, the scattered photon has a shorter wavelength and higher energy than the entering photon **(see Figure 2.22)** [267]. In RS, Stokes scattering displays higher intensity than anti-Stokes scattering are there are more molecules available in the ground vibrational state than in the high energy vibrational state. RS usually measures Stokes shifts that cover an energy level range of 200-4000 cm^{-1} [267].

2.6.5.1.2 Raman Microscopy

Raman microscopy is a combination between optical microscopy and Raman spectroscopy. The Raman instrument is mainly composed of an excitation source (laser source), a spectrometer, a sampling apparatus (microscope), and a detector (a charged coupled devices [CCD] camera). In the spectrometer, there is an optical filter, which is utilised to remove the Rayleigh scattering. Meanwhile, the gratings are applied to spatially separate the different wavelengths. The lasers in the Raman instrument have different wavelengths, including green, UV, blue, and near IR lasers. The laser beam is directed onto the specimen through a specific objective lens. Then, the laser is scattered through the same objective lens. After that, the scattered light is directed into a spectrograph and then diffracted across a CCD detector. The available pinhole is located between the detector and the objective in the utilised confocal microscopy. This pinhole allows for the depth of field to be controlled. It removes undesired signals from the focal point [267], [268]. **Figure 2.21** shows a schematic illustration of the theory of Raman spectroscopy.

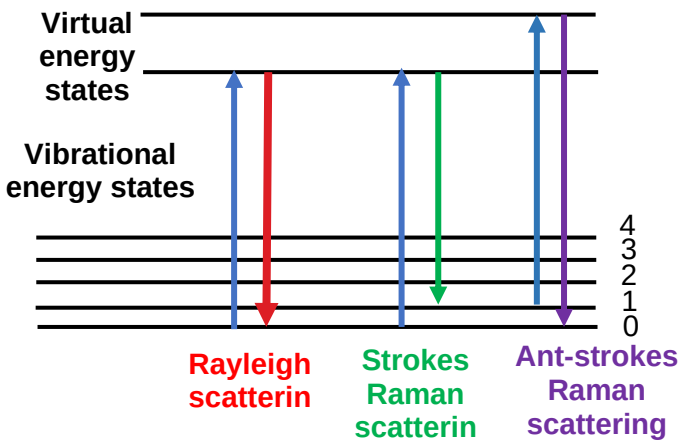

Figure 2.21 Schematic illustration of the theory of Raman spectroscopy.

2.6.5.1.3 Raman Mapping

Raman mapping (RM) is the process of collecting Raman spectra from each pixel in a desired section of the surface of an analysed sample. A Raman spectrum is collected from the desired area in coordinate space. After that, the analysed sample is moved to the next analysis point (pixel), and then another spectrum is obtained. This method also is named point-by-point mapping. There is another faster type called line scanning or mapping [268]. In this research work, a confocal Horiba-Jobin-Yvon LabRAM system (Horiba-Jobin-Yvon Ltd., Middlesex, UK) was used to determine the Raman spectra of different kinds of materials, including DXM, HPMC powder, and 7% prepared HPMC hydrogel. Moreover, Raman mapping was used to determine the line mapping of DXM in the prepared hydrogels to investigate the drug diffusion through the gelling system **(Figure 2.22)**.

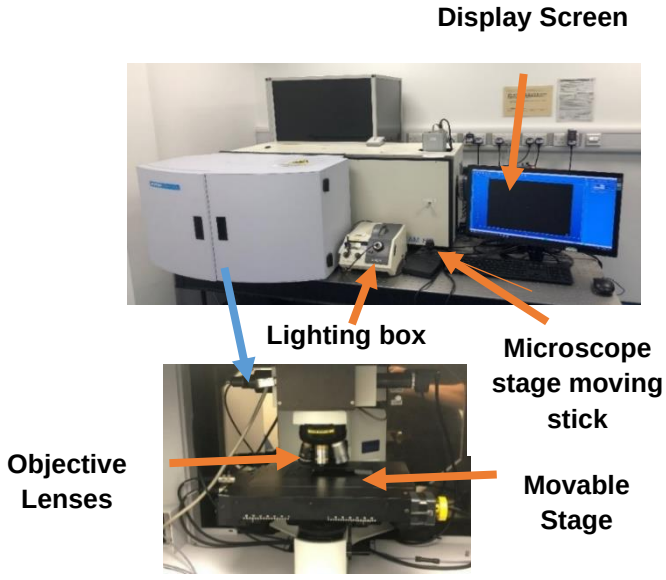

Figure 2.22 Photograph of a Raman spectroscopy instrument.

2.6.6 Study Drug Diffusion

2.6.6.1 *In vitro* Dissolution Apparatus II

In vitro dissolution testing is widely utilised to study pharmaceutical products due to many reasons, including evaluating new formulations for improvement, batch-to-batch quality of pharmaceutical products, and monitoring the quality of different API products and their performance after certain changes, such as during formulation, process, and scale-up [269]. *In vitro* dissolution analysis is a time-dependent process. This study includes many physical changes. For example, the disintegration of tablets or capsule into their primary particles, the transposition of API molecules from the solid surface, and the diffusion of API molecules across the diffusion layer adjacent to the solid surface [269]. This kind of study is routinely utilised in the lab to study pharmaceutical drug release profiles, such as from capsules, tablets, or transdermal patches. In a typical *in vitro* dissolution test, a prepared dosage form is placed within a dissolution vessel that has a fixed volume of medium with a specific apparatus. This dissolution media is mixed at a specific rate. After that, the amount of API dissolved in the selected medium is monitored using different instruments, including high-performance liquid chromatography

(HPLC) or UV spectrophotometric determination. Then, the data are reported as a percentage (%) of API released versus sampling time. The *in vitro* dissolution methods can be developed to fit the tested drug release profile, including for controlled release or immediate release [269].

Different types of US Pharmacopoeia (USP) dissolution apparatuses are available for testing different pharmaceutical dosage forms. The first type is apparatus I, which is called a basket apparatus, and the second one is apparatus II, which is called a paddle apparatus. Both are commonly utilised in the quality control testing of tablets and capsules with different release profiles, including delayed-release, immediate-release, and extended-release properties. A large volume of dissolution media (500-1000 mL) can be used with both types I and II. The third type is called apparatus III, which is named the reciprocating cylinder. The fourth type is apparatus IV, and it is called the flow-through cell apparatus. The hydrodynamics of types III and IV are thought to be closer to the human physiological conditions in the gastrointestinal tract (GIT) than types I and II. Moreover, type III is widely used for testing extended-release (ER) and immediate-release (IR) dosage forms (DF). In contrast, type IV is commonly used for poorly soluble API and ER API. The fifth type is apparatus V, and it is called the paddle over the disk, while the sixth type is apparatus VI, which named cylinder. Both types are for analysing a transdermal dosage form [269].

In this thesis, a dissolution apparatus I (Dis8000, Copley Scientific Limited, UK) was used to analyse the permeability of DXM through the Strat-M® membrane that covered the created pores over the prototype 3D printed ear devices. After that, the concentration of the DXM transport through the membrane and devices pores was analysed by UV vis spectroscopy (Cary, 50 Bio, Australia). Apparatus I was selected because the basket prevents the loaded device from floating, and it facilitated the drug release through the printed pores from the developed 3D printed ear medical prototype device **(Figure 2.23)**.

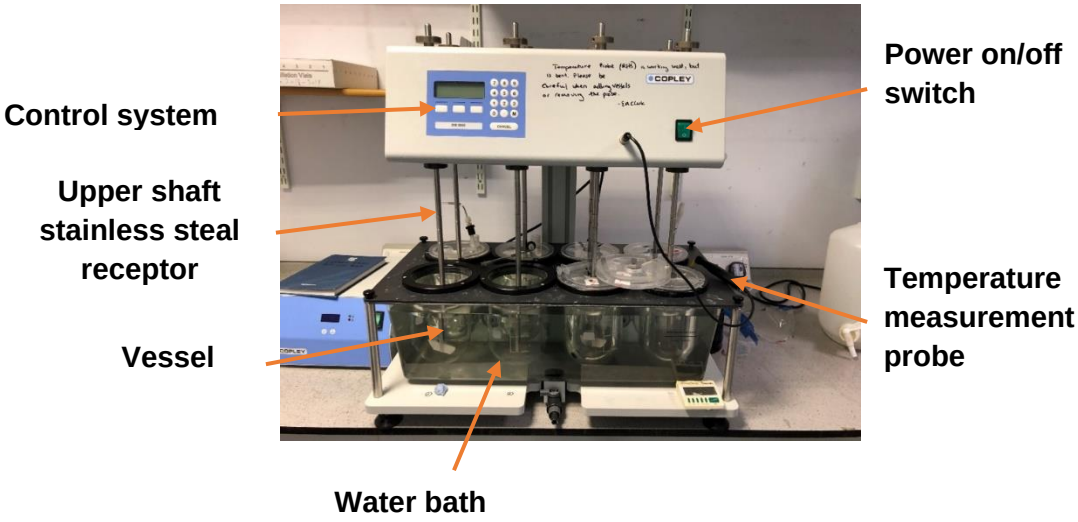

Figure 2.23 Photograph of a dissolution apparatus instrument.

Chapter 3 Developing a 3D Print External Ear Prototype Medical Device

3.1 The Novelty

The novelty described in this chapter lies in the development of a 3D printed ear prototype device with circular and square pores for future drug release by an FDM 3D printer.

3.2 Introduction

The main aim of this chapter is to develop a personalisable in-ear prototype medical device using 3D printing technologies, including FDM and SLA printers. Moreover, this manufactured device will be designed in such as way that it could in future incorporate a gelling system that could be loaded with an anti-inflammatory drug to provide the desired sustained drug release for the treatment of AOE patients (7 days).

This aim of this chapter is achieved by the meeting the following objectives:

Different 3D ear prototype devices are printed with a range of basic and realistic geometries using different kinds of 3D printing techniques and materials. The simple shapes are utilised to investigate the utilised hydrogel properties. However, more realistic shapes are utilised to study the drug release. SEM is used to image the layers of the printed devices. A calliper is used to measure the dimensions of the printed devices to ensure the designed dimensions can be achieved with the printer. DSC and HSM are used to investigate the polymer (PLA) T_g and T_m and the morphological changes of the thread layer. **Figure 3.1 and 3.2** show all stages of development of the ear medical prototype device.

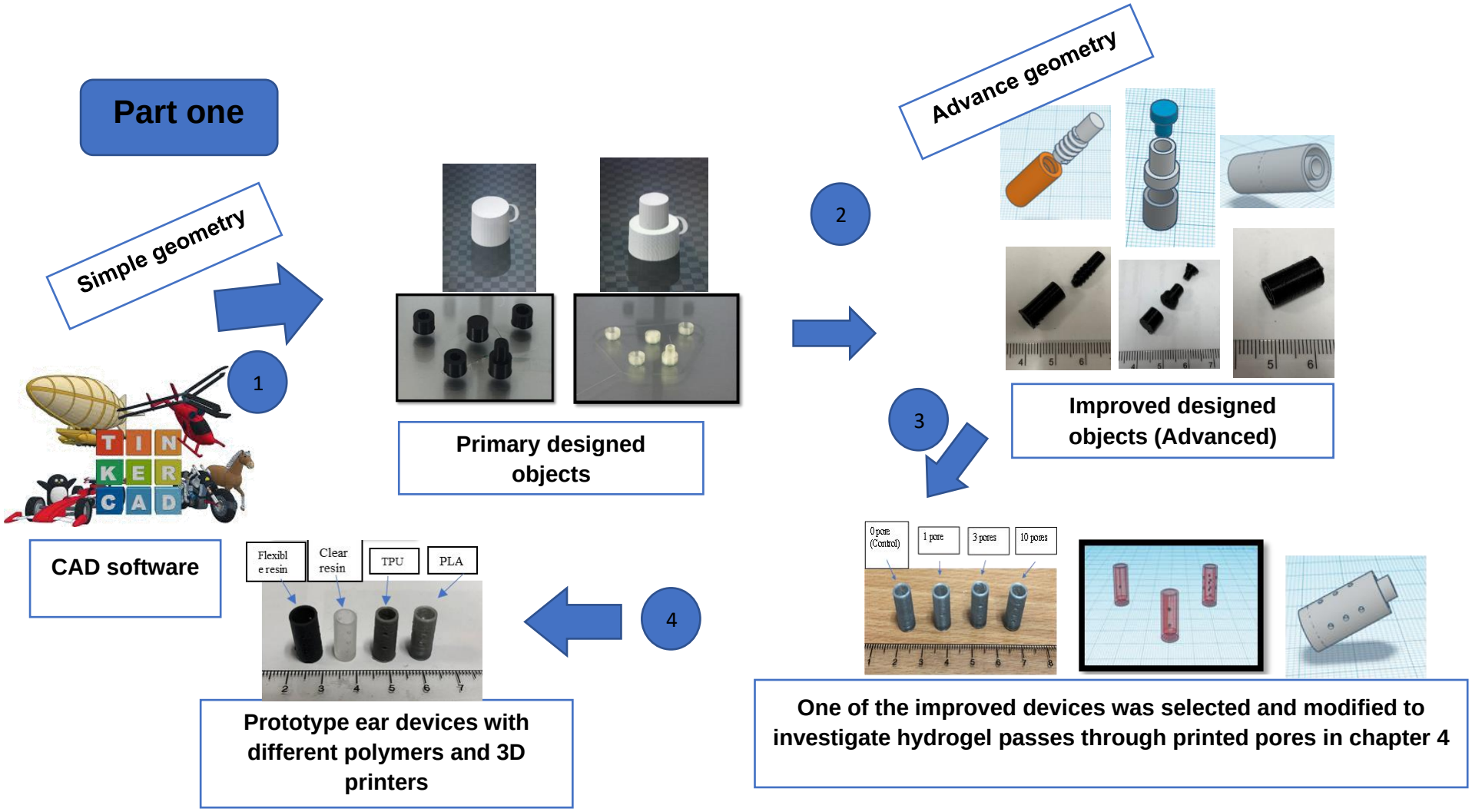

Figure 3.1 Schematic diagram representing all stages of manufacturing the porotype ear device with simple and advanced geometries using different 3D printing techniques and materials.

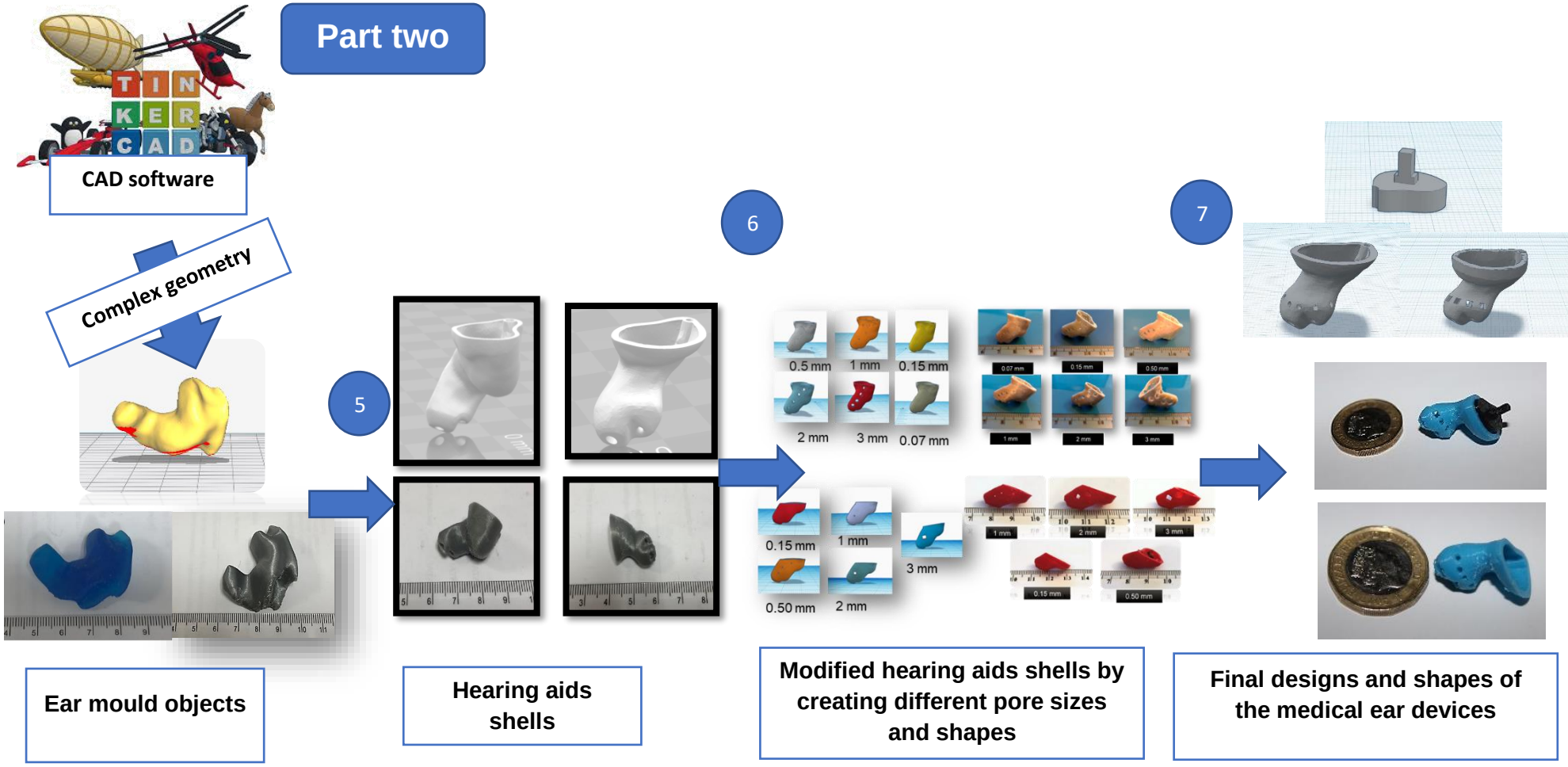

Figure 3.2 Schematic diagram representing all stages of manufacturing ear porotype device with complex geometries using an FDM printer.

3.3 Experimental section

This chapter includes the design, modification, and manufacture of ear prototype medical devices with different ranges of realistic geometries, materials and 3D printing technologies, as illustrated in **Figures 3.1 and 3.2.**

3.3.1 Design, Modification, and Optimization of Different Ear Prototype Medical Devices

This methodology comprises different parts. In the beginning, two different objects were designed using the Materialise Magics CAD software (version 21.1, Materialise, Belgium). The first object was created as depicted in **Figure 3.3 A**. This cylindrical disk has a height of 3 mm and a diameter of 5 mm. The second multi-cylinder object was designed as illustrated in **Figure 3.3 B**. This item is composed of two parts. The bottom section has a height of 3 mm and a diameter of 5 mm. The top section has a height of 3 mm and a diameter of 3 mm. Both object designs were saved as stereolithography (.STL) files, and they were imported into Cura Ultimaker software (version 2.6.2, Ultimaker, Netherlands).

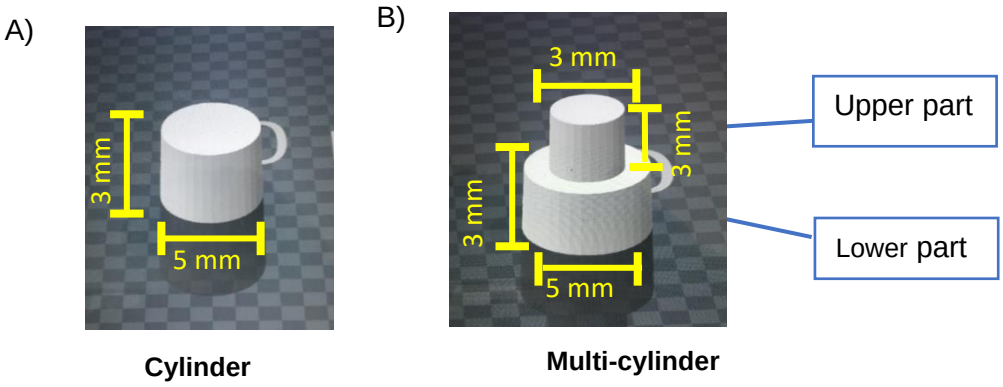

Figure 3.3 Schematic illustration of the primarily designed objects. A) The first design (cylindrical) and B) the second design (multi-cylinder) or (multi-parts). Both objects were designed using Materialise Magic software.

Subsequently, the primarily designed objects were modified to achieve more advanced ear prototype devices, as seen in **Figure 3.1 (No. 2)**. These devices were designed by an online CAD software named Tinkercad (https://www.tinkercad.com/). Then, the produced files were imported and printed by the Ultimaker^{2+} printer. **Figure 3.4** presents the different designs for the ear prototype devices suggested to be used for external ear canal drug delivery, including A) hollow cylinder design, B) ear tablet design, and C) screw designs. All dimensions are presented in **Table 3.1.**

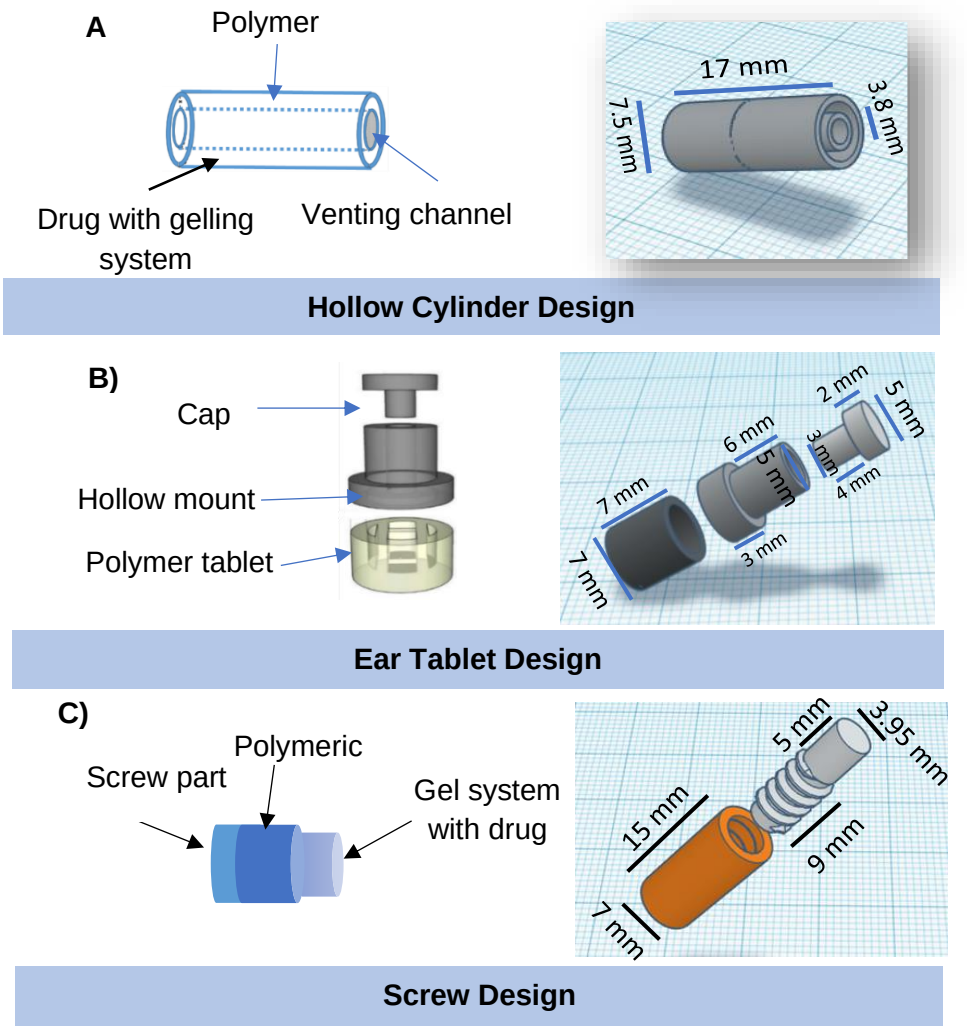

Figure 3.4 Number of suggested designs for the ear prototype medical devices (left) and their designs, drawn using Tinkercad CAD software (right), including A) hollow cylinder design, B) ear tablet design and C) screw design.

Table 3.1 The dimensions of the designed advanced ear prototype devices.

Designs			Designed	
			Diameter (mm)	Height (mm)
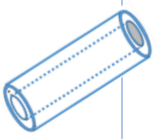 A) Hollow cylinder	Inner cylinder		3.8	17
	Outer cylinder		7.5	
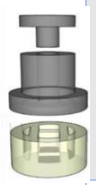 B) Ear tablet	Top	Top cylinder	5	2
		Bottom cylinder	3	4
	Middle	Top	5	6
		Bottom	7	3
	End		7	7
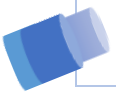 C) Screw	Top		3.95	5
	screw		3.95	9
	Hollow cylinder		7	15

Different devices were printed and modified to investigate the release of the selected hydrogels through the fabricated devices. The detailed information is discussed in **chapter 4 (Figure 3.1, No.3).** Subsequently, we investigated polymers that had a rubbery material property to allow deformation upon insertion into the ear if required. Therefore, two different polymers were utilised to print multiple ear prototype devices, as shown in **Figure 3.1 (NO.4)**. The idea in this part was to investigate whether using rubbery materials, such as TPU with the FDM printer or flexible resin with the SLA printer, are preferable to the hard thermoplastic PLA polymer for use with patients.

Firstly, the Ultimaker^{2+} was employed to print some of the 3D ear prototype items using TPU thread. The manufacturing steps are illustrated in **chapter 2, section 2.4.1**. **Figure 3.5** shows the CAD design of one of the 3D printed ear prototype devices. The outer dimensions of this 3D object are z = 13 mm, y = 7 mm, and x = 7 mm.

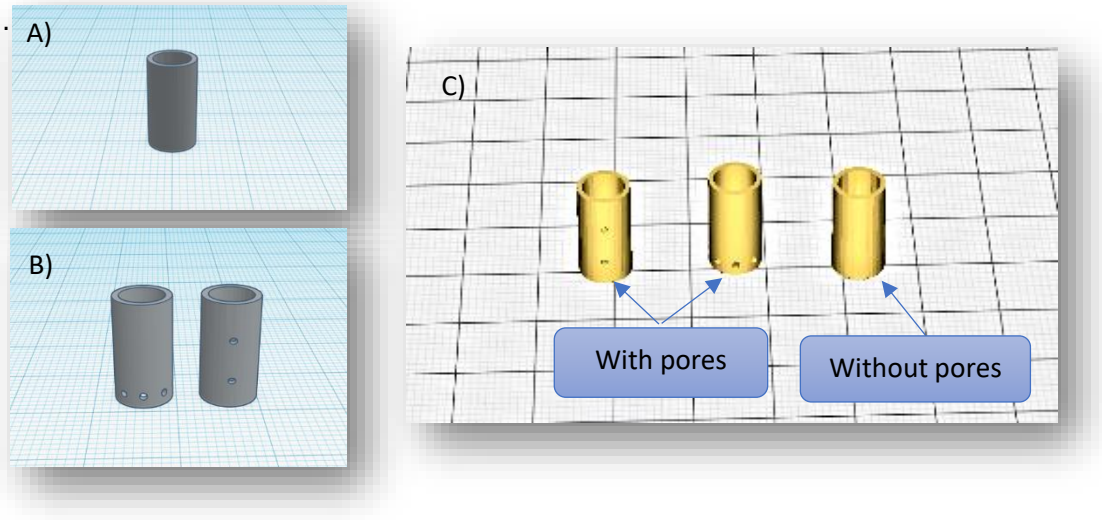

Figure 3.5 Schematic illustration of the hollow cylinder designed objects using the Tinkercad online software; A) without pores, B) with different pore orientations, and C) using the Cura software.

Secondly, SLA Formlabs 2 was utilised to fabricate an ear item using the flexible resin. The printing steps are detailed in **chapter 2, section 2.4.2**. **Figure 3.6** shows the CAD design of one of the 3D printed ear prototype devices containing several pores.

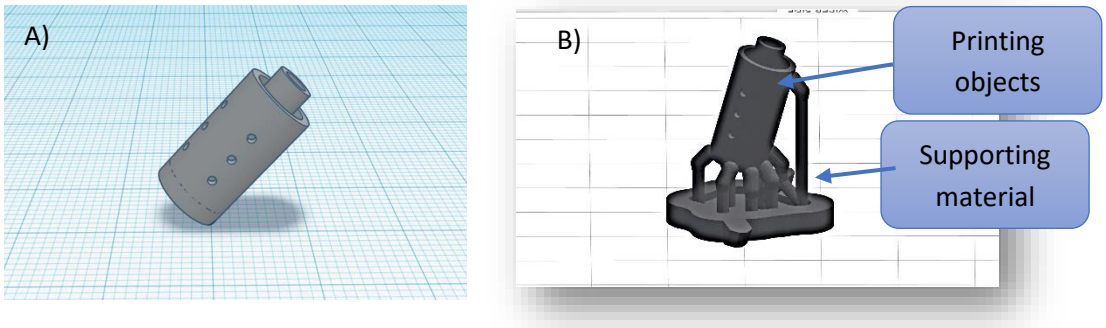

Figure 3.6 Schematic illustration of the hollow cylinder designed objects using A) the Tinkercad online software, and B) the Formlabs preform software.

In this thesis, we utilised the different polymers with various features (hard or rubbery) to find the proper polymer that can be printed with uniformly distributed layers and produce printed objects that have no cracks or pores in their walls. Moreover, the surface of the printed objects should be smooth and not have a rough texture.

Subsequently, we moved to **part two,** as shown in **Figure 3.1.** In this part, the hard thermoplastic polymer (PLA) was utilised to conduct the remaining experiments. In addition, sophisticated ear prototype devices, which has a design similar to the external ear canal, were modified and printed with the FDM 3D printer **(Figure 3.7)**.

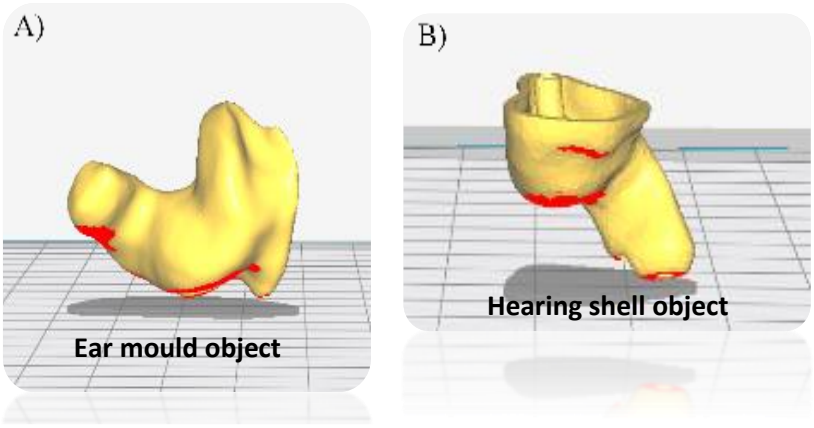

Figure 3.7 Schematic diagram of an A) ear mould object and B) a hearing aid shell object. Both images were captured from the Tinkercad online CAD software.

The CAD file (.stl) of an ear mould object was obtained from the online website "https://grabcad.com/library/ear-canal" **(Figure 3.7A).** The outer dimensions of this object are Z = 31.55 mm, X = 34.47 mm, and Y = 25.19 mm. Furthermore, another object was obtained from the same website, namely (https://grabcad.com/library/in-the-ear-hearing-aid-shells-1) **(Figure 3.7B).** The outer dimensions of this object are Z =18.23 mm, X =19.68 mm, and Y =17.88 mm.

The hearing aid shell file was modified by creating several pores in the shell wall with different shapes and dimensions. The Tinkercad software was used to produce different circular pore sizes, 3, 2, 1, 0.50, 0.15, and 0.07 mm in diameter, respectively **(Figure 3.8)**. Different square pore sizes were also created in the shell object, which had side lengths of 3, 2, 1, 0.50, and 0.15 mm, respectively **(Figure 3.9).** The main idea in this part is to find the smallest pores that the 3D printer (Ultimaker^{2+}) can print. Moreover, the dimensions of the created pores were measured to

investigate whether the designed and printed pores were similar in dimensions or not and to investigate the quality of the utilised printer. Furthermore, one of the created pore sizes, as noted, is to be selected and modified in one of the prototype ear devices to be used to investigate the hydrogel system release through the created pores. This is detailed in (**chapter 4**)**.** In addition, the selected pore dimension will be utilised to fabricate with the final developed prototype ear device. All files were imported into the Cura software and then printed with the Ultimaker^{2+} FDM printer.

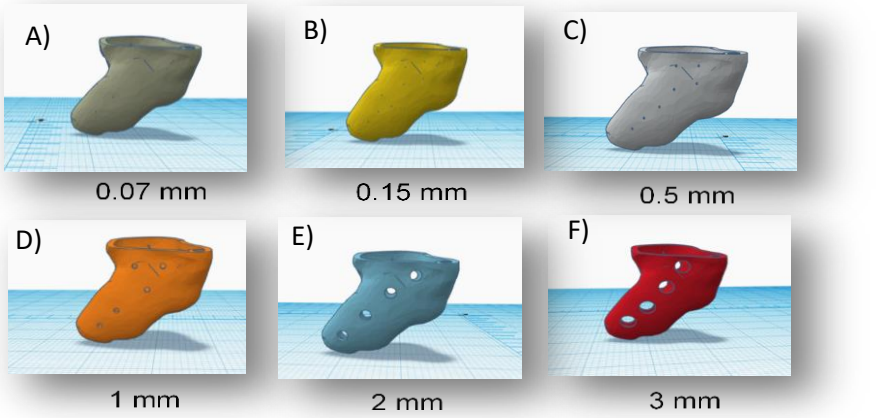

Figure 3.8 Schematic illustration of the hearing aid shell with different circular pore sizes. A) 0.07 mm, B) 0.15 mm, C) 0.5 mm D) 1 mm, E) 2 mm and F) 3 mm in diameter.

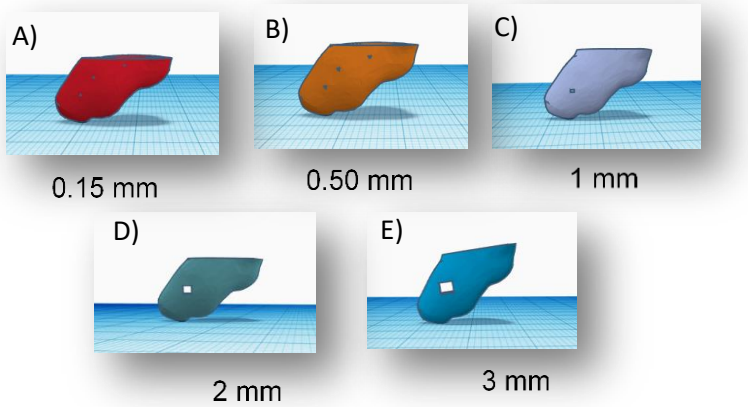

Figure 3.9 Schematic illustration of the hearing aid shell with different square pore sizes. A) 0.15 mm, B) 0.5 mm C) 1 mm, D) 2 mm, and E) 3 mm per side.

Finally, two ear medical devices were designed using the same software. The created pores with the dimension of 1 mm in diameter and per side were reorganized on the hearing shells in such a way to cover the beginning of the ear canals. The first device had circular pores (nine pores) 1 mm in diameter. The second device had 8 square pores with a dimension of 1 mm per side. Also, a cap was designed to close the upper part of the designed shells to prevent any escape of the injected materials and also facilitate the insertion and removal of the device within the patient's ears **(Figure 3.10 A-C)**.

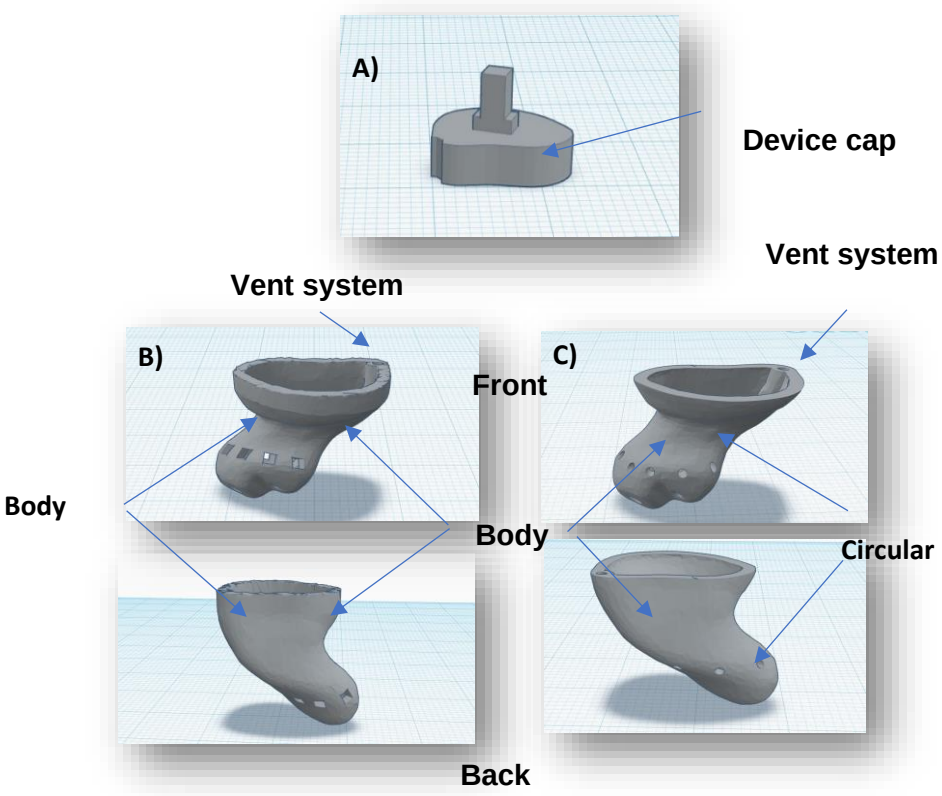

Figure 3.10 Schematic presentation of the developed PLA ear medical prototype ear devices. A) A hearing aid shell cap, B) composed of 1 mm in diameter of circular pores, and C) composed of 1 mm square pores. These devices were modified using Tinkercad online software.

3.3.2 Fabrication of the Designed and Modified Objects by Different 3D Printers

In this part, two different 3D printing instruments were utilised, namely the FDM Ultimaker^{2+} and SLA Formlabs 2, to print different 3D prototype ear objects out of numerous materials with various characteristics (rubbery or hard). Then, one of the printers was selected to print the final designed ear prototype device with the proper shape, uniformly distributed layers and without cracking in its wall. After that, this device is utilised in the final experimental chapter **(Chapter 5)** to study the DXM release with the dissolution apparatus equipment.

3.3.2.1 The FDM Ultimaker^{2+} 3D Printer

The FDM Ultimaker^{2+} 3D printer was employed to fabricate all the designed and modified objects. Moreover, it was also used to fabricate the ear devices obtained online, namely A) the ear mould object and B) the hearing aid shell object. The files were created and modified using the CAD software (Materialise magic and Tinkercad) and imported into the Cura software. The different printing parameters were adjusted, including infill percentage (%), printing speed (mm/s), layer height (mm), wall thickness (mm), top/bottom thickness (mm), printing temperature (℃), and build plate temperature (℃) **(Figure 3.11)**. Subsequently, the produced files were saved as Gcode commands and transferred to the printer's SanDisk memory cards. The printing steps are described in **chapter 2**, **section 2.4.1.**

The most commonly utilised CAD file format is .STL in the 3D printing CAD software. After the.STL file is prepared, the designed model is converted to an X, Y and Z based code, which the utilise 3D printer can read. This code is named g-code, and the 3D printer uses the X, Y and Z directs to navigate the utilised code.

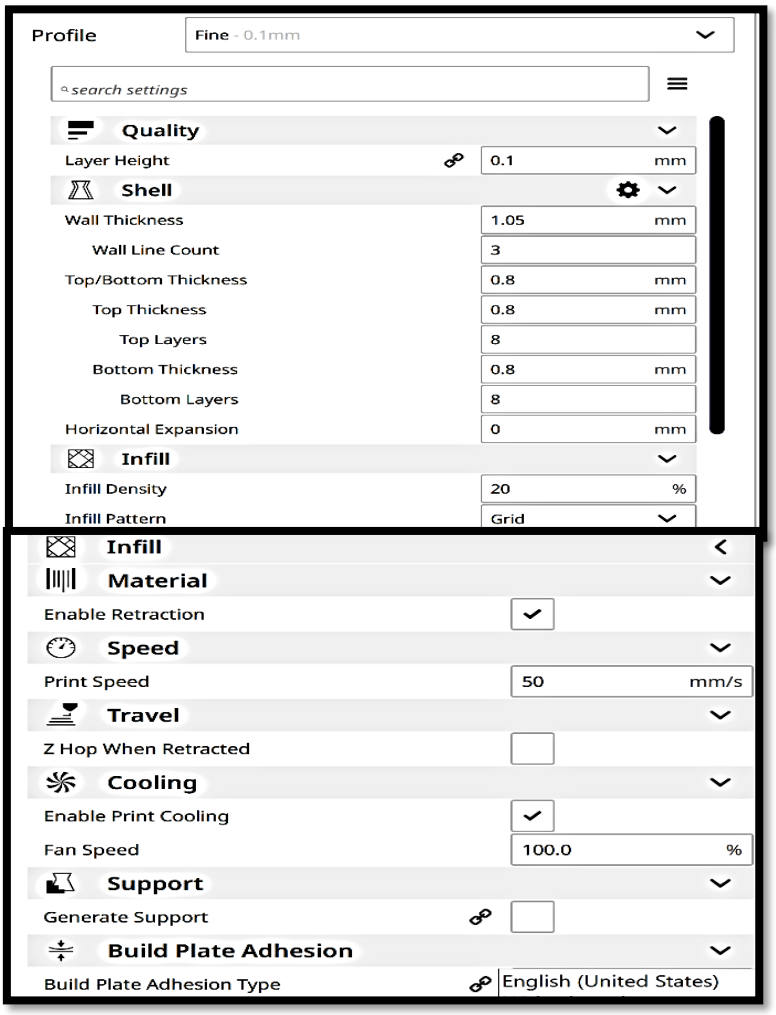

Figure 3.11 The FDM 3D printing parameters in the Cura software.

3.3.2.2 The SLA Formlabs 2 3D Printer

Likewise, the SLA Formlabs 2 3D printer was utilised to print the different ear objects. This printer was equipped with a 405 nm laser, and enable the fabrication of the obtained 3D models with a resolution of 300 µm. The ear prototype devices files were imported into the SLA desktop printer software (Preform software, version 2.11.1). The printing parameters of the SLA printer were set to the used resins. **Figure 3.12** shows the SLA preform software printing parameters.

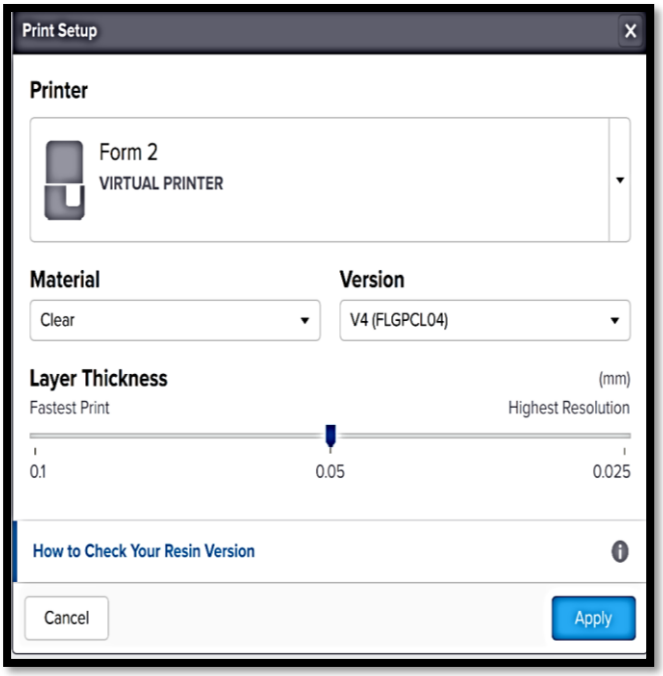

Figure 3.12 The SLA Formlab 2 printing parameter and print setup.

3.3.3 Characterisation of the Utilised FDM Thread and the Printed Ear Prototype Devices

3.3.3.1 Thermal Analysis of the Printing Filament to Determine their Glass Transition (T_g) and Melting Point Temperatures (T_m) by DSC

DSC (Perkin Elmer DSC 8000, Waltham, MA, USA) was used to conduct the thermal analysis of the 3D printed PLA commercial filament and to determine the T_m and the T_g of this polymer. In the beginning, the PLA commercial filament was cut using an appropriate accurately weighed within a size range of 5-10 mg. Then, the measured sample was placed within a new Tzero aluminium hermetic pan (02304636, Germany). After that, the pan was covered by a new lid (B0143018, Germany) and then sealed with a Perkin Elmer crimper press. DSC analysis was conducted from room temperature to 200℃. The heating rate of the DSC was fixed at 10℃/min, and nitrogen gas was utilised as a purge gas with a flow rate of 50 ml/min. All DSC measurements were performed in triplicates (n=3).

3.3.3.2 HSM to Observe the Morphological Changes of the Printing Filaments and their T_g and T_m

HSM experiments were performed to observe the T_m of the commercial PLA filaments and compare it with the results obtained from the DSC experiment. Also, this method was performed to observe the morphological changes of the PLA polymer. The PLA filament was cut into small microlayers at a size of 5 microns using an ultramicrotome (RMC, PowerTome PC) instrument. Then, a microlayer was placed between two circular glass coverslips (VWR, 631-0155, Lutterworth, Leicestershire, UK) located above a heating stage within the controlling temperature plate (Linkam, T95-PE, Tadworth, UK) **(Figure 3.13)**. The hot stage plate was placed onto an optical microscope stage (Prior, PX023POL, Cambridge, UK). This microscope was equipped with a Q-Imaging camera (QICAM, FAST1394, Surrey, Canada). The PLA sample was heated from room temperature up to 160℃ with the heating rate of 2℃/min. The holding time was set for 2 min at 160℃. Several images were captured using Linksys32 software and taken with a lens magnification of 4x.

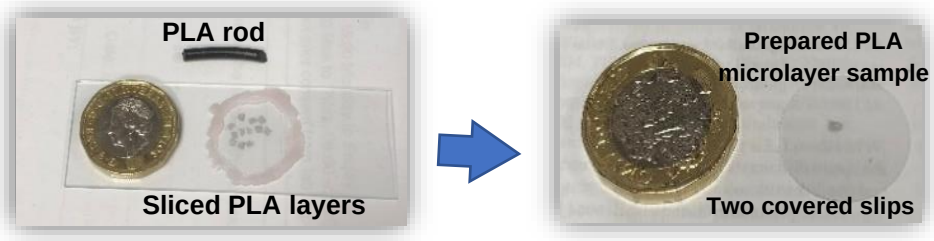

Figure 3.13 Photographs of the PLA rod, prepared PLA microlayers and HSM prepared sample.

3.3.3.3 Measurement of the Printed Objects Using a Calliper to Study the Quality of Printer

The printed ear prototype items dimensions were measured with an electronic digital calliper (Hardened stainless®) to characterise the FDM printed items and to ensure that the Ultimaker^{2+} printer delivers the quality to print the dimensions that were similar to or as produced in the CAD software (Materialise Magics software and Tinkercad software).

3.3.3.4 Microscopic Observation of the Designed Printed Objects

3.3.3.4.1 Scanning Electron Microscopy (SEM)

A Hitachi SEM (TM3030, Japan) was utilised to characterise the structure of the primary designed manufactured objects **(Figure 3.14).** A conductive carbon tape was mounted onto a specimen stub. Subsequently, the printed samples were placed on adhesive carbon tape. After that, the prepared samples were placed inside a vacuum sputter coater chamber (Leica EM SCD005 sputter coater) and coated with gold for 120 seconds at an accelerating voltage of 25 mA. After the coating, the samples were placed in the SEM specimen stage, and many images were obtained for the samples.

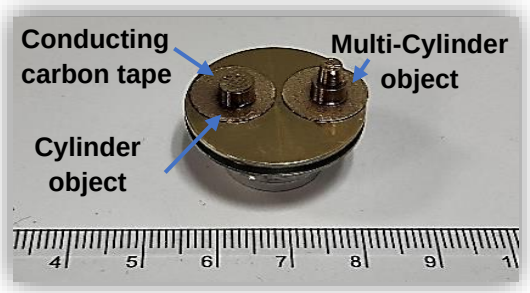

Figure 3.14 Photograph of the printed PLA objects after coating with gold.

Additionally, a Philips XL30 SEM (FEI Company, Hillsboro, OR) was utilised to characterise the structure of the FDM fabricated ear items with advanced and complex geometries. All prepared steps are mentioned at the beginning of this section; however, for the ear mould object during the preparation of the samples, a conductive carbon cement was utilised

and mounted onto a specimen stub instead of the carbon tape to hold large objects. Moreover, the samples were covered from the ends by conductive tape, and several images were obtained for the samples using Philips (FEI) XL30 SEM, (Philips Electronics Co., Eindhoven, Netherlands).

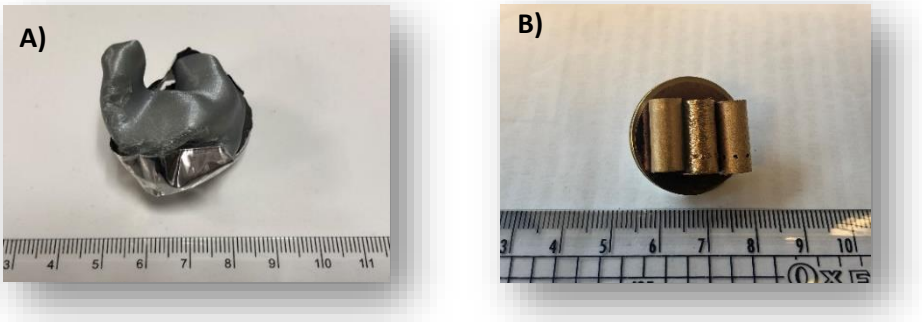

Figure 3.15 Photographs images of the PLA printed A) ear mould object and B) hollow cylinder objects coated with gold.

3.3.3.4.2 Optical Microscopy (OPM)

A Leica optical microscope (Lecia, MZ16) was utilised to investigate the dimensions of the printed pores and compare them with the designed pores. This microscope was equipped with a digital camera (Leica EC3) and two light sources boxes (Lecia, KL 1500 LCD and Lecia CLS 100x). The printed samples were placed on the microscope stage, and several images were captured under 2x magnification**.** After that, the captured images were uploaded and analysed using ImageJ software to determine the dimensions of the printed pores according to (**Eq.1&2).** The diameter of the printed pores with a circular shape was calculated and plotted in a graph. Also, as mentioned above, many objects were fabricated with different square pore sizes using the same printing parameters as for the circular pore devices. Various images were captured by using the same microscope and uploaded to ImageJ software. The results were analysed using (**Eq 3&4).** The sides of the printed pores were calculated and plotted in a graph.

Equation 1 $A = \pi r^2$ *

Equation 2 $P = 2\pi r$ *

Equation 3 $A = \alpha^2$ *

Equation 4 $P = 4\alpha$ *

*A= area of the circle, r = radius, P = perimeter, α = side

3.4 Results and Discussion

3.4.1 3D Printing of the 3D printed Ear Prototype Device Primary Designed Object

At the beginning of this chapter, a commercial PLA filament (black colour) was utilised, loaded into the Ultimaker^{2+} printer, and passed through a 0.6 mm head nozzle to fabricate the designed CAD prototype devices with simple geometries (cylinder and multi-cylinder objects) **as illustrated in section 2.2.1.**

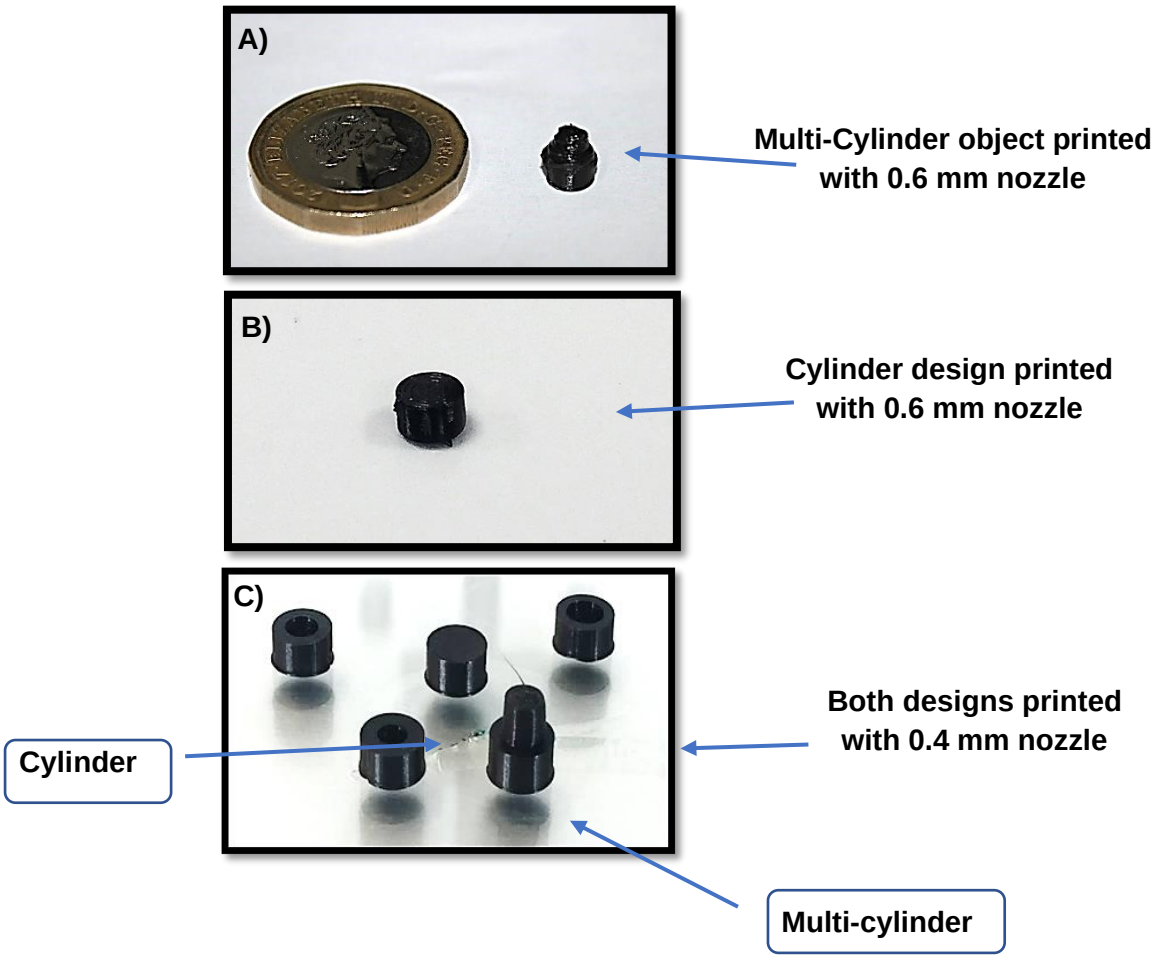

Figure 3.16 The morphology of the 3D printed PLA primary devices with different printing nozzles; A) 0.6 mm nozzle, and B) 0.4 mm nozzle. The adjusted printing parameters are shown in Table 3.2.

Several challenges were encountered during this part of the printing, including a) the production of 3D printed objects with an acceptable morphology as indicated through the design software and b) the optimization of the printing parameters.

Figure 3.16 A and B demonstrates the morphology of the PLA printed devices. The PLA filament was loaded into the FDM Ultimaker^{2+} printer, and the printing parameters were set according to **Table 3.2**. However, we found that the printed objects morphology still needed to be improved to meet the designed specifications. Therefore, the head nozzle size was changed to 0.4 mm, and some of the printing parameters were optimized.

Table 3.2 The 3D printing parameters for both PLA designs (cylinder and multi-cylinder).

Printing parameters	Cylinder	Multi-cylinder
Wall thickness (mm)	1.05	1.59
Layer thickness (mm)	0.06	0.15
Top/bottom thickness (mm)	0.72	1.2
Printing speed (mm/second)	20	20
Printing Temperature (ºC)	190	190
Building plate Temperature (ºC)	60	60
Infill (%)	100	100
Supporting materials	No	No
Adhesion	No	No

The first printed device **(Figure 3.16 C)** looked like a cylinder with the external dimensions 5.15 mm diameter and 2.97 mm height. The second device was observed as a multi-cylinder with the outer dimensions of 5.04 mm diameter and 2.92 mm height for the bottom part **(Figure 3.16 C)**. The top had the external dimensions of 3.79 mm diameter and 2.93 mm in height. These devices did not possess an acceptable morphology similar to the designed device. Therefore, the printing parameters were altered to improve the morphology of the printed devices. After the nozzle and printing parameters were changed, we found that the printed objects became better in terms of their morphological shapes than those printed with the 0.6 mm nozzle and old printing parameters. Furthermore, we found that by reducing the printing speed, changing the thickness of the layer, and changing building plate temperature improved the morphology of the printed objects.

PLA was selected in this thesis because it is one of the most common commercial polymers used with FDM 3D printers. Moreover, this polymer is biocompatible, thermostable, safe, and approved by the FDA for several biomedical and clinical applications [223], [270]. It has also been used in many different medical studies related to FDM 3D printing technology [271]–[274]. Several other polymers have been used with FDM 3D printers in the literature to fabricate DDS, such as PVA, PVP, PCL, EVA, and methacrylic acid co-polymers (Eudragit) [275]. Furthermore, FDM was used in this research because it is widely utilised commercially, and it can customise and manufacture complex structures [276], [277]. This kind of printing technology is also used in pharmaceutical studies. For instance, it is used to print tablets (printlets) [278], implants [251], and nanocapsules [279].

3.4.1.1 Morphological Observation of the Printed Layers Using SEM

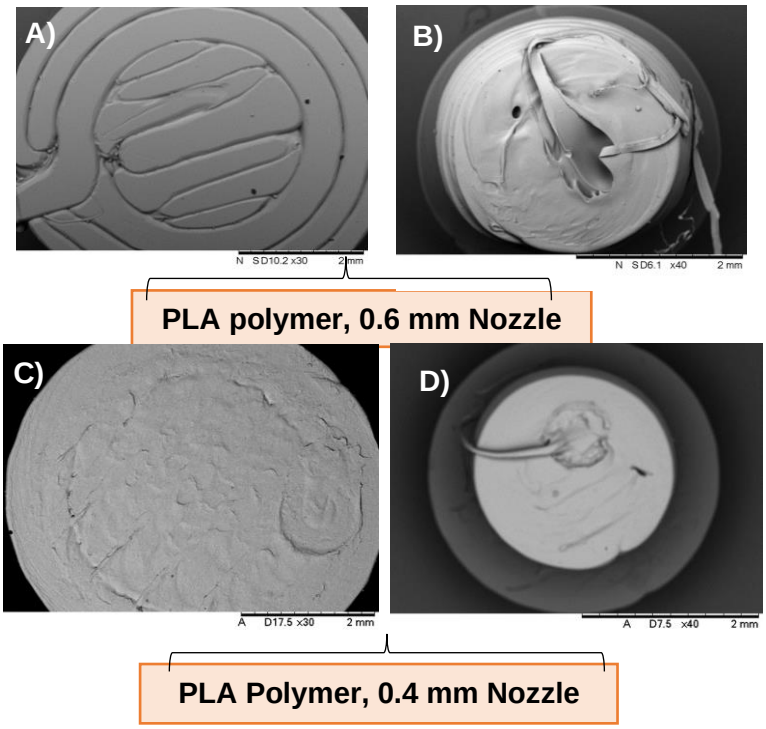

Figure 3.17 SEM images of the manufactured primary designed PLA 3D printed objects under various magnifications. Top views of A) cylinder and B) multi-cylinder objects after printing with the 0.6 mm FDM nozzle. C) A cylinder and D) a multi-cylinder after printing with the 0.4 mm FDM nozzle. The adjusted printing parameters are shown in Table 3.2.

The morphology of the printed ear prototype devices was characterised using a Hitachi SEM (TM3030, Japan). **Figure 3.17** shows SEM images of the primarily designed objects (cylinder and multi-cylinder devices) under various magnifications (30x and 40x). The SEM image of the cylinder device **(Figure 3.17A)** displays the organised printed layers of the PLA filament; further, these layers are uniformly connected. In addition, there were no pores between the fabricated and connected layers. Conversely, the multi-cylinder device image demonstrates the upper cylinder's smaller part with unorganised layers and an unacceptable morphology, as shown in the designed file.

To improve the morphology of the printed objects, the printer nozzle and some of the printing parameters were changed. Subsequently, various devices were fabricated until the desired morphologies were achieved. The printing parameters were determined for both objects and are shown in **Table 3.3.**

Figure 3.17 C & D presents the SEM images of the PLA printed devices after changing the printing parameters and head nozzle. Both devices have acceptable shapes, and they was no overlapping between layers or pores in the printed or connected layers **(Figure 3.17 C)**. The multi-cylinder printed device possesses some additional extensions above the top layer that can be treated after printing **(Figure 3.17 D)**. The SEM results show that the FDM Ultimaker^{2+} printer provides 3D objects with uniformly distributed layers and lacks any pores.

Table 3.3 The modified 3D printing parameters for both PLA designs (cylinder and multi-cylinder).

Printing parameters	Cylinder
Wall thickness (mm)	0.8
Layer height (mm)	0.1
Top/bottom thickness (mm)	0.8
Printing speed (mm/second)	20
Printing Temperature (ºC)	190
Building plate Temperature (ºC)	50
Infill (%)	100
Supporting materials	No
Adhesion	No

3.4.1.2 Measurements of the Printed Devices with Simple Geometries

Table 3.4 The printed devices with the PLA polymer for A) the cylinder and B) multi-cylinder design (n=3).

A)

	DM (mm)	DF (mm)	HT (mm)
1	4.99	5.29	2.95
2	5.00	5.23	2.77
3	4.96	5.37	2.93
Average ± SD	4.98 ± 0.0	5.30 ± 0.1	2.88 ± 0.1

B)

	Upper part (mm)		Lower part (mm)		
	DM	**HT**	**DM**	**HT**	**DF**
1	3.25	3.02	5.03	2.95	5.32
2	3.29	3.23	5.04	2.84	5.24
3	3.22	3.04	5.03	2.90	5.36
Average ± SD	3.25 ± 0.0	3.10 ± 0.1	5.03 ± 0.0	2.90 ± 0.1	5.31 ± 0.1

DM, Diameter of the printed device from the middle, DF, Diameter of the first layer that contact to the printable build plate, HT, Height

Table 3.4 presents the measurements of the printed prototype devices for both designs using the 0.4 mm printing nozzle and PLA loaded thread. The original measurements of the cylinder design were 5 mm in diameter and 3 mm in height. The measures for the second design were 3 mm in diameter and 3 mm in height for the top part. The bottom part was 5 mm in diameter and 3 mm in height.

The results revealed that the designed and printed objects presented no substantial differences. The difference can be controlled through an alteration of the printing parameters, and nozzle sizes. We found in this experiment that the resolution of the printing objects was improved by decreasing the printing speed and using smaller nozzles. We succeeded in printing both primary designed 3D objects with the FDM 3D printer. Therefore, the Ultimaker^{2+} was selected, and various ear prototype devices were designed and printed with the Tinkercad software.

3.4.1.3 Thermal analysis of the FDM Printing Filaments

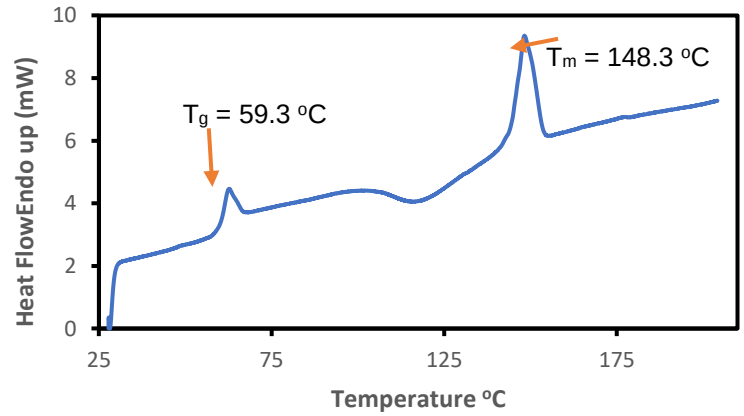

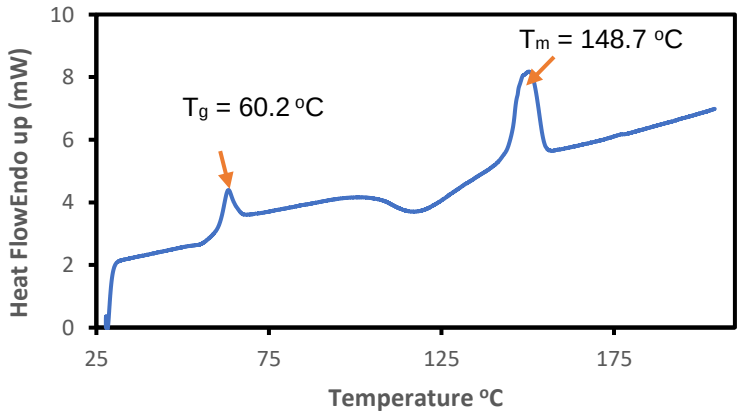

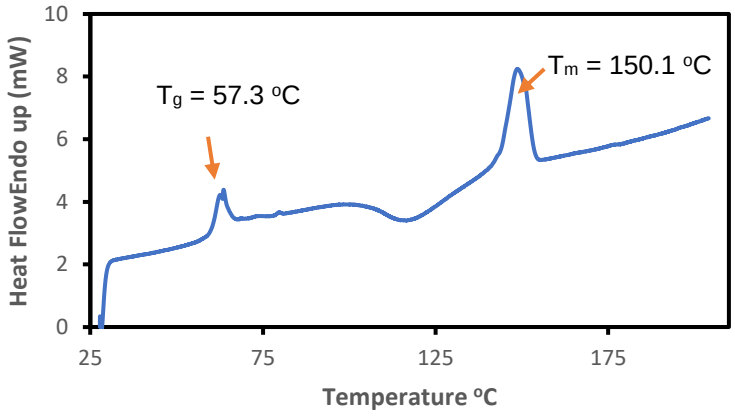

Figure 3.18 DSC thermogram of the PLA 3D printing Ultimaker filament. (The endotherm upwards in the thermogram) n=3.

Table 3.5 The DSC thermogram results of the PLA commercial filament (n=3).

Sample	Tg (°C)	Tm (°C)
Run 1	59.3	148.3
Run 2	60.2	148.7
Run 3	57.3	150.1
Mean ± SD	58.9 ± 1	149.01± 0.8

It is important to characterise the utilised polymer and record its T_g and T_m, because, the quality of the 3D printing is negatively affected if the applied temperature is too low or too high in relation to the T_g and T_m of the polymer. Consequently, the head temperature needs to be adjusted in accordance with the T_m of the used filament to ensure melting/softening but not degradation. **Figure 3.18** shows the DSC thermal results of the commercial PLA sample. The T_m, T_g, and broad crystallisation peaks can be observed in the DSC thermogram [280], [281]. The first event that was seen is the T_g at an average of 58.9 ± 1℃, close to what is reported in the literature (60-65℃) [282]. The second

observed peak is an exothermic transition peak at around 118℃. This crystallisation process is related to the exothermal self-nucleation of the crystalline phases that happen after the T_g temperature [280]. Also, this value is within the range previously reported (111-147℃) [281]. The final detected peak is an endothermic peak at 149℃, which is the T_m. The detected temperature is somewhat less than that stated in some studies, which are 166.7℃ and 157℃, respectively [280], [281]. These differences may be due to the additive materials used with the PLA commercial filaments to promote good printing properties. They may also be due to the prior heat treatment produced by the extruder [281], [283].

3.4.1.4 Morphological Changes of the FDM Printing Filaments

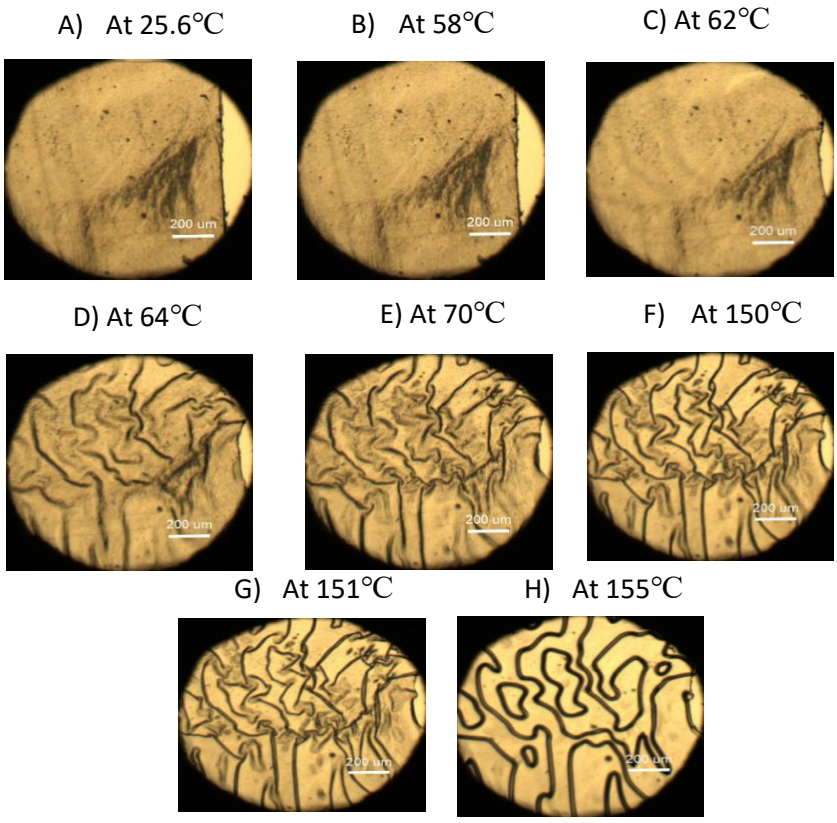

Figure 3.19 The optical images of the PLA commercial filament at various temperatures starting from room temperature up to the 155℃ using HSM.

Figure 3.19 shows the bright-field images of the commercial PLA filament sample during the ramp cycle using 4x magnification. The HSM experiment demonstrated the morphological changes of the PLA microlayer from room temperature up to 160℃. The PLA commercial

filament rod was cut into thin microlayers. Then, it was placed between two glass coverslips to make sure that the heat spread equally throughout the PLA sample and to facilitate the observation of the morphological changes of the PLA polymer.

The T_g of the PLA sample was detected at 58℃ **(Figure 3.19 A),** and then the sample continued to change in morphology until the temperature reached 70℃ **(Figure 3.19 B-E)**. After that, the Tm was detected at 150℃ **(Figure 3.19 F)**, and the sample morphology continued to change until the PLA microlayer wholly melted at 155℃ **(Figure 3.19 F-H)**. The T_g and T_m results are consistent with those obtained from the thermal analysis study of the PLA using DSC. It is difficult to detect the changes if the PLA rod is cut as a large irregular particle. Subsequently, we moved to more advanced ear prototype devices, as seen in **Figure 3.20**. The parameters used to print those devices are Presented in **Table 3.5.**

3.4.2 Advanced 3D Printed Ear Prototype Devices

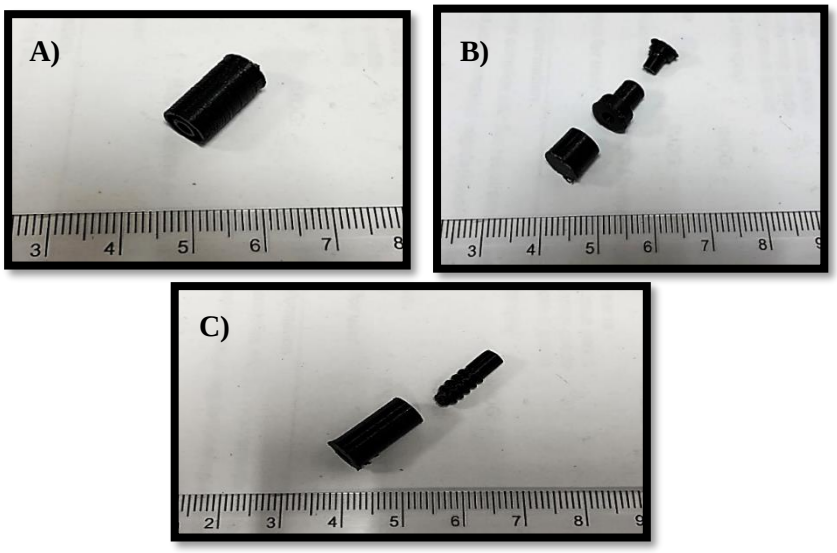

Figure 3.20 The photographs of the PLA 3D printed ear advanced prototype devices created using the 3D Ultimaker^{2+} FDM printer. A) Hollow cylinder design, B) ear tablet design, and C) screw design. The adjusted printing parameters are shown in Table 3.6.

Table 3.6 The 3D printing parameters for the FDM 3D printed advanced ear prototype devices

Printing parameters	All designs
Wall Thickness (mm)	1.05
Layer Height (mm)	0.1
Top/Bottom Thickness (mm)	0.8
Printing Speed (mm/second)	30
Printing Temperature (ºC)	190
Building Plate Temperature (ºC)	10
Infill (%)	100
Supporting Materials	No
Adhesion	Brim

Table 3.7 The differences in dimensions between the designed and printed advanced ear prototype devices.

Designs			Designed		Printed	
			Diameter (mm)	Height (mm)	Diameter (mm)	Height (mm)
Hollow cylinder	Inner cylinder		3.8	17	3.78	15.30
	Outer cylinder		7.5		7.47	
Ear tablet	Top	Top cylinder	5	2	5.15	2.05
		Bottom cylinder	3	4	3.08	3.95
	Middle	Top	5	6	5	6.02
		Bottom	7	3	7.06	2.97
	End		7	7	6.99	6.95
Screw	Top		3.95	5	4.17	5.68
	screw		3.95	9	4.17	9.04
	Hollow cylinder		7	15	6.99	14.95

- The data not shown

Figure 3.20 shows the suggested advanced ear prototype devices after printing with the FDM 3D printer. The measurements of the printed devices can be found in **Table 3.7.** The measurement results of the printed devices' heights and dimeters also revealed that the designed and printed objects presented no substantial differences dimensions. The difference can also be controlled through an alteration of the printing parameters. The idea in this part is to design and print an ear prototype device that can in future

incorporate a gelling system that contains an anti-inflammatory drug to treat people suffering from AOE in the early stages of this disease.

In this part, we succeed in printing the suggested 3D advanced designs with the FDM Ultimaker^{2+} 3D printer. However, we found some limitations with those devices, which may affect patient compliance. Firstly, two of those prototype devices (hollow cylinder design and screw design) lack venting systems that can be used to release ear pressure within the patient's ear canal during the insertion of the ear devices and also pushing the gelling system that contains the medication **(Figure 3.20 B and C).** Thus, using vent systems would help to release the air pressure within the patient's auditory canal and make it equal to the ambient air pressure of the external ear [284]–[286]**.** Secondly, the loaded hydrogel can only be passed from the front section of the designed devices **(Figure 3.20)**. The released hydrogel may affect a portion of the patient's ear rather than the whole affected area. Also, when the whole loaded hydrogel passes through the devices, it may block the ear canal. Consequently, it may affect the hearing of treated patients. Yang et al. developed a DDS (a gelling system, antibiotic drug, and chemical penetration enhancer) that can be applied locally to the area near the TM through the ear canal to deliver the antibiotic drug (ciprofloxacin) to the middle ear through the TM layers. Thus, it can be used to treat middle ear OM. They found that the gelling system that they used, as well as any existing ear wax, may produce hearing loss. In addition, they found that the injected hydrogel may take three weeks to be fully biodegraded [287].

After the PLA was used to print the ear prototype devices, we decided to move to rubbery materials, such as TPU and flexible resin, to print several of the suggested advanced designs to investigate whether using polymers with rubbery characteristics are better than solid polymers. The idea in this part is to use soft materials to avoid any problems that may occur with the solid polymers, such as scratches on the skin wall or pain. The FDM (Ultimaker^{2+}) was employed to print the hollow cylinder device,

as shown in **Figure 3.21 A & B**. The printing steps and printing parameters are detailed in **section 2.4.1** and **Table 3.8**.

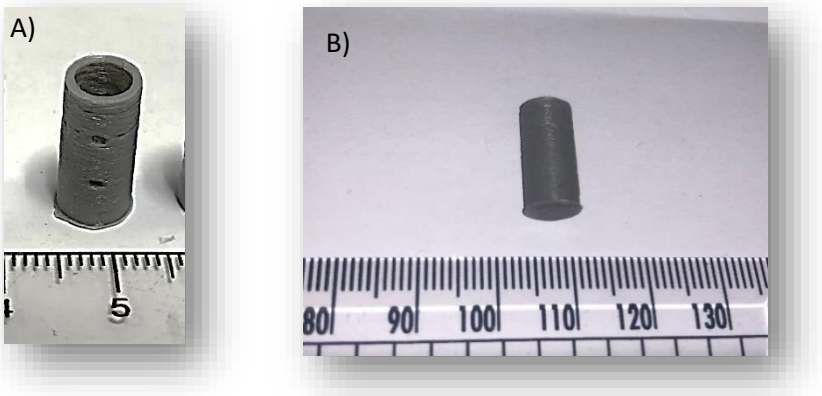

Figure 3.21 Photographs of the TPU printed prototype ear devices produced by an Ultimaker^{2+} FDM printer; A) with pores and B) without pores. The adjusted printing parameters were shown in Table 3.8.

Table 3.8 The 3D printing parameters for the FDM 3D printed ear prototype devices using TPU polymer.

Printing parameters	TPU Hollow Cylinder
Wall Thickness (mm)	0.06
Layer Height (mm)	0.1
Top/Bottom Thickness (mm)	0.8
Printing Speed (mm/second)	10
Printing Temperature (°C)	230
Building Plate Temperature (°C)	60
Infill (%)	20
Supporting Materials	No
Adhesion	Brim
Nozzle (mm)	0.25

Also, an SLA printer (Formlabs 2) was employed to print the hollow cylinder device, as shown in **Figure 3.22**. The printing steps are detailed in **section 3.2.3.2**. The printing parameters were set according to the flexible resin polymer.

Figure 3.22 Photograph of the flexible resin printed prototype device by the Formlabs 2 SLA printer.

3.4.2.1 Morphological Observation of the Printed Layers

3.4.2.1.1 SEM

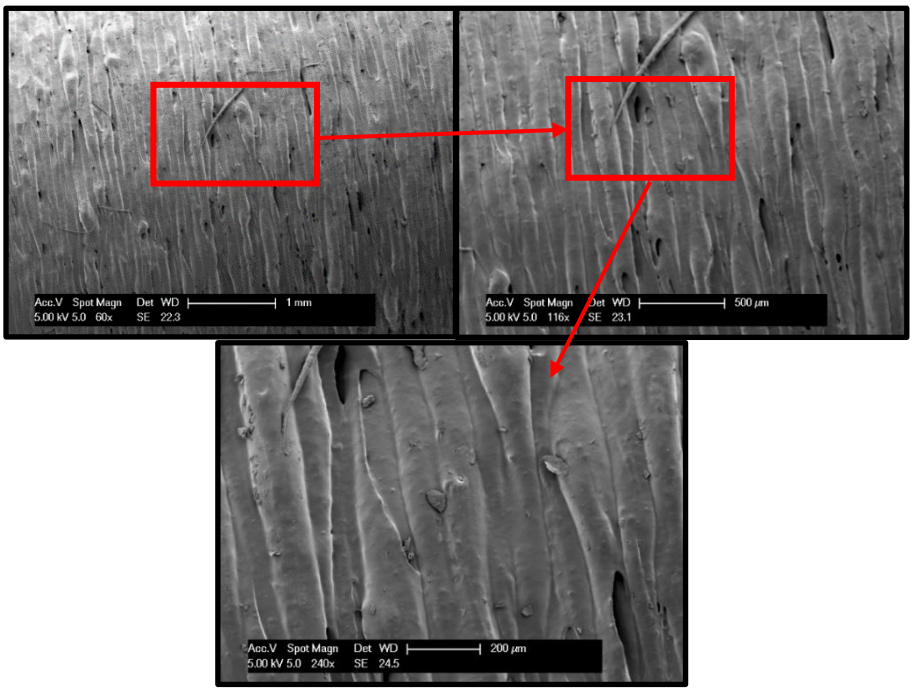

Figure 3.23 The SEM images of the TPU 3D printed prototype ear object produced using a desktop FDM Ultimaker^{+2} printer. The adjusted printing parameters are shown in Table 3.8.

Figure 3.23 presents the SEM images of the FDM TPU printed prototype ear object with various distances, including 1 mm, 500 µm, and 50 µm. The SEM images of this object display the printed layers of the TPU filament; further, these layers are connected. However, some overlap

between the printed layers. Also, there are some pores and extremities on the surface of the printed items.

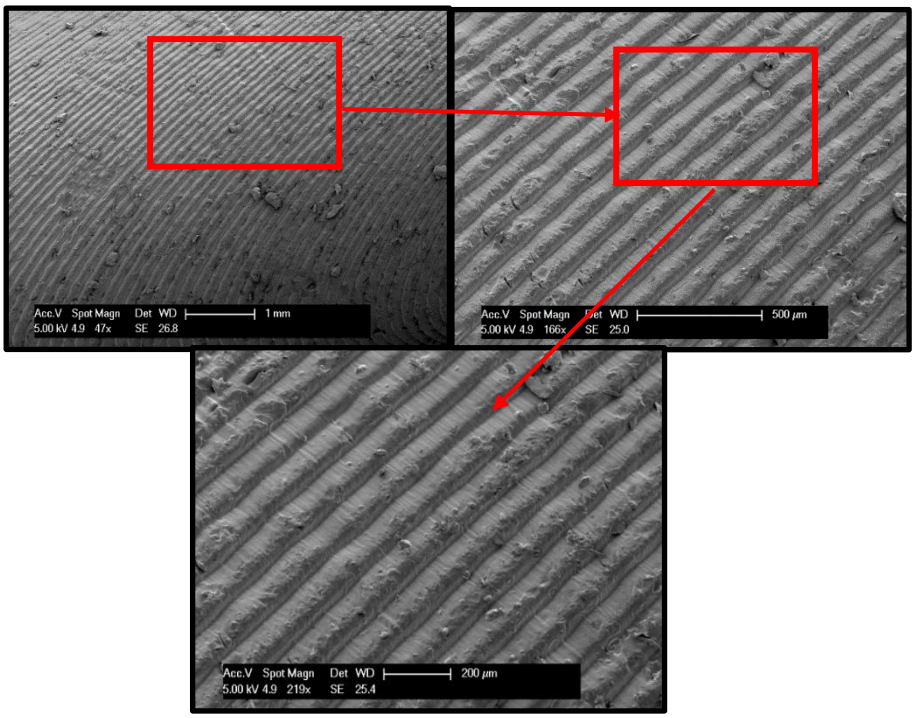

Figure 3.24 The SEM images of the flexible resin 3D printed prototype ear object with the desktop SLA Formlabs 2 printer.

Figure 3.24 presents the SEM images of the SLA flexible resin printed prototype ear object at different distances, namely 1 mm, 500 µm, and 50 µm. The SEM images of this object display the organised fabricated layers of the flexible cured resin; further, these layers are uniformly connected. Moreover, there is no overlapping between the cured resin layers. Also, some roughness is observed on the surface of the printed items.

3.4.2.1.2 Optical microscopy

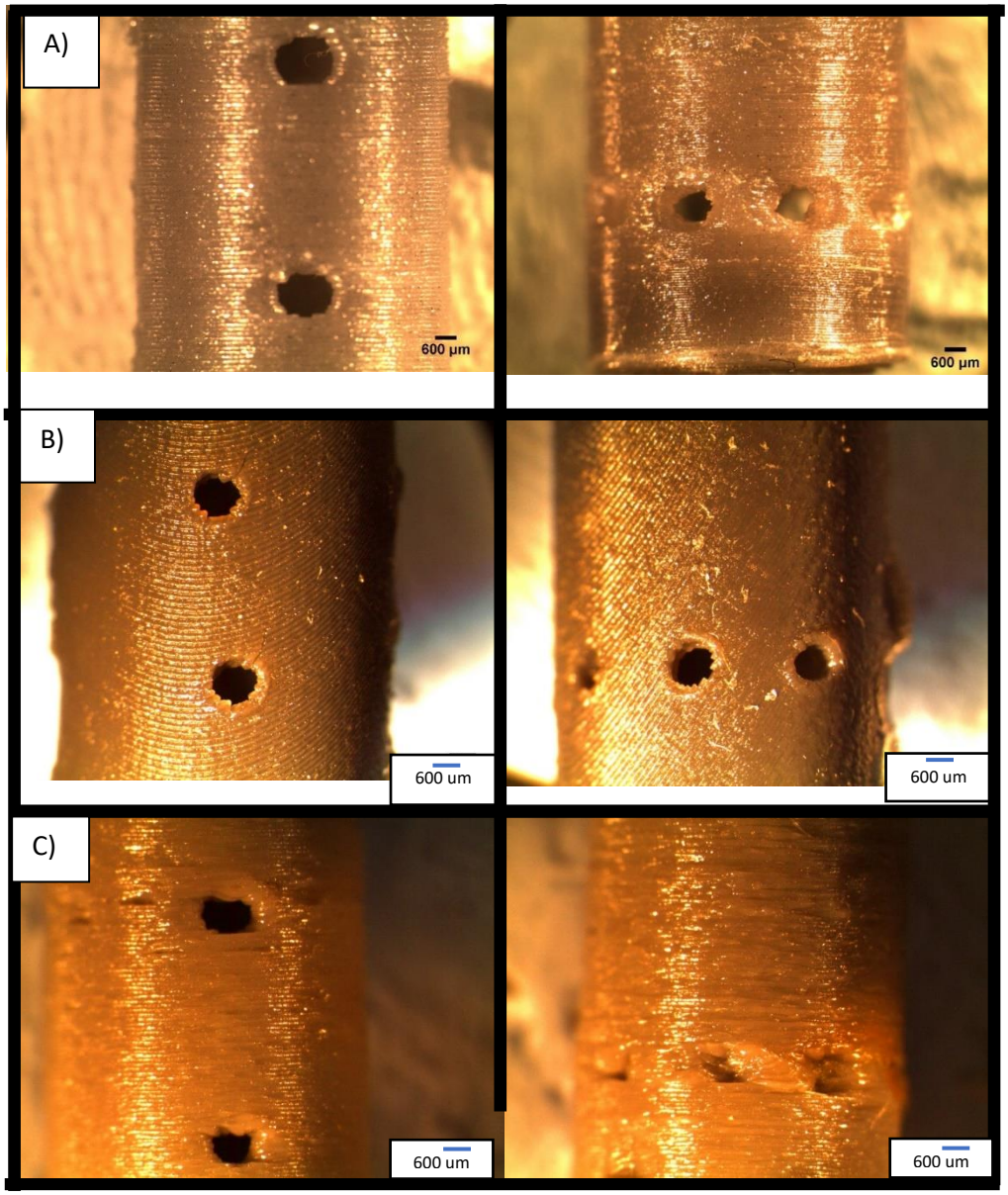

Figure 3.25 Optical microscope images captured with different magnifications of the different prototype 3D printed prototype devices. A) PLA, B) flexible resin, and C) TPU printed prototype devices.

Figure 3.25 shows the optical microscopy images of the printed devices made with different materials and printers, including PLA, TPU, and flexible resin. The results show that the TPU polymer failed to print the pores when they are near the device base; however, the pores were successfully printed using the other materials.

In this part, we found some limitations after using flexible resin and TPU materials. The TPU printed prototype device was cracked after it was squeezed multiple times (2-3 times). Meanwhile, the flexible resin printed device was directly cracked after it had been squeezed the first time **(Figure 3.26)**. Thus, the flexible resin printed prototype device was weaker than the TPU printed prototype device. Furthermore, the prototype ear devices made from soft polymers (TPU and flexible resin) may squeeze an incorporated gelling system with a loaded drug during the insertion into the patient's ears. This may affect the hearing of the patients because it can clog the ear canal. In addition, the printed devices could not prevent the swelling of the ear canal, because they were not hard enough in the late stages. Therefore, we decided to move forward to more hard material, namely the PLA polymer, to fabricate more sophisticated devices with similar ear canal designs, venting systems and enough solid characteristics to avoid any ear complications.

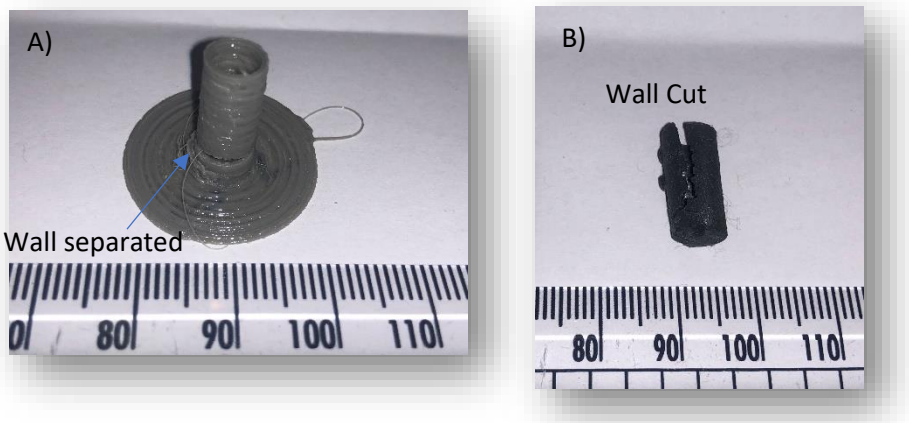

Figure 3.26 The A) TPU, and B) flexible resin printed devices with a crack in their walls after squeezing.

The human ear is a complex organ, and it has a unique ear canal shape. The canal size is different from person to person, as mentioned in the introduction section. Therefore, we decided to move to more complicated devices that have a design that mimics the inner shape of the human ear canal. The next part describes the devices that have designs similar to the inner ear.

3.4.3 Ear Prototype Devices with Complex Geometries Similar to Ear Canal

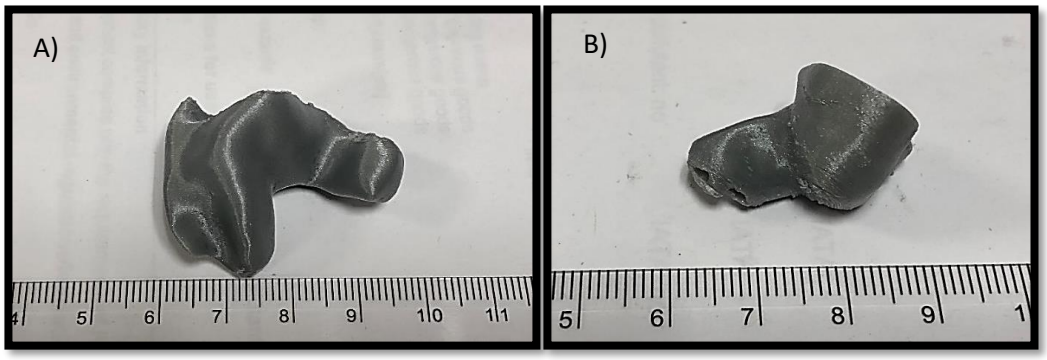

Figure 3.27 Photographs of the PLA FDM printed A) ear mould and B) hearing aid shell objects. The adjusted printing parameters are shown in Table 3.9.

At the beginning of this part, the idea was to print ear prototype devices that have a similar shape to the human ear's internal design. Therefore, an ear mould object was obtained from an online source, as detailed in **section 3.1.1**. The attained file was printed with the Ultimaker^{2+} commercial printer.

Usually, two techniques are utilised to measure the human ear canal dimensions. The first technique is scanning the ear impression. The produced file is then converted into a CAD system and printed with 3D printing technology [288], [289]. The ear impression creates a 3D image of the external ear. It can be produced by the following steps. First, the patient's ear needs to be examined via otoscopy to find any abnormalities or inflammations, whether in the canal or the TM. Then, the canal needs to be cleaned of any cerumen or debris. After that, the otoblock, which is made from cotton or foam, is prepared and placed beyond the second bend as close as possible to the TM. Subsequently, the impression materials are mixed and inserted into a proper syringe to be injected to cover the inner area of the canal until the otoblock. Then, the patient needs to wait until the injected materials are cured for about 6 minutes. Finally, the ear impression is removed [290].

The second method uses a digital Oto-scan device. This method is very new. The Oto-scan device can be used by a specialist to measure the inner canal dimensions of the human ear. Then, the collected data are transferred to CAD software, and the produced file can be modified and printed using 3D printing technology [291], [292]. The FDM Ultimaker^{2+} was employed and loaded with the PLA thread (silver colour), and it was passed through a 0.4 mm nozzle to fabricate the downloaded files, as illustrated in **section 3.2.2**.

Figure 3.27 describes the FDM ear mould item. The ear mould object was selected as a complex structure to be printed using 3D printing technology (FDM) to determine which printer provides good morphological resolutions. Also, the ear mould object mainly describes the internal cavity shape and features of a human ear. Additionally, the ear mould object can be modified by any available CAD software to design different types of hearing aid shells to incorporated with the hearing aid components and used for hearing impaired patients. The printing parameters of this object are given in **Table 3.9**. The ear mould object was successfully printed using Ultimaker^{2+} 3D printer.

Table 3.9 The 3D printing parameters for the FDM 3D printed ear mould object.

Printing Parameters	Ear Mould Design
Wall Thickness (mm)	0.8
Layer Height (mm)	0.1
Top/bottom Thickness (mm)	0.8
Printing Speed (mm/second)	50
Printing Temperature (ºC)	190
Building Plate Temperature (ºC)	10
Infill (%)	100
Supporting Materials	No
Adhesion	No

3.4.3.1 Morphological Observation of the Printed Layers

3.4.3.1.1 SEM

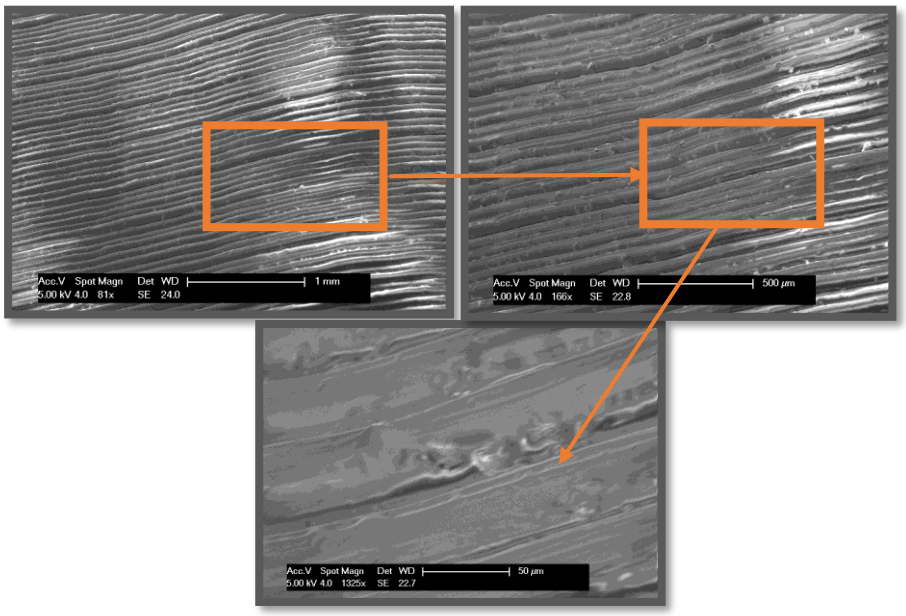

Figure 3.28 SEM images of the PLA printed ear mould object made with the FDM Ultimaker^{2+} printer. The adjusted printing parameters are shown in Table 3.9.

Figure 3.28 represents the SEM images of the FDM printed ear mould. The SEM images display the organised printed layers of the PLA filament; further, these layers are uniformly connected, and there is no overlapping between each layer. Moreover, there are no pores evident on the surface of the printed object, which indicates that the printer gives a proper resolution of the printed materials.

Therefore, we also employed the Ultimaker^{2+} to fabricate a hearing aid shell file, and we succeeded in printing the hearing aid shell attained file **(Figure 3.27)**. The utilised printing parameters are the same as illustrated in **Table 3.9.** Then, the CAD file of this downloaded object was modified by creating different pore sizes, in two different shapes (circular and square shapes), as noted previously. The idea was to investigate whether the printer had the quality to provides the same dimensions of the designed shapes.

Currently, commercially available hearing aid devices are manufactured using two different 3D printing technologies, namely SLS and SLA. In the SLS 3D printing process, a powder material, such as nylon powder, is utilised to fabricate the hearing aid shells layer by layer. This manufacturing process is explained in chapter 1, section 1.4.1.2. However, in SLA 3D printing technology, a photoreactive acrylic liquid resin is photocured by a UV laser to build the hearing aids shells layer by layer. This fabrication process is explained in chapter 2, section 2.6.2.2. The hearing aid shells that manufactured by the SLA printing procedure had a slightly smoother finish than those shells fabricated by the SLS printing procedure. The smoother surface is due to the fact that the powder has a more discontinuous nature than liquid resin. The thickness of each layer printed by the laser process is typically 0.1-0.25 mm. The thinner the printed layer, the smoother the primary hearing aid shell surface [293]. The layer in our model printed by the FDM 3D printer is 0.8 mm. The laser printers manufacture hearing aid shells with thinner layers than the FDM. Both printing technologies, namely the laser and the fused deposition technologies, provide printed objects with smooth surfaces.

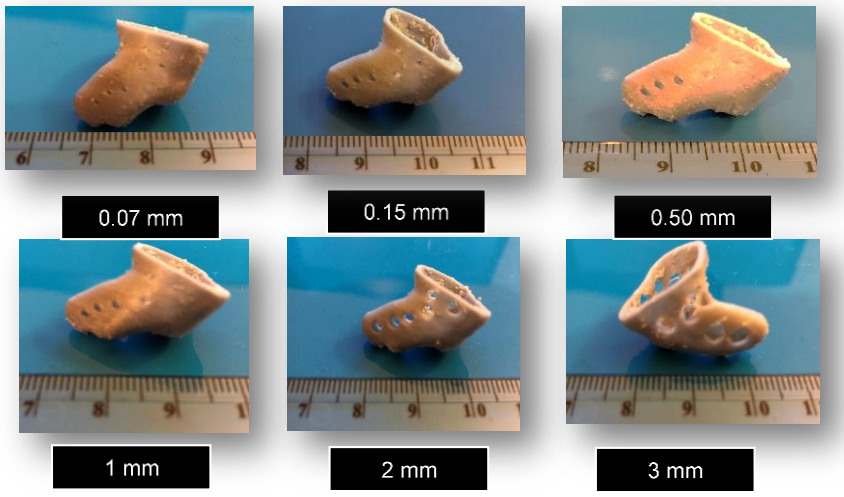

Figure 3.29 Photographs of the PLA printed hearing aid shells with different sizes of circular pores, at 0.07, 0.15, 0.50, 1, 2, and 3 mm in diameter. The adjusted printing parameters are shown in table 3.10A.

We succeeded in printing the hearing aid shells with circular and square pores with the different pore dimensions as noted **(Figure 3.29, and 3.30)**. The Ultimaker^{2+} was used to print the hearing aid shells containing the different pore sizes and shapes, as noted. The printing parameters are presented in **Table 3.21.** The manufactured objects have good morphological resolutions. The manufacture parameters are illustrated in **Table 3.10 A.**

The infill percentage, build plate temp, and printing temp were 100%, 10℃ and 190℃, respectively, for all printed shells. Also, the utilised plate adhesion type was the brim. The smallest pore size printed by the printer was 0.07 mm in diameter, and the printed shells had good morphological quality, especially for the smallest pore sizes.

Table 3.10 The 3D printing parameters for the FDM 3D printed HA shell.

Printing parameters	A) HA shell circular pores	B) HA shell square pores
Wall Thickness (mm)	1.05	1.05
Layer Height (mm)	0.06	0.1
Top/Bottom Thickness (mm)	0.72	0.8
Printing Speed (mm/second)	20	50
Printing Temperature (ºC)	190	190
Building Plate Temperature (ºC)	10	10
Infill (%)	100	100
Supporting Materials	No	No
Adhesion	No	No

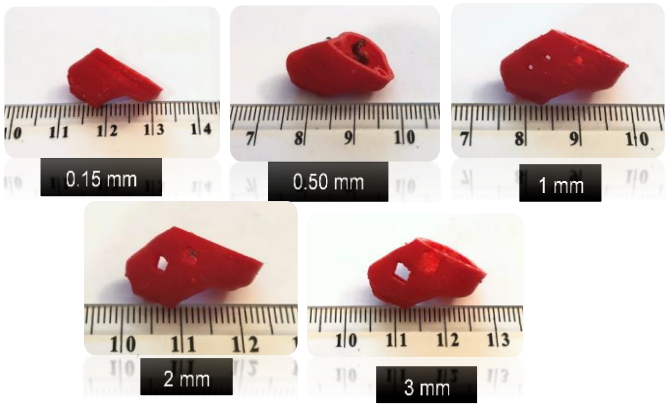

Figure 3.30 Photographs of the PLA printed hearing aid shells with different sizes of square pores without supporting material mode, with pore side lengths of 0.15, 0.50, 1, 2, and 3 mm. The adjusted printing parameters are shown in Table 3.10B.

In this part, the hearing aid shell CAD file was modified by creating square pores of different sizes, as noted above. We aimed to compare the ability of the printer to print the square shape and find the smallest pore sizes that could be printed and compare this with printed circular pores. The printed square objects were fabricated with the printing parameters shown in **Table 3.10B**. The fabricated shells with small pore sizes were clogged, as seen in for the 0.15 mm pore sizes. The printed objects had a proper resolution in shape**,** and the smallest square pore size that was printed was 0.50 mm in diameter **(Figure 3.30)**.

In this experiment, it is essential to leave adequate space between the designed pores to facilitate the printer in depositing the layers without affecting the shape or dimensions of the nearby pores. The pores may merge if they are too close to each other. Moreover, the morphological shape of the printed devices with small pore sizes (0.15 mm, and 0.50 mm, 1 mm) were better than those printed with larger pores (2 mm and 3 mm). In addition, the supporting materials built within the 3D printed hearing shells had square pores 3 mm and 2 mm in sizes. However, this did not affect the smaller pore size (1 mm, and 0.50 mm) **(Figure 3.31).** Finally, selecting a proper orientation of the 3D objects during the optimization with the CAD software is essential. Consequently, the printed items' shapes were not affected **(Figure 3.32)**.

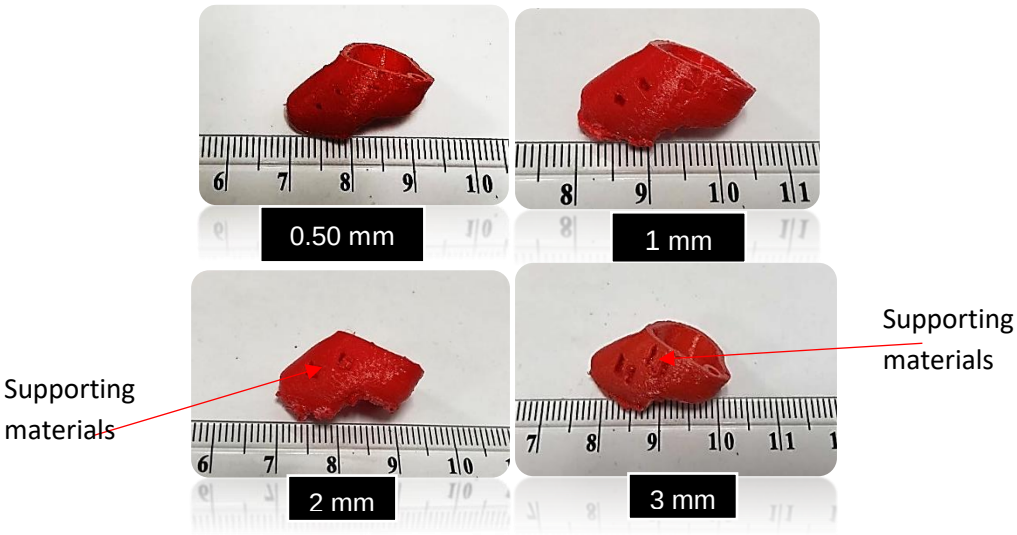

Figure 3.31 Photographs of the PLA printed hearing aid shells with different sizes of square pores in the supporting material mode, at 0.50, 1, 2, and 3 mm per side. The adjusted printing parameters are shown in Table 3.10.

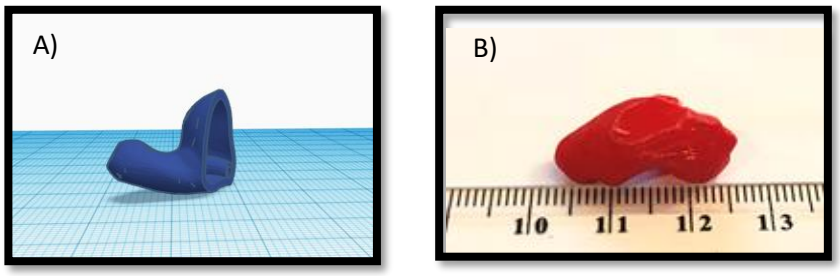

Figure 3.32 A) Hearing aid shell oriented on the side with Tinkercad online software, and B) photograph of the PLA printed hearing aid shell showing a defect in the wall. The adjusted printing parameters are shown in Table 3.10.

3.4.3.1.2 Optical Microscopy of the 3D Printed Pores

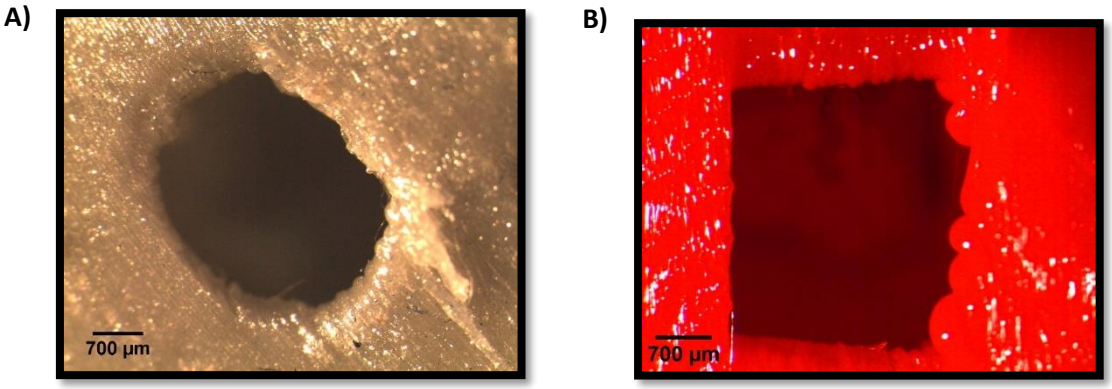

Figure 3.33 Optical microscopy images for different PLA 3D printed prototype devices with different shapes; A) circular pore (3 mm in diameter), and B) square pore (3 mm per side). The adjusted printing parameters are shown in Table 3.10 A and B.

This experiment was conducted to determine whether the used FDM printer could fabricate the devices with the same pore dimensions as the design. Different hearing aid shells were printed with different circular pore sizes, as noted. After that, the optical microscope was utilised and manually calibrated to capture different images under 2x magnification**.** Then, the captured images were analysed using the ImageJ software.

Figure 3.33 photographs of A) circular pore (3 mm in diameter), and B) square pore (3 mm per side). The other sizes for both shapes can be found in the **index section**.

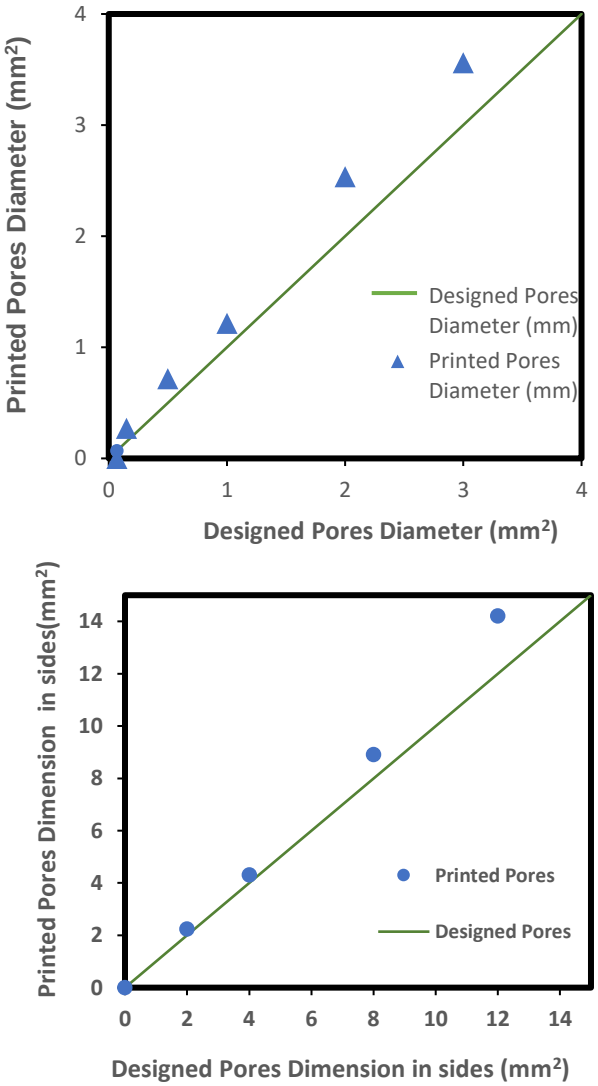

Figure 3.34 Diagram of the printed and designed circular pores dimensions (top) and square pore dimensions (bottom). The straight line of both figures represents the dimensions of the designed pores.

Figure 3.34 shows the diagram of the printed and designed circular and square pore measurements. There is a difference in sizes between the dimensions of the fabricated and designed pores, and these differences increase with increasing pores sizes for both designs. The printed shell designed with a 0.07 mm circular pore size was printed without pores. However, the printed shells developed with 0.07 mm and 0.15 mm square pores were printed without pores. Finally, the 1 mm pores for both shapes (square & circular) were selected and reorganised within the hearing aid shell. They were distributed at the beginning of the shell to cover the beginning of the canal area. The developed device consists of a cap and a hearing aid shell with different pore shapes and numbers. The first one is composed of 9 pores, while the second one comprises 8 pores **(Figure 3.35)**. The printing parameters that were utilised are shown in **Table 3.11**. However, with the square pores, an adhesion type was utilised to make the shell more adhesive to the building plate.

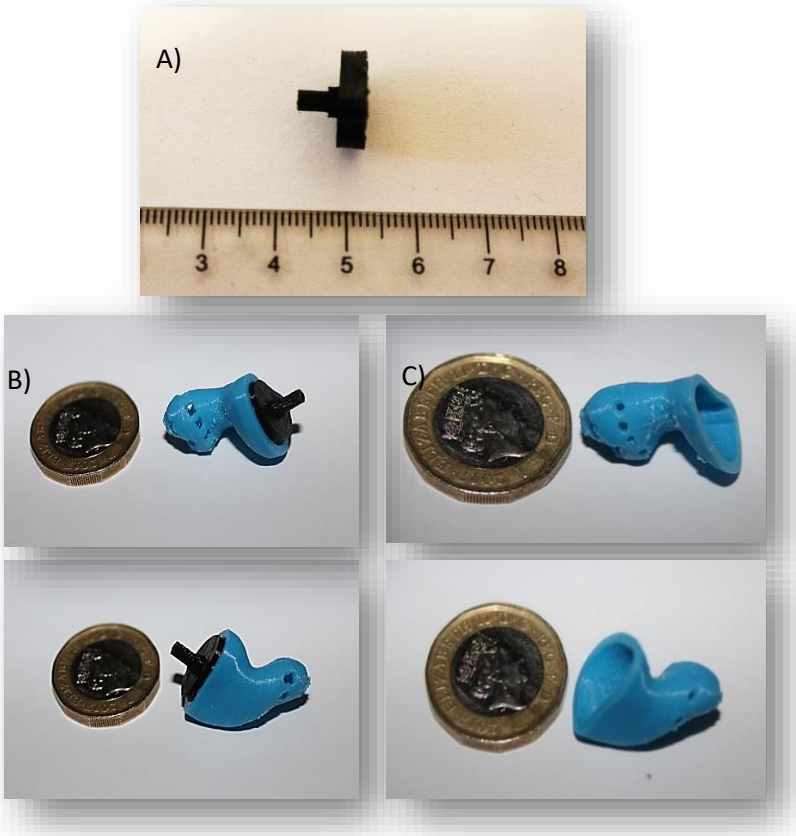

Figure 3.35 Photographs of the developed printed ear medical prototype device; A) the cap, b) the ear prototype device with square pores (1 mm per side), and C) the ear prototype device with circular pores (1 mm in diameter).

Table 3.11 The 3D printing parameters for the developed 3D printed ear prototype device and cap.

Printing parameters	Cap	Shell with circular pores
Nozzle (mm)	0.25	
Wall Thickness (mm)	0.88	
Layer Height (mm)	0.06	
Top/bottom Thickness (mm)	0.72	
Printing Speed (mm/second)	10	20
Printing Temperature (ºC)	190	
Building Plate Temperature (ºC)	10	
Infill (%)	50	30
Supporting Materials	No	Yes
Adhesion	No	No

The formulations of the different concentrations of the HPMC hydrogel system, their rheological properties, and their passing through the FDM printed circular pores are discussed in detail in the following chapter.

3.5 Conclusion

In this chapter, different ear prototype devices were printed with different 3D printers, namely the FDM Ultimaker^{2+} and SLA Formlabs 2, and different materials, namely PLA, TPU, flexible resin, and tough resin. The SEM images showed that the different ear prototype devices produced by the FDM 3D printer using PLA polymer had good morphological resolutions, and there were no overlaps between the printed layers. The optical microscope results of the printed shells pores showed that there were differences in the pore area between the designed and printed pores, and these differences increase with increasing pore sizes. We thus successfully developed 3D printed ear medical prototype devices. The work in this chapter is the first step towards further work in the dissertation. In the next chapter, we aim to formulate a hydrogel system and investigate the release of the created gelling system through the pores of the fabricated devices (1 mm in diameter) at room temperature and 37℃ to select the concentration that can pass slowly through the pores of the printed device.

Chapter 4 Investigation of the Release of Hydroxypropyl Methylcellulose Gelling System Through Different 3D Printed Ear Prototype Devices

4.1 The Novelty

In this work, various FDM 3D printing ear prototype devices with different circular pore numbers and locations are manufactured. In addition, the flow of various formulated HPMC hydrogels concentrations through the pores of the printed devices is studies.

4.2 Introduction

Hydrogels are a 3D configuration of water-soluble polymeric networks that can hold large quantities of water or biological fluids. Hydrogels can be produced from particularly any hydrophilic (water-soluble) polymer and involve a wide range of bulk physical properties and chemical compositions. Moreover, hydrogels can be prepared in different physical forms, including coatings, slabs, films, and microparticles [294]. Because of the ability of hydrogels to absorb a significant quantity of aqueous fluids, they mimic the natural structure of human body tissues, making them essential for biomedical applications, including artificial organ and contact lens design, diagnostics [295], tissue engineering [296] and importantly drug delivery [297].

Hydrogels are highly porous materials and can be easily modified by manipulating their cross-link density in the gel matrix and their aqueous fluid affinity. Furthermore, the porosity of the hydrogel system allows the loading of APIs into the gel matrix and the subsequent release of drugs at a rate dependent on the diffusion coefficient of small molecule or macromolecule APIs over the gel network [298]. There are several benefits in using this kind of dosage form for drug delivery, such as the hydrophilicity, biocompatibility, controlled API release, prolonged drug release at the site of action, easy formulation and modification, decreased systemic side effects, improved patient compliance by decreasing the frequency of daily dosing, targeted specific site of action, reduced daily cost to the patient due to reduced dosage, ability to be

injected, and the avoidance of extensive drug loss through the first-pass metabolism [297], [299]–[301]. Many literature reviews have discussed hydrogels in detail, including their classification, types, preparation, application, and release mechanisms [300], [302]–[304].

In this chapter, the HPMC polymer was selected because it is one of the most commonly cellulose ethers utilised as a gel-forming polymer. It has been reported in the literature that the HPMC polymer forms a hydrogel dosage form [305], [306]. HPMC is a very useful hydrophilic polymer in the formulation of controlled drug delivery preparations [307]. This polymer undergoes the phenomenon of thermoreversible gelation, which happens when the temperature of an HPMC solution is raised above a critical temperature known as reversible thermal gelation. In this phenomenon, the solution viscosity decreases when the temperature of the solution increases. However, as the temperature of the HPMC solution increases, the temperature of this solution undergoes a marked increase upon reaching the initial gelation temperature. Above the gelation temperature, the HPMC polymer chains associate through hydrophobic chains' interactions that occur between the methoxyl substituted groups [308]. The association of methoxyl substituted groups occurs as a result of the dehydration of the hydration sheath that is available around the methoxyl-rich regions of the cellulose backbone, in comparison with the other regions that contain low hydrophobic methoxyl substitution [309], [310]. The intermolecular hydrophobic methoxyl bonding regions form "junction zones" which result in the formation of the HPMC polymer chains 3D gelling networks [311], [312]. This gelation phenomenon also leads to the separation of phases, which is thermo-reversible at cooling [309], [310]. There are different grades of cellulose ether, and each one has a characteristic thermal gelation temperature range due to the relative balance of hydrophilic and hydrophobic substituents. A grade that has a high content of methoxyl substitution levels has in lower gel temperature, whereas a group that has a high content of hydroxyalkyl substitution has a higher gel temperature [311].

In our model, it is important to have a gelling system that can be loaded into the developed ear prototype device and also has the viscosity to stay within the printed device for the treatment regimen of OE, which is 7 days. Moreover, the gelling system needs to be released in small amounts to contact the canal wall and facilitate the drug reaching the inflamed area. It is important not to use a gelling system that can completely release after insertion into the ear canal because this might affect the patients' hearing by blocking the ear canal or affecting the movement of the eardrum.

As mentioned in **chapter 1**, the effective management of OE disease is through the use of locally acidifying solutions, local analgesics and/or antibiotic ear drops alone or in combination with steroid ear drops [214]. Although ear drops medications have many benefits, they also have several drawbacks. The ear drops require multiple daily dosing over 7-10 days. Also, OE patients need to lie on their sides with the affected ear up while administering their drops medications. Furthermore, the patients require someone else to provide their drops while they are lying down. Some studies showed that the effectiveness of the treatment could be increased by someone else applying the drops to the patients [215], [216].

Therefore, we ideally need a one-time application of a constant drug release system, which would decrease the requirement for multiple daily drug dosing and improve patient compliance. It could be beneficial to incorporate a gelling system with the API drug within a 3D printed ear prototype device to deliver the API at the site of action while maintaining the hearing of the patient.

The idea in this thesis is to develop a 3D printed ear medical prototype device with pores **(as detailed in chapter 3).** This device can be loaded with a gelling system (HPMC hydrogel) that can stay within the device, and it can be released from the printed device pores to contact the wall of the ear canal to prolong the release of the loaded drug **(see chapter**

5). Also, the loaded hydrogel can facilitate a constant drug release for the treatment period of AOE (7 days).

4.3 Aims and Objectives

This chapter investigates the release of different concentrations of HPMC hydrogels through several FDM 3D printed ear prototype devices with various pore numbers and locations. Rheometry is utilised to characterise the formulated HPMC hydrogels. Various rheological tests are performed, including amplitude sweep tests, frequency sweep tests and viscosity measurements. The Ultimaker^{2+} FDM 3D printer is utilised to fabricate several 3D printed ear prototype devices with different pore numbers and locations. The release of the prepared hydrogels through the pores of the printed device is investigated at two different temperatures (37℃) and room temperature (25℃). Finally, one of the investigated HPMC hydrogel concentrations is selected to be utilised in the next chapter as a vehicle to provide sustained drug release through the developed ear prototype medical device.

4.4 Experimental Section

All materials utilised in this chapter are illustrated in **chapter 2, section 2.1.**

4.4.1 Preparation of Different Concentrations of the HPMC Hydrogels

In the beginning, several hydrogels were prepared with different concentrations of the HPMC polymer, namely 1-7%, 9%, 10%, 15% and 20% (w/w). The detailed preparation steps are illustrated in **chapter 2, section 2.6.1.**

4.4.2 3D Printing of Ear Prototype Devices with Different Pore Numbers

In this part, different PLA printed devices were manufactured using the Ultimaker^{2+} 3D printer. The printed devices contained several circular pores, including one, three, and ten pores **(Figure 4.1)**. The designed pores were 1 mm in diameter. This method was utilised to investigate the release of the prepared samples through the printed pores and to

determine whether the flowing of the gelling system would be affected by changing the pore number, location, storage temperature and viscosity of the polymer. The detailed manufacturing steps are illustrated in **chapter 2, section 2.4.1.**

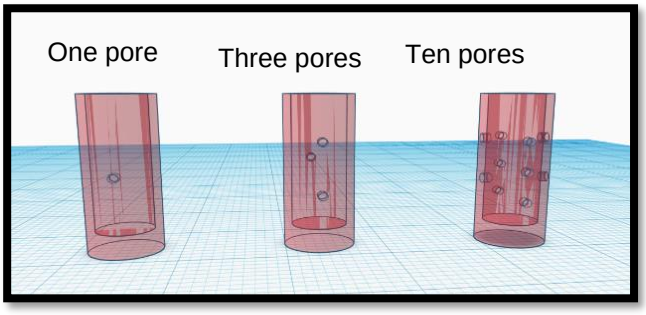

Figure 4.1 Schematic illustration of the FDM 3D printed prototype ear devices with circular pores. The printed devices contain various numbers of pores, including one, three, and ten pores 1 mm in diameter.

4.4.3 Characterization of the Prepared Hydrogels

4.4.3.1 Examining the Rheological Properties of the Prepared HPMC Hydrogels

An Anton Paar (MCR 302, Anton Paar, Germany) rheometer was used to study the rheological behaviours of the prepared HPMC hydrogels. Also, it was utilised to determine the formulations considered hydrogel systems, whereby the key characteristic of a hydrogel system is when the storage modulus (G') is more than the loss modulus (G''). Furthermore, the viscosities of the prepared HPMC hydrogels was determined to find the viscosity behaviour by increasing the shear rate. The software utilized to analyse the data was Rheoplus. The rheometer was equipped with a parallel plate (PP) geometry with a diameter of 25 mm to perform the rheological tests. This type of geometry was utilized with the HPMC formulations given in the literature [313], [314]. A freshly prepared sample from each hydrogel concentration was mounted carefully to the middle of a Peltier temperature-controlled plate using the correct plastic tool. Then, any trapped air bubbles were removed from the sample using a plastic dropper. After that, the upper plate of the

rheometer was lowered to a programmed point to provide a gap of 1 mm between the upper and lower plates. Then, the excess loaded amount of the mounted sample was removed from the edges of the upper plate rheometer. Different rheological tests were performed, namely the amplitude sweep (AS), frequency sweep (FS) tests, and viscosity measurements. Rheology is also known as the study of the deformation of a tested sample resulting from the application of a stress/strain [312].

A) Amplitude Sweep Test

The AS tests were conducted on the prepared samples (2-7% HPMC hydrogels w/w) to determine the linear viscoelastic region (LVER) of each sample, whereby the G″ and G′ remained on a constant plateau. The samples of hydrogels were exposed to increasing strain from 0.01% to 100% [315]. The temperature of the experiments was performed at 37℃. The measurements were made in triplicate for the prepared samples.

The rheological tests are performed within the LVER of the tested samples as the measurements needed to be independent of strain or stress [310]. The changes outside this linear region may be produced from the destruction of the tested sample by the rheometer (e.g. shear-thinning behaviour) [311].

B) Frequency Sweep Test

The frequency sweep test provides information about a sample's viscoelastic properties as a function of frequency [316]. The FS test helps to distinguish the tested sample into entangled solution, dilute solution, physical gels or chemical gels [317]. This experiment was performed in the LVER of the loaded sample. The FS tests of the prepared samples were performed over the range of 0.01 Hz to 10 Hz [318]. The FS experiments were conducted at 37 ^{o}C [315]. The strain was 0.1%. The tests were made in triplicate for the prepared samples. This method was utilised to find the behaviours of the tested samples by increasing the shear rate.

C) Viscosity Measurements

The flow curves were performed for the prepared samples. They provided the viscosity of the tested samples at defined shear rates. The shear rate was in the range of 0.01-1000 s^{-1}. The tests were made in triplicate for the prepared samples. This method was utilised to find the differences between the viscosities of the tested samples.

4.4.3.2 Investigating the Passing of the Prepared HPMC Hydrogels Through the 3D Prototype Printed Device Pores

4.4.3.2.1 Investigating the Passing of the Hydrogels Through the Printed Pores at Room Temperature and 37℃

A) Devices Placed at Room Temperature (25℃ ± 0.5℃)

Briefly, several hollow cylinder prototype ear devices were designed with different circular pore numbers, including one pore, three pores, and ten pores, using the Tinkercad online software. Then, the designed devices were printed using the FDM Ultimaker^{2+} 3D printer **(section 4.3.2**). The printed pores dimensions were 1 mm in diameter, which was selected in **chapter 3** because it produced an acceptable morphological shape, and its dimension was closed to the designed model **(chapter3, section 3.4.3.1.2)**. Subsequently, different concentrations of HPMC hydrogels were formulated. The hydrogel preparation steps are detailed in **chapter 2, section 2.6.1**.

Afterwards, the prepared hydrogels were loaded by inside the printed ear prototype devices using a plastic syringe. Then, the top open part of each device was covered with a parafilm membrane. After that, the devices were cleaned on the outside by a proper tissue to remove the excess amount of sample from the walls of the devices. Then, each device was weighed using an electronic balance. After that, they were placed separately within a scintillation vial (20 mL) and placed on the top bench at room temperature (25 ± 0.5℃) **(Figure 4.2)**. Next, the devices were

weighed at different time points, namely 0.0833, 0.5, 1, 7, 10, 24, and 48 hours. The devices were cleaned each time before being weighed.

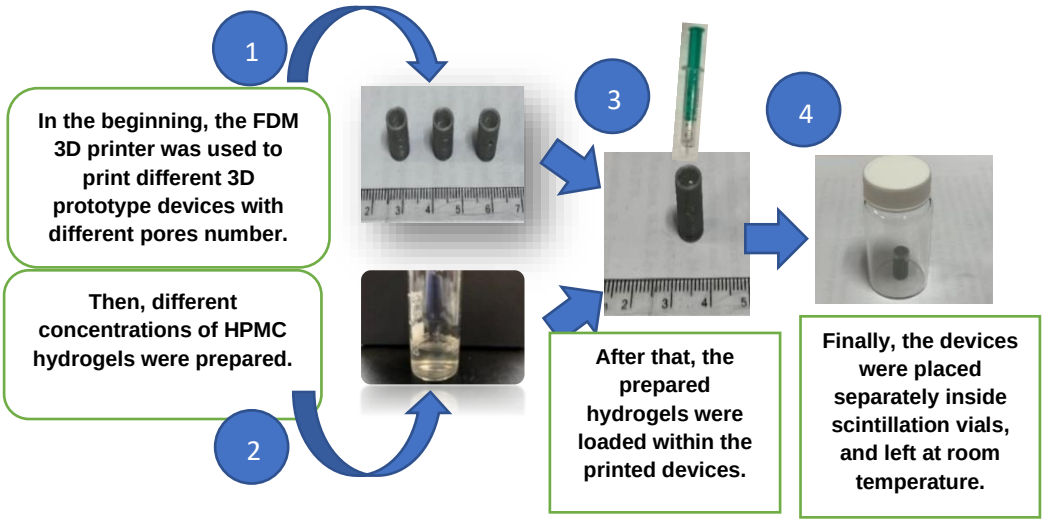

Figure 4.2 Schematic illustration of the preparation steps to study the hydrogels flowing through the pores of the printed devices at room temperature.

B) Devices Placed at 37℃

Based upon the analysis of the results at room temperature, different concentrations of HPMC hydrogels were prepared, including 4%, 6% and 7% of HPMC hydrogel (w/w). The same procedures as before, were done. However, each sample was placed within an incubator oven (Thermo Scientific Heratherm, Waltham, MA, USA) at 37℃.

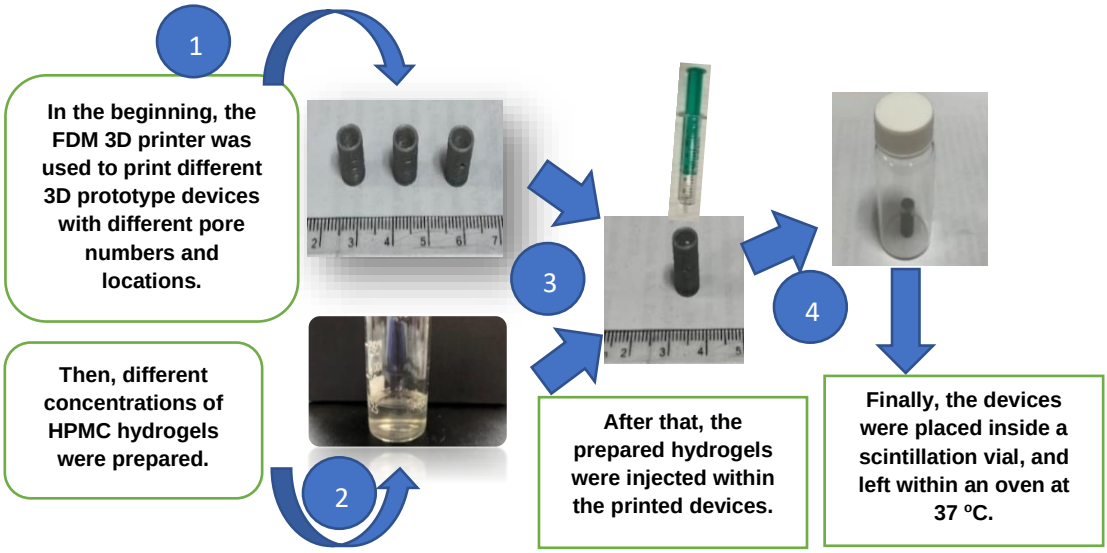

Figure 4.3 Schematic illustration of the preparation steps to study the hydrogels flowing through the pores of the printed prototype device at 37℃.

4.5 Statistics

Two-way ANOVA was employed in this chapter using the GraphPad Prism software (version 8.1.2) to analyse the results of the different concentrations of HPMC hydrogels that flowed through the printed devices with different pore numbers and at different temperatures (25℃ and 37℃).

4.6 Results and discussion

4.6.1 Hydrogels with Different Concentrations of HPMC

In this thesis, different concentrations of HPMC hydrogels were successfully prepared according to the preparation method outlined in **chapter 2, section 2.6.1. Figure 4.4** shows the different HPMC concentrations after their manufacture. The remaining results for the other concentrations are available in **the appendix section 4.A.** The formed gelling systems were colourless, not entirely clear, and contained some air bubbles.

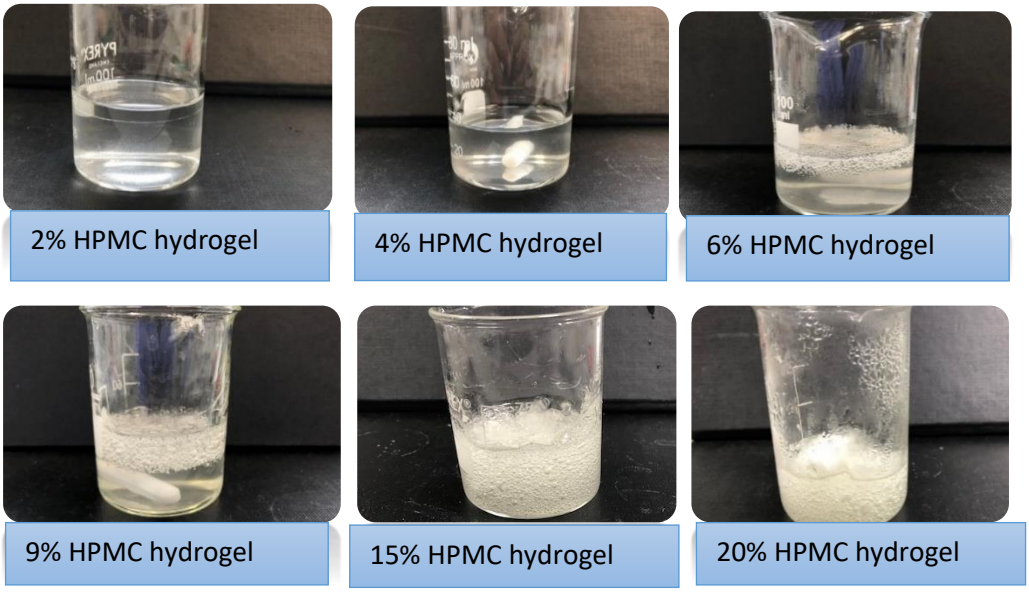

Figure 4.4 Photographs of the prepared HPMC hydrogels with different concentrations, namely 2%, 4%, 6%, 9% 15%, and 20% HPMC w/w.

Some challenges were faced during the preparation of the HPMC hydrogels. Several air bubbles were produced after the HPMC polymer was added to the heated water under stirring. The amount of formed air bubbles increased by raising the polymer contents and the magnetic bar speed rotations. The HPMC polymer needs to be added slowly to avoid any compact mass formation, which cannot be dissolved easily to form the gelling system. The prepared formulations were placed at - 4℃ in a refrigerator to remove the air bubbles from the gelling systems. **Figure 4.5** showed two different prepared concentrations of HPMC (6% and 7% HPMC (w/w)) after they were cleared of air bubbles.

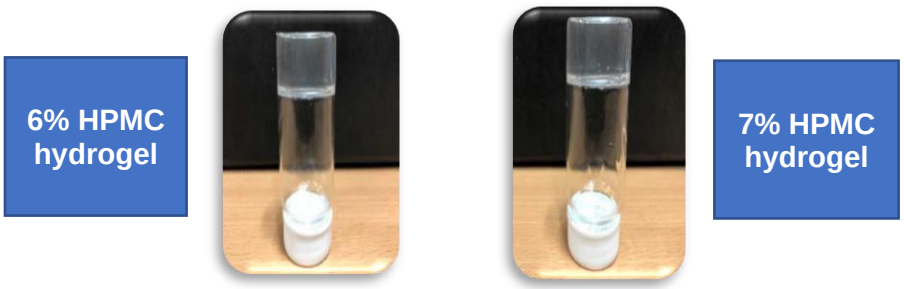

Figure 4.5 Photographs of the prepared HPMC hydrogels with 6% and 7% of the prepared HPMC hydrogels after being cleared of air bubbles.

In this experiment, it was found that the formulations with high concentrations of HPMC polymer took more time to be cleared of air bubbles than the formulations with the lower concentrations of the polymer. For example, the formulated HPMC concentrations with 1-4% HPMC hydrogels were cleared of air bubbles within 24 hours after stored in the refrigerator. In contrast, the concentrations with 5-7% HPMC hydrogels were cleared of air bubbles after two days' storage in the refrigerator. Also, we found that concentrations of more than 7% took more than two days to be cleared of the air bubbles. The forming of air bubbles in the formulations imply the viscosity of the formulated sample.

In this chapter, we select different HPMC concentrations (1-7% HPMC hydrogels w/w). The concentrations with more than the 7% HPMC were excluded because they formed many air bubbles and required more than two days to be cleared. Furthermore, the selected concentrations were within the water-soluble cellulose derivatives for hydrogels reported in the literature (1-10% by weight) [319]. The rheometer analysed the selected concentrations to determine their viscoelastic behaviours and their viscosities. Then, their flow from the 3D printed prototype devices with different pore numbers was investigated to find the proper concentration that can be loaded to the printed device developed in chapter 3. Also, the gelling system needed to be able to remain for the treatment period of AOE (7 days).

4.6.2 Rheological Characterisation of the Prepared Hydrogels

The rheological experiments were performed to study the effect of adding HPMC contents on the viscoelastic behaviours and viscosities of the selected concentrations (1-7% HPMC w/w). It is important to have a gelling system that can be loaded and stay within a 3D printing fabricated prototype device for an extended period **(section 4.6.3).**

The rheological analysis studies were carried out by measuring G″ and G′, as a function of strain, and frequency. G′ is defined as a measure of the elastic response of an object, and it measures the deformation energy stored by the tested sample during the application of shear. After

removal of the applied load from the tested samples, this energy is fully available, and it acts as a driving force for reforming or compensating for the previous deforming of the structure [316]. On the other hand, G″ is defined as a measure of the viscous response of an object, and it measures the deformation energy that is used up by the tested sample during the application of shear. The energy loss from the tested materials displays irreversible deformation behaviour [316]. As mentioned before, different rheological tests were performed on the selected formulations, including AS tests, FS tests, and viscosity measurements.

It is important to have a gelling system that is easy to clear of the air bubbles produced during the preparation procedure because they might affect the rheological analysis results. Moreover, it is also important to have a gelling system clear of air bubbles with a shear-thinning behaviour that can be easily injected into the fabricated ear prototype devices. Finally, it needs to have the proper viscosity, so it does not release fastly from the ear prototype devices **(section 4.6.4).**

4.6.2.1 Amplitude Sweep Test

The AS test is the first rheological experiment was performed on the selected concentrations of the HPMC formulations. This test was established to define the LVER for the tested samples. The AS tests were conducted at 37℃ and strain values ranging from 0.001 to 100%.

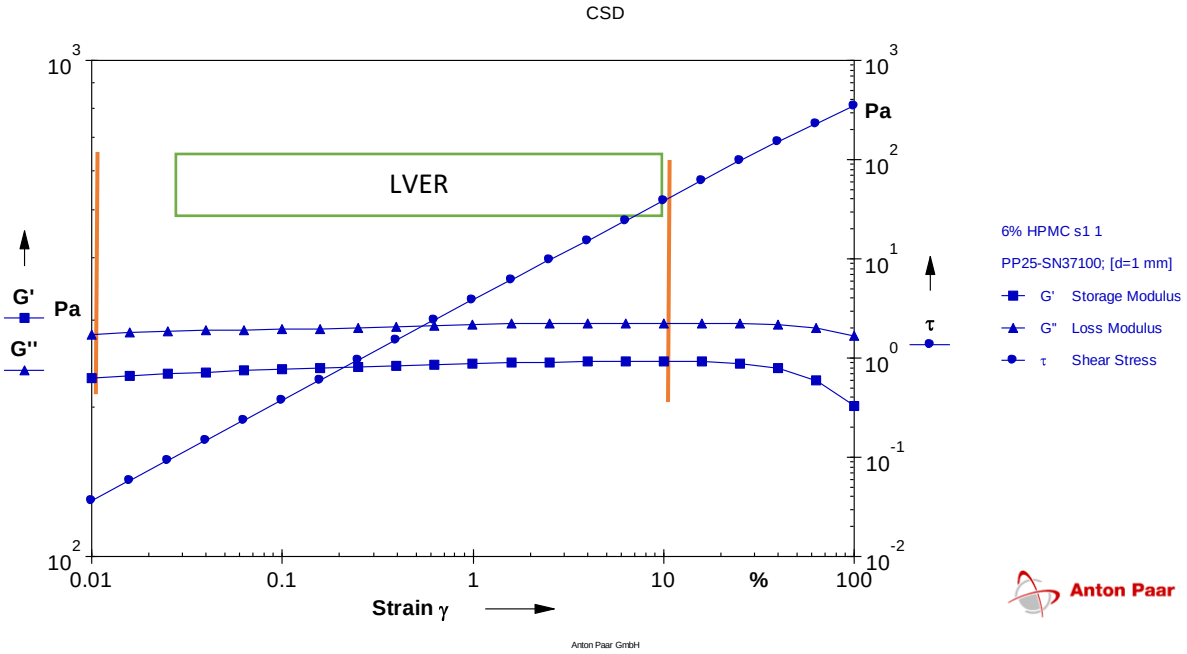

Figure 4.6 Dynamic amplitude sweep on a 6% w/w HPMC formulation sample with respect to G″ and G′.

Figure 4.6 represents the AS test graph for one of the formulated gelling systems, which is the 6% HPMC hydrogel. This figure shows a typical graph for the AS test results. The shear strain is compared against both moduli (G′ and G"), and the graph shows the LVER of the prepared formulation. This linear region where deformation occurred was not considered to damage the internal structure of the tested sample. The AS experiments were done for all the selected formulations (2-7% HPMC), and the results are illustrated in **Figure 4.7**. The LVER were found within the range of 0.01% to 10% of the shear strain for all samples. Moreover, all tested samples showed non-linearity starting at >10% of shear strain**.**

The results showed that both moduli (G′ and G″) were increased with increasing polymer (HPMC) concentration. Their decrease after the LVER may have resulted from the destruction of the tested samples. The formulation with 1% HPMC was excluded from the rheological analysis as it had very low viscosity, and this formulation may need to be tested with a concentric cylinder geometry, which is generally utilized for low viscosity systems. Moreover, it is a useful alternative geometry for testing

the viscoelastic properties of dilute solutions or suspensions due to their increased sensitivity afforded by the large surface area [320]. The yield stress of the G' values resulting from the tested hydrogels (2-7% HPMC w/w) was to be found approximately between the 20% and 30% strain.

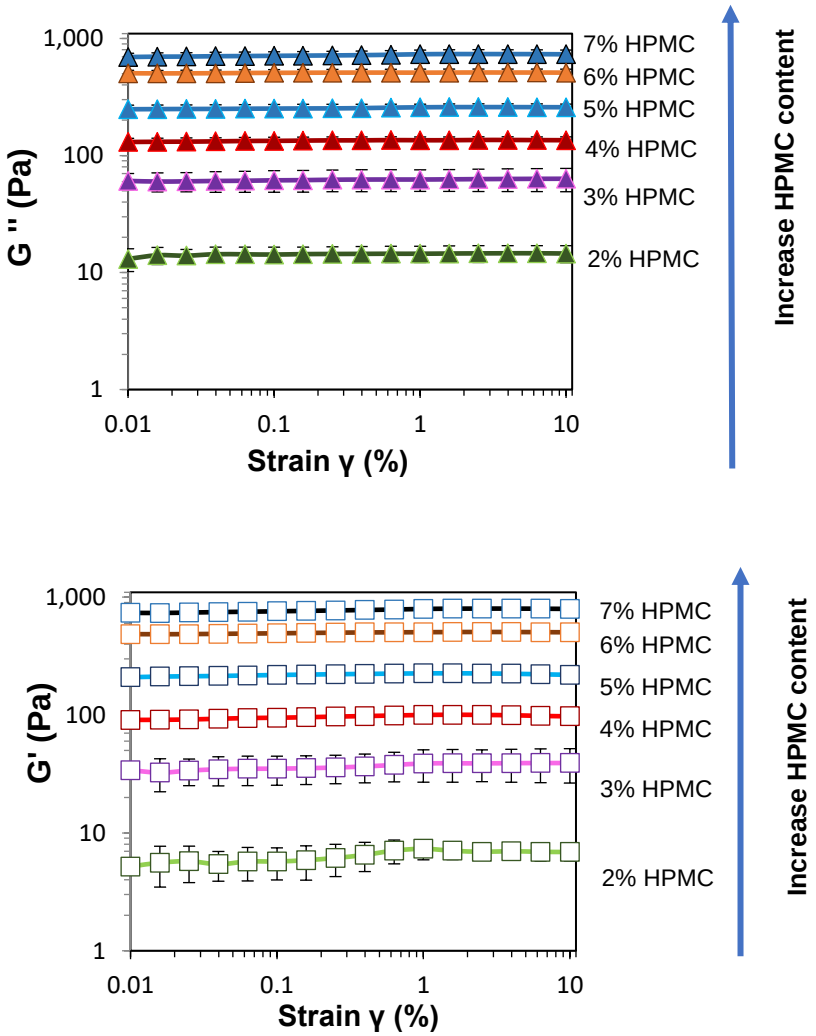

Figure 4.7 Dynamic amplitude sweep test of the prepared hydrogels with different concentrations of HPMC, namely 2-7% (w/w).

4.6.2.2 Frequency Sweep Test

Frequency sweeps are oscillatory tests that are conducted at variable frequencies, a constant amplitude value, and a controlled temperature [316]. All experiments were conducted at 37℃ for all samples.

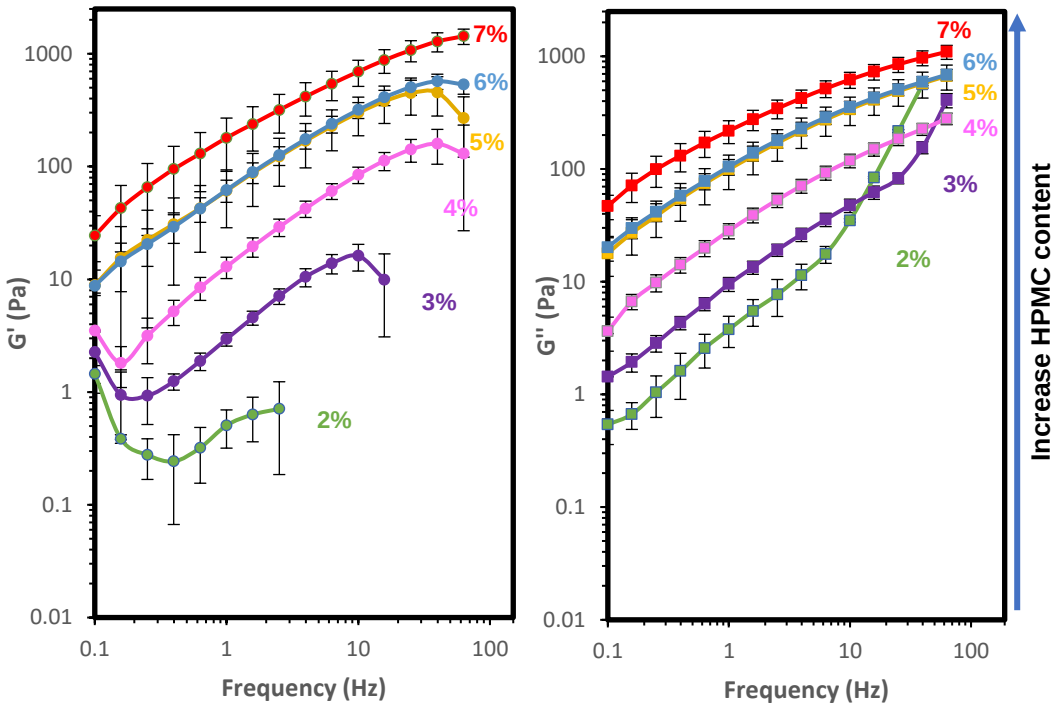

Figure 4.8 Frequency sweep test data of the tested hydrogels with different concentrations of HPMC, namely 2-7% (w/w).

The results in **Figure 4.8** show that both moduli (G′ and G″) increased with increasing frequency. Moreover, G″ is more than G' for the lower concentrations of the tested samples (2-6% HPMC w/w), and the differences between both are decreased with increasing polymer concentrations. The samples of the HPMC preparations from 2% to 6% showed a liquid-like behaviour as the G″ was higher than the G′. However, the 7% HPMC hydrogel (w/w) was different, exhibiting a liquid-like behaviour at low frequency as G″ was higher than G′. The G′ became more than the G″ after a frequency of 15 Hz, indicating that the sample started to show elastic-like behaviour properties **(Figure 4.9)**.

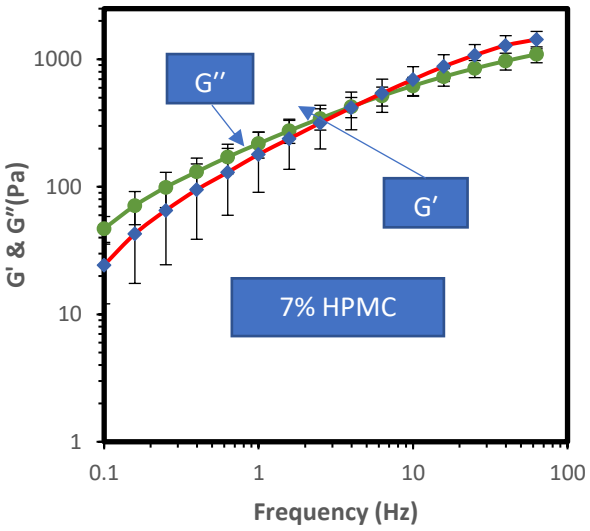

Figure 4.9 Frequency sweep test data of the tested hydrogels with 7% HPMC hydrogel concentration (w/w).

4.6.2.3 Viscosity Measurements (Flow Curve)

Another rheological test was conducted for all selected samples, namely the viscosity measurement **(Figure 4.9).**

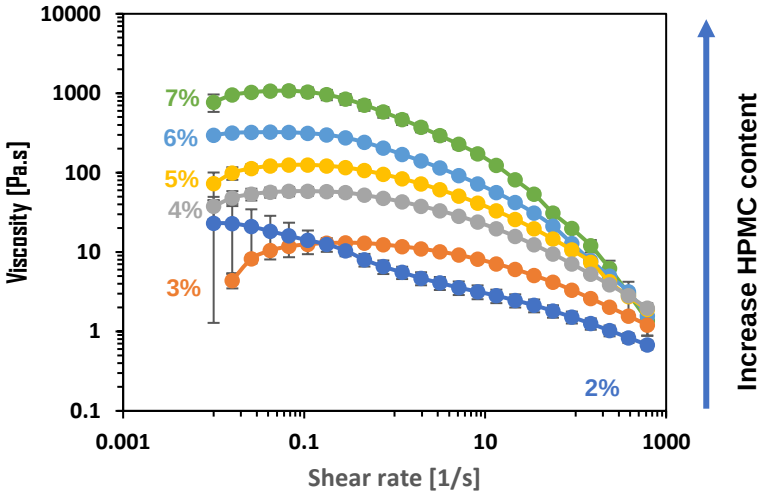

Figure 4.10 Viscosity measurement of the prepared HPMC hydrogels, including 2-7% HPMC hydrogel (w/w).

The results in **Figure 4.10** present the flow curve for all prepared HPMC concentrations with 2% to 7% HPMC hydrogels w/w. The data showed that the viscosities of the tested concentrations decreased with increasing shear rate. For example, the 6% HPMC hydrogel viscosity was reduced as the shear rate changed from around 269 Pa to 1.75 Pa. The decreases in viscosities with the increases in the shear rate indicate that the tested samples exhibited non-Newtonian shear-thinning behaviours. The viscosities of the tested samples increased with increasing HPMC polymer content, and they decreased with increasing the shear rate. The reason behind the decreases in the viscosity might be the disentanglement and orientation of the HPMC networks in the flow field. As the shear stress raises, more chains are rearranged along the direction of the shear, and thus the viscosity is reduced [321], [322]. When the tested sample was subjected to lower stress, the viscosity was higher because random molecular orientations showed resistance to flow [323].

The shear-thinning behaviour of a gelling system facilitated its flow by decreasing the viscosity under shear stress during injection by the syringe within the printed devices [324]. Moreover, it facilitated the flow of the gelling system through the pores through the disentanglement of the polymer networks due to the sample weight inside the devices [325]. The utilised rheological measurements showed that the differences between G″ and G′ decreased with increasing HPMC content, and the formulations changed from liquid-like behaviour to elastic-like behaviour with increasing HPMC content. Also, the viscosities of the samples were affected by increasing HPMC content. The flow curve results showed that the hydrogels had shear-thinning behaviours.

4.6.3 3D Printing of the FDM Printed Prototype Devices with Circular Pores

Different ear prototype devices were printed to investigate the releases of the selected samples **(Figure 4.10)**.

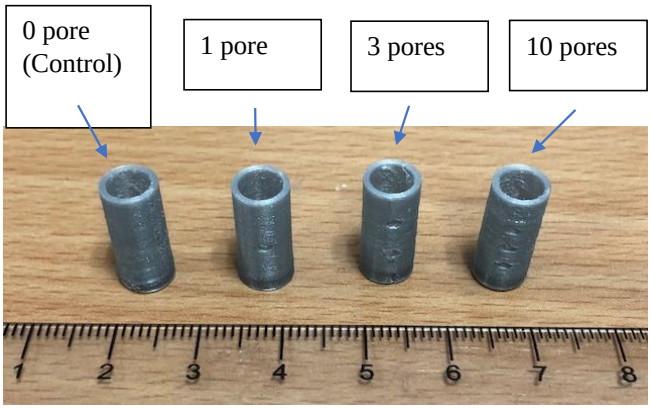

Figure 4.11 Photograph of the PLA Ultimaker^{2+} printed prototype ear devices with different pore numbers. The adjusted printing parameters are illustrated in Table 4.1.

Figure 4.11 shows the different 3D printed ear prototype devices (hollow cylinder devices). These devices were designed with the Tinkercad online software and then fabricated using the Ultimaker^{2+} FDM 3D printer. The commercial PLA polymer was utilized to fabricate the designed prototype devices, with different pore numbers, namely one, three, and ten pores. The printed parameters are presented in **Table 4.1.**

These devices were printed to investigate the flow of the selected hydrogels through the printed pores. Subsequently, one of the tested concentrations was selected and loaded with one of the anti-inflammatory drugs for use within the developed ear prototype devices (see chapter 3 for the developed ear prototype device design). The drug release investigated in **chapter 5.**

The printed devices were 7 mm in diameter and 15 mm in height. The dimensions selected as being within the range of the average external canal of an adult, as mentioned in the introduction section.

Table 4.1 The 3D printing parameters for the FDM 3D printed ear prototype devices using PLA polymer.

Printing parameters	Hollow Cylinder
Wall Thickness (mm)	1.05
Layer Height (mm)	0.1
Top/Bottom Thickness (mm)	0.8
Printing Speed (mm/second)	30
Printing Temperature (ºC)	190
Building plate Temperature (ºC)	60
Infill (%)	100
Supporting Materials	No
Adhesion	No
Nozzle (mm)	0.4

4.6.4 Hydrogel Flow Through the Printed Devices at Room Temperature and Body Temperature

This part investigates the flow of the selected formulations (2-7% HPMC w/w) through the pores of the printed devices at different temperatures, namely room temperature (25 ± 0.5℃) and body temperature (37℃). Various parameters were considered during this method, including the pore numbers, storage temperatures, viscosities of the prepared samples and pore locations. The aim was to have a gelling concentration of HPMC that can be loaded to the 3D printed ear prototype device using a suitable syringe with the loaded hydrogel remaining there for an extended period, i.e. the treatment period for AOE (7 days). The loaded hydrogel needed to pass through the printed pores at certain amounts. Consequently, it could contact the ear canal and deliver the loaded drug **(see chapter 5).**

In the beginning, the flows of the selected hydrogels (2-7% HPMC w/w) were studied at room temperature to select the concentrations that could be loaded into the fabricated prototype devices and remain there for an extended period. **Figure 4.11 A-C** shows the results of the percentage flows of the selected HPMC samples (2-7% HPMC w/w).

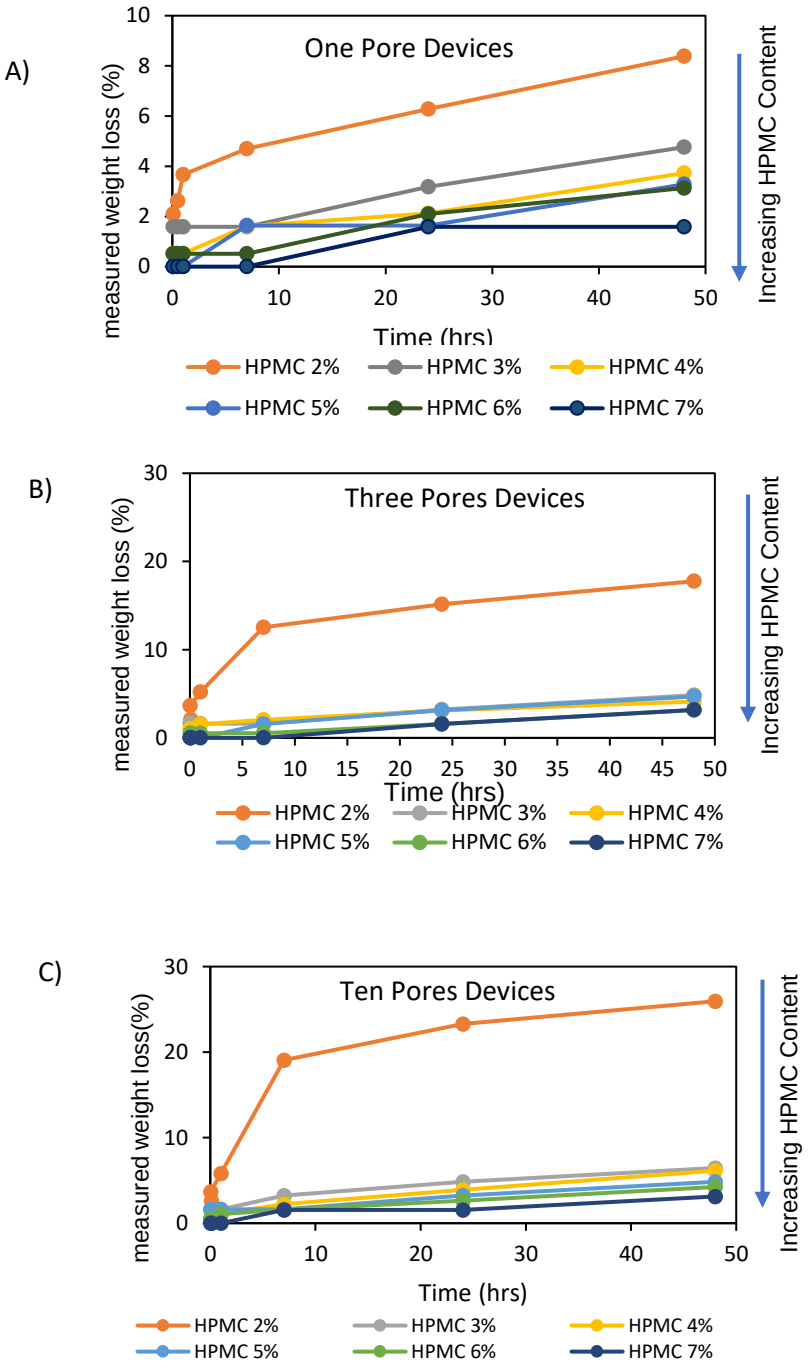

Figure 4.12 The percentage flows of the selected HPMC hydrogels (2-7% HPMC w/w) through the printed devices containing (A) one pore, (B) three pores, and (C) ten pores after storage at room temperature (n=1).

The effect of pore numbers on the sample flows was studied at room temperature, as shown in **figure 4.12**. The aim was to determine the impact of increasing the number of pores on the release of the utilised concentrations. The concentrations that flowed more quickly were

excluded. The results showed that the percentage flows of the selected samples increased as the pore numbers were increased for all samples. For instance, the percentage flow of the 2% HPMC sample was increased with an increasing number of pores. The percentage flows through the pores were found to be about ≈ 8.30% through the one-pore devices, ≈ 18% through the three-pores devices, and 26% through the ten-pores devices after ≈ 48 hours. Moreover, the 4% HPMC hydrogel percentage flows through the pores were found to be about ≈ 3.73% through the one-pore devices, ≈ 4.20% through the three-pores devices, and ≈ 6.15% through the ten-pores devices after 48 hours. The flows of the samples were increased due to the increase in the open area. The same effects for the percentage flow were found for other concentrations. The 2% concentration was excluded as it flowed quickly, losing about 26% within two days. Moreover, this concentration was watery. We selected the concentrations 4% and 6% of the HPMC preparations to continue the study, distinguishing their viscosities by excluding the 5% HPMC sample. The aim was to determine whether the flows through the same and different pore numbers would be affected by changing the viscosities**(Figure 4.13)**.

A)

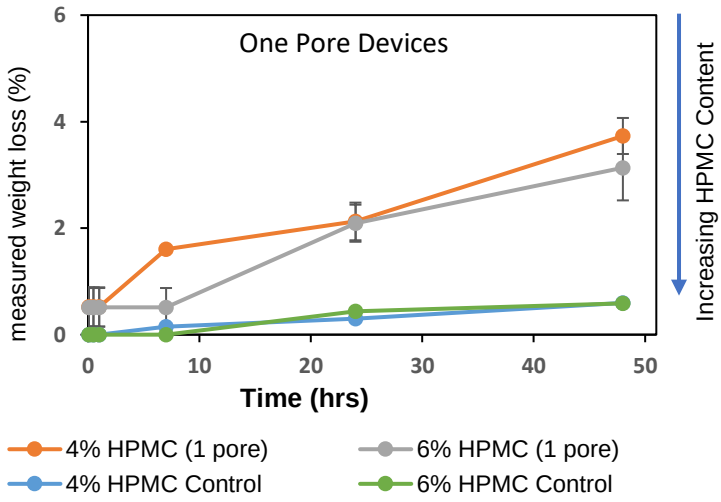

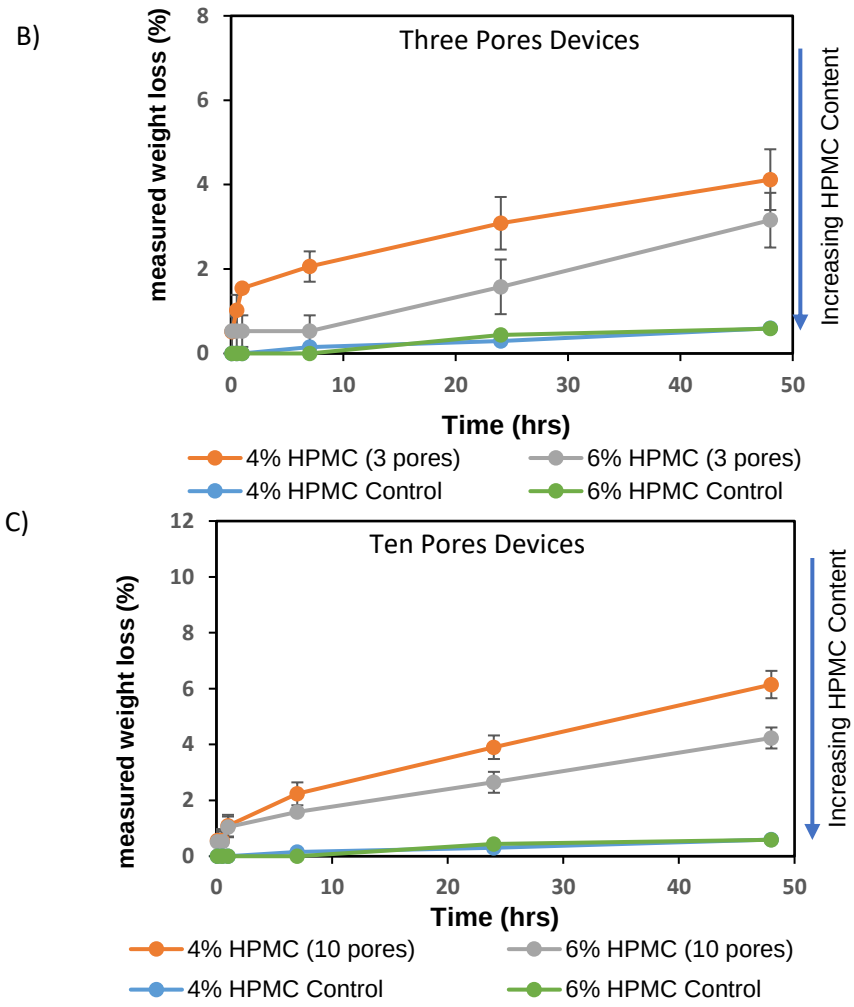

Figure 4.13 Comparison of the percentage flows of the A) 4%, and B) 6% HPMC samples through the printed devices containing different pore numbers, namely one, three, and ten pores (n=3).

Figure 4.13 shows the results of the percentage flows of the 4% and 6% HPMC hydrogels through all pores (one, three, and ten pores). It was found that the percentage flows of the samples decreased when the concentrations of HPMC increased for devices with the same number of pore. For example, the percentage flow of the 4% HPMC hydrogel through the three-pores devices was about ≈ 6.15%, while the percentage flow of the 6% HPMC was 4.25%. The viscosity was increased by increasing the HPMC content **(Figure 4.13B)**. Moreover,

the 4% HPMC sample percentage flow through the ten pores was about 6.14%, while it was about 4.23% for the 6% HPMC sample **(Figure 4.13C)**. The flowing of the tested samples through the printed pores decreased due to the corresponding increase in viscosity. The increase in viscosity may lead to an increase in the resistance to the flow of the sample within the device wall. The literature reports that the flowability of a sample is inversely proportional to its viscosity [326]. The statistical analyses (two-way ANOVA tests) showed that the percentage flows between the 4% and 6% HPMC hydrogels through the printed devices containing one, three, and ten pores did not have any significant differences. Subsequently, the effect of temperature on the samples was investigated. In this part, the 6% HPMC hydrogel was selected to be investigated at 37℃ to show whether the flow would be affected by the changes **(Figure 4.13)**. Also, this concentration reached 4% flow after 48 hours of study, and the 4% concentration of HPMC reached 6% flow through the ten-pore devices. Thus, the 6% concentration was selected.

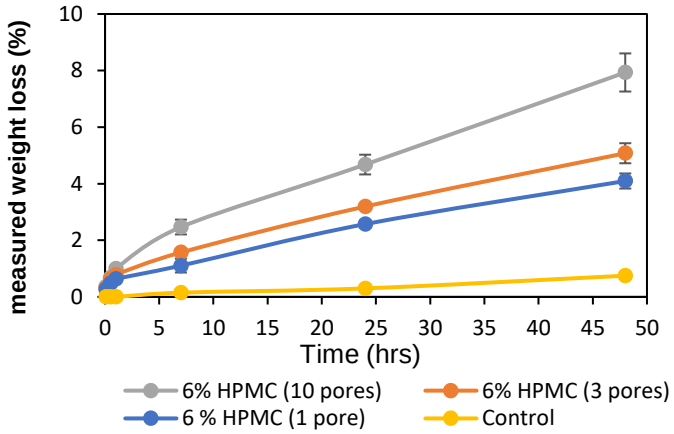

Figure 4.14 The percentage flow of the 6% HPMC hydrogel through the printed devices containing one, three, and ten pores after storage at 37℃.

Figure 4.14 shows the percentage flows of the 6% HPMC sample through the printed pores (one, three, and ten pores) at 37℃. It was found that with the change in temperature to 37℃, the percentage flow of the tested sample through the printed pores increased. For instance, the percentage flow through the printed pores of the 6% HPMC sample

increased as the temperature changed from 25℃ to 37℃. The percentage flow of the 6% gelling system through the ten-pore devices was about 8%, while it was about 4% through the same number of pores at room temperature. The increase in the flows may have been due to the macromolecules of the gelling system being mediated by the increase in temperature, thus promoting the loss of the crosslinked chains and leading to a decrease in the viscosity [327].

The statistical analysis of the data showed that the percentage flows of the 6% HPMC hydrogel were significantly different in terms of the percentage flowed through the one-pore and three-pore devices versus the ten-pore devices after seven hours (p-values of 0.0005, and 0.0248, respectively). Furthermore, the percentage flows of this sample through one pore and three pores versus ten pores devices are significantly different after 24 hours. The p-values were about <0.0001 and 0.0002, respectively. In addition, the percentage flows through the one-pore, and three-pore versus ten-pore devices were significantly different, with p-values of <0.0001 for both flows. In addition, the percentage flowed through the one-pore versus the three-pore devices were significantly different, with a p-value of 0.0135. Afterwards, the 7% HPMC hydrogel was selected to be compared with the 6% HPMC sample at 37℃ with ten-pore devices to determine whether their releases were significantly different or not **(Figure 4.14).**

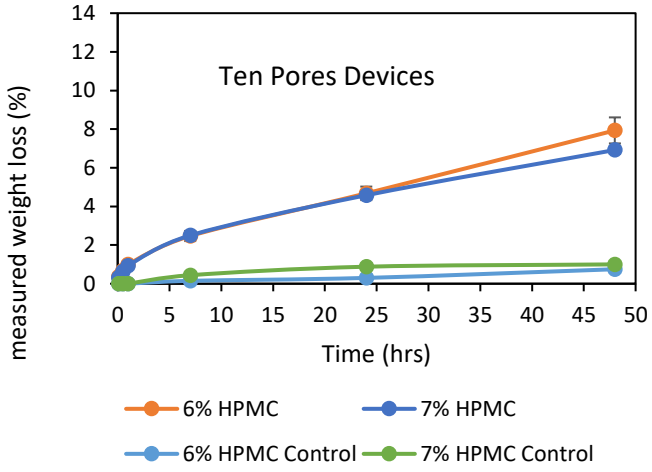

Figure 4.15 The percentage flow of the 6% and 7% HPMC hydrogels through the printed devices containing ten pores after storage at 37℃.

Figure 4.15 presents the results of the percentage flows of the 6% and 7% HPMC samples through the printed devices with ten-pores. The samples release through the pores were studied at 37℃. There were no significant differences between both concentrations in terms of their flows through the printed pores.

Afterwards, the pore locations were changed to show whether the flow of the gelling systems would change **(Figure 4.15)**. The newly designed device was modified to have eight pores instead of ten pores to allow an appropriate distance between the designed pores and facilitate the printing of the devices without any problems emerging in the fabricated pores. The printing parameters that were utilised to print the newly designed devices were the same as the parameters used to print the previously designed devices **(Table 4.1).** The 6% HPMC hydrogel was selected for comparison with the previous devices **(Figure 4.15).**

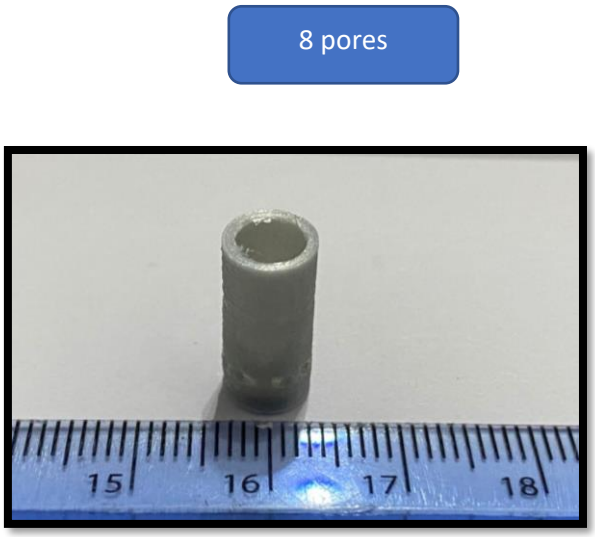

Figure 4.16 Photograph of the newly designed PLA prototype devices showing eight pores near the base of the printed devices. The adjusted printing parameters are illustrated in Table 4.1.

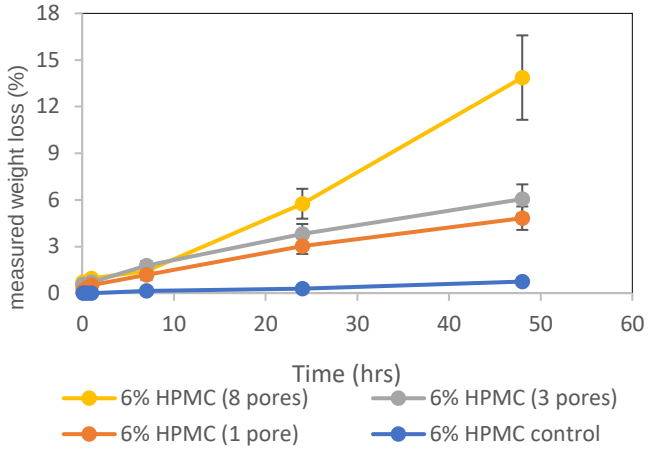

Figure 4.17 The percentage flows of the 6% HPMC hydrogel w/w, through the newly designed printed devices containing one, three, and eight pores after storage at 37℃.

Figure 4.17 shows the results of the 6% HPMC sample flow through all modified pores. It was found that as the pore number increased, the percentage flowing of the tested 6% HPMC sample also increased. For instance, the percentage flow through the pores was increased to ≈ 13.86% through eight pores, ≈ 6% through three pores, and ≈ 4.8% through one pore after 48 hours. The statistical analysis of the data showed that there was a significant difference in the percentage flows through the eight-pore versus the one-pore devices for the 6% HPMC sample, with a p-value of <0.0001. Moreover, there was a significant difference in the percentage flows through the eight-pore versus the three-pore devices, and the p-value was 0.0001. Finally, the percentage flows of the 6% HPMC samples through the previous and modified designed devices are compared in **Figure 4.17.**

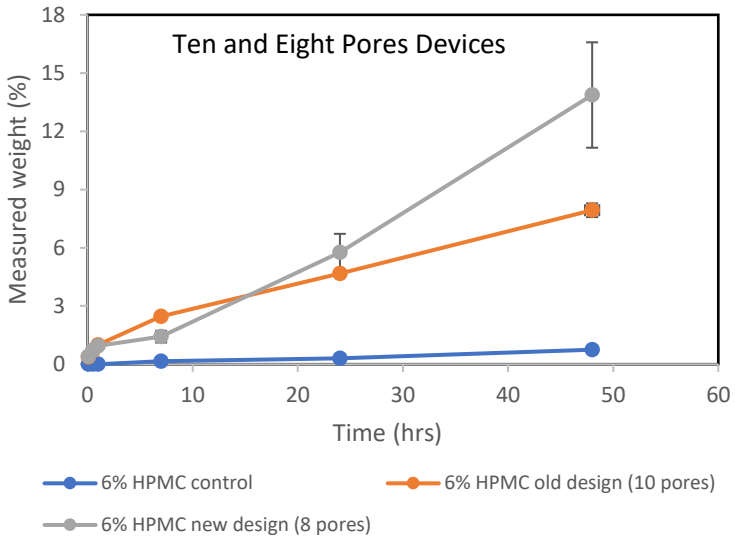

Figure 4.18 The percentage flows of the 6% HPMC hydrogel w/w through the newly designed printed devices containing eight pores and the previously designed devices containing ten pores after storage at 37℃.

Figure 4.18 shows the comparison between the percentage flows of the 6% HPMC samples through the old and modified devices. The statistical analysis (two-way ANOVA test) showed that there were no significant differences between the percentage flows through both designs. Furthermore, according to the results, there were no statistical differences between the 6% and 7% HPMC samples in terms of their flows through the ten-pore devices. The release of the 7% gelling sample through the printed devices was reached around 7% in two days, while the 6% HPMC sample release reached about 8% during the same period. Also, the gel flow experiments showed that when the pore locations of the 6% HPMC changed, there were no significant differences in their flowing. In our model, the 7% HPMC hydrogel was selected to be utilised in the next chapter as a vehicle for the extended release of an anti-inflammatory drug through the printed device developed in chapter 1. The control samples showed that some flows might lose some of the contained water during the experiment.

4.7 Conclusion

In this chapter, different concentrations of HPMC hydrogels were successfully prepared. Moreover, various 3D FDM printed ear prototype devices with various pore numbers and locations were successfully fabricated to investigate the flows of the prepared formulations through the printed pores. The rheological data showed that the LVER of the selected samples was between 0.01% to 10% shear strain. Moreover, the low concentrations of the HPMC samples (1-6% HPMC w/w) showed liquid-like behaviours as the G'' was more than the G' modulus. The differences between both moduli decreased with increasing HPMC polymer in the preparations. Furthermore, the 7% HPMC w/w sample showed an elastic-like behaviour after 15 Hz frequency. The G' became more than the G" moduli. In addition, the flow curve data showed that the HPMC samples exhibited non-Newtonian shear-thinning behaviours after the shear rate of the rheometer was increased. The results of the percentage flows for the selected samples were affected by various factors, including increasing the pore numbers, decreasing the concentrations of the HPMC polymer, raising the temperature from room temperature to the body temperature, and changing the pore locations on the prototype devices. The 7% HPMC was selected to be studied in the next chapter as a vehicle for the sustained release of anti-inflammatory medication utilized in the treatment of AOE.

Chapter 5: Investigation of Dexamethasone Release through the Fabricated Ear Prototype Medical Device

5.1 The Novelty

In this chapter, DXM was formulated into a tablet to be inserted within the selected HPMC concentration (7% HPMC w/w) gelling system, which can be utilised as a vehicle for sustained DXM release in a planned for zero-order manner. Moreover, an FDM 3D printer was utilised to develop a 3D ear medical prototype device that contains several circular pores. Subsequently, the developed device was loaded with the 7% HPMC hydrogel, and DXM tablet. The device can be utilised in the external ear of a patient suffering from AOE. Also, a synthetic skin simulation membrane (Strat-M® membrane) was used with the USP dissolution apparatus I (basket) to study the potential delivery of the drug into the skin. The Strat-M® membrane mimics human skin.

5.2 Introduction

Skin is the largest organ of the human body, accounting for about 10% of total human body mass. It is a complex organ and offers an attractive route for drug delivery. It works as both a protective barrier and a sensory organ. Also, it is involved in the maintenance of homeostasis. The human skin is composed of different layers, namely the epidermis, dermis, and subcutaneous hypodermis **(Figure 5.1)** [328], [329].

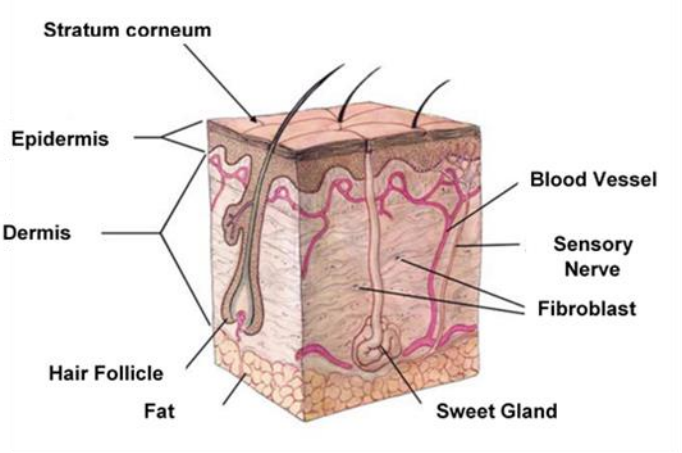

Figure 5.1 Cross-section of the human skin showing the different layers and components [330].

The skin covers the human ear pinna, and it continues directly into the ear canal. Moreover, it covers the outer surface of the TM. The skin that covers the auditory canal is thin, and it is closely adherent to the cartilage and bone of the canal **(chapter 1, section 1.1).** The outer layer of the epidermis is called the stratum corneum [331] and is commonly the rate-limiting step in successful drug delivery [332], [333]. Several techniques have been utilised to change the natural barrier of the stratum corneum, such as physical penetration enhancements, chemical penetration enhancements, and drug modification [334].

Different models, such as *in vivo* and *in vitro* models, can be utilised to assess the rate and extent of API absorption for transdermal drug delivery. Drug permeation can be regularly studied using a Franz diffusion cells instrument [335]. Several membranes can also be used to study API permeation with the Franz diffusion cells, such as animal skins (rodent, pig), human skin (skin from cosmetic surgery, surgical biopsies, and cadavers), and synthetic membranes (Strat-M® membrane and cellulose acetate). Biological skins (human and

animal skins) are preferred because they are closest to *in vivo* human skin. The biological models have some drawbacks, including a short half-life, special storage requirements, complex sample preparation, high study costs, safety issues, and high variability [328], [336].

Synthetic membranes are frequently used to decrease the need for biological membranes in pilot studies. There is a requirement for synthetic membranes that have both lipophilic and hydrophilic drug pathways as healthy skin in human [328]. Synthetic membranes have some advantages, including faster preparation time compared to biological membranes, controlled membrane thickness, low storage space, and relatively low cost [332], [333].

The Strat-M® membrane is a polymeric-synthetic membrane that can be used to study transdermal drug diffusion. Moreover, this membrane is predictive of drug diffusion in human skin without lot-to-lot variability, storage and safety limitations [328]. This membrane was designed to a structure and chemical features similar to that of human skin layers. It is also similar in a limited number of aspects in terms of structure and lipid chemistry. The membrane has a thickness of about 300 µm. It is constructed of different layers, including a tight top layer similar to the stratum corneum (epidermis), two layers of porous polyethersulfone, and one layer of a polyolefin non-woven fabric support **(Figure 5.2)**. These synthetic layers become increasingly porous, open, and large in thickness to mimic the various layers of human skin. The Strat-M® membrane contains lipids, such as cholesterol, free fatty acids, and ceramides, in a ratio similar to what is available in healthy human skin. The Strat-M® membrane can be used for testing and optimizing API formulations during early-stage drug/formulation development. Moreover, it can also be used in the early stages of formulation development in the

screening of different materials, including pesticides, APIs, cosmetic actives, personal care products, and chemical protective formulations [337].

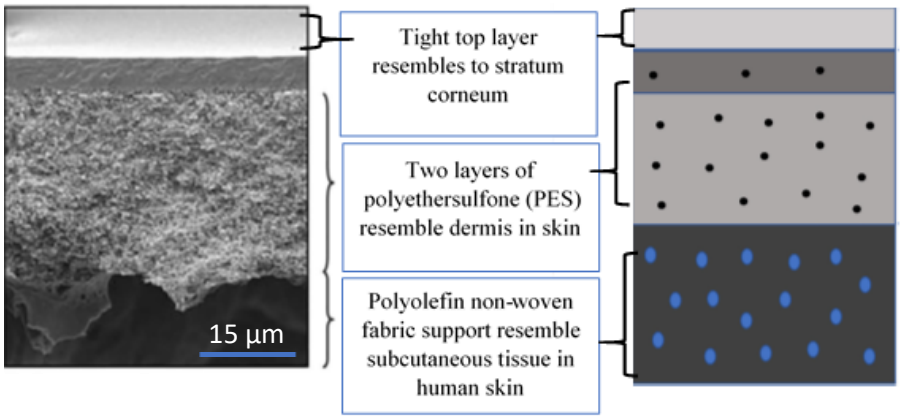

Figure 5.2 Cross-section (on the left side) and schematic illustration of the synthetic Strat-M® membrane (on the right side) [328], [337].

5.3 Aims and Objectives

This chapter investigates the *in vitro* release properties of the various manufactured DXM tablets, including DXM/methyl-β-CD and DXM/lactose, through the developed 3D printed ear prototype device **(chapter 3)** loaded with the selected 7% HPMC hydrogel w/w **(chapter 4)**.

A single hydraulic compression press instrument was utilised to fabricate the DXM into tablet dosage form using two different excipients, including methyl-β-CD and lactose. A Raman spectroscopy instrument was utilised to investigate the diffusion of the fabricated DXM tablets through the selected HPMC hydrogel concentration (7% HPMC w/w). A food colouring dye was used to investigate the passing of the colour through the pores of the 3D printed prototype device loaded with the selected hydrogel. A UV-visible spectrophotometer and a United States Pharmacopeia

Convention (USP) type I apparatus were utilised to study the DXM release from the pores of the 3D printed prototype devices loaded with the selected hydrogel and covered by Strat-M® synthetic membranes.

5.4 Experimental Section

All materials utilised in this chapter were described in **chapter 2**, **section 2.1.**

5.4.1 Preparation of the DXM Tablets

In the beginning, a manual 15-tonne hydraulic press (Atlas™, Specac, Orpington, UK) was used to compress two different tablets, including DXM/methyl-β-CD, and DXM/lactose. With this kind of instrument, the utilised powders can be compressed into small tablets one at a time. The tablets were manufactured through several steps: First, the powders (drug and excipients) were weighed accurately using a Mettler Toledo electronic balance, and then they were mixed manually using with a suitable spatula in a weighing boat for 5 minutes. Subsequently, the lower punch was placed under the die mould. Afterwards, the weighed powders were placed inside the mould cavity pocket, and then the upper punch was placed above the set powders. Subsequently, the whole sets were placed at the bottom piston inside the hydraulic instrument. Finally, the filled powders were compacted using the hydraulic pump handle to increase the pressure of the pressing face on the top of the filled powders until the desired pressure was achieved. The force used was 5 tonnes for 1 minute. **Figure 5.3** presents the 6 mm diameter punches and die that were utilised to fabricate the drug tablets. The procedures used in fabricating the DXM/methyl-β-CD and DXM/lactose tablets are illustrated in **Figure 5.4** and **Figure 5.5.**

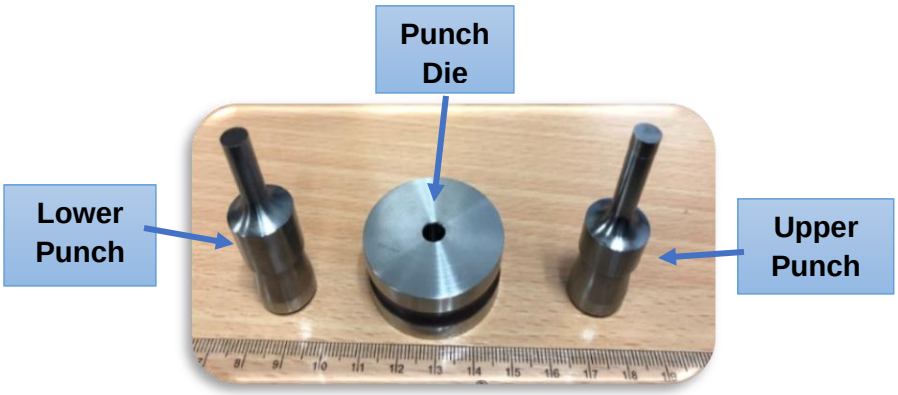

Figure 5.3 Photograph of the 6 mm diameter upper punch, lower punch and punch die used to compress various DXM tablets.

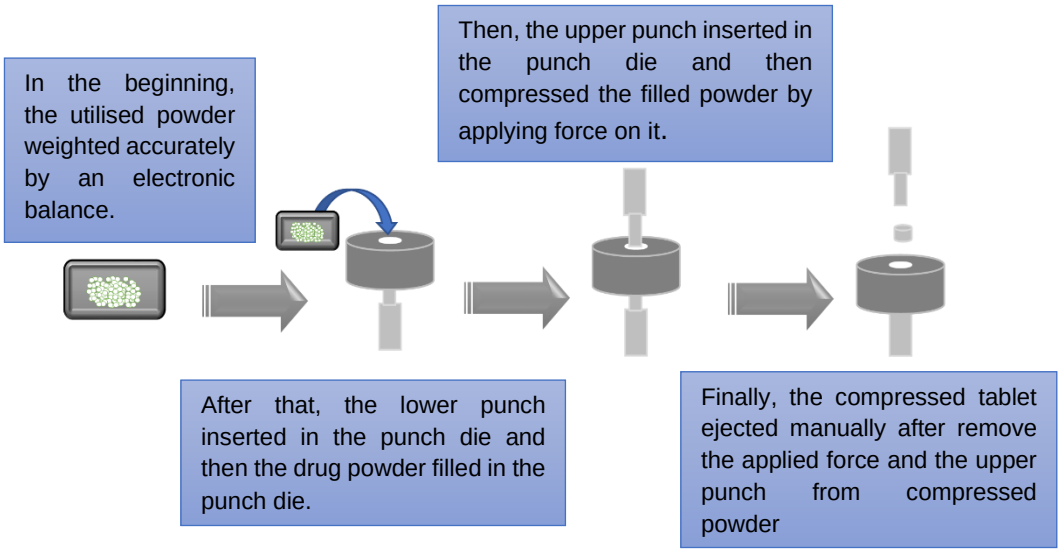

Figure 5.4 Schematic illustration of the manufacturing steps used to press the different tablets, including DXM/methyl-β-CD, methyl-β-CD (as a control), and lactose (as control), using the single hydraulic press tabletting instrument.

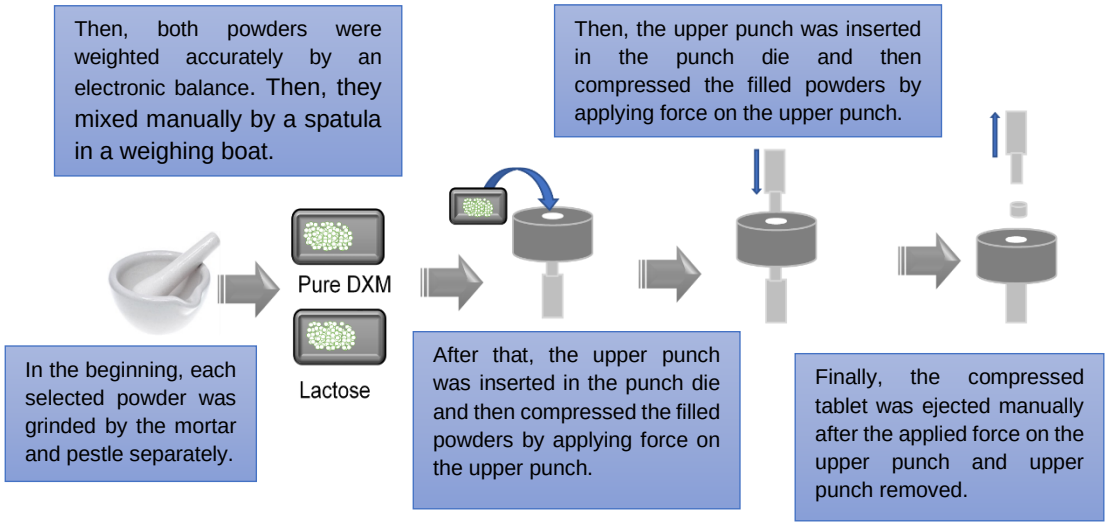

Figure 5.5 Schematic illustration of the manufacturing steps for compressing the DXM/lactose powders using the single hydraulic press instrument.

5.4.2 Investigate the DXM Diffusion Through the HPMC Hydrogel

5.4.2.1 Raman Spectroscopy

A confocal Horiba-Jobin-Yvon LabRAM system (Horiba-Jobin-Yvon Ltd., Middlesex, UK) was used to investigate the DXM diffusion through the selected 7% HPMC hydrogel w/w. This instrument was equipped with different laser excitation capabilities, including UV (325 nm), red (660 nm), green (532 nm), and NIR (785 nm), as mentioned **in chapter 2**. In this work, the NIR (785 nm) laser was utilised for all samples with a 300 µm confocal hole, 600 lines/mm grating, 100 filter percentage, 2 seconds accumulation time, and a spectral range of 1100-1700 cm^{-1}. The Raman spectrophotometer was connected to an Olympus BX41 microscope that was fitted with different objective lenses, including 10x, 40x, 50x, and 100x. Two objectives lenses were utilised in this work, including the 50x for

calibration and focusing the samples, and the 10x for selecting the area for detection. The LabSpec 6 software was utilised to analyse the Raman data.

Based on the previous chapter, the selected HPMC hydrogel (7% HPMC w/w) was freshly prepared **(chapter two, section 2.6.1)**. Then, a measured amount (1 mL) of the prepared hydrogel was filled within the middle of a 35 mm Petri dish. Subsequently, the Petri dish was placed overnight on the top lab bench to allow the loaded hydrogel to settle down and the air bubbles to clear. Afterwards, a tablet with DXM/methyl-β-CD complex was fabricated using the hydraulic manual press instrument **(chapter 2, Section 5.3.2.1)**. Subsequently, the manufactured tablet was placed above the middle of the prepared hydrogel loaded into the Petri dish **(Figure 5.6)**. Subsequently, Raman line mapping was done for the prepared sample at different times, including zero-time, one day, three days, and seven days. **Figure 5.7** shows the preparation steps for the prepared sample for the investigation of DXM diffusion through the prepared hydrogel using the Raman spectroscopy. The Raman data were analysed and plotted using the R software.

.

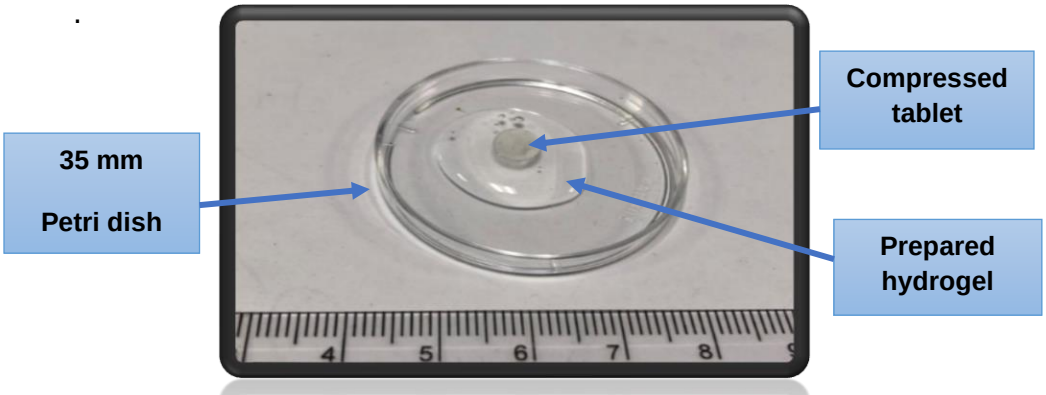

Figure 5.6 Photograph of the Raman prepared sample before the line mapping, showing the loaded hydrogel (7% HPMC w/w) in the middle of the Petri dish, and the manufactured DXM/methyl-β-CD tablet at the middle of the hydrogel.

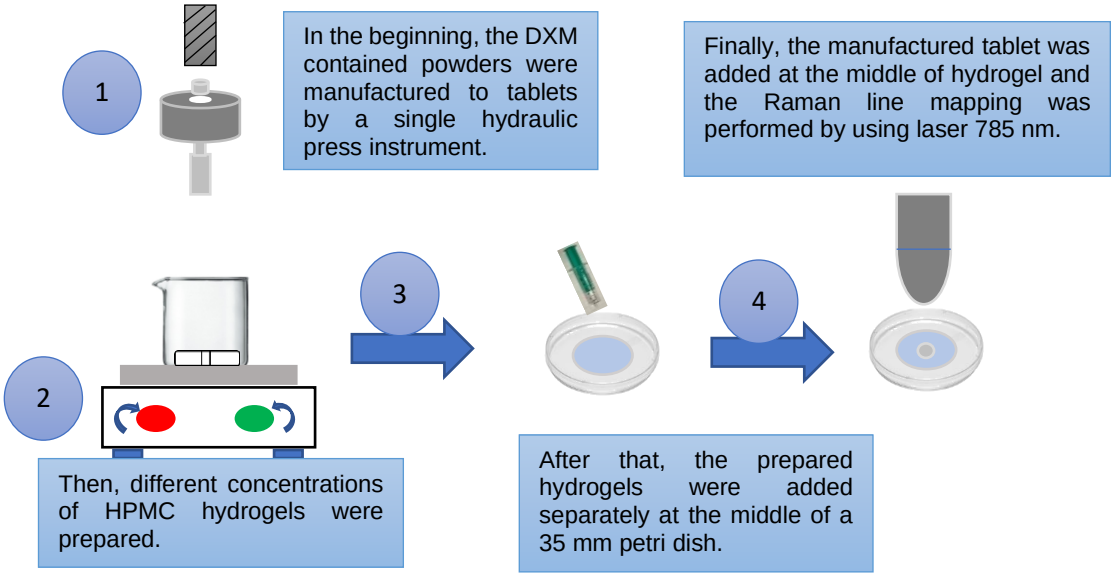

Figure 5.7 Schematic illustration of the preparation steps for the prepared sample for the Raman spectroscopy study.

5.4.2.2 Study the passing of a Food Dye Through the Pores of the Prototype Printed Device

Based on the previous optimisation in chapter 4, the 6% HPMC hydrogel concentration was selected to see if it could provide a sustained release of a drug or drug-like molecule. However, the selected anti-inflammatory drug (DXM) is not coloured. Therefore, we utilised a food dye to see whether we could obtain the release of a small molecule which is similar in molecular mass to our drug from the 6% HPMC hydrogel. Such a simple visual release model was considered effective and efficient.

In this part, the 7% HPMC hydrogel was loaded within a small glass container with a height of 3.9 cm and a diameter of 3 cm. Afterwards, the container was placed overnight within a cold temperature at 2℃ in order to allow the hydrogel to settle, and the air bubbles to be cleared. Subsequently, the developed ear prototype device in

chapter 3 was utilised based on the printing designs, process, and parameters detailed in **chapter 3, section 3.3.3**. The top of the printed device was covered with a parafilm membrane with an open area to allow the addition of the prepared hydrogel and food dye to the device. Afterwards, the prepared hydrogel was loaded within the printed device by a suitable syringe. Subsequently, the loaded device was placed in the hydrogel in a glass container. After that, food dye (0.5 mL) was added to the top part of the loaded hydrogel available within the device. Finally, several images were captured by a digital camera at different times to show the release of the dye through the printed pores **(Figure 5.8)**.

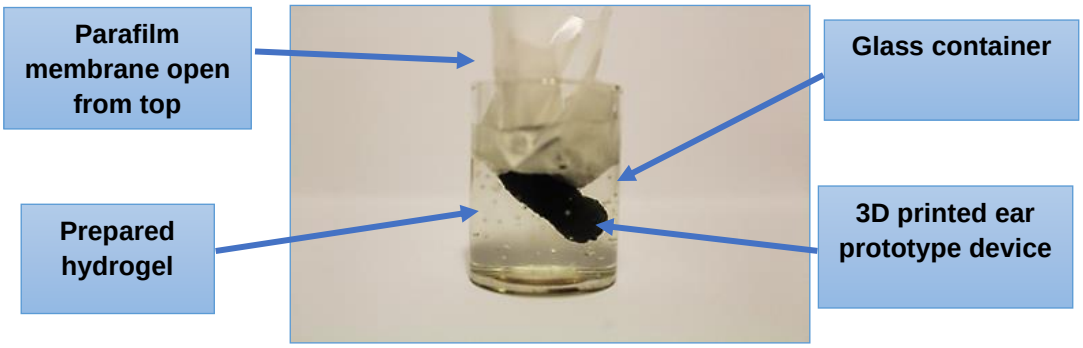

Figure 5.8 Photograph of the prepared sample for investigating the release of a food colour dye through the pores of the printed device. The black colour in the picture represents the printed ear prototype device suspended in the loaded HPMC hydrogel. The top white colour represents the covered parafilm membrane. The glass vial has a diameter of 3 cm.

5.4.3 Standard Stock Solution and Sample Preparations

A PBS solution was freshly prepared and adjusted with a pH ≈ 7.4. Subsequently, a standard solution of DXM was prepared by accurately weighing 10 mg of the received powder using an electronic balance. After that, the weighed amount was transferred to a 250 mL glass beaker. Then, 80 mL of PBS was measured accurately using a gradual cylinder and added to the beaker. Next,

the glass container was placed under sonication for 15 minutes. This solution was considered the stock solution and its concentration was 0.125 mg/ml. Finally, different sample concentrations, including 1.25, 3.125, 6.25, 12.5, 25, 37.5, and 50 µg/mL, were prepared for creating a working calibration curve covering the dissolved concentrations of the DXM in the dissolution medium. The prepared concentrations were diluted with PBS from the prepared stock solution. Finally, a 1 mL sample from each concentration was placed within a UV quartz and analysed using a UV spectrophotometer.

5.4.4 Optimal Detection Wavelength

An amount of the stock solution (1 mL) was withdrawn using a suitable pipette and inserted into a UV quartz. Then, it was scanned using the UV spectrophotometer in a range of 200-800 nm to determine the absorbance wavelength of the DXM.

5.4.5 Limit of Detection (LOD) and Limit of Quantification (LOQ)

Different concentrations were prepared, including 1.25, 3.125, 6.25, 12.5, and 25 µg/mL, to determine the LOD and LOQ. The absorbance was scanned from 200 to 400 nm, and it was detected at 241 nm. LOD and LOQ were calculated as $3.3\sigma/S$ and $10\sigma/S$, respectively. The σ is the standard deviation of the intercept, and S is the slope of the calibration plots.

5.4.6 *In vitro* DXM Permeability Across Synthetic Membrane

The DXM permeability across a synthetic membrane was measured. A Strat-M® membrane (Merck Millipore, USA) and 12-well culture plates, containing the acceptor chamber and the donor compartment, were used. The Strat-M® membrane **(Figure 5.9)** was carefully placed at the bottom of the donor compartment (Transwell insert), and a tight rubbery ring was placed around the set membrane to hold it tightly and prevent any liquid escaping from the donor

compartment. Also, it allowed the DXM to be passed through the covered membrane **(Figure 5.10)**. The dimensions of the utilised Transwell plate are presented in **Figure 5.11.**

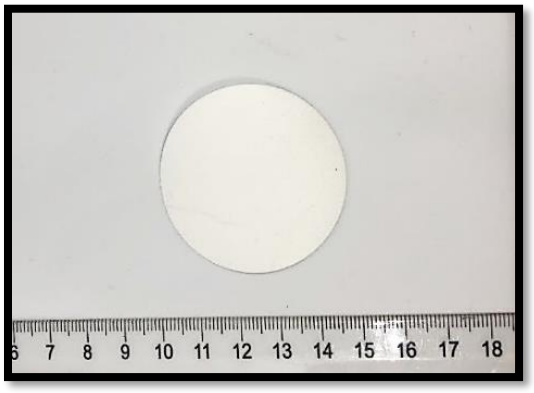

Figure 5.9 Photograph of the Strat-M® membrane with a size of 47 mm in diameter.

In this experiment, an amount of DXM was accurately weighed (0.65 mg) using an electronic balance and placed within a test tube 200 µL of PBS with a pH of 7.4. Afterwards, the test tube was shaken for three minutes to allow the drug particles to dissolve. After that, the required amount was pipetted directly into the donor compartment, while the acceptor compartment was filled with three mL of PBS alone; the plate was then placed at room temperature. Then, at different time points (0, 1, 5, 24 hours), 1 mL aliquots of the PBS-receiving media were sampled from the acceptor compartments, and a fresh amount (1 mL) of PBS was placed in the same chamber. The withdrawn samples were analysed with a UV spectrophotometer, with a wavelength of 243 nm. The experiment parameters were obtained from the literature [338], [339]. The aim was to investigate whether the DXM would pass through the Strat-M® membrane.

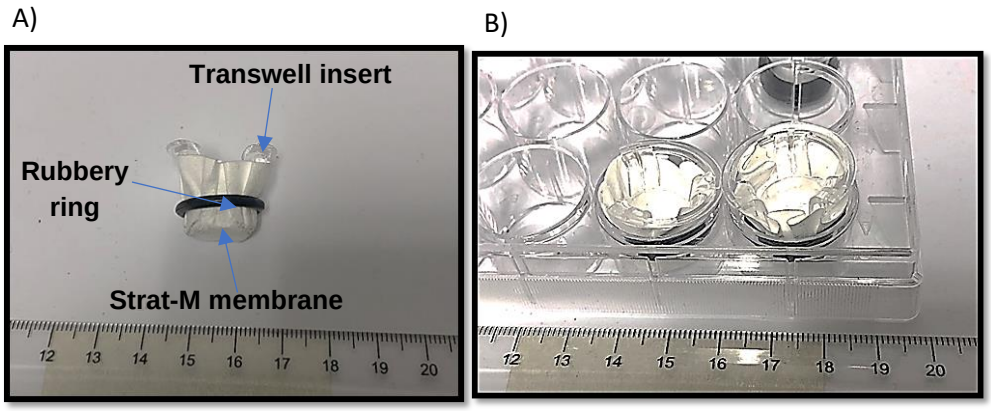

Figure 5.10 Photographs of A) side view of a Transwell insert covered from the bottom by a Strat-M® membrane and rubber ring; B) a top view of a Transwell insert covered from the bottom by a Strat-M® membrane and rubber ring.

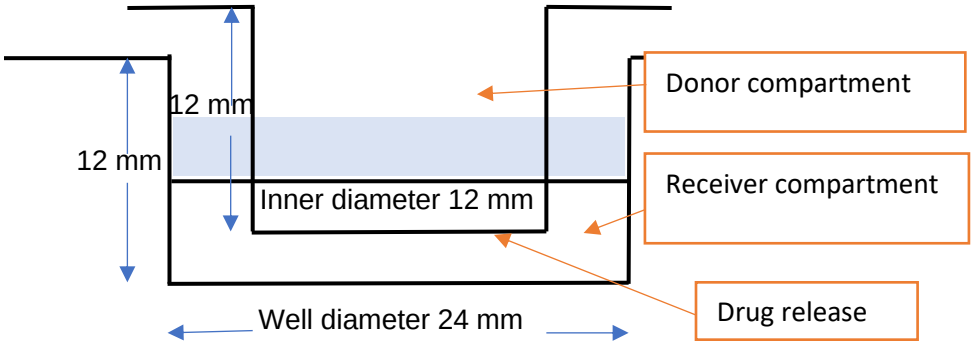

Figure 5.11 The dimensions of a 12-well plateTranswell.

5.4.6.1 Study the DXM Drug Release through the 3D Printed Ear Medical Prototype Device by using Dissolution Apparatus I (Basket)

The *in vitro* drug release study of DXM was achieved using a type I USP apparatus (basket) [340]. The main aim was to incorporate an amount (0.8 mL) of the prepared HPMC hydrogel within the manufactured ear prototype device with circular pores and then place the compressed drug tablet containing 2 mg of DXM within the

injected hydrogel to facilitate the sustained release of the contained drug.

The dissolution method consisted of several steps**.** Firstly, various tablets were fabricated using a single hydraulic press tabletting instrument; these were DXM/methyl-β-CD inclusion complex tablets (n=3), DXM/lactose mixture tablets (n=3), lactose tablets (as control), and Methyl-β-CD tablets (as control) **(Figure 5.14, N.O 1)**. The manufacturing steps are outlined at the beginning of this chapter **(section 5.3.2.1).** Subsequently, the 7% HPMC hydrogel was freshly prepared (w/w) **(Figure 5.14, N.O. 2).** The formulation steps are detailed in **chapter 2, section 2.6.1.** Finally, the various 3D FDM ear prototype devices were printed using an Ultimaker^{2+} printer **(Figure 5.14, N.O. 3).** The full manufacturing steps and utilised parameters are detailed in (**chapter 3).**

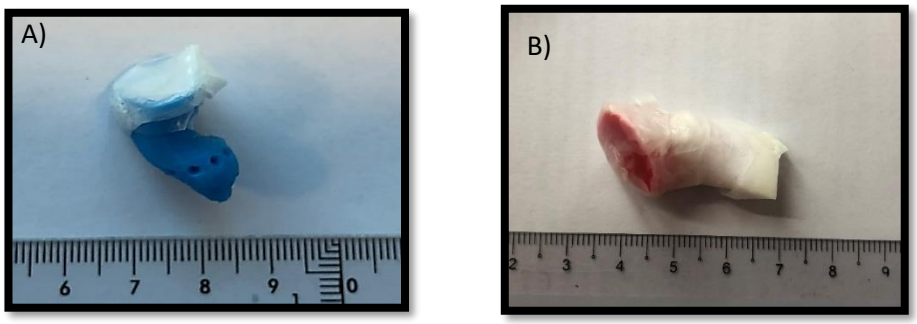

Figure 5.12 Photographs of the prepared ear prototype device sample covered with a parafilm; A) without the Strat-M® membrane and B) with the Strat-M® membrane.

An amount (0.8 mL) of the prepared HPMC hydrogel with the concentration of 7% was injected in the printed prototype devices. Afterwards, the prepared tablets were added separately into the middle of the injected hydrogels. Subsequently, the top of each device was covered by a parafilm sheath to prevent any of the drug or the loaded hydrogel from escaping from the top part. After that, some of the devices were covered with a synthetic Start-M®

membrane. The shiny side of the membrane (epidermis) was facing the pores and walls of the device. Each device was added separately to the dissolution apparatus basket **(Figure 5.13)**, and each basket was loaded into a 900 mL dissolution apparatus vessel. Each vessel was filled with 200 mL PBS with a pH of 7.4. The rotating speed of the basket was set to 100 rpm for 7 days, with the water bath temperature set at 37℃ for the whole experiment. The sampling schedule was predetermined at different time points, including 0, 5, 15, 30, 60, 300, 600, 1440, 2880, 4320, 5760, 7200, 8640, and 10080 minutes. Each time an amount of the dissolution medium (5 mL) was drawn using a sterile plastic 5 mL syringe. After each sampling time, the same volume of the prepared PBS blank was replenished into each apparatus vessel. Each sample was analysed using the UV spectrophotometric instrument (Agilent UV, Nottingham, UK) at a wavelength (λ max) of 241 nm by taking 1 mL from the withdrawing samples and filling it into a UV quartz using a suitable pipette. **Figure 5.14** shows the schematic preparation steps prior to the dissolution study.

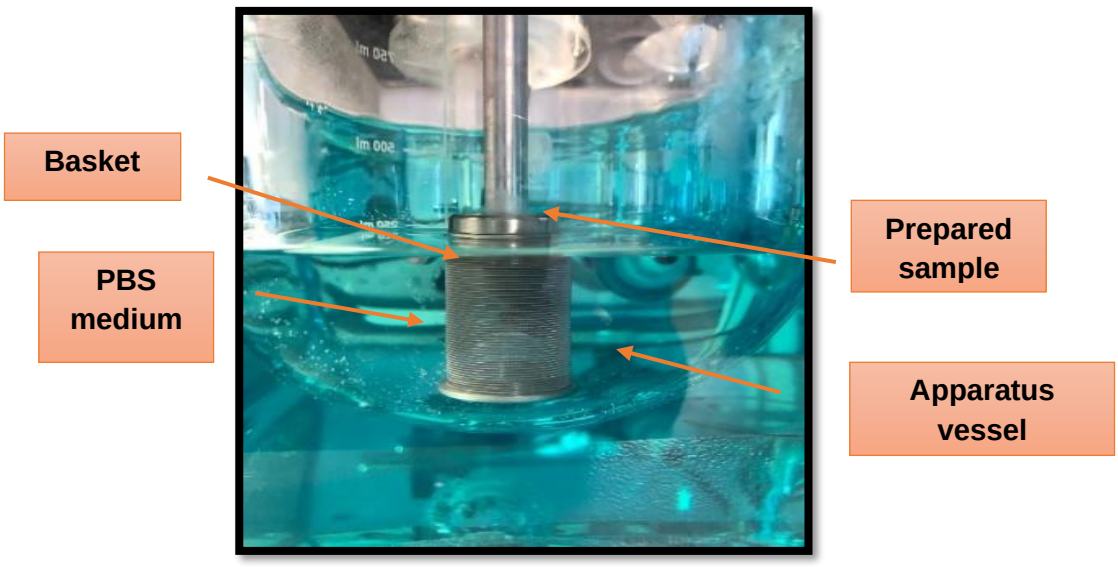

Figure 5.13 The dissolution apparatus containing a prepared device within a basket.

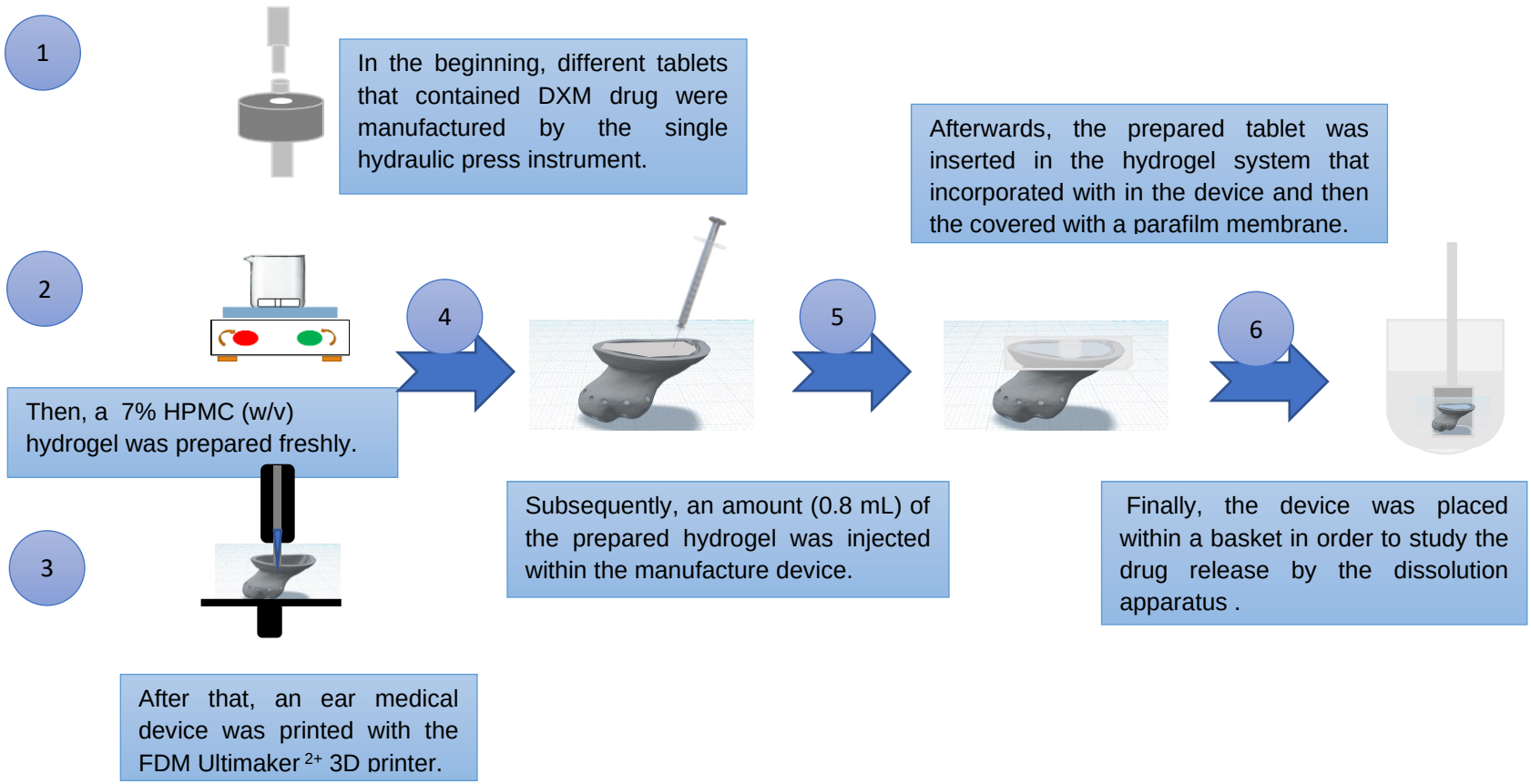

Figure 5.14 Schematic description of all preparation steps prior to the *in vitro* dissolution test.

5.5 Results and Discussion

5.5.1 Morphology of the Manufactured DXM Tablets

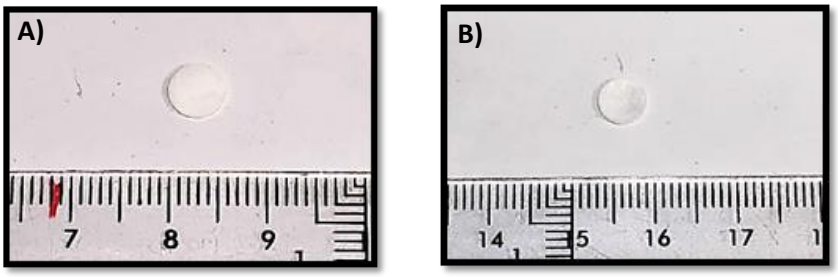

Figure 5.15 Photographs of the compressed tablets; A) DXM/lactose mixture tablet and B) DXM/methyl-β-CD inclusion complex tablet.

In this chapter, different tablets were successfully compressed using a single hydraulic tablet compressing instrument. The first compressed tablet comprised of DXM and DXM/methyl-β-CD powders **(Figure 5.15 A)**. However, the second tablet was compromised of DXM and lactose mixture powders **(Figure 5.15 B)**. The methyl-β-CD and lactose tablets are described in the appendix section **(Figure 5.C1 in appendix).** The printed tablets were 6 mm in diameter.

Some difficulties were experienced during the compression method, specifically in compressing the active drug (DXM) without any excipients in the utilised punches **(Figure 5.3)** as the dosage amount of DXM was very small (2 mg). This dose is the normal concentration utilised to treat patients affected by AOE for 7 days [341]. Furthermore, the manufactured tablets were very thin, fragile, and broke during handling. Thus, various excipients were added to facilitate the compression of the drug tablets.

In this study, methyl-β-CD was selected for many reasons. This excipient can increase the aqueous solubility of low or poor water-soluble drugs. Additionally, it increases their stability and bioavailability [342]. Also, it can enhance the permeation of

hydrophobic drugs through the human biological membrane. Furthermore, it has good compatibility with APIs, minimal lubrication requirements [343], and substantial compressibility compared to other fillers utilised in direct compression. Finally, it also has good flowability and floodability [344]–[346].

In this work, methyl-β-CD used to increase the aqueous solubility of DXM in the prepared HPMC hydrogel system. Also, β-CD can be used as a binder, filler or disintegrated powder to form a tablet with the API. Additionally, it can be used to control the release of the APIs [342]. CDs have been used in different drug delivery systems, including transdermal, ocular, rectal, nasal, and oral drug delivery systems [347]. Methyl-β-CD has a lipophilic cavity located in the centre. Therefore, it forms inclusion complexes with various lipophilic drugs (e.g., DXM) by taking part in a drug molecule or the whole of the molecule. Hence, in this system, it is possible to create aqueous drug/methyl-β-CD inclusion complexes of lipophilic APIs [348].

On the other hand, lactose is utilised as it is commonly used as a binder or filler excipient in tablet manufacture. This excipient has many advantages, including its availability, compatibility with APIs and other excipients, and water solubility [349]. Lactose has been widely used in the literature as an excipient with DXM to formulate tablet dosage forms [350]–[352].

After the DXM tablets were fabricated, two methods used to investigate whether the added materials, such as DXM tablet and the dye, would distribute through the prepared hydrogel.

5.5.2 Raman Spectroscopy

The main aim of this method was to investigate whether the DXM in the DXM/methyl-β-CD tablet could distribute through the prepared HPMC hydrogel (7% HPMC w/w). In the beginning, the Raman spectra of the utilised materials were determined **(Figure 5.16 and 5.17)** to identify the major DXM molecular peak and determine whether this peak interfered by other materials molecular peaks at the same region. Identifying the main DXM molecular peak was useful for studying the diffusion of the drug through the utilised hydrogel system.

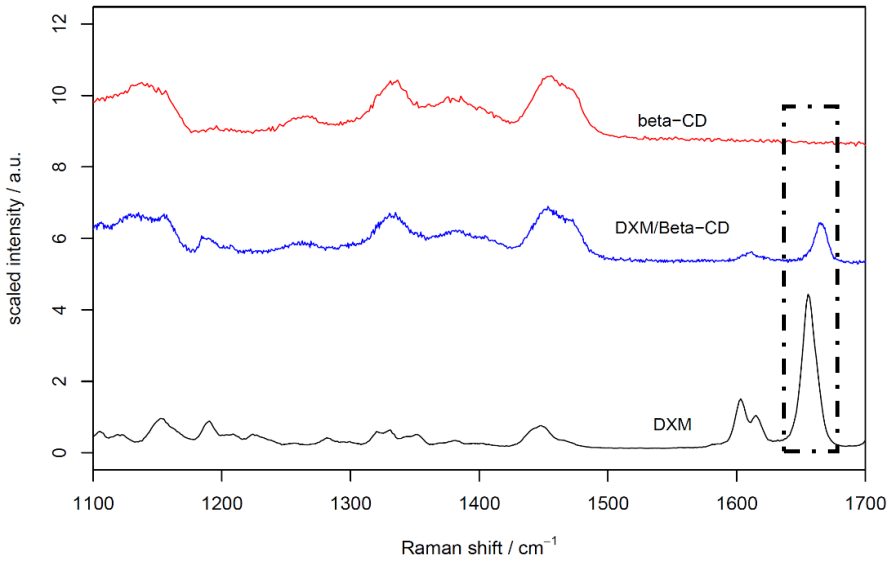

Figure 5.16 The Raman spectra of the dry DXM as received, beta-CD powder as received, and DXM/methyl-β-CD inclusion complex powder as received.

Figure 5.16 presents the main molecular peaks in the DXM Raman spectra in the region of 1100-1700 cm^{-1}. A characteristic peak of DXM was detected at 1660 cm^{-1}, which is related to the C=O group. This peak was also observed for DXM/methyl-β-CD complex powder and did not emerge in the methyl-β-CD powder Raman spectrum. This peak was slightly shifted in the region of the methyl-β-CD spectra due to the inclusion complexation between the DXM and the

β-CD polymer [353]. Moreover, it did not interfere with another peak in the methyl-β-CD powder Raman spectrum. There were two other molecular regions related to the DXM in the 2960 cm^{-1} and 3060 cm^{-1} regions, and these are related to the C-H and =C-H molecular groups, respectively [354]. However, these regions are not evident in **figure 5.17** and in the region 1000-1700 cm^{-1}, which was line mapped in the next step.

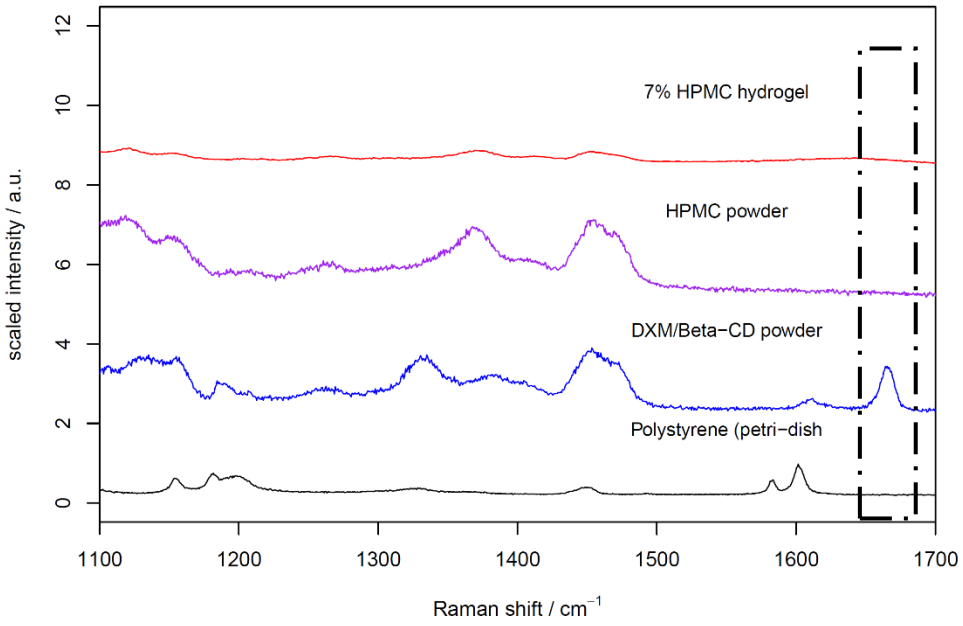

Figure 5.17 Raman spectra of the received materials and prepared hydrogel. From bottom to top, polystyrene (Petri dish), DXM/methyl-β-CD complex powder (as received), HPMC powder (as received), and freshly prepared 7% HPMC hydrogel.

Figure 5.17 shows the Raman spectra of the utilised materials, including the DXM/methyl-β-CD powder, the HPMC powder, a freshly prepared 7% HPMC hydrogel, and the polystyrene (Petri-dish container). The results represent the characteristic peak for DXM in the 1660 cm^{-1} region, and this peak does not interfere with other materials' molecular peaks in the same molecular region. All the previous spectra for DXM [354]–[357], polystyrene [358], [359], HPMC [360], [361], and methyl-β-CD [362] were identified in the

literature. After the characteristic peak was identified for the DXM, the mapping technique was conducted for the prepared sample (HPMC hydrogel containing a compressed DXM/methyl-β-CD tablet). In the beginning, two images were taken for the dry prepared tablet and the prepared sample **(Figure 5.18 A and B)**.

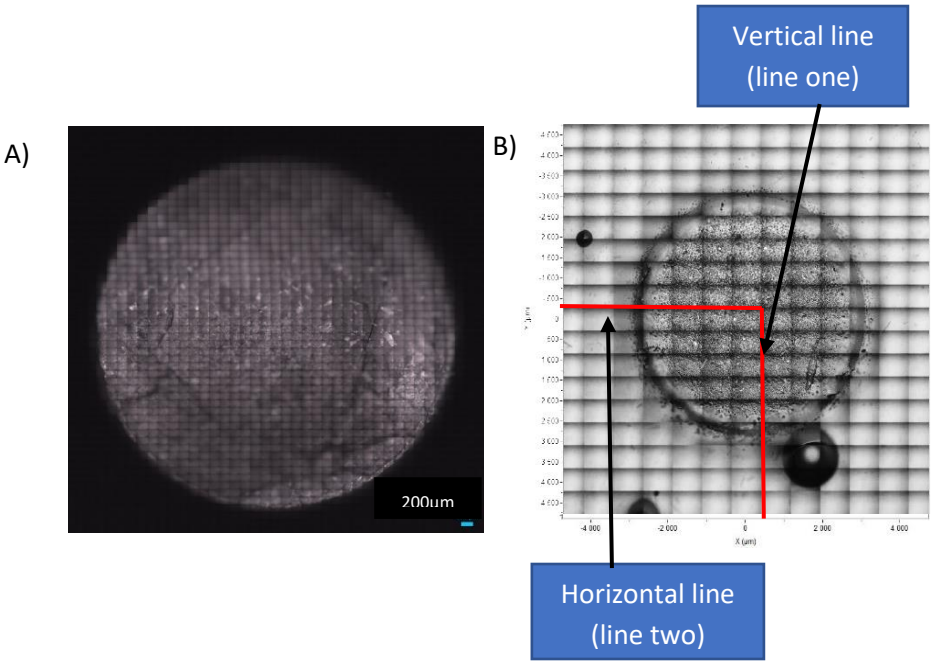

Figure 5.18 Raman optical image of A) a DXM/methyl-β-CD tablet under 10x magnification, and B) after the tablet was placed above the 7% HPMC hydrogel at the middle of a Petri dish under 10x magnification at the beginning of the study. The images were formed by stitching many images together.

At the beginning of this experiment, optical images were taken of one of the compressed dry DXM/methyl-β-CD tablets to show the morphological shape and surface of the prepared tablet **(Figure 5.18 A).** This image was taken under 10x magnification to facilitate taking a larger area than other objectives. The required area was selected, and multiple images were taken by clicking the mosaic tool. Subsequently, other images were taken of the prepared tablet after it was placed in the middle of the prepared sample at the top of

hydrogel **(Figure 5.18 B).** Afterwards, two-line mapping (horizontal and vertical) was conducted for the sample at the different time point (0, 1, 3, 7 days) to investigate the diffusion of the DXM in the hydrogel **(Figure 5.19 A and B).**

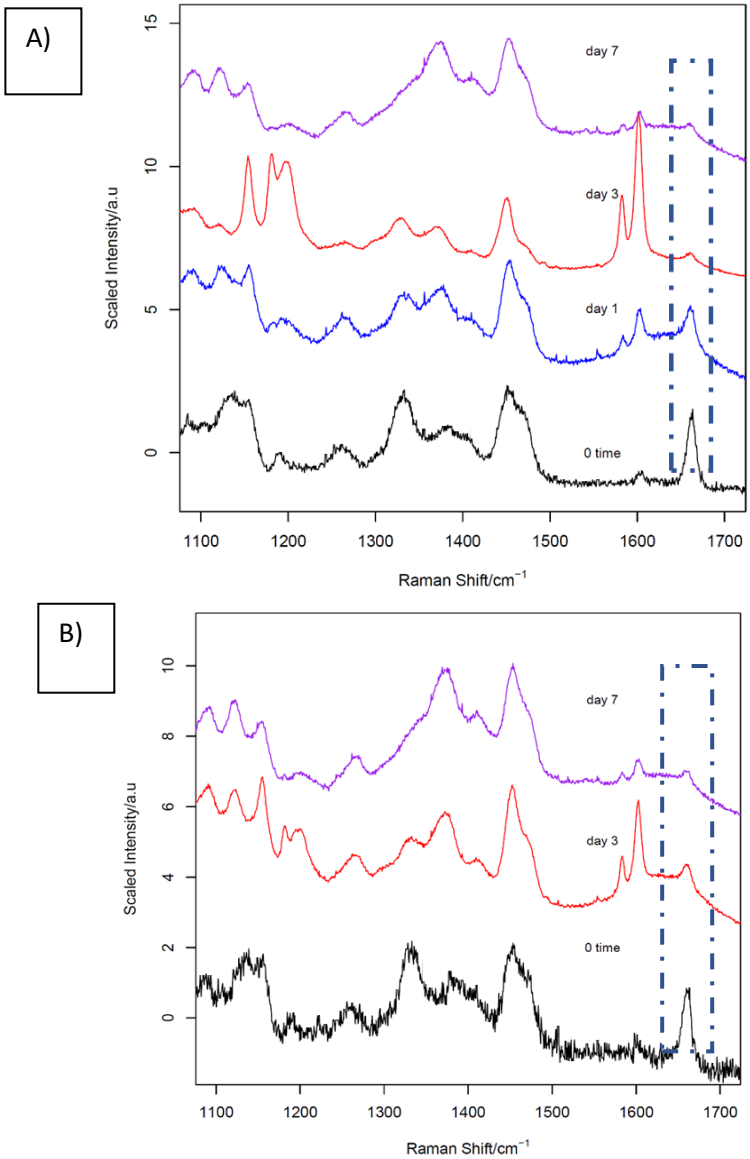

Figure 5.19 Raman Spectra of the DXM/methyl-β-CD tablets in 7 % HPMC hydrogel after being line mapped at different times, including 0-time, 1 day, 3 days and 7 days. A) The first line mapping Raman spectra (the horizontal line) and B) the second line mapping Raman spectra (the vertical line).

Figure 5.19 presents the Raman spectra after the line mapping (line one) collected from the prepared samples from day 0 to day 7. The analysed area was taken from the middle of the placed tablet (0 µm) to an area of the placed hydrogel, as seen in appendix section **Figure 5. C2,** to investigate the distribution of the DXM in the hydrogel. Some characteristic bands with high intensities were detected at day 0, including 1660, 1450, 1330, 1260, 1190 cm^{-1}. The band that appears at 1660 cm^{-1} is characteristic for DXM, as mentioned before, and is related to carbonyl group C=O molecular group. As a result, the identified peak showed that its intensity decreased from day 0 to day 7. Also, the area under the curves (AUC) was found for each of the characteristic peaks **(horizontal line)** from day 0 to day 7, namely as 679.13, 390.37, 240.57, and 23.17, respectively. Moreover, the peak intensity of the carbonyl group changed, namely at day 0, 1, 3, and 7 it was 0.05, 0.04, 0.03, and 0.02 a.u., respectively **(Figure 5.19 A)**. Moreover, the AUC for day 0 to day 7 **(vertical lines) w**as 321.05, 154.90, 105.90, and 28.6, respectively. The peak intensity of the carbonyl group changed between day 0, 3, and 7, namely from 0.04 to 0.03 to 0.02 a.u., respectively **(Figure 5.19 B)**. The results show that the DXM diffused through the prepared hydrogel.

Many challenges were faced during this experiment. Firstly, the prepared hydrogel placed in the middle of the Petri dish needed to be placed there for 24 hours to avoid the hydrogel moving during the Raman mapping test, which would have affected the results. Moreover, the hydrogel was also placed there for 24 hours to facilitate the removal of any air bubbles that would have affected the Raman reading of the spectra. Also, the utilised container could not have any tall edges as these may have hit the Raman objective and affected the Raman reading due to the moving of the sample

container by the objective. Finally, the HPMC hydrogel was transparent, and it was challenging to focus the objective on a specific area to conduct the full or line mapping.

In the next step, the release of a food colour dye through the printed pores was investigated. The release of the colouring agent through the printed pores loaded with the HPMC hydrogel was captured using a digital camera to determine whether the dye release through the all printed pores. In this part, we aimed to investigate the release of a colouring agent with a similar molecular mass to DXM through the pores of the printed device that loaded with the HPMC hydrogel. Our drug is colourless after dissolving in the hydrogel, and thus we aimed to investigate the release of the colouring agent visually using a simple model.

5.5.3 Food Dye Passing Through the Printed Pores via the HPMC Hydrogel

In this part, a food dye was utilised to investigate the passing of the dye through the printed pores **(Figure 5.20)**. Our aim was to see whether the dye would be passed through all pores.

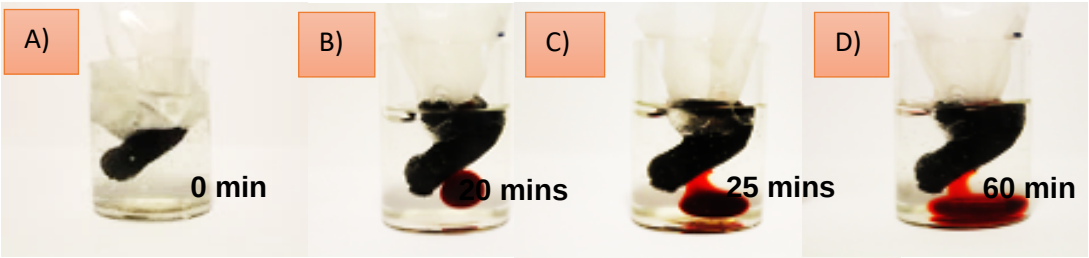

Figure 5.20 Photographs of a food colour dye (sunset red dye) passing through the pores of an ear prototype device filled with and immersed in the 6% HPMC hydrogel. It shows the dye passing at A) zero-time, B) 20 min, C) 25 min, and D) 60 min after the experiment started.

Figure 5.20A-D shows the passing of a commercially available food colouring dye (sunset red) through the pores of the printed prototype ear device with 6% HPMC hydrogel and at different times. The utilised colouring agent contains various excipients, including sodium carboxymethylcellulose, propylene glycol, sorbitol, and a colouring dye. The results showed that the dye passed through the printed pores were located at the base of the immersed devices. This may have occurred due to gravity [363], the concentration of the added dye, and the lack of movement of the immersed devices. The diffusion of the dye through the hydrogel depends on the concentration gradient. Moreover, the diffusion might have been affected by the viscosity of the hydrogel, the particle size of the utilised dye, the hydrogel properties (porosity, degree of crosslinking and elasticity), the chemical compositions of the hydrogel, temperature, the solubility of the utilised material [364]–[367]. Different concentrations of HPMC hydrogels were utilised (4 and 5% HPMC hydrogels (see the appendix section)).

Using this method, the immersed devices experienced no movement similar to the real movement of a human. Hence, this method needs some modifications to investigate the passing of the dye through the pores during device movement. Moreover, this experiment was carried out at room temperature. It may be necessary to use another temperature (37℃) in future to see its effect on the passing of the dye. Furthermore, we may need to use less added dye to see the effect of concentration on the passing of the dye through the printed pores. In addition, we may need to use a smaller container to reflect the size of the human ear canal.

5.5.4 Calibration of the Curve Using UV spectroscopy

In the beginning, the UV-vis spectrometer scanned the DXM sample from 200 to 800 nm, and DXM chromatic peak was observed at 241 nm **(Figure 5.21)**. The detected wavelength matches what was published in the literature [218], [368], [369].

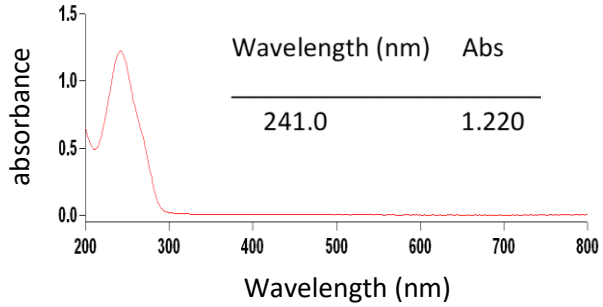

Figure 5.21 The UV absorbance sensitivity of DXM (as received) was 241 nm.

Subsequently, the standard curve for the DXM was constructed for the Transwell and dissolution tests of the formulated tablets (DXM/methyl-β-CD and DXM/lactose tablets) **(Figure 5.23)**.

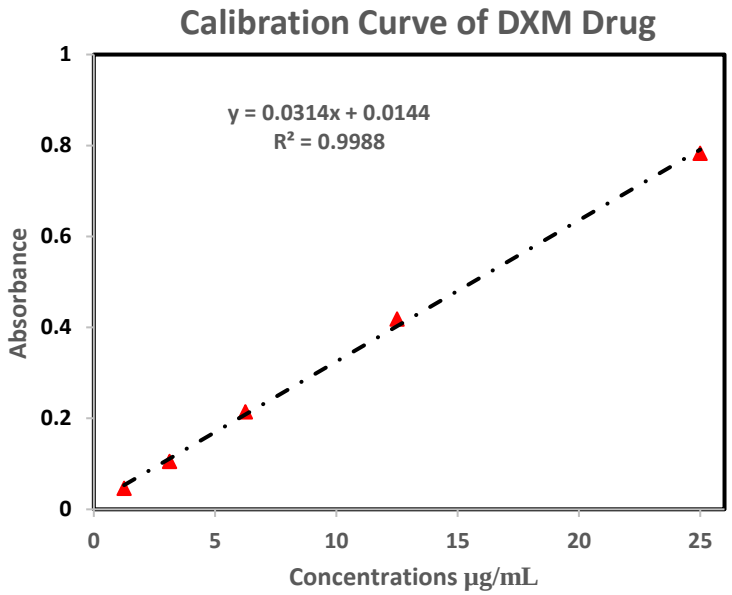

Figure 5.22 Calibration curve of DXM solution.

In this part, different concentrations were diluted from the prepared stock solution, including 1.25, 3.125, 6.25,12.5, and 25 µg/mL, in to construct the calibration curve to verify the linearity. The stock drug concentration was diluted into different sample concentrations, which were scanned by a UV-vis spectrometer to create a standard curve to verify the linearity. **Table 5.1** presents the values obtained from the DXM calibration curve, including the slope, intercept, and R^2. The coefficient of determination was $R^2 = 0.9988$. The LOD for DXM was 0.052 µg/mL, and the LOQ was 0.159 µg/mL.

Table 5.1 Values obtained from the DXM calibration curve.

	Value
Slope	0.0314
Intercept	0.0144
R^2	0.9988

5.5.5 *In Vitro* DXM Release and Permeability Through the Synthetic Membrane

5.5.5.1 Preliminary *in vitro* Permeability Studies of DXM

In this part, various preliminary studies were performed, including the Transwell penetration study utilising the Strat-M® membrane and the USP dissolution (apparatus one) study of the drug release through the printed pores without the Strat-M® membrane.

5.5.5.1.1 Transwell Release Study

The permeability of DXM through the Strat-M® membrane was measured at room temperature using a Transwell® 12-well plate modified by covering a Transwell insert with the Start-M® membrane **(Figure 5.10)**. The aim was to investigate whether the DXM molecules could permeate through the covered membrane for use

with the device developed in the dissolution apparatus study. Usually, diffusion studies are conducted using either an animal skin model, such as porcine skin or a human skin model. But, there are some limitations of these skin models (See the introduction section for other limitations) [370].

Different studies have been performed comparing the release profile of APIs through a Strat-M® membrane, human, other synthetic membrane or animal models [337], [371]–[373].

A Strat-M® membrane with the size of 47 mm (4.7 cm) in diameter was selected in this study because it can cover the whole area surrounding the Transwell insert. Moreover, it can prevent any escape of the aqueous medium from the donor compartment edges to the receiver compartment. Therefore, the drug can be only passed through the utilised membrane from the opening area of the bottom part of the Transwell insert.

Several challenges were faced in this experiment. Firstly, using small synthetic membrane size (25 mm in diameter) could not prevent aqueous solutions from escaping from the donor compartment sides to the receiver compartment. Moreover, it required a tight closing of the larger membrane (47 mm) at the side, to hold the membrane with the insert to facilitate the withdrawal of the samples and adding the refreshing media. Moreover, it needed to facilitate the drug passing through the membrane from the open part of the Transwell insert. **Figure 5.23** shows the *in vitro* drug release profile of DXM through the covered synthetic membrane, which is the Strat-M® membrane.

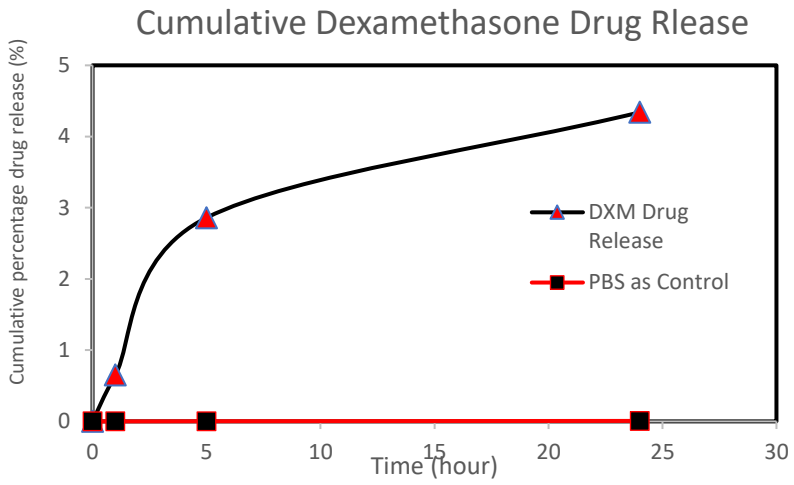

Figure 5.23 Cumulative DXM release through the Strat-M® membrane covering the Transwell insert.

The DXM release from the printed ear prototype device pores and its permeability through the Strat-M® membrane was examined for 24 hours. The results in **Figure 5.23** show that 4.34% of the starting drug load had permeated through the Strat-M® membrane at 24 hours. The permeation of DXM through the synthetic membrane was at a small percentage, which might have been because the loaded concentration of the DXM in the donor compartment was high. Also, the receiver compartment was saturated with DXM, which might have been due to the low amount of PBS medium utilised in the experiment. This experiment was done to confirm whether the DXM could pass through the Strat-M® membrane. The results confirmed that DXM did pass through the membrane. Consequently, the membrane can be utilised in future with the dissolution apparatus study to investigate the drug release through the printed pores of the 3D devices developed in **chapter 3**. In this study, we also used methyl-β-CD with the DXM powder to investigate whether DXM still permeates through the membrane. The results show that the DXM still permeated through the membrane at a low concentration for the same reasons as the DXM alone **(see the appendix section).**

Subsequently, we moved to the next step, which was studying the DXM release through the created pores in the final 3D developed prototype printed device using one of the dissolution apparatus techniques, namely the basket model.

5.5.5.1.2 *In Vitro* Release of DXM through the Printed Pores Without Using the Strat-M® Membrane

This experiment consisted of two parts. The first was using the 3D printed devices without covering the created pores with the synthetic Strat-M® membrane. In this part, two different formulations were investigated to determine which one could provide sustained DXM release for 7 days, which is the same period for which AOE patients are treated with ear drops. For instance, Ciprodex is used to treat some patients suffering from AOE for 7 days [374].

In this part, we aimed to investigate the release of DXM through the printed pores using two different tablets. One of the prepared tablets (DXM/methyl-CD) can dissolve faster than the other tablet (DXM/lactose). The dissolution apparatus V (paddle over disk) and dissolution apparatus VI (cylinder) are mostly used for testing the transdermal dosage forms [375], [376]. However, we selected apparatus I for many reasons, including the fact that the basket can prevent any movement or floating of the loaded FDM printed ear medical device. In addition, it facilitates the drug release through the printed pores and spreading in all directions near the beginning of the printed device. With the other transdermal apparatus types, some of the printed pores may have been affected, preventing the drug release through them. Also, the loaded medical device may move or float if it is not fixed to the insertion place.

In this experiment, several ear prototype devices with 1 mm in diameter circular pores were utilised **(chapter 3, section 3.3.5)**, and these were each loaded with 0.8 mL of 7% HPMC hydrogel (w/w). Then, each device was inserted with a tablet containing either the DXM/methyl-β-CD inclusion complex or the DXM/lactose mixture. The dissolution study was run in triplicate for both formulations (n=3).

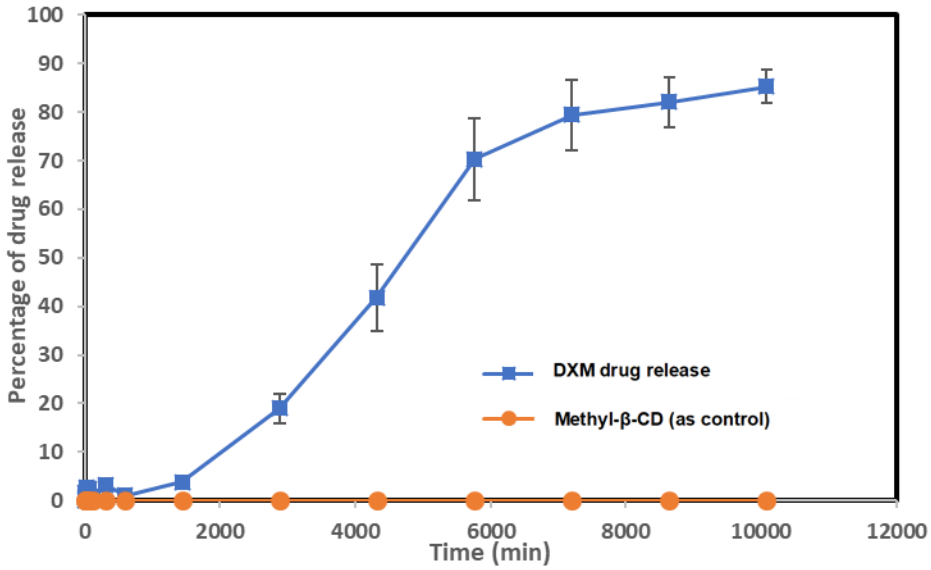

Figure 5.24 Dissolution profile of DXM tablets in pH 7.4; DXM/methyl-β-CD and as received methyl-β-CD, through the printed devices with circular pores without synthetic membrane cover. The error bars in this chart are the standard error in the mean, where n=3.

Figure 5.24 shows the *in vitro* drug release profile of DXM/methyl-β-CD through the loaded 7% HPMC hydrogel and via the printed pores without using the Strat-M® membrane. The dissolution data presented in this figure show that the formulation (DXM/methyl-β-CD) displayed sustained release over 7 days. Also, it was found that the DXM release started during the first five minutes (0.6%) and reached 85.3% on day 7. This experiment was done in triplicate, and the drug concentrations in the three tablets was 2.01±0.09 mg.

Afterwards, another tablet (DXM/lactose) was compressed and investigated using the same device and gelling system **(Figure 5.25)**

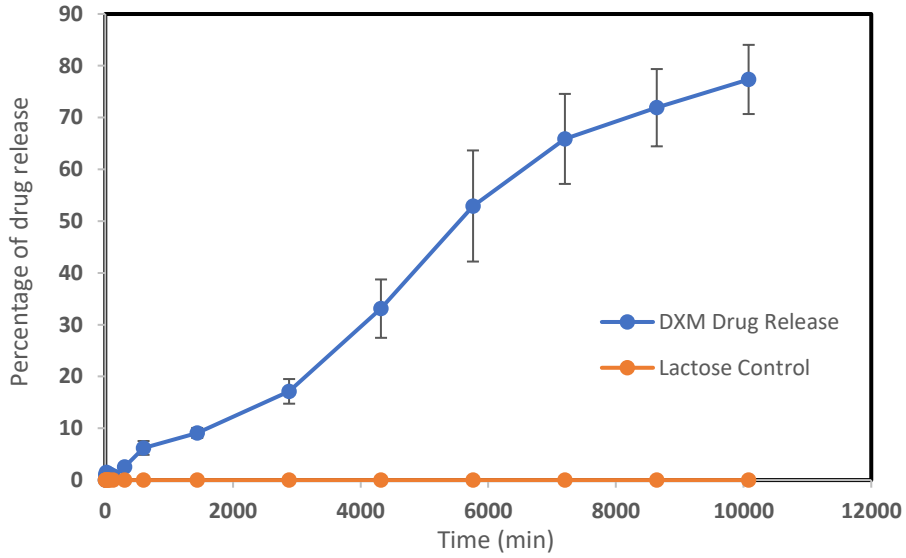

Figure 5.25 Dissolution profile of DXM compressed tablets in pH 7.4; DXM/lactose and received lactose, through the printed devices with circular pores without synthetic membrane cover. The error bars in this chart are the standard error in the mean where n=3.

Figure 5.25 shows the *in vitro* drug release profile of the DXM/lactose through the loaded 7% HPMC hydrogel and via the printed pores without using the Strat-M® membrane. The dissolution data show that the formulation displayed a sustained release over the same period as with the previous formulation, namely 7 days. The release of the DXM started during the first five minutes (1%) and reached 77.36% on day 7. This experiment was done in triplicate, and the drug concentrations in the three tablets was 2.06 ± 0.24 mg.

In both experiments, the standard curve was created in pH 7.4 dissolution PBS medium to determine the concentration of each withdrawn sample after the UV measurements. Also, the percentage of the DXM release was calculated and plotted vs the time in the curve.

The second formulation, which is DXM/lactose tablet, was selected for several reasons. Firstly, it gives a slower release of DXM than the other formulation, i.e. DXM/methyl-β-CD. With the DXM/lactose formulation, the percentage release of DXM at day 7 was 77.36%, while for the other formulation (DXM/methyl-β-CD) it was 85.3%. In the DXM/lactose formulation, all the three replicates provided a sustained release of DXM for 7 days. However, some of the replicates of the DXM/methyl β-CD finished before day 7. Figure 5.25 shows that the percentage release of DXM gradually increased until it reached day 7. However, the DXM release in Figure 5.24 reduced after it reached day five.

Subsequently, we moved forward with the DXM/lactose formulation, and the Strat-M® membrane was utilised for the dissolution study (Figure 5.26).

5.5.5.2 *In vitro* DXM Release through the printed pores Covered with Strat-M® Membrane

Based on the results of the preliminary studies, the DXM/lactose tablet was utilised. The same procedures as in the previous section, were done. However, the printed ear prototype devices were covered from the outside with the Strat-M® membrane. The dissolution study was run in triplicate (n=3).

Figure 5.28 shows the *in vitro* drug permeability through the synthetic Stat-M Membrane covering the FDM printed ear prototype device. This printed device was loaded with a DXM/Lactose tablet and 7% HPMC hydrogel. The results show that the formulation displayed sustained release over the same period, which was 7 days. The release of the DXM started after 5 minutes of running the experiment, reaching 62.94% on day 7. The *in vitro* permeability of

the DXM in the DXM/lactose mixture tablet experiment was repeated in triplicate, and the graph is illustrated in the appendix section.

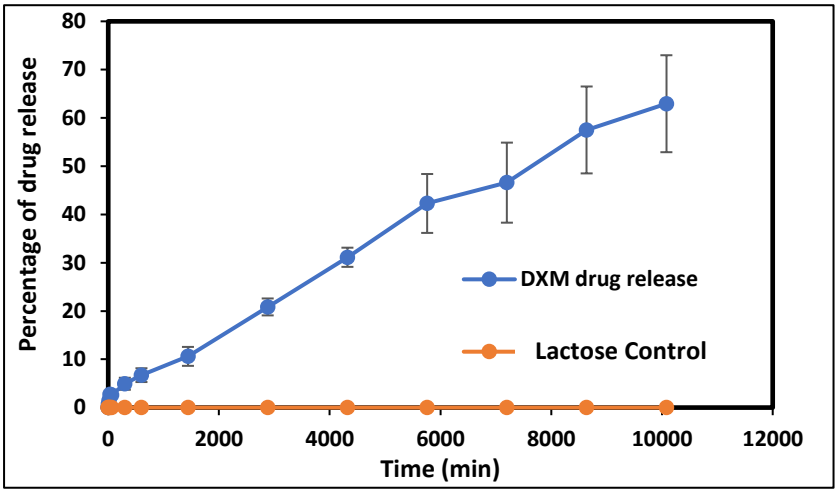

Figure 5.26 *In vitro* drug permeability of DXM through the covered synthetic membrane at pH 7.4

In this thesis, we designed a system that incorporated a tablet into a gelling system. The tablet contained DXM, whereby its concentration reached the solubility limit after contact with the gelling system. The rate-limiting of the DXM release into the dissolution medium was controlled by the diffusion rate through the gelling system and its permeability through the covering Strat-M membrane. The DXM permeated at a constant rate through the covered synthetic Strat-M membrane **(Figure 5.27)**.

There are some advantages of using a tablet dosage form in our model, including the fact that it might offer a very easy dosing method for OE patients. The patient might take different tablets containing different drugs, such as DXM and ciprofloxacin. Moreover, the patients might use different tablets containing different DXM doses. Furthermore, the patients might take tablets with different dissolving rates and rates of diffusion through the loaded gelling system. For

instance, they might use a quickly dissolving tablet, such as DXM/CD, or a slowly dissolving tablet, such as DXM/lactose. When the DXM/CD tablet is placed within the loaded gelling system, the loaded CD dissolves rabidly, and the DXM is released and precipitates within the loaded gelling system. Then, the drug starts to diffuse through the gelling system and the 3D printed pores. After that, the DXM permeates through the covered synthetic membrane, which simulates the external auditory canal skin, to the surrounding dissolution medium. The synthetic membrane covering the 3D printed ear prototype device controlled the release of DXM to the dissolution medium.

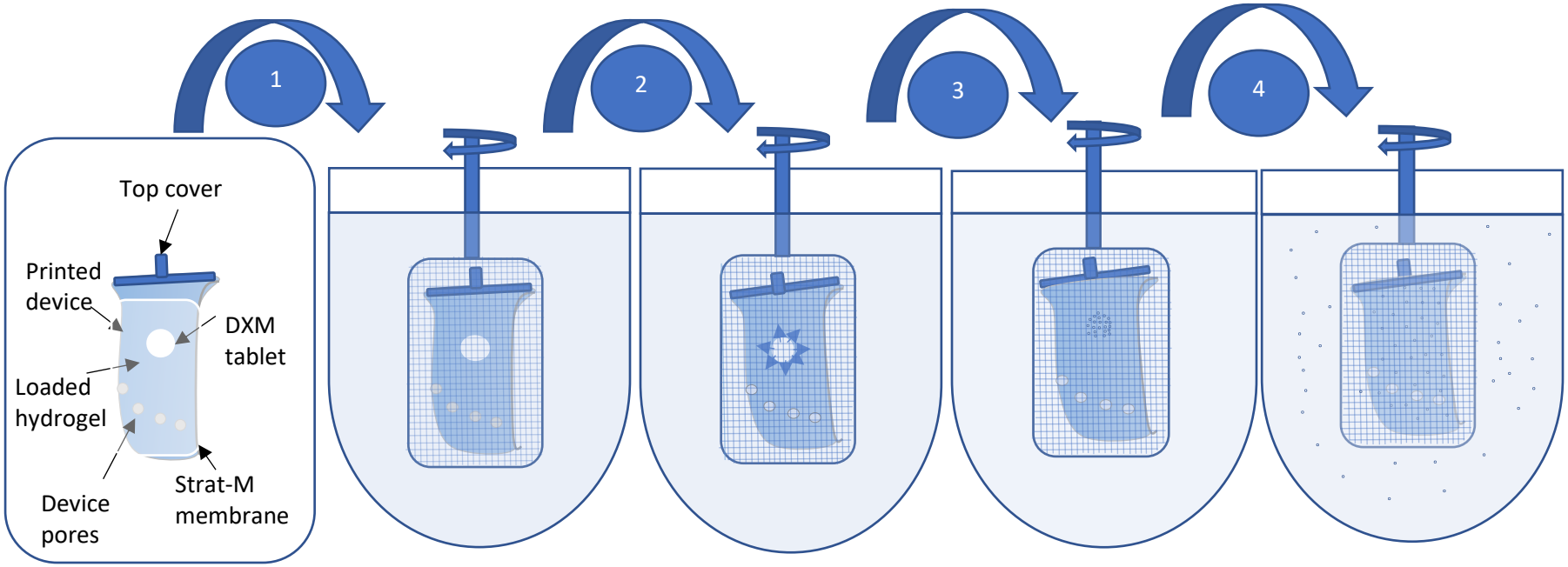

Figure 5.27 Schematic diagram of the DXM permeability mechanism through the covering Strat-M membrane.

5.6 Conclusion

In this chapter, we successfully compressed two different tablet formulations, namely DXM/methyl-β-CD and DXM/lactose tablets, using a single hydraulic compression instrument. Moreover, the diffusion of the DXM was successfully detected by Raman spectroscopy. The Raman results showed that the intensity and AUC of the characterised molecular peak, which was located at 1660 cm^{-1}, decreased from day 1 to day 7. This indicates that the drug diffused through the selected 7% HPMC hydrogel. Additionally, the diffusion of different colouring agents were investigated through the HPMC hydrogel system, and the results confirmed that the utilised dyes successfully passed through some of the printed pores. The utilised method needs some modifications in future. The *in vitro* Transwell release study confirmed that the DXM permeated through the utilised Strat-M® membrane, whereby this membrane covered the developed ear prototype device in order to study the drug release using the dissolution apparatus I. The results showed that the DXM had a sustained release over 7 days, which is the treatment period for OE patients using ear drops. Hence, the covering synthetic membrane influenced the release of DXM into the dissolution medium.

Chapter 6 General Conclusions and Future Work

6.1 Conclusions

This dissertation aimed to develop a medical prototype device for use in the ear using 3D printing. The developed device incorporates a gel-based drug delivery system. An anti-inflammatory drug would be able to show a sustained release after being inserted into a patient's external ear canal for the treatment of AOE. OE infections of the outer ear affect a large proportion of the population, including children, adolescents, and adults [1].

The device proposed here could allow a one-time application of an extended-release drug system that would minimise the current requirement for multiple daily applications, thereby likely improving patient compliance and bringing significant benefits compared to current OE treatments. To achieve this, an FDM 3D printing technique was utilised to fabricate an ear medical prototype device containing several circular pores. The fabricated device can be designed such a way as to mimic the internal dimensions of an individual's external auditory canal. Moreover, the printed device can incorporate a gelling system as a vehicle for an OE ear drug to be slowly released and delivered at the site of action for an extended period. The loaded drug used mimics the therapeutic dose that currently utilised anti-inflammatory ear drops (DXM). To date, no report has shown an ear medical device that contains a gelling system in addition to the API drug to be utilised to treat OE patients.

The work presented in chapter 3 developed different ear prototype devices utilising different 3D printing techniques, including FDM (Ultimaker^{2+}) and SLA (Formlabs 2). Several materials were used to fabricate the designed devices, namely PLA, TPU, flexible resin, and tough resin. PLA was selected for use with the Ultimaker^{2+} 3D printer to manufacture the final designed ear medical prototype device with circular pores (1 mm in diameter). The SEM investigations showed that the PLA

printed devices had the proper distribution of the deposited layers and that there were no overlaps and cracks between the printed layers. DSC and HSM investigated the T_m of the PLA polymer for this to be considered during the printing.

After the final design of the ear prototype device was achieved, the second step was initiated in chapter 4 by formulating a gelling system using HPMC polymer. Various concentrations were prepared, and rheologically characterised to determine the rheological behaviour and viscosities of the prepared samples. The prepared hydrogel displayed shear-thinning behaviour. Several concentrations were prepared and their flows were investigated through several printed devices with different pore configurations at various temperatures (25℃ and 37℃). The results showed that the ability of the prepared hydrogels to emerge from the pores (as required to make contact with the skin in use) was affected by increasing the pore number, raising the temperature from 25℃ to 37℃, increasing the HPMC polymer concentration and changing the designs of the devices by changing the pore locations. A 7% HPMC hydrogel was selected to be utilised as a vehicle for sustained drug release. This concentration provided an elastic-like behaviour during the rheology test, and it facilitated a slower release than the 6% HPMC hydrogel through the printed devices for 2 days.

Finally, the anti-inflammatory drug, DXM was formulated into different tablet dosage forms using a single hydraulic compression press. Different excipients were utilised, including β-CD and lactose. Then, the DXM diffusion through the prepared HPMC hydrogel (7% HPMC) was successfully investigated using Raman spectroscopy. Finally, the *in vitro* permeability of the DXM through the Synthetic-M membrane was examined using a USP apparatus I (basket). The results showed that the incorporated tablet (DXM/lactose) within the printed prototype device successfully passed the Strat-M® membrane (used as a certified model of the human skin) and reached 62.94% DXM percentage release at day 7.

Some challenges may occur during the usage of the PLA 3D printed in-ear prototype device, including:

- The printed ear prototype device might break the epithelial layers of the patient's external auditory canal after removal from and reinsertion of the printed devices in the canal area, producing some ear problems. The printed device might need to be lubricated by the same gelling system before insertion into the human canal. Moreover, the device needs to be inserted into the patient's ear under the supervision of an audiologist.
- The ear prototype device surface might be contaminated with the microorganisms, which may cause some ear problems if they inserted into the patient's ears. The patients need to clean their hands before holding the printed devices.
- The printed pores might not cover the entire inflamed area; therefore, their locations may need to be optimised.
- The gelling system might flow completely from the printed device and block the area between the TM and the inserted device and thus affect the patient's hearing.

6.2 Future Work

The ideas presented in this work may be continued in several ways:

- Human (assessment of comfort and use) trial: The external auditory canals of several patients suffering from early-stage AOE could be scanned by an Otoscan device under the supervision of an audiologist [292]. The audiologist needs to check the patients' ear canals. The patients would need to be free from any ear complications, such as ear occlusion, canal oedema, or canal defects. Then, the ear dimensions data could be transferred to CAD software to be modified to the design achieved in chapter 3. Subsequently, the CAD files could be transferred to a commercially available FDM 3D printer to fabricate the ear prototype devices. Afterwards, the patients may use the printed devices under the

supervision of an audiologist to avoid any complications. Then, a survey could be done about the device use and ear feeling and to obtain feedback from the patients. We have an agreement in place and some ethical approval for a comfort trial with patients. In future, the process can be moved forward by taking the ear dimensions of several patients.

- The ear medical prototype device designs developed in this thesis might be improved by changing the utilised polymer to a potentially more comfortable and compliant rubbery polymer that is still hard enough to hold and release the formulation and not be squeezed during the ear insertion. Also, the device needs to be hard enough to withstand the formulation loading and insertion within the patient's ear canal.
- The drug release through the printed ear prototype device with circular pores might be optimised further by changing the pore number, shape (square), size, and location as well as the hydrogel viscosity.
- The formulated tablets might be improved by adding additional excipients, such as a filler, lubricant or binder, to be fabricated in large quantities utilising a rotary compressing tabletting instrument. Also, a stability test may be performed on the utilised tablet. Additionally, another drug might be used and compressed with the DXM to form a tablet, such as ciprofloxacin, to be used against bacterial infections that can occur in the ear canal. Also, it might be possible to add chemical permeation enhancers, such as sodium dodecyl sulfate, limonene, and bupivacaine, to treat ME infections (AOM). The chemical permeation enhancers could enhance the API flux through an intact TM into the ME [339].
- It might be useful to incorporate the developed ear medical prototype device with hearing aid components to act as drug-eluting hearing aids for use with patients suffering from OE and hearing problems. The patients could thus be treated for AOE without affecting their hearing. The hearing aids could be optimised in such a way that they

can be covered with a printed shell that contains an antibiotic drug, a steroid, and a hydrogel formulation.

References

[1] J. Wipperman, “Otitis Externa,” *Prim. Care Clin. Off. Pract.*, vol. 41, no. 1, pp. 1–9, 2014.

[2] J. D. Osguthorpe and D. R. Nielsen, “Otitis externa: Review and clinical update,” *Am. Fam. Physician*, vol. 74, no. 9, pp. 1510–1516, 2006.

[3] P. G. Shekelle *et al.*, “Management of acute otitis media: update,” *Evid. Reporttechnology Assess.*, no. 198, p. 1, 2010.

[4] A. S. Coco, “Cost-effectiveness analysis of treatment options for acute otitis media,” *Ann. Fam. Med.*, vol. 5, no. 1, pp. 29–38, 2007.

[5] I. Syed and C. Aldren, “Meniere’s disease: an evidence based approach to assessment and management,” *Int. J. Clin. Pract.*, vol. 66, no. 2, pp. 166–170, 2012.

[6] T. Meyer, “Intratympanic treatment for tinnitus: a review,” *Noise Health*, vol. 15, no. 63, p. 83, 2013.

[7] M. J. Ruckenstein, “Autoimmune inner ear disease,” *Curr. Opin. Otolaryngol. Head Neck Surg.*, vol. 12, no. 5, pp. 426–430, 2004.

[8] M. M. Vio and R. H. Holme, “Hearing loss and tinnitus: 250 million people and a US $10 billion potential market,” *Drug Discov. Today*, vol. 10, no. 19, pp. 1263–1265, 2005.

[9] “World Health Organization; 2018. Prevention of blindness and deafness. Available from - Google Search.” https://www.google.co.uk/search?q=World+Health+Organization%3B+2018.+Prevention+of+blindness+and+deafness.+Available+from (accessed Aug. 14, 2019).

[10] R. Esterberg *et al.*, “Fish in a Dish: Drug Discovery for Hearing Habilitation,” *Drug Discov. Today Dis. Models*, vol. 10, no. 1, 2013.

[11] B. Yueh *et al.*, “Screening and Management of Adult Hearing Loss in Primary Care: Scientific Review,” *JAMA*, vol. 289, no. 15, pp. 1976–1985, 2003.

[12] N. El Kechai *et al.*, “Recent advances in local drug delivery to the inner ear,” *Int. J. Pharm.*, vol. 494, no. 1, pp. 83–101, 2015.

[13] R. W. Sander, “Otitis Externa: A Practical Guide to Treatment and Prevention,” *Am. Fam. Physician*, vol. 63, no. 5, p. 927, 2001.

[14] K. D. Brown *et al.*, “Diseases of the External Ear, Chapter 47,” in *Current Diagnosis & Treatment Otolaryngology--Head and Neck Surgery,* Third edition., pp. 645–660, 2011.

[15] C. E. Rash, “Basic Anatomy of the Hearing System,” *Helmet-Mounted Disp. Sensat. Percept. Cogn. Issues*, p. 302, 2009.

[16] P. S. Roland *et al.*, “disorders of the external auditory canal,” *J Am Acad Audiol*, vol. 8, pp. 367–378, 1997.

[17] J. K. Kim and J. H. Cho, “Change of external auditory canal pH in acute otitis externa,” *Ann. Otol. Rhinol. Laryngol.*, vol. 118, no. 11, pp. 769–772, 2009.

[18] P. M. Devesa *et al.*, “External auditory canal pH in chronic otitis externa,” *Clin. Otolaryngol. Allied Sci.*, vol. 28, no. 4, pp. 320–324, 2003.

[19] F.E. Lucente, “Anatomy, Histology, and Physiology,” *Phila. WB Saunders Co*, pp. 1–16, 1995.

[20] H. K. Vaddi *et al.*, “Ocular, Nasal, and Otic Drug Delivery,” in *in Gibaldi’s Drug Delivery Systems in Pharmaceutical Care*, ASHP, pp. 59–78, 2007.

[21] D. H. Keefe *et al.*, “Ear-canal impedance and reflection coefficient in human infants and adults,” *J. Acoust. Soc. Am.*, vol. 94, no. 5, pp. 2617–2638, 1993.

[22] X. Liu *et al.*, "Otic drug delivery systems: formulation principles and recent developments," *Drug Dev. Ind. Pharm.*, vol. 44, no. 9, pp. 1395–1408, 2018.
[23] H. F. Schuknecht and M. R. Gacek, "Cochlear Pathology in Presbycusis," *Ann. Otol. Rhinol. Laryngol.*, vol. 102, no. 1_suppl, pp. 1–16, 1993.
[24] M. Igarashi *et al.*, "Morphometric Comparison of Endolymphatic and Perilymphatic Spaces in Human Temporal Bones," *Acta Otolaryngol. (Stockh.)*, vol. 101, no. 3–4, pp. 161–164, 1986.
[25] X. Khoo *et al.*, "Formulations for trans-tympanic antibiotic delivery," *Biomaterials*, vol. 34, no. 4, pp. 1281–1288, 2013.
[26] E. Hoskison *et al.*, "Drug delivery to the ear," *Ther. Deliv.*, vol. 4, no. 1, pp. 115–124, 2012.
[27] A. N. Salt and K. Hirose, "Communication pathways to and from the inner ear and their contributions to drug delivery," *Hear. Res.*, vol. 362, pp. 25–37, 2018.
[28] S. K. Juhn, "Barrier Systems in the Inner Ear," *Acta Otolaryngol. (Stockh.)*, vol. 105, no. sup458, pp. 79–83, 1988.
[29] X. Shi, "Pathophysiology of the cochlear intrastrial fluid-blood barrier (review)," *Hear. Res.*, vol. 338, pp. 52–63, 2016.
[30] S. Iurato, "Diseases of the Auricle and of the External Auditory Canal," in *Otorhinolaryngology, Head and Neck Surgery*, Springer Berlin Heidelberg, pp. 43–54, 2010.
[31] G. Dickson and J. Wipperman, "Otitis Media and Externa," in *Family Medicine*, Springer, Cham, pp. 1–9, 2015.
[32] R. M. Rosenfeld *et al.*, "Clinical practice guideline: Acute otitis externa," *Otolaryngol. Head Neck Surg.*, vol. 134, no. 4, Supplement, pp. S4–S23, 2006.
[33] J. D. Russell *et al.*, "What causes acute otitis externa?," *J. Laryngol. Otol.*, vol. 107, no. 10, pp. 898–901, 1993.
[34] I. A. Van Asperen *et al.*, "Risk of otitis externa after swimming in recreational fresh water lakes containing Pseudomonas aeruginosa," *Bmj*, vol. 311, no. 7017, pp. 1407–1410, 1995.
[35] A. E. Tarazi *et al.*, "Fungal Malignant Otitis Externa: Pitfalls, Diagnosis, and Treatment," *Otol. Neurotol.*, vol. 33, no. 5, p. 769, 2012.
[36] C. L. Lum *et al.*, "Antibacterial and antifungal properties of human cerumen," *J. Laryngol. Otol.*, vol. 123, no. 4, pp. 375–378, 2009.
[37] R. M. Rosenfeld *et al.*, "Clinical Practice Guideline: Acute Otitis Externa," *Otolaryngol. Neck Surg.*, vol. 150, no. 1_suppl, pp. S1–S24, 2014.
[38] B. W. Kesser, "Assessment and management of chronic otitis externa," *Curr. Opin. Otolaryngol. Head Neck Surg.*, vol. 19, no. 5, p. 341, 2011.
[39] P. Schaefer and R. F. Baugh, "Acute otitis externa: an update," *Am. Fam. Physician*, vol. 86, no. 11, pp. 1055–1061, 2012.
[40] V. Kaushik, T. Malik, and S. R. Saeed, "Interventions for acute otitis externa," *Cochrane Database Syst. Rev.*, no. 1, 2010.
[41] D. Hajioff and S. MacKeith, "Otitis externa," *Clin Evid*, vol. 12, no. 4, pp. 755–763, 2004.
[42] W. L. Dibb, "Microbial aetiology of otitis externa," *J. Infect.*, vol. 22, no. 3, pp. 233–239, 1991.
[43] M. T. Halpern *et al.*, "Treatment patterns for otitis externa," *J. Am. Board Fam. Pract.*, vol. 12, no. 1, pp. 1–7, 1999.
[44] S. I. McCoy *et al.*, "Antimicrobial prescribing for otitis externa in children," *Pediatr. Infect. Dis. J.*, vol. 23, no. 2, pp. 181–183, 2004.

[45] Van Balen *et al.*, "Clinical efficacy of three common treatments in acute otitis externa in primary care: randomised controlled trial," *BMJ*, vol. 327, no. 7425, pp. 1201–1205, 2003.
[46] D. N. Fairbanks, "Otic topical agents," *Otolaryngol. Head Neck Surg. Off. J. Am. Acad.* , vol. 88, no. 4, pp. 327–331, 1980.
[47] P. Schaefer and R. F. Baugh, "Acute Otitis Externa: An Update," *Am. Fam. Physician*, vol. 86, no. 11, pp. 1055–1061, 2012.
[48] G. M. Wall *et al.*, "Ciprofloxacin 0.3%/dexamethasone 0.1% sterile otic suspension for the topical treatment of ear infections: a review of the literature," *Pediatr. Infect. Dis. J.*, vol. 28, no. 2, pp. 141–144, 2009.
[49] K. M. Harmes, R. A. Blackwood, H. L. Burrows, J. M. Cooke, R. V. Harrison, and P. P. Passamani, "Otitis media: diagnosis and treatment," *Am. Fam. Physician*, vol. 88, no. 7, pp. 435–440, Oct. 2013.
[50] C.-Y. Eng and A. S. El-Hawrani, "The pH of commonly used topical ear drops in the treatment of otitis externa," *Ear. Nose. Throat J.*, vol. 90, no. 4, pp. 160–162, 2011.
[51] A. M. Ayoob and J. T. Borenstein, "The role of intracochlear drug delivery devices in the management of inner ear disease," *Expert Opin. Drug Deliv.*, vol. 12, no. 3, pp. 465–479, 2015.
[52] R. E. Clifford *et al.*, "Low-dose D-methionine and N-acetyl-L-cysteine for protection from permanent noise-induced hearing loss in chinchillas," *Otolaryngol. Neck Surg.*, vol. 145, no. 6, pp. 999–1006, 2011.
[53] I. Seggas *et al.*, "Intratympanic steroid therapy for sudden hearing loss: a review of the literature," *Otol. Neurotol.*, vol. 32, no. 1, pp. 29–35, 2011.
[54] X. Wang *et al.*, "Principles of inner ear sustained release following intratympanic administration," *The Laryngoscope*, vol. 121, no. 2, pp. 385–391, 2011.
[55] T. Rivera *et al.*, "Drug delivery to the inner ear: strategies and their therapeutic implications for sensorineural hearing loss," *Curr. Drug Deliv.*, vol. 9, no. 3, pp. 231–242, 2012.
[56] J. T. Borenstein, "Intracochlear Drug Delivery Systems," *Expert Opin. Drug Deliv.*, vol. 8, no. 9, pp. 1161–1174, 2011.
[57] H. Liu *et al.*, "Current strategies for drug delivery to the inner ear," *Acta Pharm. Sin. B*, vol. 3, no. 2, pp. 86–96, 2013.
[58] A. A. McCall *et al.*, "Drug delivery for treatment of inner ear disease: current state of knowledge," *Ear Hear.*, vol. 31, no. 2, p. 156, 2010.
[59] A. K. Dash and G. C. Cudworth, "Therapeutic applications of implantable drug delivery systems," *J. Pharmacol. Toxicol. Methods*, vol. 40, no. 1, pp. 1–12, 1998.
[60] S. S. Iyer *et al.*, "Profiling in vitro drug release from subcutaneous implants: a review of current status and potential implications on drug product development," *Biopharm. Drug Dispos.*, vol. 27, no. 4, pp. 157–170, 2006.
[61] Y. Shi and L. C. Li, "Current advances in sustained-release systems for parenteral drug delivery," *Expert Opin. Drug Deliv.*, vol. 2, no. 6, pp. 1039–1058, 2005.
[62] L. W. Kleiner, J. C. Wright, and Y. Wang, "Evolution of implantable and insertable drug delivery systems," *J. Controlled Release*, vol. 181, pp. 1–10, 2014.
[63] V. Aswani *et al.*, "Implants," in *Advanced Drug Delivery*, 1 edition., C. H. Lee and K. Cheng, Eds. Hoboken, N.J: Wiley-Blackwell, 2013, pp. 183–200.

[64] B. D. Ratner, “Reducing capsular thickness and enhancing angiogenesis around implant drug release systems,” *J. Control. Release Off. J. Control. Release Soc.*, vol. 78, no. 1–3, pp. 211–218, 2002.
[65] S. Stewart *et al.*, “Implantable polymeric drug delivery devices: Classification, manufacture, materials, and clinical applications,” *Polymers*, vol. 10, no. 12, p. 1379, 2018.
[66] M. Danckwerts and A. Fassihi, “Implantable Controlled Release Drug Delivery Systems: A Review,” *Drug Dev. Ind. Pharm.*, vol. 17, no. 11, pp. 1465–1502, 1991.
[67] W. Tian *et al.*, “The influence of advancing age on implantation of drug-eluting stents,” *Catheter. Cardiovasc. Interv. Off. J. Soc. Card. Angiogr. Interv.*, vol. 88, no. 4, pp. 516–521, 2016.
[68] L. Claes and A. Ignatius, “Development of new, biodegradable implants,” *Chir. Z. Alle Geb. Oper. Medizen*, vol. 73, no. 10, pp. 990–996, 2002.
[69] M. Sarat and A. Dash, “special dosage forms and drug delivery systems,” in *Pharmaceutics: Basic Principles and Application to Pharmacy Practice*, 1 edition., S. Singh and J. Tolman, Eds. Academic Press, 2013.
[70] K. H. Rademacher *et al.*, “Global introduction of a low-cost contraceptive implant,” in *Critical Issues in Reproductive Health*, Springer, 2014, pp. 285–306, 2014.
[71] G. R. da Silva *et al.*, “Implants as drug delivery devices for the treatment of eye diseases,” *Braz. J. Pharm. Sci.*, vol. 46, no. 3, pp. 585–595, 2010.
[72] J. B. Christoforidis *et al.*, “Intravitreal Devices for the Treatment of Vitreous Inflammation,” *Mediators Inflamm.*, vol. 2012, p. e126463, 2012.
[73] J. L. Bourges *et al.*, “Intraocular implants for extended drug delivery: Therapeutic applications,” *Adv. Drug Deliv. Rev.*, vol. 58, no. 11, pp. 1182–1202, 2006.
[74] A. A. Exner and G. M. Saidel, “Drug-eluting polymer implants in cancer therapy,” *Expert Opin. Drug Deliv.*, vol. 5, no. 7, pp. 775–788, 2008.
[75] T. Htay and M. W. Liu, “Drug-eluting stent: a review and update,” *Vasc. Health Risk Manag.*, vol. 1, no. 4, p. 263, 2005.
[76] R. H. Allen vol. “Chapter 18 - Hormonal Contraception,” in *Williams Textbook of Endocrinology (Thirteenth Edition)*, S. Melmed, K. S. Polonsky, P. R. Larsen, and H. M. Kronenberg, Eds. Philadelphia: Content Repository Only!, pp. 664–693, 2016.
[77] M. S. Lesniak and H. Brem, “Targeted therapy for brain tumours,” *Nat. Rev. Drug Discov.*, vol. 3, no. 6, pp. 499–508, 2004.
[78] J. Tambaca *et al.*, “Mechanical behavior of fully expanded commercially available endovascular coronary stents,” *Tex. Heart Inst. J.*, vol. 38, no. 5, p. 491, 2011.
[79] B. Affandi *et al.*, “Five-year experience with Norplant®,” *Contraception*, vol. 36, no. 4, pp. 417–428, 1987.
[80] S. Uhm *et al.*, “Home or office etonogestrel implant insertion after pregnancy: a randomized trial,” *Contraception*, vol. 94, no. 5, pp. 567–571, 2016.
[81] D. R. Friend, “Advances in vaginal drug delivery,” *Drug Deliv Transl Res*, vol. 1, pp. 183–184, 2011.
[82] T. M. Mulders and T. O. Dieben, “Use of the novel combined contraceptive vaginal ring NuvaRing for ovulation inhibition,” *Fertil. Steril.*, vol. 75, no. 5, pp. 865–870, 2001.
[83] M. M. Baum *et al.*, “An intravaginal ring for the simultaneous delivery of multiple drugs,” *J. Pharm. Sci.*, vol. 101, no. 8, pp. 2833–2843, 2012.

[84] B. R. Goldspiel and D. R. Kohler, “Goserelin acetate implant: a depot luteinizing hormone-releasing hormone analog for advanced prostate cancer,” *DICP*, vol. 25, no. 7–8, pp. 796–804, 1991.
[85] M. Westphal *et al.*, “A phase 3 trial of local chemotherapy with biodegradable carmustine (BCNU) wafers (Gliadel wafers) in patients with primary malignant glioma,” *Neuro-Oncol.*, vol. 5, no. 2, pp. 79–88, 2003.
[86] N. L. Elstad and K. D. Fowers, “OncoGel (ReGel/paclitaxel)—Clinical applications for a novel paclitaxel delivery system,” *Adv. Drug Deliv. Rev.*, vol. 61, no. 10, pp. 785–794, 2009.
[87] P. Schlegel, “A review of the pharmacokinetic and pharmacological properties of a once-yearly administered histrelin acetate implant in the treatment of prostate cancer,” *BJU Int.*, vol. 103, pp. 7–13, 2009.
[88] K. L. Macoul and D. Pavan-Langston, “Pilocarpine ocusert system for sustained control of ocular hypertension,” *Arch. Ophthalmol.*, vol. 93, no. 8, pp. 587–590, 1975.
[89] N. Haghjou *et al.*, “Sustained release intraocular drug delivery devices for treatment of uveitis,” *J. Ophthalmic Vis. Res.*, vol. 6, no. 4, p. 317, 2011.
[90] I. B. Wong *et al.*, “Sustained-release ganciclovir implant as prophylaxis for cytomegalovirus retinitis in a child undergoing bone marrow transplantation,” *Eye*, vol. 27, no. 7, p. 890, 2013.
[91] M. Itzoe and M. Guarnieri, “New developments in managing opioid addiction: impact of a subdermal buprenorphine implant,” *Drug Des. Devel. Ther.*, vol. 11, p. 1429, 2017.
[92] J. C. Nickel *et al.*, “Continuous intravesical lidocaine treatment for interstitial cystitis/bladder pain syndrome: safety and efficacy of a new drug delivery device,” *Sci. Transl. Med.*, vol. 4, no. 143, pp. 143ra100–143ra100, 2012.
[93] R. Dammerman *et al.*, “Pharmacokinetics and safety of risperidone subcutaneous implants in stable patients with schizophrenia,” *Clin. Pharmacol. Drug Dev.*, vol. 7, no. 3, pp. 298–310, 2018.
[94] A. C. Anselmo and S. Mitragotri, “An overview of clinical and commercial impact of drug delivery systems,” *J. Controlled Release*, vol. 190, pp. 15–28, 2014.
[95] L. W. Kleiner, J. C. Wright, and Y. Wang, “Evolution of implantable and insertable drug delivery systems,” *J. Controlled Release*, vol. 181, pp. 1–10, May 2014, doi: 10.1016/j.jconrel.2014.02.006.
[96] A. Kumar and J. Pillai, “Chapter 13 - Implantable drug delivery systems: An overview,” in *Nanostructures for the Engineering of Cells, Tissues and Organs*, A. M. Grumezescu, Ed. William Andrew Publishing, pp. 473–511, 2018.
[97] J. Jacob *et al.*, “Biopolymer based nanomaterials in drug delivery systems: A review,” *Mater. Today Chem.*, vol. 9, pp. 43–55, 2018.
[98] R. K. Verma *et al.*, “Formulation aspects in the development of osmotically controlled oral drug delivery systems,” *J. Controlled Release*, vol. 79, no. 1, pp. 7–27, 2002.
[99] A. Dash and G. Cudworth, “Therapeutic applications of implantable drug delivery systems,” *J. Pharmacol. Toxicol. Methods*, vol. 40, no. 1, pp. 1–12, 1998.
[100] B. D. Ulery *et al.*, “Biomedical Applications of Biodegradable Polymers,” *J. Polym. Sci. Part B Polym. Phys.*, vol. 49, no. 12, pp. 832–864, 2011.
[101] S. Lyu and D. Untereker, “Degradability of Polymers for Implantable Biomedical Devices,” *Int. J. Mol. Sci.*, vol. 10, no. 9, pp. 4033–4065, 2009.

[102] Y. Fu and W. J. Kao, “Drug release kinetics and transport mechanisms of non-degradable and degradable polymeric delivery systems,” *Expert Opin. Drug Deliv.*, vol. 7, no. 4, pp. 429–444, 2010.
[103] J. Siepmann and F. Siepmann, “Mathematical modeling of drug delivery,” *Int. J. Pharm.*, vol. 364, no. 2, pp. 328–343, 2008.
[104] S. B. Lin *et al.*, “Segmental orientation studies of polyether polyurethane block copolymers with different hard segment lengths and distributions,” *Colloid Polym. Sci.*, vol. 263, no. 2, pp. 128–140, 1985.
[105] S. L. Fialho and A. da Silva Cunha, “Manufacturing techniques of biodegradable implants intended for intraocular application,” *Drug Deliv.*, vol. 12, no. 2, pp. 109–116, 2005.
[106] M. Jivraj *et al.*, “An overview of the different excipients useful for the direct compression of tablets,” *Pharm. Sci. Technol. Today*, vol. 3, no. 2, pp. 58–63, 2000.
[107] H. K. Makadia and S. J. Siegel, “Poly lactic-co-glycolic acid (PLGA) as biodegradable controlled drug delivery carrier,” *Polymers*, vol. 3, no. 3, pp. 1377–1397, 2011.
[108] A. Santovena *et al.*, “A mathematical model for interpreting in vitro rhGH release from laminar implants,” *Int. J. Pharm.*, vol. 309, no. 1–2, pp. 38–43, 2006.
[109] M. J. Dorta *et al.*, “Potential applications of PLGA film-implants in modulating in vitro drugs release,” *Int. J. Pharm.*, vol. 248, no. 1–2, pp. 149–156, 2002.
[110] N. Umeki *et al.*, “Preparation and evaluation of biodegradable films containing the potent osteogenic compound BFB0261 for localized delivery,” *Int. J. Pharm.*, vol. 404, no. 1–2, pp. 10–18, 2011.
[111] A. I. Prata *et al.*, “Preparation of dexamethasone ophthalmic implants: a comparative study of in vitro release profiles,” *Pharm. Dev. Technol.*, vol. 23, no. 3, pp. 218–224, 2018.
[112] J. Breitenbach, “Melt extrusion: from process to drug delivery technology,” *Eur. J. Pharm. Biopharm.*, vol. 54, no. 2, pp. 107–117, 2002.
[113] N. Follonier *et al.*, “Various ways of modulating the release of diltiazem hydrochloride from hot-melt extruded sustained release pellets prepared using polymeric materials,” *J. Controlled Release*, vol. 36, no. 3, pp. 243–250, 1995.
[114] Y. Shi *et al.*, “Early endothelial progenitor cells as a source of myeloid cells to improve the pre-vascularisation of bone constructs,” *Eur Cell Mater*, vol. 27, pp. 64–79, 2014.
[115] C. Schubert *et al.*, “Innovations in 3D printing: a 3D overview from optics to organs,” *Br. J. Ophthalmol.*, vol. 98, no. 2, pp. 159–161, 2014.
[116] C. L. Ventola, “Medical Applications for 3D Printing: Current and Projected Uses,” *Pharm. Ther.*, vol. 39, no. 10, pp. 704–711, 2014.
[117] J. Banks, “Adding Value in Additive Manufacturing : Researchers in the United Kingdom and Europe Look to 3D Printing for Customization,” *IEEE Pulse*, vol. 4, no. 6, pp. 22–26, 2013.
[118] A. Pîrjan and D.-M. Petroşanu, “The Impact Of 3d Printing Technology On The Society and Economy,” *J. Inf. Syst. Oper. Manag.*, vol. 7, no. 2, pp. 360–370, 2013.
[119] B. C. Gross “Evaluation of 3D printing and its potential impact on biotechnology and the chemical sciences,” *Anal. Chem.*, vol. 86, no. 7, pp. 3240–3253, 2014.
[120] M. O. Oyewumi, “3D Printing Technology in Pharmaceutical Drug Delivery: Prospects and Challenges,” *Biomol. Res. Ther.*, 2015.

[121] I. D. Ursan *et al.*, "Three-dimensional drug printing: A structured review," *J. Am. Pharm. Assoc.*, vol. 53, no. 2, pp. 136–144,
[122] A. Melocchi *et al.*, "Hot-melt extruded filaments based on pharmaceutical grade polymers for 3D printing by fused deposition modeling," *Int. J. Pharm.*, vol. 509, no. 1, pp. 255–263, 2016.
[123] J. Long *et al.*, "Application of Fused Deposition Modelling (FDM) Method of 3D Printing in Drug Delivery," *Curr. Pharm. Des.*, vol. 23, no. 3, pp. 433–439, 2017.
[124] B. C. Gross *et al.*, "Evaluation of 3D Printing and Its Potential Impact on Biotechnology and the Chemical Sciences," *Anal. Chem.*, vol. 86, no. 7, pp. 3240–3253, 2014.
[125] X. Cui *et al.*, "Thermal Inkjet Printing in Tissue Engineering and Regenerative Medicine," *Recent Pat. Drug Deliv. Formul.*, vol. 6, no. 2, pp. 149–155, 2012.
[126] W. E. Katstra *et al.*, "Oral dosage forms fabricated by Three Dimensional Printing™," *J. Controlled Release*, vol. 66, no. 1, pp. 1–9, 2000.
[127] C. W. Rowe *et al.*, "Multimechanism oral dosage forms fabricated by three dimensional printing™," *J. Controlled Release*, vol. 66, no. 1, pp. 11–17, 2000.
[128] J. T. Santini *et al.*, "A controlled-release microchip," *Nature*, vol. 397, no. 6717, pp. 335–338, 1999.
[129] L. G. Cima and M. J. Cima, ''*Preparation of medical devices by solid free-form fabrication methods*.'' Google Patents, 1996.
[130] D. C. Monkhouse *et al.*, "A complex-aided fabrication process for rapid designing, prototyping and manufacturing," *WO Pat.*, vol. 29202, 2000.
[131] D. Monkhouse *et al.*, "*Dosage forms exhibiting multi-phasic release kinetics and methods of manufacture thereof*." Google Patents, 2001.
[132] D. G. Yu *et al.*, "Three-dimensional printing in pharmaceutics: Promises and problems," *J. Pharm. Sci.*, vol. 97, no. 9, pp. 3666–3690, 2008.
[133] C. W. Hull, *Apparatus for production of three-dimensional objects by stereolithography*. Google Patents, 1986.
[134] C. M. Madla *et al.*, "3D Printing Technologies, Implementation and Regulation: An Overview," in *3D Printing of Pharmaceuticals*, American Association of Pharmaceutical Scientists, pp. 21–40, 2018.
[135] J. Wang *et al.*, "Stereolithographic (SLA) 3D printing of oral modified-release dosage forms," *Int. J. Pharm.*, vol. 503, no. 1, pp. 207–212, 2016.
[136] F. P. W. Melchels *et al.*, "A poly(d,l-lactide) resin for the preparation of tissue engineering scaffolds by stereolithography," *Biomaterials*, vol. 30, no. 23, pp. 3801–3809, 2009.
[137] S. Kumar, "Selective laser sintering: A qualitative and objective approach," *JOM*, vol. 55, no. 10, pp. 43–47, 2003.
[138] S. H. Ko *et al.*, "All-inkjet-printed flexible electronics fabrication on a polymer substrate by low-temperature high-resolution selective laser sintering of metal nanoparticles," *Nanotechnology*, vol. 18, no. 34, p. 345202, 2007.
[139] Nikolay K. Tolochko *et al.*, "Absorptance of powder materials suitable for laser sintering," *Rapid Prototyp. J.*, vol. 6, no. 3, pp. 155–161, 2000.
[140] B. Duan *et al.*, "Three-dimensional nanocomposite scaffolds fabricated via selective laser sintering for bone tissue engineering," *Acta Biomater.*, vol. 6, no. 12, pp. 4495–4505, 2010.
[141] K. F. Leong *et al.*, "Building Porous Biopolymeric Microstructures for Controlled Drug Delivery Devices Using Selective Laser Sintering," *Int. J. Adv. Manuf. Technol.*, vol. 31, no. 5, pp. 483–489, 2006.

[142] A. Waldbaur *et al.*, "Let there be chip—towards rapid prototyping of microfluidic devices: one-step manufacturing processes," *Anal. Methods*, vol. 3, no. 12, pp. 2681–2716, 2011.
[143] D.-G. Yu *et al.*, "Novel oral fast-disintegrating drug delivery devices with predefined inner structure fabricated by Three-Dimensional Printing," *J. Pharm. Pharmacol.*, vol. 61, no. 3, pp. 323–329, 2009.
[144] "3D Printed Organs Aid Surgeons." https://www.engineering.com/3DPrinting/3DPrintingArticles/ArticleID/5575/3D-Printed-Organs-Aid-Surgeons.aspx (accessed Jun. 05, 2019).
[145] A. C. DDS By Gregory S. Jacob, "Three-Dimensional Printing of Dentures Using Fused Deposition Modeling | Inside Dental Technology." https://www.aegisdentalnetwork.com/idt/2013/08/three-dimensional-printing-of-dentures-using-fused-deposition-modeling (accessed Jun. 05, 2019).
[146] A. Goyanes *et al.*, "Effect of geometry on drug release from 3D printed tablets," *Int. J. Pharm.*, vol. 494, no. 2, pp. 657–663, 2015.
[147] S. A. Khaled, J. C. Burley, M. R. Alexander, and C. J. Roberts, "Desktop 3D printing of controlled release pharmaceutical bilayer tablets," *Int. J. Pharm.*, vol. 461, no. 1–2, pp. 105–111, Jan. 2014, doi: 10.1016/j.ijpharm.2013.11.021.
[148] M. A. Alhnan *et al.*, "Emergence of 3D Printed Dosage Forms: Opportunities and Challenges," *Pharm. Res.*, vol. 33, no. 8, pp. 1817–1832, 2016.
[149] X. Wang *et al.*, "3D printing of polymer matrix composites: A review and prospective," *Compos. Part B Eng.*, vol. 110, pp. 442–458, 2017.
[150] W. Huang, Q. Zheng, W. Sun, H. Xu, and X. Yang, "Levofloxacin implants with predefined microstructure fabricated by three-dimensional printing technique," *Int. J. Pharm.*, vol. 339, no. 1, pp. 33–38, 2007.
[151] D. G. Yu *et al.*, "Tablets with material gradients fabricated by three-dimensional printing," *J. Pharm. Sci.*, vol. 96, no. 9, pp. 2446–2456, 2007.
[152] D.-G. Yu *et al.*, "Novel oral fast-disintegrating drug delivery devices with predefined inner structure fabricated by Three-Dimensional Printing," *J. Pharm. Pharmacol.*, vol. 61, no. 3, pp. 323–329, 2009.
[153] D.-G. Yu *et al.*, "Novel drug delivery devices for providing linear release profiles fabricated by 3DP," *Int. J. Pharm.*, vol. 370, no. 1, pp. 160–166, 2009.
[154] U. Gbureck *et al.*, "Low temperature direct 3D printed bioceramics and biocomposites as drug release matrices," *J. Controlled Release*, vol. 122, no. 2, pp. 173–180, 2007.
[155] B. M. Wu *et al.*, "Solid free-form fabrication of drug delivery devices," *J. Controlled Release*, vol. 40, no. 1–2, pp. 77–87, 1996.
[156] W. Wu *et al.*, "A programmed release multi-drug implant fabricated by three-dimensional printing technology for bone tuberculosis therapy," *Biomed. Mater.*, vol. 4, no. 6, p. 065005, 2009.
[157] C.-C. Wang *et al.*, "*Diffusion-controlled dosage form and method of fabrication including three dimensional printing*." Google Patents, 2012.
[158] C. W. Rowe *et al.*, "Multimechanism oral dosage forms fabricated by three dimensional printing™," *J. Controlled Release*, vol. 66, no. 1, pp. 11–17, 2000.
[159] K. F. Leong *et al.*, "Fabrication of porous polymeric matrix drug delivery devices using the selective laser sintering technique," *Proc. Inst. Mech. Eng. [H]*, vol. 215, no. 2, pp. 191–192, 2001.
[160] K. H. Low *et al.*, "Characterization of SLS parts for drug delivery devices," *Rapid Prototyp. J.*, vol. 7, no. 5, pp. 262–268, 2001.

[161] A. Goyanes *et al.*, "Fused-filament 3D printing (3DP) for fabrication of tablets," *Int. J. Pharm.*, vol. 476, no. 1, pp. 88–92, 2014.
[162] A. Goyanes *et al.*, "3D printing of modified-release aminosalicylate (4-ASA and 5-ASA) tablets," *Eur. J. Pharm. Biopharm.*, vol. 89, pp. 157–162, 2015.
[163] J. J. Water *et al.*, "Three-Dimensional Printing of Drug-Eluting Implants: Preparation of an Antimicrobial Polylactide Feedstock Material," *J. Pharm. Sci.*, vol. 104, no. 3, pp. 1099–1107, 2015.
[164] J. Skowyra *et al.*, "Fabrication of extended-release patient-tailored prednisolone tablets via fused deposition modelling (FDM) 3D printing," *Eur. J. Pharm. Sci.*, vol. 68, pp. 11–17, 2015.
[165] N. Sandler *et al.*, "Towards fabrication of 3D printed medical devices to prevent biofilm formation," *Int. J. Pharm.*, vol. 459, no. 1, pp. 62–64, 2014.
[166] J. A. Weisman *et al.*, "Antibiotic and chemotherapeutic enhanced three-dimensional printer filaments and constructs for biomedical applications," *Int. J. Nanomedicine*, vol. 10, pp. 357–370, 2015.
[167] S. E. Moulton and G. G. Wallace, "3-dimensional (3D) fabricated polymer based drug delivery systems," *J. Controlled Release*, vol. 193, pp. 27–34, 2014.
[168] J. Firth *et al.*, "The Role of Semi-Solid Extrusion Printing in Clinical Practice," in *3D Printing of Pharmaceuticals*, AAPS Advances in the Pharmaceutical Sciences Series, pp. 133–151, 2018.
[169] K. Chockalingam *et al.*, "Influence of layer thickness on mechanical properties in stereolithography," *rapid prototype J*, vol. 12, no. 2, pp. 106–113, 2006.
[170] S. A. Khaled *et al.*, "Desktop 3D printing of controlled release pharmaceutical bilayer tablets," *Int. J. Pharm.*, vol. 461, no. 1–2, pp. 105–111, 2014.
[171] S. A. Khaled *et al.*, "3D printing of tablets containing multiple drugs with defined release profiles," *Int. J. Pharm.*, vol. 494, no. 2, pp. 643–650, 2015.
[172] S. A. Khaled *et al.*, "3D printing of five-in-one dose combination polypill with defined immediate and sustained release profiles," *J. Controlled Release*, vol. 217, pp. 308–314, 2015.
[173] F. P. Melchels *et al.*, "A review on stereolithography and its applications in biomedical engineering," *Biomaterials*, vol. 31, no. 24, pp. 6121–6130, 2010.
[174] M. Alomari *et al.*, "Personalised dosing: printing a dose of one's own medicine," *Int. J. Pharm.*, vol. 494, no. 2, pp. 568–577, 2015.
[175] H. A. Merchant *et al.*, "Age-mediated changes in the gastrointestinal tract," *Int. J. Pharm.*, vol. 512, no. 2, pp. 382–395, 2016.
[176] M. A. Hamburg and F. S. Collins, "The path to personalized medicine," *N. Engl. J. Med.*, vol. 363, no. 4, pp. 301–304, 2010.
[177] A. C. Freire *et al.*, "Does sex matter? The influence of gender on gastrointestinal physiology and drug delivery," *Int. J. Pharm.*, vol. 415, no. 1–2, pp. 15–28, 2011.
[178] A. Awad *et al.*, "Reshaping drug development using 3D printing," *Drug Discov. Today*, vol. 23, no. 8, pp. 1547–1555, 2018.
[179] G. L. Kearns *et al.*, "Developmental pharmacology—drug disposition, action, and therapy in infants and children," *N. Engl. J. Med.*, vol. 349, no. 12, pp. 1157–1167, 2003.
[180] J. Breitkreutz and J. Boos, "Paediatric and geriatric drug delivery," *Expert Opin. Drug Deliv.*, vol. 4, no. 1, pp. 37–45, 2007.
[181] B. T. Peek *et al.*, "Accuracy of tablet splitting by elderly patients," *JAMA*, vol. 288, no. 4, pp. 451–452, 2002.

[182] W. A. Habib *et al.*, "Accuracy of tablet splitting: Comparison study between hand splitting and tablet cutter," *Saudi Pharm. J.*, vol. 22, no. 5, pp. 454–459, 2014.
[183] J. T. McDevitt *et al.*, "Accuracy of tablet splitting," *Pharmacother. J. Hum. Pharmacol. Drug Ther.*, vol. 18, no. 1, pp. 193–197, 1998.
[184] S. Hill *et al.*, "Analysis of drug content and weight uniformity for half-tablets of 6 commonly split medications," *J. Manag. Care Pharm.*, vol. 15, no. 3, pp. 253–261, 2009.
[185] J. Skowyra *et al.*, "Fabrication of extended-release patient-tailored prednisolone tablets via fused deposition modelling (FDM) 3D printing," *Eur. J. Pharm. Sci.*, vol. 68, pp. 11–17, 2015.
[186] C. W. Rowe *et al.*, "Multimechanism oral dosage forms fabricated by three dimensional printing™," *J. Controlled Release*, vol. 66, no. 1, pp. 11–17, 2000.
[187] S. J. Trenfield *et al.*, "The Shape of Things to Come: Emerging Applications of 3D Printing in Healthcare," in *3D Printing of Pharmaceuticals*, Springer, pp. 1–19, 2018.
[188] M. A. Alhnan *et al.*, "Emergence of 3D Printed Dosage Forms: Opportunities and Challenges," *Pharm. Res.*, vol. 33, no. 8, pp. 1817–1832, 2016.
[189] J. Norman *et al.*, "A new chapter in pharmaceutical manufacturing: 3D-printed drug products," *Adv. Drug Deliv. Rev.*, vol. 108, pp. 39–50, 2017.
[190] I. D. Ursan *et al.*, "Three-dimensional drug printing: a structured review," *J. Am. Pharm. Assoc. JAPhA*, vol. 53, no. 2, pp. 136–144, 2013.
[191] M. B. Hoy, "3D printing: making things at the library," *Med. Ref. Serv. Q.*, vol. 32, no. 1, pp. 94–99, 2013.
[192] C. G. Sandström, "The non-disruptive emergence of an ecosystem for 3D Printing — Insights from the hearing aid industry's transition 1989–2008," *Technol. Forecast. Soc. Change*, vol. 102, pp. 160–168, 2016.
[193] N. Guo and M. C. Leu, "Additive manufacturing: technology, applications and research needs," *Front. Mech. Eng.*, vol. 8, no. 3, pp. 215–243, 2013.
[194] Robert Bogue, "3D printing: the dawn of a new era in manufacturing?," *Assem. Autom.*, vol. 33, no. 4, pp. 307–311, 2013.
[195] Y. l. Yap and W. y. Yeong, "Additive manufacture of fashion and jewellery products: a mini review," *Virtual Phys. Prototyp.*, vol. 9, no. 3, pp. 195–201, 2014.
[196] D. H. Brean, "Asserting Patents to Combat Infringement via 3D Printing: It's No'Use," *Fordham Intellect. Prop. Media Entertain. Law J.*, vol. 23.3, 2013.
[197] J. I. Lipton *et al.*, "Additive manufacturing for the food industry," *Trends Food Sci. Technol.*, vol. 43, no. 1, pp. 114–123, 2015.
[198] X. Cui *et al.*, "Thermal inkjet printing in tissue engineering and regenerative medicine," *Recent Pat. Drug Deliv. Formul.*, vol. 6, no. 2, pp. 149–155, 2012.
[199] G. T. Klein *et al.*, "3D printing and neurosurgery--ready for prime time?," *World Neurosurg.*, vol. 80, no. 3–4, pp. 233–235, 2013.
[200] "NIH 3D Print Exchange | A collection of biomedical 3D printable files and 3D printing resources supported by the National Institutes of Health (NIH)." https://3dprint.nih.gov./ (accessed Jul. 19, 2017).
[201] R. Hampson, "Hearing aids," *Eur. Geriatr. Med.*, vol. 3, no. 3, pp. 198–200, 2012.
[202] B. Meding and A. Ringdahl, "Allergic contact dermatitis from the earmolds of hearing aids.," *Ear Hear.*, vol. 13, no. 2, pp. 122–124, 1992.

[203] D. Cockerill, “Allergies to ear moulds: a study of reactions encountered by hearing aid users to some ear mould materials,” *Br. J. Audiol.*, vol. 21, no. 2, pp. 143–145, 1987.
[204] Ç. T. Karaca *et al.*, “External auditory canal microbiology and hearing aid use,” *Am. J. Otolaryngol.*, vol. 34, no. 4, pp. 278–281, 2013.
[205] N. Ahmad et al., “Prospective study of the microbiological flora of hearing aid moulds and the efficacy of current cleaning techniques,” *J. Laryngol. Otol.*, vol. 121, no. 2, pp. 110–113, 2007.
[206] A. U. Bankaitis, “What’s growing on your patients’ hearing aids? A study gives you an idea,” *Hear. J.*, vol. 55, no. 6, p. 48, 2002.
[207] M. Mehdinejad et al., “Study of bacterial flora in children’s with hearing aid earmoulds in Ahvaz, Iran,” *Pak. J. Biol. Sci. PJBS*, vol. 13, no. 5, pp. 245–248, 2010.
[208] F. T. Orji et al., “The clinical implications of ear canal debris in hearing aid users,” *Pak. J. Med. Sci.*, vol. 30, no. 3, p. 483, 2014.
[209] R. Sander, “Otitis externa: a practical guide to treatment and prevention,” *Am. Fam. Physician*, vol. 63, no. 5, pp. 927–936, 941–942, 2001.
[210] M. N. Battikhi and S. I. Ammar, “Otitis externa infection in Jordan. Clinical and microbiological features,” *Saudi Med. J.*, vol. 25, no. 9, pp. 1199–1203, 2004.
[211] A. F. Snik et al., “Bone-anchored hearing aids in patients with sensorineural hearing loss and persistent otitis externa,” *Clin. Otolaryngol. Allied Sci.*, vol. 20, no. 1, pp. 31–35, 1995.
[212] A. F. M. Snik et al., “Evaluation of the subjective effect of middle ear implantation in hearing-impaired patients with severe external otitis,” *J. Am. Acad. Audiol.*, vol. 18, no. 6, pp. 496–503, 2007.
[213] N. Schmuziger et al., “Long-term assessment after implantation of the Vibrant Soundbridge device,” *Otology & Neurotology.*, vol. 27, no. 2, pp. 183–188, 2006.
[214] R. W. Sander, “Otitis Externa: A Practical Guide to Treatment and Prevention,” *Am. Fam. Physician*, vol. 63, no. 5, p. 927, Mar. 2001.
[215] A. M. Agius et al., “Patient compliance with short-term topical aural antibiotic therapy,” *Clin. Otolaryngol. Allied Sci.*, vol. 19, no. 2, pp. 138–141, 1994.
[216] R. J. England et al., “Accuracy of patient self-medication with topical eardrops,” *J. Laryngol. Otol.*, vol. 114, no. 1, pp. 24–25, 2000.
[217] R. Wadhwa et al., “Electrochemically controlled release of dexamethasone from conducting polymer polypyrrole coated electrode,” *J. Controlled Release*, vol. 110, no. 3, pp. 531–541, 2006.
[218] R. B. Friedrich et al., “Validation of a simple and rapid UV spectrophotometric method for dexamethasone assay in tablets,” *Quimica Nova*, vol. 32, no. 4, pp. 1052–1054, 2009.
[219] E. M. Cohen, “Dexamethasone,” in *Analytical Profiles of Drug Substances*, vol. 2, K. Florey, Ed. Academic Press, 1973, pp. 163–197, .
[220] “U S Food and Drug Administration Home Page.” https://www.fda.gov/ (accessed Oct. 23, 2018).
[221] “Home - British Pharmacopoeia.” https://www.pharmacopoeia.com/ (accessed Jan. 18, 2019).
[222] “Dexamethasone Ophthalmic: MedlinePlus Drug Information.” https://medlineplus.gov/druginfo/meds/a682869.html (accessed Jul. 11, 2019).
[223] D. Garlotta, “A Literature Review of Poly(Lactic Acid),” *J. Polym. Environ.*, vol. 9, no. 2, pp. 63–84, 2001.

[224] S. Farah et al., “Physical and mechanical properties of PLA, and their functions in widespread applications—A comprehensive review,” *Adv. Drug Deliv. Rev.*, vol. 107, pp. 367–392, 2016.
[225] D. da Silva *et al.*, “Biocompatibility, biodegradation and excretion of polylactic acid (PLA) in medical implants and theranostic systems,” *Chem. Eng. J.*, vol. 340, pp. 9–14, 2018.
[226] L. Xiao et al., “Poly (lactic acid)-based biomaterials: synthesis, modification and applications,” *Biomed. Sci. Eng. Technol.*, vol. 11, 2012.
[227] B. Wittbrodt and J. M. Pearce, “The effects of PLA color on material properties of 3-D printed components,” *Addit. Manuf.*, vol. 8, pp. 110–116, 2015.
[228] M. A. Cuiffo et al., “Impact of the Fused Deposition (FDM) Printing Process on Polylactic Acid (PLA) Chemistry and Structure,” *Appl. Sci.*, vol. 7, no. 6, p. 579, 2017.
[229] K. A. Athanasiou et al., “Sterilization, toxicity, biocompatibility and clinical applications of polylactic acid/polyglycolic acid copolymers,” *Biomaterials*, vol. 17, no. 2, pp. 93–102, 1996.
[230] R. E. Drumright et al., “Polylactic Acid Technology,” *Adv. Mater.*, vol. 12, no. 23, pp. 1841–1846, 2000.
[231] L.-Y. Li *et al.*, “Advances in functionalized polymer coatings on biodegradable magnesium alloys - A review,” *Acta Biomater.*, vol. 79, pp. 23–36, 2018.
[232] M. Banchero et al., “Characterization of ketoprofen/methyl-β-cyclodextrin complexes prepared using supercritical carbon dioxide,” *J. Chem.*, vol. 2013, 2013.
[233] T. Loftsson et al., “Cyclodextrins in drug delivery,” *Expert Opin. Drug Deliv.*, vol. 2, no. 2, pp. 335–351, 2005.
[234] T. Loftsson, “Pharmaceutical applications of β-cyclodextrin,” *Pharm. Technol.*, vol. 23, no. 12, pp. 40–50, 1999.
[235] T. Sultana *et al.*, “Characteristic profiles of the inclusion complex of omeprazole/peracylated-β-cyclodextrin formed in supercritical carbon dioxide,” *J. Incl. Phenom. Macrocycl. Chem.*, vol. 72, no. 1–2, pp. 207–212, 2012.
[236] R. L. Carrier et al., “The utility of cyclodextrins for enhancing oral bioavailability,” *J. Controlled Release*, vol. 123, no. 2, pp. 78–99, 2007.
[237] M. E. Brewster and T. Loftsson, “Cyclodextrins as pharmaceutical solubilizers,” *Adv. Drug Deliv. Rev.*, vol. 59, no. 7, pp. 645–666, 2007.
[238] A. Kusmin et al., “Quasielastic small-angle neutron scattering from heavy water solutions of cyclodextrins,” *J. Chem. Phys.*, vol. 134, no. 2, p. 024518, 2011.
[239] I. R. Schmolka, “Artificial skin I. Preparation and properties of pluronic F-127 gels for treatment of burns,” *John Wiley Sons Inc*, vol. 6, pp. 571–582, 1972.
[240] E. Doelker, “Cellulose derivatives,” in *Biopolymers I*, pp. 199–265, 1993.
[241] C. L. Li et al., “The use of hypromellose in oral drug delivery,” *J. Pharm. Pharmacol.*, vol. 57, no. 5, pp. 533–546, 2005.
[242] K. Deshmukh et al., “Biopolymer composites with high dielectric performance: interface engineering,” in *Biopolymer Composites in Electronics*, Elsevier, 2017, pp. 27–128, 2017.
[243] K. Pal et al., “Biopolymers in controlled-release delivery systems,” in *Modern biopolymer science*, Elsevier, pp. 519–557, 2009.
[244] Z. T. Chowhan, “Role of binders in moisture-induced hardness increase in compressed tablets and its effect on in vitro disintegration and dissolution,” *J. Pharm. Sci.*, vol. 69, no. 1, pp. 1–4, 1980.

[245] L. Ambrosio et al., “Superabsorbent cellulose-based hydrogels for biomedical applications,” in *Biomedical Hydrogels*, Elsevier, 2011, pp. 25–50, 2011.
[246] J. Skowyra et al., “Fabrication of extended-release patient-tailored prednisolone tablets via fused deposition modelling (FDM) 3D printing,” *Eur. J. Pharm. Sci.*, vol. 68, pp. 11–17, 2015.
[247] A. Goyanes *et al.*, “Fabrication of controlled-release budesonide tablets via desktop (FDM) 3D printing,” *Int. J. Pharm.*, vol. 496, no. 2, pp. 414–420, 2015.
[248] D. Espalin et al., “Fused deposition modeling of patient-specific polymethylmethacrylate implants,” *Rapid Prototyp. J.*, vol. 16, no. 3, pp. 164–173, 2010.
[249] T. D. Ngo et al., “Additive manufacturing (3D printing): A review of materials, methods, applications and challenges,” *Compos. Part B Eng.*, vol. 143, pp. 172–196, 2018.
[250] E. Y. Teo *et al.*, “Polycaprolactone-based fused deposition modeled mesh for delivery of antibacterial agents to infected wounds,” *Biomaterials*, vol. 32, no. 1, pp. 279–287, 2011.
[251] N. Genina et al., “Ethylene vinyl acetate (EVA) as a new drug carrier for 3D printed medical drug delivery devices,” *Eur. J. Pharm. Sci.*, vol. 90, pp. 53–63, 2016.
[252] F. P. W. Melchels et al., “A review on stereolithography and its applications in biomedical engineering,” *Biomaterials*, vol. 31, no. 24, pp. 6121–6130, 2010.
[253] M. H. Chiu and E. J. Prenner, “Differential scanning calorimetry: An invaluable tool for a detailed thermodynamic characterization of macromolecules and their interactions,” *J. Pharm. Bioallied Sci.*, vol. 3, no. 1, pp. 39–59, 2011.
[254] L. C. Thomas, “An introduction to the techniques of differential scanning calorimetry (DSC) and modulated DSC,” 2005.
[255] S.-D. Clas et al,. “Differential scanning calorimetry: applications in drug development,” *Pharm. Sci. Technol. Today*, vol. 2, no. 8, pp. 311–320, 1999.
[256] J. A. Seyforth, “Scanning Electron Microscopy (SEM): An Introduction to the use of SEM for character-ising the Surface Topology and Composition of Matter with Further Applications,” 2015.
[257] S. Byrn, et al,. “Microscopy,” in *Solid-State Properties of Pharmaceutical Materials*, pp. 142–158, 2017.
[258] N. Stieger et al,. “Hot-stage Optical Microscopy as an Analytical Tool to Understand Solid-state Changes in Pharmaceutical Materials,” *Am. Pharm. Rev. ·*, vol. 15, no. 2, 2012.
[259] C. Marriott, “Rheology,” in *Aulton’s Pharmaceutics*, 4th edition., Elsevier Ltd, pp. 94–114, 2013.
[260] S. Kazemian et al., “Review of Newtonian and non-Newtonian fluids behaviour in the context of grouts,” in *Geotechnical Aspects of Underground Construction in Soft Ground*, Taylor & Francis Group London, 2012, pp. 321–326, 2012.
[261] R G. Griskey, et al., "Rheological and pipeline flow behavior of corn starch dispersions." Journal of Rheology 29, 3349-360, 1985.
[262] A. B., Metzner, and M. Whitlock. "Flow behavior of concentrated (dilatant) suspensions." Transactions of the Society of Rheology 2.1, 239-254, 1958
[263] R. P. Chabra and J. F. Richardson, “Non-Newtonian Flow and Applied Rheology,” *Eng. Appl.*, p. 14, 2008.
[264] P. H. T. Uhlherr *et al.*, “The shear-induced solid–liquid transition in yield stress materials with chemically different structures,” *J. Non-Newton. Fluid Mech.*, vol. 125, no. 2, pp. 101–119, 2005.

[265] G. Alderborn, “Tablets and Compaction,” in *Aluton’s Pharmaceutics The Design and Manufacture of Medicines*, 4th ed., Elsevier Ltd., pp. 504–549, 2013.
[266] C. Raman, “A new radiation,” *Indian J Phys*, vol. 2, pp. 387–398, 1928.
[267] S. Byrn *et al.*, “Vibrational Spectroscopy,” in *Solid-State Properties of Pharmaceutical Materials*, First edition., John Wiley & Sons, Inc., pp. 159–178, 2017.
[268] G. P. S. Smith *et al.*, “Raman imaging of drug delivery systems,” *Adv. Drug Deliv. Rev.*, vol. 89, pp. 21–41, 2015.
[269] S. R. Byren *et al.*, “Solubility and Dissolution,” in *Solid-State Properties of Pharmaceutical Materials*, John Wiley & Sons, Inc., 2017, pp. 249–264, 2017.
[270] B. Tyler *et al.*, “Polylactic acid (PLA) controlled delivery carriers for biomedical applications,” *Adv. Drug Deliv. Rev.*, vol. 107, pp. 163–175, 2016.
[271] F. S. Senatov *et al.*, “Mechanical properties and shape memory effect of 3D-printed PLA-based porous scaffolds,” *J. Mech. Behav. Biomed. Mater.*, vol. 57, pp. 139–148, 2016.
[272] R. Suuronen *et al.*, “Bioabsorbable plates and screws: Current state of the art in facial fracture repair.,” *J. Cranio-Maxillofac. Trauma*, vol. 6, no. 1, pp. 19–27; discussion 28-30, 2000.
[273] P. A. Gunatillake and R. Adhikari, “Biodegradable synthetic polymers for tissue engineering,” *Eur. Cell. Mater.*, vol. 5, pp. 1–16; discussion 16, 2003.
[274] H. Xu *et al.*, “Rapid prototyped PGA/PLA scaffolds in the reconstruction of mandibular condyle bone defects,” *Int. J. Med. Robot. Comput. Assist. Surg. MRCAS*, vol. 6, no. 1, pp. 66–72, 2010.
[275] A. Awad *et al.*, “Fused Deposition Modelling: Advances in Engineering and Medicine,” in *3D Printing of Pharmaceuticals*, Springer, pp. 107–132, 2018.
[276] N. Sandler *et al.*, “Towards fabrication of 3D printed medical devices to prevent biofilm formation,” *Int. J. Pharm.*, vol. 459, no. 1, pp. 62–64, 2014.
[277] J. J. Water *et al.*, “Three-dimensional printing of drug-eluting implants: preparation of an antimicrobial polylactide feedstock material,” *J. Pharm. Sci.*, vol. 104, no. 3, pp. 1099–1107, 2015.
[278] J. Boetker *et al.*, “Modifying release characteristics from 3D printed drug-eluting products,” *Eur. J. Pharm. Sci.*, vol. 90, pp. 47–52, 2016.
[279] R. C. R. Beck *et al.*, “3D printed tablets loaded with polymeric nanocapsules: An innovative approach to produce customized drug delivery systems,” *Int. J. Pharm.*, vol. 528, no. 1–2, pp. 268–279, 2017.
[280] M. A. Cuiffo *et al.*, “Impact of the Fused Deposition (FDM) Printing Process on Polylactic Acid (PLA) Chemistry and Structure,” *Appl. Sci.*, vol. 7, no. 6, p. 579, 2017.
[281] X. Cao *et al.*, “DSC study of biodegradable poly(lactic acid) and poly(hydroxy ester ether) blends,” *Thermochim. Acta*, vol. 406, no. 1, pp. 115–127, 2003.
[282] J. Long *et al.*, “Application of Fused Deposition Modelling (FDM) Method of 3D Printing in Drug Delivery,” *Curr. Pharm. Des.*, vol. 23, no. 3, pp. 433–439, 2017.
[283] B. D. M. Matos *et al.*, “Evaluation of commercially available polylactic acid (PLA) filaments for 3D printing applications,” *J. Therm. Anal. Calorim.*, vol. 137, no. 2, pp. 555–562, 2019.
[284] G. Slabaugh *et al.*, “3-D shape modeling for hearing aid design [Applications Corner],” *IEEE Signal Process. Mag.*, vol. 25, no. 5, pp. 98–102, 2008.
[285] A. Winkler *et al.*, “Open Versus Closed Hearing-Aid Fittings: A Literature Review of Both Fitting Approaches,” *Trends Hear.*, vol. 20, 2016.
[286] H. Dillon, *Hearing aids*. Hodder Arnold, 2008.

[287] R. Yang *et al.*, "Treatment of otitis media by transtympanic delivery of antibiotics," *Sci. Transl. Med.*, vol. 8, no. 356, p. 356ra120, 2016.
[288] R. Cortez *et al.*, "Changing with the times: applying digital technology to hearing aid shell manufacturing," *Hear. Rev.*, vol. 11, no. 3, pp. 30–41, 2004.
[289] T. Gao and S. S. Jarng, "Design and realization of hearing aids based 3D rapid shell mold ing CADCAM," in *2009 IEEE International Symposium on Industrial Electronics*, 2009, pp. 1488–1492.
[290] H. R. Staff, "Earmolds and Hearing Aid Shells: A Tutorial Part 2," *Hear. Rev.*, vol. 13, no. 5, 2006.
[291] K. Hatzilias and J. Thompson, "3D Ear Scanning Enables a Platform for Wearable Computing," *Int. Conf. 3D Body Scanning Technol.*, pp. 27–28, 2015.
[292] A. Stojmenski, I. Chorbev, B. Joksimoski, and S. Stojmenski, "3D Printing Assistive Devices," in *Mobile Networks and Management*, 2015, pp. 446–456.
[293] K. Chung, "Challenges and Recent Developments in Hearing Aids: Part II. Feedback and Occlusion Effect Reduction Strategies, Laser Shell Manufacturing Processes, and Other Signal Processing Technologies," *Trends Amplif.*, vol. 8, no. 4, pp. 125–164, 2004.
[294] Y. Qiu and K. Park, "Environment-sensitive hydrogels for drug delivery," *Adv. Drug Deliv. Rev.*, vol. 53, no. 3, pp. 321–339, 2001.
[295] H. J. van der Linden *et al.*, "Stimulus-sensitive hydrogels and their applications in chemical (micro)analysis," *The Analyst*, vol. 128, no. 4, pp. 325–331, 2003.
[296] K. Y. Lee and D. J. Mooney, "Hydrogels for tissue engineering," *Chem. Rev.*, vol. 101, no. 7, pp. 1869–1879, 2001.
[297] T. R. Hoare and D. S. Kohane, "Hydrogels in drug delivery: Progress and challenges," *Polymer*, vol. 49, no. 8, pp. 1993–2007, 2008.
[298] B. M, A. Vadithya, and A. Chatterjee, "As A Review on Hydrogels as Drug Delivery in the Pharmaceutical Field," *Int. J. Pharm. Chem. Sci.*, vol. 1, pp. 642–661, 2012.
[299] K. Saini, "Preparation method, Properties and Crosslinking of hydrogel: a review," *PharmaTutor*, vol. 5, no. 1, pp. 27–36, 2017.
[300] P. Ghasemiyeh and S. Mohammadi Samani, "Hydrogels as Drug Delivery Systems; Pros and Cons (Review Article)," vol. 5, pp. 7–24, 2019.
[301] R. Narayanaswamy and V. P. Torchilin, "Hydrogels and Their Applications in Targeted Drug Delivery," *Mol. Basel Switz.*, vol. 24, no. 3, 2019.
[302] M. Sakthivel *et al.*, "Intelligent hydrogels for controlled drug delivery system: a review," *Int J Front Sci Technol*, vol. 3, no. 2, pp. 37–47, 2015.
[303] B. Mishra *et al.*, "Hydrogels: An Introduction to a Controlled Drug Delivery Device, Synthesis and Application in Drug Delivery and Tissue Engineering," 2017.
[304] C.-C. Lin and A. T. Metters, "Hydrogels in controlled release formulations: Network design and mathematical modeling," *Adv. Drug Deliv. Rev.*, vol. 58, no. 12, pp. 1379–1408, 2006.
[305] S. C. Joshi, "Sol-Gel Behavior of Hydroxypropyl Methylcellulose (HPMC) in Ionic Media Including Drug Release," *Materials*, vol. 4, no. 10, pp. 1861–1905, 2011.
[306] A. Sannino *et al.*, "Biodegradable cellulose-based hydrogels: design and applications," *Materials*, vol. 2, no. 2, pp. 353–373, 2009.
[307] M. K. Das and A. B. Ahmed, "Formulation and ex vivo evaluation of rofecoxib gel for topical application," *Acta Pol Pharm*, vol. 64, no. 5, pp. 461–7, 2007.
[308] J. A. Grover, "Mehtylcellulose and its Derivatives," in *Industrial Gums Polysaccharides and Their Derivatives*, Third edition., Academic Press, pp. 475–504, 1993.

[309] A. Haque *et al.*, "Thermogelation of methylcellulose. Part II: effect of hydroxypropyl substituents," *Carbohydr. Polym.*, vol. 22, no. 3, pp. 175–186, 1993.
[310] A. Haque and E. R. Morris, "Thermogelation of methylcellulose. Part I: molecular structures and processes," *Carbohydr. Polym.*, vol. 22, no. 3, pp. 161–173, 1993.
[311] N. Sarkar, "Thermal gelation properties of methyl and hydroxypropyl methylcellulose," *J. Appl. Polym. Sci.*, vol. 24, no. 4, pp. 1073–1087, 1979.
[312] A. Carlsson *et al.*, "Thermal gelation of nonionic cellulose ethers and ionic surfactants in water," *Colloids Surf.*, vol. 47, pp. 147–165, 1990.
[313] M. M. Talukdar *et al.*, "Rheological characterization of xanthan gum and hydroxypropylmethyl cellulose with respect to controlled-release drug delivery," *J. Pharm. Sci.*, vol. 85, no. 5, pp. 537–540, 1996.
[314] P. Polamaplly *et al.*, "3D printing and characterization of hydroxypropyl methylcellulose and methylcellulose for biodegradable support structures," *Polymer*, vol. 173, pp. 119–126, 2019.
[315] E. Engleder *et al.*, "Preclinical evaluation of thermoreversible triamcinolone acetonide hydrogels for drug delivery to the inner ear," *Int. J. Pharm.*, vol. 471, no. 1, pp. 297–302, 2014.
[316] T. G. Mezger, "Oscillatory tests.," in *The Rheology Handbook*, 4th edition., pp. 135–210, 2014.
[317] N. Modi, "Rheology-A pre-formulation tool for evaluating mechanical andthermal properties of transdermal formulations," PhD Thesis, Long Island University, The Brooklyn Center, 2017.
[318] L. K. Widjaja *et al.*, "Hyaluronic acid-based nanocomposite hydrogels for ocular drug delivery applications," *J. Biomed. Mater. Res. A*, vol. 102, no. 9, pp. 3056–3065, 2014.
[319] L. Vlaia *et al.*, "Cellulose-derivatives-based hydrogels as vehicles for dermal and transdermal drug delivery," *Emerg. Concepts Anal. Appl. Hydrogels*, vol. 2, p. 64, 2016.
[320] T. G. Mezger, "Measuring systems," in *The rheology handbook*, 4th edition., Vincentz Network GmbH & Co. KG, pp. 233–290, 2014.
[321] X. Xu *et al.*, "Shear thinning behavior of linear polymer melts under shear flow via nonequilibrium molecular dynamics," *J. Chem. Phys.*, vol. 140, no. 17, p. 174902, 2014.
[322] J. M. Katona *et al.*, "Rheological properties of hydroxypropylmethyl cellulose/sodium dodecylsulfate mixtures," *J. Serbian Chem. Soc.*, vol. 79, no. 4, pp. 457–468, 2014.
[323] X. H. Yang and W. L. Zhu, "Viscosity properties of sodium carboxymethylcellulose solutions," *Cellulose*, vol. 14, no. 5, pp. 409–417, 2007.
[324] J. Li and D. J. Mooney, "Designing hydrogels for controlled drug delivery," *Nat. Rev. Mater.*, vol. 1, no. 12, 2016.
[325] T. G. Mezger, "Rotational tests," in *The Rheology Handbook*, 4th edition., pp. 33–88, 2014.
[326] A. D. Padsalgikar, "Applications of Plastics in Cardiovascular Devices," in *Plastics in Medical Devices for Cardiovascular Applications*, Ed. William Andrew Publishing, pp. 133–176, 2017.
[327] Z. Hao *et al.*, "Rheological properties and gel characteristics of polysaccharides from fruit-bodies of Sparassis crispa," *Int. J. Food Prop.*, vol. 21, no. 1, pp. 2283–2295, 2018.

[328] A. Haq *et al.*, "Membrane properties for permeability testing: Skin versus synthetic membranes," *Int. J. Pharm.*, vol. 539, no. 1–2, pp. 58–64, 2018.
[329] P. C. Mills and S. E. Cross, "Transdermal drug delivery: basic principles for the veterinarian," *Vet. J.*, vol. 172, no. 2, pp. 218–233, 2006.
[330] M. O. Visscher, "Update on the Use of Topical Agents in Neonates," *Newborn Infant Nurs. Rev.*, vol. 9, no. 1, pp. 31–47, 2009.
[331] M. Leider and D. Tanenbaum, "Surface area of the skin," *J. Invest. Dermatol.*, vol. 52, no. 4, pp. 313–314, 1969.
[332] S. N. Andrews *et al.*, "Transdermal delivery of molecules is limited by full epidermis, not just stratum corneum," *Pharm. Res.*, vol. 30, no. 4, pp. 1099–1109, 2013.
[333] A. Baroni *et al.*, "Structure and function of the epidermis related to barrier properties," *Clin. Dermatol.*, vol. 30, no. 3, pp. 257–262, 2012.
[334] I. B. Pathan and C. M. Setty, "Chemical penetration enhancers for transdermal drug delivery systems," *Trop. J. Pharm. Res.*, vol. 8, no. 2, 2009.
[335] T. J. Franz, "Percutaneous absorption. On the relevance of in vitro data," *J. Invest. Dermatol.*, vol. 64, no. 3, pp. 190–195, 1975.
[336] B. Godin and E. Touitou, "Transdermal skin delivery: predictions for humans from in vivo, ex vivo and animal models," *Adv. Drug Deliv. Rev.*, vol. 59, no. 11, pp. 1152–1161, 2007.
[337] A. Haq *et al.*, "Strat-M® synthetic membrane: Permeability comparison to human cadaver skin," *Int. J. Pharm.*, vol. 547, no. 1, pp. 432–437, 2018.
[338] Y. R *et al.*, "Treatment of otitis media by transtympanic delivery of antibiotics," *Sci Transl Med*, vol. 8, pp. 1–22, 2016.
[339] X. Khoo *et al.*, "Formulations for Trans-Tympanic Antibiotic Delivery," *Biomaterials*, vol. 34, no. 4, pp. 1281–1288, 2013.
[340] "USP–NF | USP-NF." http://www.uspnf.com/ (accessed Apr. 20, 2018).
[341] J. W. Kutz Jr *et al.*, "Ciprofloxacin 0.3%+ dexamethasone 0.1% for the treatment for otitis media," *Expert Opin. Pharmacother.*, vol. 14, no. 17, pp. 2399–2405, 2013.
[342] J. Conceição *et al.*, "Cyclodextrins as excipients in tablet formulations," *Drug Discov. Today*, vol. 23, no. 6, pp. 1274–1284, 2018.
[343] C. Scavone *et al.*, "Efficacy and Safety Profile of Diclofenac/Cyclodextrin and Progesterone/Cyclodextrin Formulations: A Review of the Literature Data," *Drugs RD*, vol. 16, no. 2, pp. 129–140, 2016.
[344] F. J. Otero-Espinar *et al.*, "Cyclodextrins in drug delivery systems," *J. Drug Deliv. Sci. Technol.*, vol. 20, no. 4, pp. 289–301, 2010.
[345] S. Anguiano-Igea *et al.*, "Rheological properties of the complex clofibrate-β-cyclodextrin," in *Proc. Intern. Symp. Control Rel. Bioact. Mater.*, vol. 21, pp. 728–729, 1994.
[346] R. F. Shangraw *et al.*, "Characterization of the tableting properties of β-cyclodextrin and the effects of processing variables on inclusion complex formation, compactibility and dissolution," *Drug Dev. Ind. Pharm.*, vol. 18, no. 17, pp. 1831–1851, 1992.
[347] G. Tiwari *et al.*, "Cyclodextrins in delivery systems: Applications," *J. Pharm. Bioallied Sci.*, vol. 2, no. 2, pp. 72–79, 2010.
[348] J. K. Kristinsson *et al.*, "Dexamethasone-cyclodextrin-polymer co-complexes in aqueous eye drops. Aqueous humor pharmacokinetics in humans.," *Invest. Ophthalmol. Vis. Sci.*, vol. 37, no. 6, pp. 1199–1203, 1996.

[349] M. Jivraj *et al.*, "An overview of the different excipients useful for the direct compression of tablets," *Pharm. Sci. Technol. Today*, vol. 3, no. 2, pp. 58–63, 2000.
[350] H. Soroush *et al.*, "Formulation Optimization and Assessment of Dexamethasone Orally Disintegrating Tablets Using Box-Behnken Design," *Iran. J. Pharm. Res. IJPR*, vol. 17, no. 4, pp. 1150–1163, 2018.
[351] J. Li and Y. Wu, "Lubricants in Pharmaceutical Solid Dosage Forms," *Lubricants*, vol. 2, no. 1, pp. 21–43, 2014.
[352] S. S. Soebagyo, "The effect of the particle size of magnesium stearate on the dissolution of dexamethasone from interactive mix tablet," *Maj Farm Indones*, vol. 5, pp. 52–58, 1994.
[353] A. R. Rojas-Mena *et al.*, "Preparation and characterization of holmium-beta-cyclodextrin complex," *Adv. Mater. Phys. Chem.*, vol. 5, no. 03, p. 87, 2015.
[354] K. Wormuth, "Characterization of Therapeutic Coatings on Medical Devices," in *Confocal Raman Microscopy*, First., The Springer Series in Optical Sciences, pp. 203–223, 2010.
[355] L. Li *et al.*, "Rapid Detection of Six Glucocorticoids Added Illegally to Dietary Supplements by Combining TLC with Spot-Concentrated Raman Scattering," *Molecules*, vol. 23, no. 7, p. 1504, 2018.
[356] E. C. O. da Silva *et al.*, "Drug-induced anti-inflammatory response in A549 cells, as detected by Raman spectroscopy: a comparative analysis of the actions of dexamethasone and p-coumaric acid," *The Analyst*, vol. 144, no. 5, pp. 1622–1631, 2019.
[357] G. Stevenson *et al.*, "Polyterthiophene as an electrostimulated controlled drug release material of therapeutic levels of dexamethasone," *Synth. Met.*, vol. 160, no. 9, pp. 1107–1114, 2010.
[358] J. R. Anema *et al.*, "Surface-enhanced Raman scattering from polystyrene on gold clusters," *J. Raman Spectrosc.*, vol. 41, no. 7, pp. 745–751, 2010.
[359] S. M. Asiala *et al.*, "Surface-Enhanced, Spatially Offset Raman Spectroscopy (SESORS) in Tissue Analogues," *ACS Appl. Mater. Interfaces*, vol. 9, no. 30, pp. 25488–25494, 2017.
[360] F. Adar, "Characterizing Modified Celluloses Using Raman Spectroscopy," *Spectroscopy*, pp. 22–27, 2016.
[361] C. M. Oh *et al.*, "Influence of Hydroxypropyl Methylcellulose on Metronidazole Crystallinity in Spray-Congealed Polyethylene Glycol Microparticles and Its Impact with Various Additives on Metronidazole Release," *AAPS PharmSciTech*, vol. 16, no. 6, pp. 1357–1367, 2015.
[362] T. Suzuki *et al.*, "Modification of physical properties of poly(L-lactic acid) by addition of methyl-β-cyclodextrin," *Beilstein J. Org. Chem.*, vol. 10, pp. 2997–3006, 2014.
[363] B. Pokusaev *et al.*, "Diffusion of nano-particles in gels," *Chem. Eng. Trans.*, vol. 47, pp. 91–96, 2016.
[364] K. Samprovalaki *et al.*, "Investigation of the diffusion of dyes in agar gels," *J. Food Eng.*, vol. 111, no. 4, pp. 537–545, 2012.
[365] N. Fatin-Rouge *et al.*, "Size Effects on Diffusion Processes within Agarose Gels," *Biophys. J.*, vol. 86, no. 5, pp. 2710–2719, 2004.
[366] S. P. Zustiak, H. Boukari, and J. B. Leach, "Solute diffusion and interactions in cross-linked poly(ethylene glycol) hydrogels studied by Fluorescence Correlation Spectroscopy," *Soft Matter*, vol. 6, no. 15, 2010.
[367] K. Pal *et al.*, "Polymeric hydrogels: characterization and biomedical applications," *Des. Monomers Polym.*, vol. 12, no. 3, pp. 197–220, 2009.

[368] N. M. Vacanti *et al.*, “Localized delivery of dexamethasone from electrospun fibers reduces the foreign body response,” *Biomacromolecules*, vol. 13, no. 10, pp. 3031–3038, 2012.
[369] C. Zhang *et al.*, “Rethinking Cleaning Validation for API Manufacturing,” *Pharm. Technol.*, pp. 42–54, 2018.
[370] A. Haq *et al.*, “Membrane properties for permeability testing: Skin versus synthetic membranes,” *Int. J. Pharm.*, vol. 539, no. 1, pp. 58–64, 2018.
[371] D. Karadzovska and J. E. Riviere, “Assessing vehicle effects on skin absorption using artificial membrane assays,” *Eur. J. Pharm. Sci.*, vol. 50, no. 5, pp. 569–576, 2013.
[372] D. E. M. Haron *et al.*, “In vitro and in vivo evaluation of a novel testosterone transdermal delivery system (TTDS) using palm oil base,” *Iran. J. Basic Med. Sci.*, vol. 18, no. 12, pp. 1167–1175, 2015.
[373] C. H. Salamanca *et al.*, “Franz Diffusion Cell Approach for Pre-Formulation Characterisation of Ketoprofen Semi-Solid Dosage Forms,” *Pharmaceutics*, vol. 10, no. 3, p. 148, 2018.
[374] P. S. Roland *et al.*, “Topical ciprofloxacin/dexamethasone otic suspension is superior to ofloxacin otic solution in the treatment of children with acute otitis media with otorrhea through tympanostomy tubes,” *Pediatrics*, vol. 113, no. 1, pp. e40–e46, 2004.
[375] J. B. Dressman and J. Krämer, *Pharmaceutical dissolution testing*. Taylor & Francis Boca Raton, FL:, 2005.
[376] M. Siewert *et al.*, “FIP/AAPS guidelines to dissolution/in vitro release testing of novel/special dosage forms,” *Aaps Pharmscitech*, vol. 4, no. 1, pp. 43–52, 2003.

Appendix A

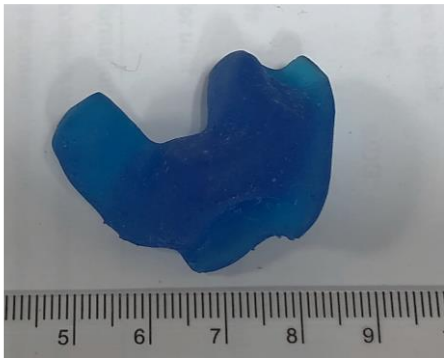

Figure 3.A1 Photographic image of the SLA printed ear mould objects.

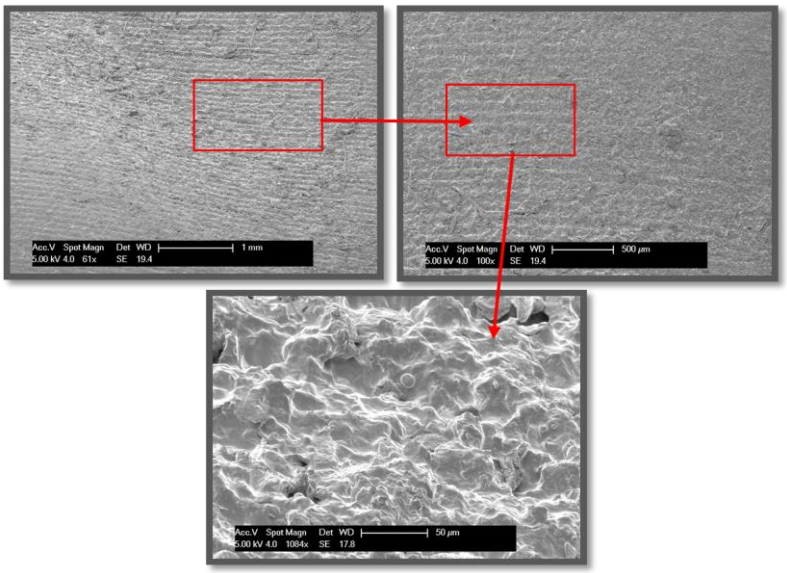

Figure 3. A2 The SEM images of the 3D printed ear mould object with the desktop SLA Formlabs 1 printer.

Figure 3. A3 Photographic images of the FDM PLA 3D printed ear anatomy.

Appendix B

❖ Preparation of Hydrogels

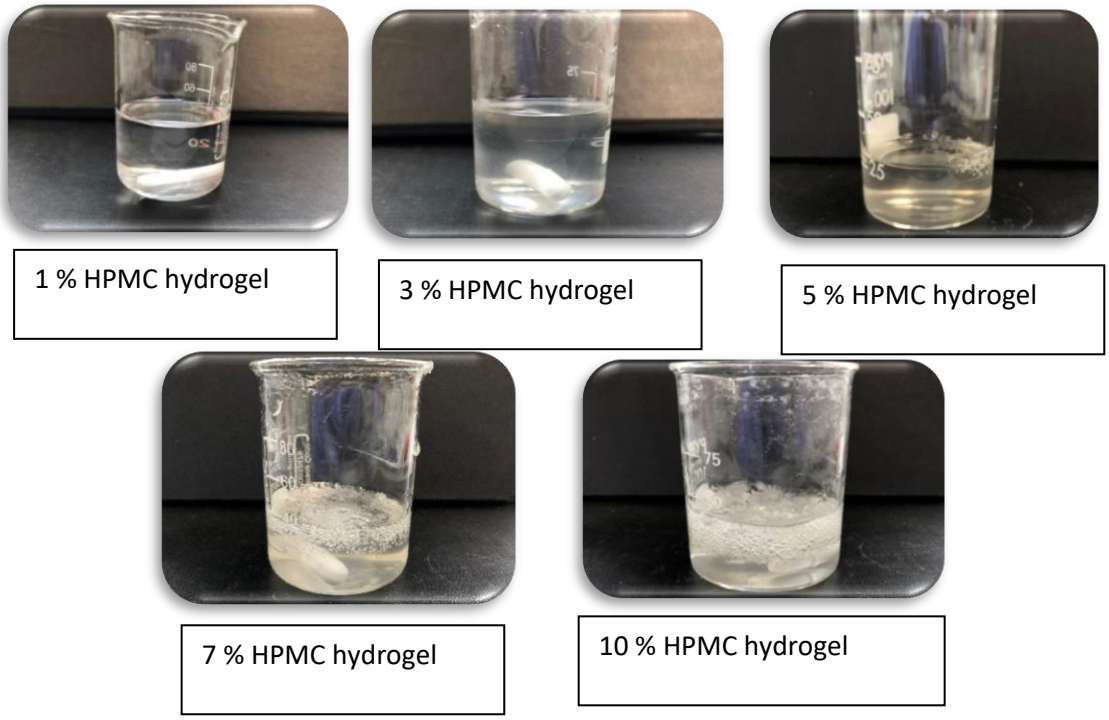

Figure 4. B1 Photographic images of the prepared HPMC hydrogels with different concentrations, including 1%, 3%, 5%, 7%, 10% and 15% HPMC w/w.

Figure 4. B2 Photographic image of the formed compact mass of the HPMC powder during the preparation of an HPMC hydrogel system.

Appendix C

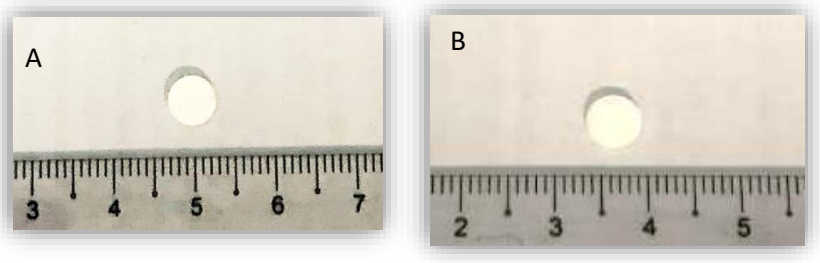

Figure 5.C1 photographic images of the compressed A) Lactose as, and B) Methyl-Beta-CD. Both used as a control in the in-vitro drug release test.

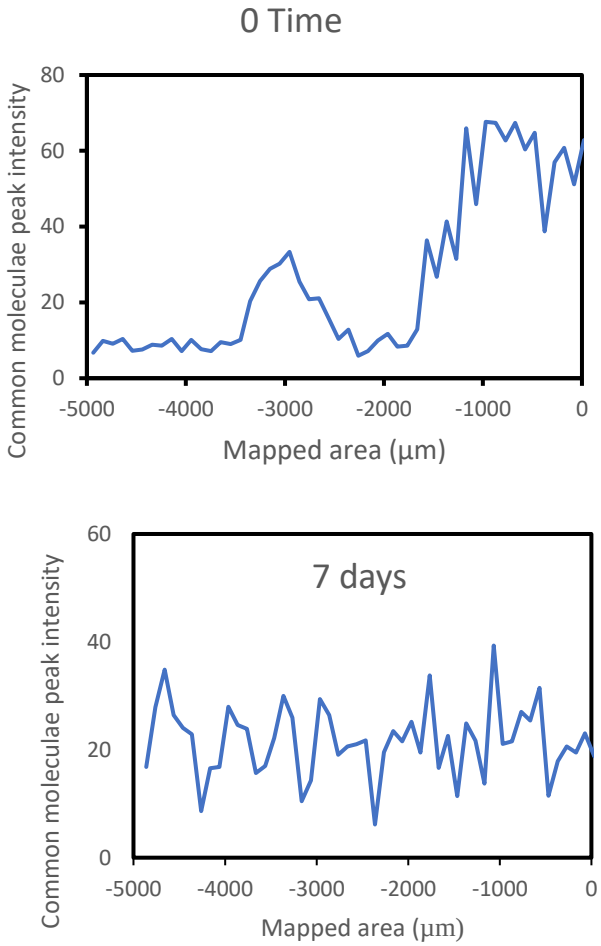

Figure 5.C2 Raman line mapping (horizontal line) of carbonyl molecular peak of DXM drug in 7 % HPMC hydrogel at different time, including 0-time, and 7 days.

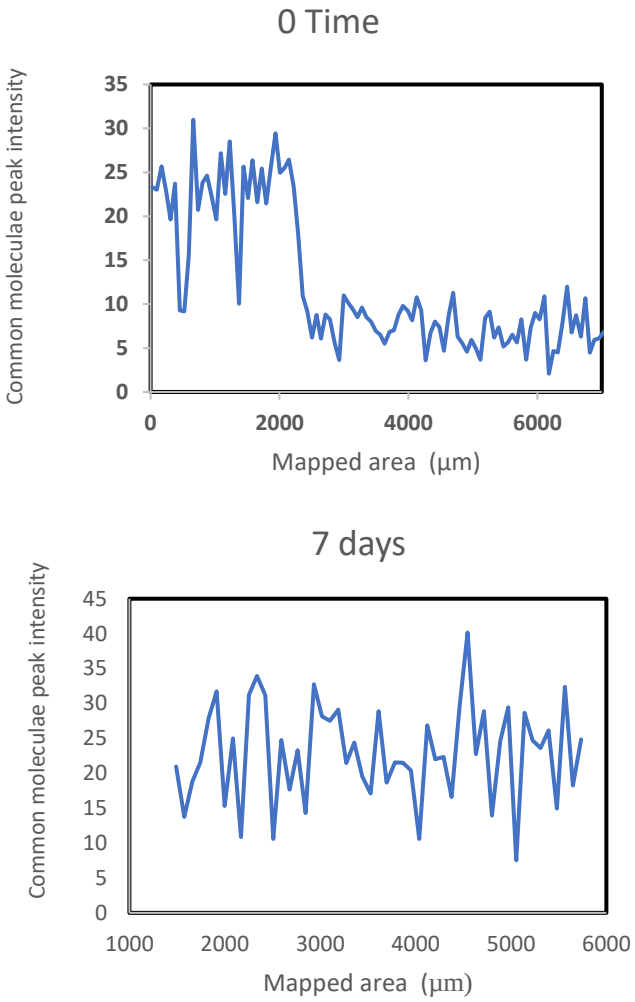

Figure 5.C3 Raman line mapping (horizontal line) of carbonyl molecular peak of DXM drug in 7 % HPMC hydrogel at different time, including 0-time, and 7 days.

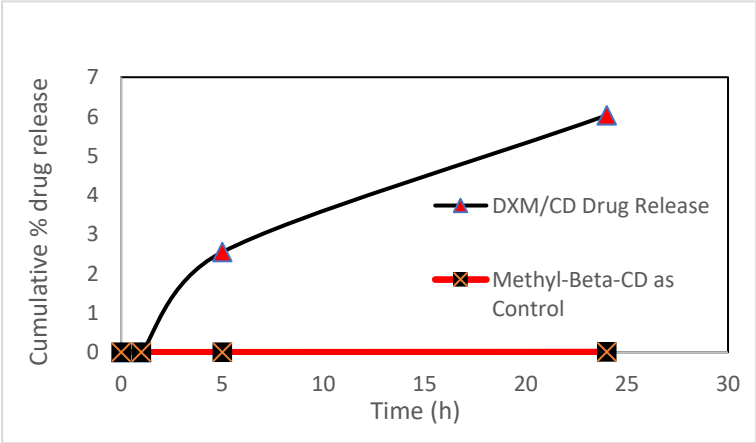

Figure 5. C4 Cumulative % of DXM/Me-β-CD complex drug release through the Strat-M® membrane that covered the Transwell.

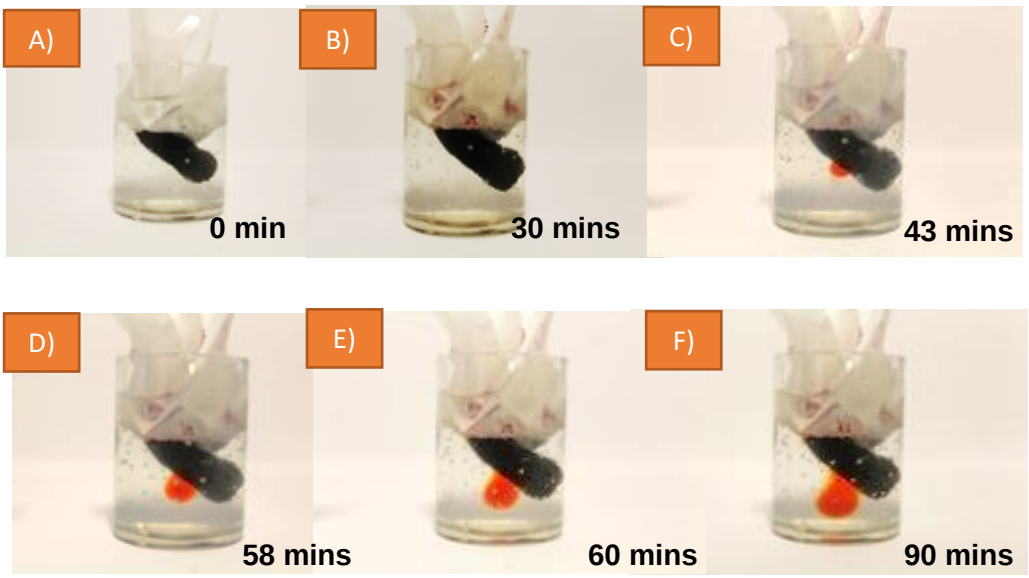

Figure 5. C6 Photographic images of a food colour dye pass through the pores of an ear prototype device that filled and immersed with 5% HPMC hydrogel. It shows the dye passes at A) zero-time, B) 30, C) 43, D) 58, E) 60, and 90 mins after the experiment started.

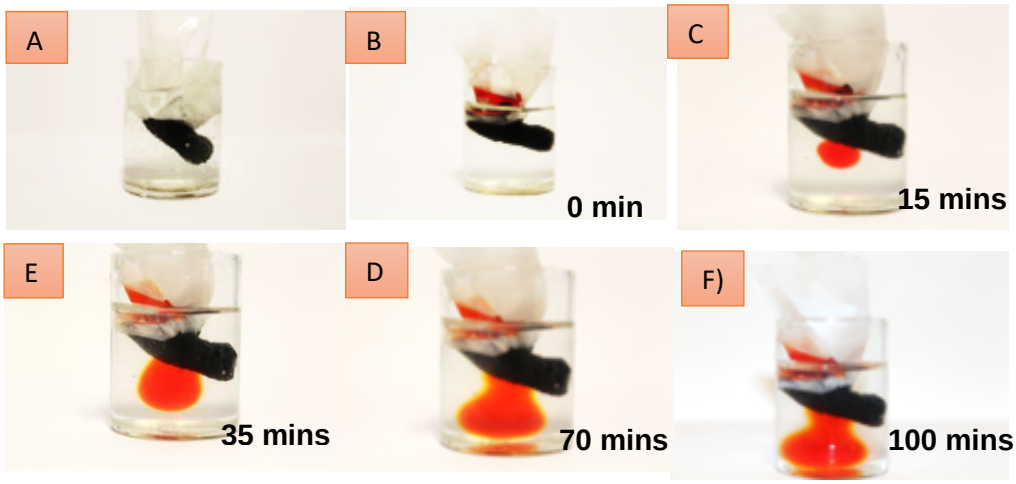

Figure 5.C7 Photographic images of a food colour dye (sunset yellow) pass through the pores of an ear prototype device that filled and immersed with 4% HPMC hydrogel. It shows the dye passes at A) zero-time, B) 15 min, C) 35 min, D) 70 min, and E) 100 min after the experiment started.

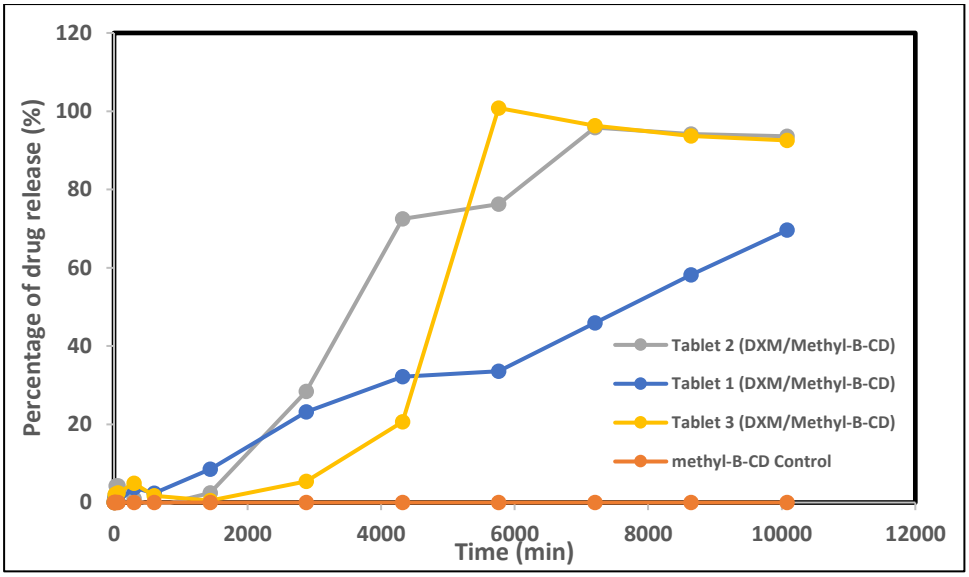

Figure 5. C8 Represents the percentage amount of the DXM drug release in PH 7.4 of PBS from the compressed (DXM/methyl-β-CD complex) tablet n=3.

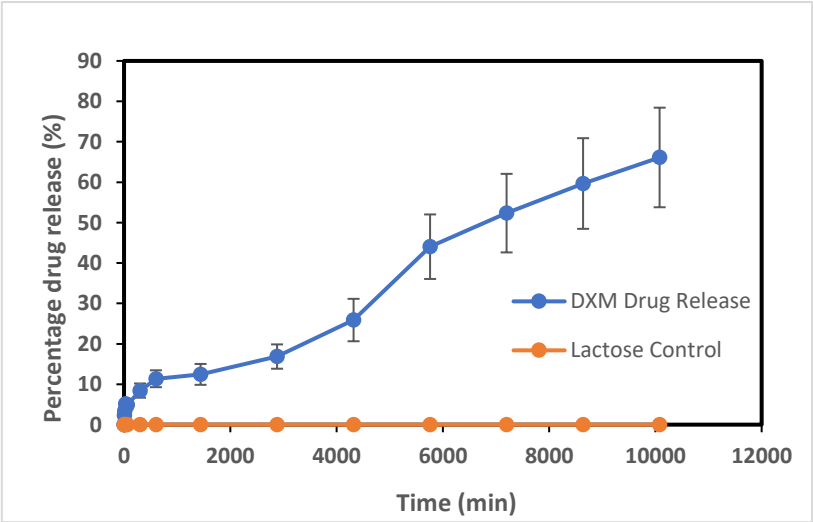

Figure 5. C9 The repeat of the In-vitro drug release profile of DXM drug in pH 7.4 through the printed devices with circular pores with synthetic membrane cover (n=3).